technische universität
dortmund

Biophysical Insights into the Ras–Membrane Ballet:

Orientational Flexibility, Conformational Substates and Mechanosensitivity of Ras Proteins

Dissertation
zur Erlangung des akademischen Grades eines
Doktors der Naturwissenschaften
(Dr. rer. nat.)

eingereicht an
der Fakultät Chemie der
Technischen Universität Dortmund

vorgelegt von

Shobhna Kapoor
Aus Delhi, Indien

Dortmund 2012

technische universität
dortmund

Biophysical Insights into the Ras–Membrane Ballet:

Orientational Flexibility, Conformational Substates and Mechanosensitivity of Ras Proteins

Dissertation
For the achievement of the academic degree of the
Doctors in Natural Sciences
(Dr. rer. nat.)

Submitted to
The Department of Chemistry
TU Dortmund University

By

Shobhna Kapoor
From Delhi, India

Dortmund 2012

Declaration/Erklärung

The work described in this Dissertation was performed from August 2009 to September 2012 at the Department of Chemistry, TU Dortmund University under the guidance of Prof. Dr. Roland Winter.

I hereby declare that I performed the work independently and did not use any other but the indicated aids.

Die vorliegende Arbeit wurde in der Zeit von August 2009 bis September 2012 an der Fakultät Chemie der Technischen Universität Dortmund unter der Anleitung von Prof. Dr. Roland Winter durchgeführt.

Hiermit versichere ich an Eides statt, dass ich die vorliegende Arbeit selbstständing und nur mit den angegebenen Hilfsmitteln angefertigh habe.

Dortmund 2012

Shobhna Kapoor

1st Examiner

Prof. Dr. Roland Winter
Department of Chemistry
Physical Chemistry-I, Biophysical Chemistry
TU Dortmund University
Dortmund

2nd Examiner

Prof. Dr. Martin Engelhard
Department of Physical Biochemistry
Max Planck Institute of Molecular Physiology
Department of Chemitsry
TU Dortmund University
Dortmund

To my loving parents

Acknowledgments

It gives me immense pleasure in expressing my heartfelt gratitude towards all the people who have helped in bringing my PhD research work to the present form.

At the very outset, I would like to express my sincere regards and gratitude to my supervisor and an outstanding mentor, Prof. Dr. Roland Winter. His indispensable guidance and invaluable suggestions have benefitted me tremendously during the course of this work. This thesis evolved out of a series of brainstorming discussions with him. His interpretations on every single work I undertook are themselves a course in critical thought upon which I will always draw. I especially value his efforts in dealing with innumerable redrafts of papers, conference posters and talks despite his grueling schedule. His encouraging attitude and positive approach have undoubtedly enhanced my learning abilities and will always be with me. It has been a truly enriching experience to work with him and learn a lot about different aspects of scientific research.

Words cannot adequately express my gratitude to Prof. Dr. Claus Czeslik for his invaluable suggestions and constant troubleshooting through the experimental and technical difficulties.

I am thankful to Prof. Dr. Roland Winter and Prof. Dr. Martin Engelhard for examining my thesis work and investing their precious time.

I owe my sincere thanks to Prof. Dr. Herbert Waldmann and his group for their generous provision of the exotic semi-synthetic Ras proteins, which is the heart of this work. His profound insights and critical comments on the scientific papers published in collaboration deserve a special mention.

I declare in candid appreciation, the role of Prof. Dr. Roger S. Goody with whom I carried out the stopped-flow measurements. I am grateful to him for taking out time for me despite his grueling schedule and sharing his profound knowledge.

I would like to thank Dr. Ingrid. R. Vetter for performing the required calculations for IRRAS simulation. I deeply acknowledge the relentless efforts of Mirko Erlkamp for performing the IRRAS simulations.

A profound sense of gratitude is owed to Dr. Katrin Weise for her support and imparting her knowledge, experienced suggestions and painstaking efforts to teach me the AFM technique. Her "eagle eye" proofreading through posters and paper drafts is highly acknowledged.

Dr. Andreas Kerth and Dr. Anette Meister from the Martin-Luther-Universität Halle-Wittenberg and Dr. Andrea Gohlke are deeply acknowledged for their valuable time and key suggestions in troubleshooting through the technical difficulties encountered in the IRRAS method.

I have been highly fortunate in getting a chance to meet and work with very warm and dedicated people " My group members". I would like to thank the present and past members of Winter's group in no particular order: Janine Seeliger, Alexander Werkmüller, Mirko Erlkamp, Juny Koo, Sebastian Grobelny, Christopher Rosin, Yong Zhai, Marie Kahse, Jonas Markgraf, Irene Perov, Simone Möbitz, Dr. Katrin Weise, Dr. Werner Horstmann, Dr. Denise Zacher, Dr. Andrea Golhke, and Dr. Chrsitoph Jeworrek with a special mention of Dr. Daniel Sellin, for providing a very hospitable and productive environment.

A Special thank is rendered to Andrea Kreusel and Bertina Schuppan in compensating for my 'ein bischen' (little) knowledge of the German language that helped me tremendously during my stay.

I am highly indebted to all my teachers and professors from the bachelor's and master's level, for inculcating in me a correct and healthy scientific attitude and to face every difficulty with high and positive spirit. I thank all my friends with a special mention of "The Tribe" for always being there in my low times.

It has been an honour to be a member of the esteemed International Max Planck Research School. I owe immensely to the IMPRS committee for considering me eligible for this school and putting their trust in me. I highly acknowledge the generous funding and resources from the Max-Plank-Gesellschaft and Technische Universität Dortmund that enabled me to pursue this work. Words cannot adequately describe the support provided by Dr. Waltraud-Hoffmann Goody and Christa Hornemann, both professionally and personally, during my stay in Germany.

I would like to thank the American Chemical Society, Elsevier, National Academy of Sciences, Nature, and Springer for their permissions to include the copyrighted materials.

I would like to single out Dr. Rishikesh Narayan for his incisive criticism and insights that constantly challenged and enriched my ideas. His tireless efforts in supporting me through the thick and thin, painstakingly proofreading my thesis, listening to my incessant ranting, and always being there for me are gratefully acknowledged.

Last, but not the least I would like to acknowledge with full heart the encouragement, support, and love from my parents, Prof. Dr. Anup K. Kapoor and Prof. Dr. Satwanti Kapoor and my brother, Anuj Kapoor. In the same breath I would like to respectfully thank my paternal grandparents, P. S. Kapoor and Kamla Kapoor, and my maternal grandparents, Ris. S. Singh and Shanti Devi, for always encouraging me to pursue higher studies.

Abbreviations

Å	Ångström (1 Å = 0.1 nm = 10^{-10} m)
Aa	Amino acid
AFM	Atomic force microscopy
ATR	Attenuated Total Internal Reflection
CaM	Calmodulin
cAMP	Cyclic adenosine monophosphate
Chol	Cholesterol
CBD	Chitin binding domain
cGMP	Cyclic guanosine monophosphate
CS	Conformational substate
Da	Dalton
Dansyl	5-Dimethylaminonaphtalin-1-sulfonyl
DAC	Diamond anvil cell
DMPC	1,2-Dimyristoyl-***sn***-glycero-3-phosphocholine
DOPC	1,2-dioleoyl-*sn*-glycero-3-phosphocholine
DOPG	1,2-dioleoyl-*sn*-glycero-3-phospho-(1'-*rac*-glycerol) sodium salt
DPPC	1,2-dipalmitoyl-*sn*-glycero-3-phosphocholine
DPPG	1,2-dipalmitoyl-***sn***-glycero-3-phospho-(1'-***rac***-glycerol) sodium salt
EF	Equilibrium fluctuation
EGF	Epidermal growth factor
EGFR	Epidermal growth factor receptor
EPL	Expressed protein ligation
ER	Endoplasmic reticulum
ERK	Extracellular signal-regulated kinases
Far	Farnesyl
FLIM	Fluorescence lifetime imaging microscopy
FIM	Functionally important motions
Fmoc	Fluorenylmethyloxycarbonyl
FRET	Föster (fluorescence) resonance energy transfer
FSD	Fourier self-deconvolution
FT-IR	Fourier transform infrared
FWHH	Full width at half height
GAP	GTPase activating protein
GDF	GDI displacement factor
GDI	GDP dissociation inhibitor

GDP	Guanosine diphosphate
GEF	Guaninenucleotide exchange factor
GG	Geranylgeranyl
GIXD	Grazing incidence X-Ray diffraction
GNBPs	Guanine Nucleotide Binding Proteins
GppNHp	Guanosine-5′-(βγ-imino)triphosphate
GTP	Guanosine triphosphate
GUV	Giant unilameller vesicle
HD	Hexadecyl
HHP	High hydrostatic pressure
HP	High pressure
HP-FTIR	High pressure Fourier transform infrared spectroscopy
HVR	Hypervariable region
HWHH	Half width at half height
IRRAS	Infrared reflection absorption spectroscopy
Icmt	Isoprenylcysteine carboxyl methyltransferase
IRE	Internal reflection element
l_d	Liquid–disordered
l_o	Liquid–ordered
LUV	Large unilamellar vesicle
MAPK	Mitogen activated protein kinase
MD	Molecular dynamics
MEK	MAP kinase kinase
MESNA	2-mercaptoethane sulfonate Na; Na – sodium
MIC	Maleimidocaproyl
NMR	Nuclear magnetic resonance
N-Rh-DHPE/*N*-Rh-PE	*N*-(lissamine rhodamine B sulfonyl)-1.2-dihexadecanoyl-*sn*-glycero-3-phosphoethanolamine triethylammonium salt
OD	Optical density
Pal	Palmitoyl
PDEδ	Delta subunit of cyclic-guanosine-monophosphate phosphodiesterase
PDB	Protein data bank
PM	Plasma membrane
PTM	Posttranslational modification
Ras	Rat adeno sarcoma
Rce1	Ras and a factor converting enzyme-1
RPT	Ras palmitoyltransferase
RT	Room temperature
RTK	Receptor tyrosine kinase

RU	Resonance unit
SPR	Surface plasmon resonance
SOS	Son of Sevenless
s_o	Solid–ordered
SM	Sphingomyelin
StBu	S-tert-butyl
Tris	Tris(hydroxymethyl)aminomethane
wt %	weight percent

Contents

List of Figures

Chapter 1

Chapter 2

Chapter 3

Chapter 4

Chapter 5

Chapter 6

Chapter 7

Chapter 9

List of Tables

List of Fluorophores

BODIPY-FL

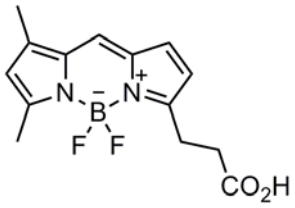

***N*-Rh-DHPE**

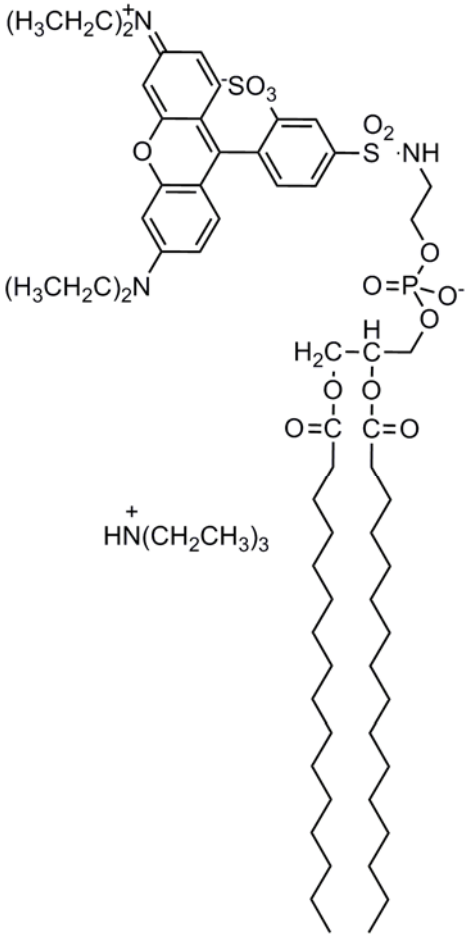

Dansyl amide

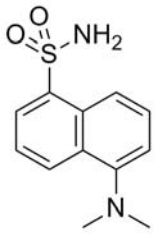

I

INTRODUCTION AND AIMS

(A) INTRODUCTION

1.1 Guanine Nucleotide Binding Proteins

Guanine nucleotide binding proteins (GNBPs), also referred to as G-proteins, are a family of proteins that bind to guanine nucleotides and transmit signals across the cell. Together with the regulators of G-protein signalling (RGS), associated effectors, and other interaction partners, GNBPs constitute the pivotal nodal points in the cellular signal transduction pathways. They mediate cellular processes ranging from proliferation, differentiation, apoptosis, and cell migration to vesicular transport. Ras, the founding member of the large superfamily of small GTPase,[1] serves as a prototype for the family of GNBPs. Small GTPase is a monomeric form of G-protein homologous to the alpha subunit of heterotrimeric G-proteins, but can independently bind and hydrolyse GTP to GDP.[2] *ras* was the first oncogene to be discovered,[3] and its history can be traced back to 1964, when Jennifer Harvey uncovered the *Harvey murine* virus *gene* that caused rapid formation of sarcoma tumour in rats.[4] Following the identification of *Harvey murine* virus, *Kirsten murine* virus sarcoma was discovered in 1967;[5] they subsequently became established as the human H-Ras and K-Ras oncogenes, respectively. Linking these *genes* to cause Rat adeno sarcoma resulted in the basis for their current gene names (i.e. *ras*) and the discoverer's name a basis for distinguishing them from each other (i.e. H-Ras and K-Ras from Harvey and Kirsten virus *ras genes*, respectively). By the end of 1982, another transforming *gene* was detected in the human neuroblastoma cell lines, and was designated as N-Ras; the third member of the *ras gene* family.[6-7] The pioneering work of Scolnick and colleagues in early 1980s revealed that

[1] Cox, A.D., and Der, C.J. **(2010)**. Ras history: The saga continues. *Small GTPases 1*, 2-27.
[2] Hurley, J.B., Simon, M.I., Teplow, D.B., Robishaw, J.D., and Gilman, A.G. **(1984)**. Homologies between signal transducing G proteins and ras gene products. *Science 226*, 860–862.
[3] Parada, L.F., Tabin, C.J., Shih, C., and Weinberg, R.A. **(1982)**. Human EJ bladder carcinoma oncogene is homologue of Harvey sarcoma virus ras gene. *Nature 297*, 474–478.
[4] Harvey, J.J. **(1964)**. Unidentified Virus Which Causes Rapid Production of Tumours in Mice. *Nature*. *204*, 1104–1105.
[5] Kirsten, W.H., and Mayer, L.A. **(1967)**. Morphologic responses to a murine erythroblastosis virus. *J. Natl. Cancer Inst. 39*, 311–335.
[6] Shimizu, K., Goldfarb, M., Perucho, M., and Wigler, M. **(1983)**. Isolation and preliminary characterization of the transforming gene of a human neuroblastoma cell line. *Proc. Natl. Acad. Sci. U.S.A. 80*, 383–387.

the proteins encoded by viral[8] and vertebrate[9] *ras genes* display high affinities for the guanine nucleotides,[10] and are attached to the plasma membrane (PM).[11-12] These, along with other renowned studies in Ras research, codified Ras as a membrane-associated, GTP-binding protein. Fuelled by the role Ras proteins play as control elements in the signal transduction pathways,[2] coupled with subsequent mutations that have been implicated in human cancers,[13] intensive research on the structure, biology, biochemistry, and biophysics of Ras proteins continues to this day.[14]

Ras, like other GNBPs, shuttles between the inactive 'off' state (GDP-bound) and the active 'on' state (GTP-bound) with nearly equal affinities (Fig. 1.1).[15] Switching 'on' of Ras is an intrinsically slow process, despite tenfold higher concentration of GTP in cells.[16] This renders the inactive form as the steady state conformation. Activation of GNBPs is expedited by the activity of Guanine Nucleotide Exchange Factors (GEFs), which catalyse the release of GDP [for example: H-Ras activation is sixfold faster in the presence of the exchange factor, SOS].[17] Once activated, Ras undergoes a conformational change in its tertiary structure,[15] which is recognised by the "effector" domain of the downstream proteins. Ras

---

[7] Hall, A., Marshall, C.J., Spurr, N.K., and Weiss, R.A. **(1983)**. Identification of transforming gene in two human sarcoma cell lines as a new member of the ras gene family located on chromosome 1. *Nature 303*, 396–400.

[8] Shih, T.Y., Weeks, M.O., Young, H.A., and Scolnick, E.M. **(1979)**. Identification of a Sarcoma Virus-Coded Phosphoprotein in Nonproducer Cells Transformed by Kirsten or Harvey Murine Sarcoma-Virus. *Virology 96*, 64–79.

[9] Langbeheim, H., Shih, T.Y., and Scolnick, E.M. **(1980)**. Identification of a normal vertebrate cell protein related to the p21 src of Harvey murine sarcoma virus. *Virology*. *106*, 292–300.

[10] Scolnick, E.M., Papageorge, A.G., and Shih, T.Y. **(1979)**. Guanine nucleotide-binding activity as an assay for src protein of rat-derived murine sarcoma viruses. *Proc. Natl. Acad. Sci. U.S.A. 76*, 5355–5359.

[11] Willingham, M.C., Pastan, I., Shih, T.Y., and Scolnick, E.M. **(1980)**. Localization of the src gene product of the Harvey strain of MSV to plasma membrane of transformed cells by electron microscopic immunocytochemistry. *Cell 19*, 1005–1014.

[12] Papageorge, A., Lowy, D., and Scolnick, E.M. **(1982)**. Comparative biochemical properties of p21 ras molecules coded for by viral and cellular ras genes. *J. Virol. 44*, 509–519.

[13] Bos, J.L. **(1989a)**. Ras Oncogenes in Human Cancer - a Review. *Cancer Research 49*, 4682–4689.

[14] Karnoub, A.E., and Weinberg, R.A. **(2008)**. Ras oncogenes: split personalities. *Nat. Rev. Mol. Cell Biol. 9*, 517–531.

[15] Vetter, I.R., and Wittinghofer, A. **(2001)**. The guanine nucleotide-binding switch in three dimensions. *Science 294*, 1299–1304.

[16] Van Dyke, K., Robinson, R., Urquilla, P., Smith, D., Taylor, M., Trush, M., and Wilson, M. **(1977)**. An analysis of nucleotides and catecholamines in bovine medullary granules by anion exchange high pressure liquid chromatography and fluorescence. Evidence that most of the catecholamines in chromaffin granules are stored without associated ATP. *Pharmacology 15*, 377–391.

[17] Chardin, P., Camonis, J.H., Gale, N.W., van Aelst, L., Schlessinger, J., Wigler, M.H., and Bar-Sagi, D. **(1993)**. Human Sos1: a guanine nucleotide exchange factor for Ras that binds to GRB2. *Science 260*, 1338–1343.

proteins are essentially weak GTP-hydrolases (GTPases), as they lack a critical Asp residue[18] necessitating the assistance of adroitly named GTPase Activating Proteins (GAPs) [for instance: the intrinsic rate of GTP hydrolysis in N-Ras is 4.2 x 10^{-4} s^{-1}, which is increased hundredfolds by its cognate GAP][19-20]. The ability of Ras proteins to interact with different nucleotides and presenting their "active state" distinguishable from their "inactive state" aptly designate them as molecular switches (Fig. 1.1).

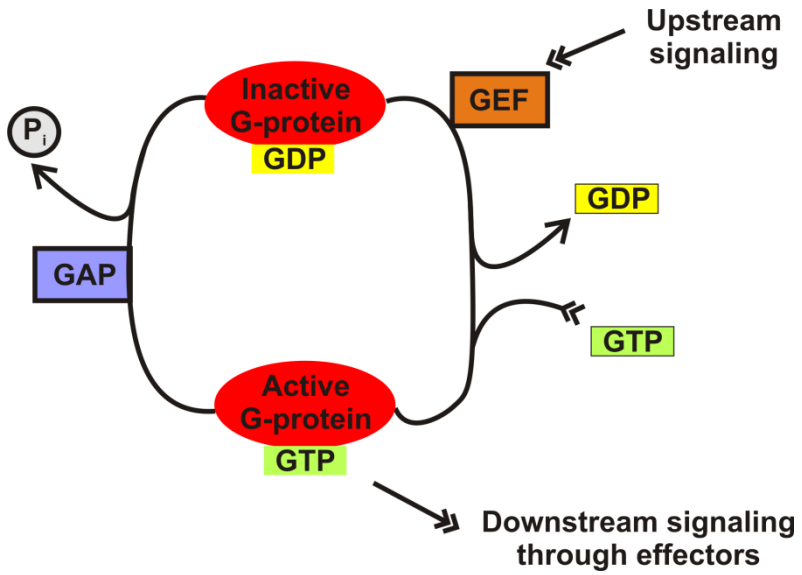

Figure 1.1: Schematic representation of the GTPase cycle. G-protein shuttles between the **GDP-bound** (inactive) and the **GTP-bound** (active) states. This cycle is regulated by **GEFs** and **GAPs** stimulating GTP-loading and hydrolysis, respectively.

1.2 Structural Outline of the Ras G-Domain Fold

The first crystal structure of Ras was independently solved by the groups of Kim[21] and Wittinghofer.[22] A comparison of all the available crystal structures of GNBPs reveals an

[18] Wittinghofer, A., Scheffzek, K., and Ahmadian, M.R. **(1997)**. The interaction of Ras with GTPase-activating proteins. *FEBS Lett 410*, 63–67.
[19] Neal, S.E., Eccleston, J.F., Hall, A., and Webb, M.R. **(1988)**. Kinetic analysis of the hydrolysis of GTP by p21N-ras. The basal GTPase mechanism. *J. Biol. Chem. 263*, 19718–19722.
[20] Trahey, M., and McCormick, F. **(1987)**. A cytoplasmic protein stimulates normal N-ras p21 GTPase, but does not affect oncogenic mutants. *Science 238*, 542–545.
[21] de Vos, A.M., Tong, L., Milburn, M.V., Matias, P.M., Jancarik, J., Noguchi, S., Nishimura, S., Miura, K., Ohtsuka, E., and Kim, S.H. **(1988)**. Three-dimensional structure of an oncogene protein: catalytic domain of human c-H-ras p21. *Science. 239*, 888–893.

evolutionary preserved universal structural core, the G-domain.[15] The approximately 21 kDa G-domain fold (comprising of 166–167 aa) consists of five helices surrounding six-stranded beta sheets on both sides—a structural motif unique to the α/β family of proteins (Fig. 1.2).

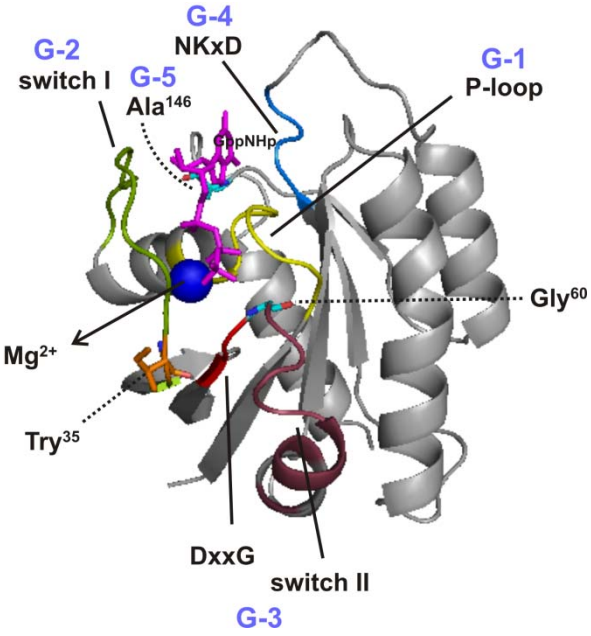

Figure 1.2: Ribbon diagram of the G-domain fold. Conserved sequence elements and switch regions depicted in different colours, as stated. The nucleotide, Mg^{2+}, Thr^{35}, Gly^{60}, and Ala^{146} are shown in the ball and stick representation.

A number of conserved sequence elements, namely G1–G5, line up along the nucleotide binding site.[23] The G-1 motif, also known as the P-loop (phosphate-binding loop), comprises the sequence "GxxxxGKS" (x, is any amino acid), and interacts with the nucleotide's α- and β-phosphates. The G-2 motif harbours the "constant" threonine (at position 35 in Ras), which binds to the γ-phosphate and coordinates with the Mg^{2+} via its side chain. Similarly, the conserved aspartate (at position 57 in Ras) of the G-3 motif (DxxG) binds to the Mg^{2+} indirectly via a water molecule, and glysine (at position 60 in Ras) makes a contact with the

[22] Pai, E.F., Kabsch, W., Krengel, U., Holmes, K.C., John, J., and Wittinghofer, A. **(1989)**. Structure of the guanine-nucleotide-binding domain of the Ha-ras oncogene product p21 in the triphosphate conformation. *Nature 341*, 209–214.
[23] Bourne, H.R., Sanders, D.A., and McCormick, F. **(1991)**. The GTPase superfamily: conserved structure and molecular mechanism. *Nature 349*, 117–127.

γ-phosphate. The G-4 (NKxD) and G-5 (SAL/K) motifs are important for the nucleotide specificity; rendered by the bifurcated contact of aspartate (at position 119 in Ras, G-4 motif), and the main-chain interaction from alanine (at position 146 in Ras, G-5 motif) to the guanine base, respectively.

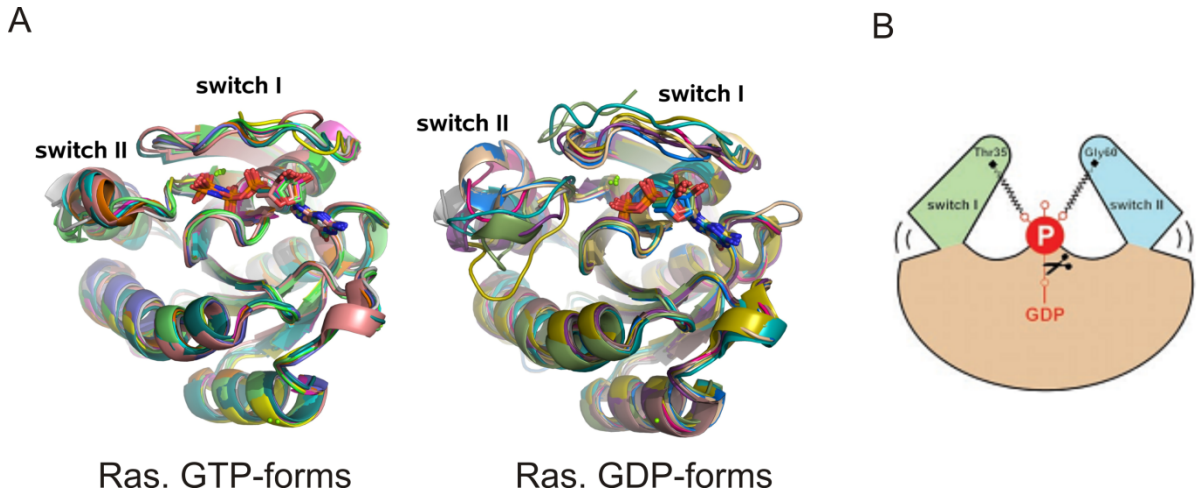

Figure 1.3: Molecular switch determinants in Ras. (**A**) Higher flexibility of the switch regions in Ras.GDP-forms compared with Ras.GTP-forms. (**B**) Schematic representation of the Switch I and II regions bound to the γ-phosphate via Thr^{35} and Gly^{60} in the active state, which relax upon GTP hydrolysis. Reproduced from ref. 15. Reprinted with permission from AAAS.

The structural determinants for the molecular switching mechanism in Ras are mainly confined to the G-2 and G-3 motifs; termed Switch I (aa 32-38) and Switch II (aa 59-67), respectively.[24] These regions only show increased flexibility in the GDP-bound state (Fig. 1.3 **A**). The abolishment of H-bonds from Thr^{35} (of Switch I) and Gly^{60} (of Switch II) to the γ-phosphate (Figure 1.3 **B**) relaxes the switch regions in the inactive state, thus best describing this conformational change as the "loaded-spring mechanism". However, the degree of conformational change between the inactive and active states differs among other members of the Ras superfamily, and may involve other structural elements. For example, Ran experiences a great degree of conformational change when its Switch I leads to the

[24] Milburn, M.V., Tong, L., deVos, A.M., Brunger, A., Yamaizumi, Z., Nishimura, S., and Kim, S.H. **(1990)**. Molecular switch for signal transduction: structural differences between active and inactive forms of protooncogenic ras proteins. *Science 247*, 939–945.

unfolding of an extra β-strand and the dramatic relocation of its N-terminal switch.[25] Likewise, the Switch I of Arf exhibits a β-sheet register shift leading to the expulsion, and thereafter membrane insertion of its N-terminal helix.[26]

1.3 Ras Signalling

The most fundamental responses of cells to extracellular stimuli are proliferation and differentiation, and the major signalling cascade mediating these responses is the mitogen-activated protein kinase (MAPK) cascade. This pathway can be activated when one of several extracellular ligands (e.g. epidermal growth factor (EGF)) binds to the different PM bound receptors (e.g. trans-membrane epidermal growth factor receptor (EGFR)). The cytoplasmic domain of EGFR is the receptor tyrosine kinase (RTK), which undergoes dimerisation and autophosphorylation upon stimulation (Fig. 1.4).

A major breakthrough linking Ras to MAPK signalling emerged in the early 90s with the following disclosure: EGFR stimulation increases Ras-GTP binding, thus placing Ras downstream of membrane-associated kinases.[27] Soon it was realised that Ras activation is also mediated by G-proteins, adhesion molecules, and second messengers, aptly falling under the category of signalling convergence. Another major epiphany in the Ras signal transduction during that time was the identification of a Raf serine/threonine kinase that bound to Ras, preferentially in the active state, thus inheriting the distinction of the *first* Ras effector.[28-29] Ras-dependent activation of Raf, and Raf-dependent activation of ERK and

[25] Vetter, I.R., Nowak, C., Nishimoto, T., Kuhlmann, J., and Wittinghofer, A. **(1999)**. Structure of a Ran-binding domain complexed with Ran bound to a GTP analogue: implications for nuclear transport. *Nature 398*, 39–46.
[26] Goldberg, J. **(1998)**. Structural basis for activation of ARF GTPase: mechanisms of guanine nucleotide exchange and GTP-myristoyl switching. *Cell 95*, 237–248.
[27] Kamata, T., and Feramisco, J.R. **(1984)**. Epidermal Growth-Factor Stimulates Guanine-Nucleotide Binding-Activity and Phosphorylation of Ras Oncogene Proteins. *Nature 310*, 147–150.
[28] Van Aelst, L., Barr, M., Marcus, S., Polverino, A., and Wigler, M. **(1993)**. Complex formation between RAS and RAF and other protein kinases. *Proc. Natl. Acad. Sci. U.S.A. 90*, 6213–6217.
[29] Moodie, S.A., Willumsen, B.M., Weber, M.J., and Wolfman, A. **(1993)**. Complexes of Ras.GTP with Raf-1 and mitogen-activated protein kinase kinase. *Science 260*, 1658–1661.

MEK, came to be known as the Ras–Raf–MEK–ERK protein kinase cascade (Fig. 1.4). [30-31] This linear description is an oversimplification of complex Ras signalling, as distinct components are known to exist in different cascade tiers of the MAPK pathway, regulating a variety of functions. Multiplicity of the cascade's substrate (i.e. molecules Ras acts upon) includes, among others, transcription factors, protein kinases, phosphatases, and regulators of apoptosis. This attributes to the divergence of Ras signalling.

Signal transduction in an abridged depiction of the Ras/MAPK cascade is, in itself, full of complex interactions that embody the Ras GTPase cycle. As mentioned above, extracellular stimuli promotes autophosphorylation of RTKs. RTKs then bind to the 'adapter protein' GRB2, which through its domain, binds to the Son of Sevenless (SOS); an important Ras-GEF. This binding evokes the recruitment of SOS to the PM, where the close proximity of membrane-bound Ras to SOS forms the crucial prerequisite for Ras activation. Activated Ras has a diverse range of effector molecules,[32] of which RAF serine-threonine kinase (MAPKKK = MAP kinase kinase kinase) is the most abundant. Following Ras activation, a sequential phosphorylation and activation of protein kinases along the different tiers of the pathway takes place. Activated RAF-kinase phosphorylates MEK (MAPKK = MAP kinase kinase), which further activates ERK (MAP kinase). Phosphorylated ERK travels into the nucleus and phosphorylates transcription factors, finally leading to cell proliferation, survival, and differentiation (Fig. 1.4). Misregulation of the Ras/MAPK pathway, due to mutations in the *ras genes* (RASopathies)[33] emphasises the essential role of Ras in normal cell development.

[30] Kyriakis, J.M., App, H., Zhang, X.F., Banerjee, P., Brautigan, D.L., Rapp, U.R., and Avruch, J. **(1992)**. Raf-1 activates MAP kinase-kinase. *Nature 358*, 417–421.
[31] Howe, L.R., Leevers, S.J., Gomez, N., Nakielny, S., Cohen, P., and Marshall, C.J. **(1992)**. Activation of the MAP kinase pathway by the protein kinase raf. *Cell 71*, 335–342.
[32] Mitin, N., Rossman, K.L., and Der, C.J. **(2005)**. Signaling interplay in Ras superfamily function. *Curr. Biol. 15*, R563–574.
[33] Tidyman, W.E., and Rauen, K.A. **(2009)**. The RASopathies: developmental syndromes of Ras/MAPK pathway dysregulation. *Curr. Opin. Genet. Dev. 19*, 230–236.

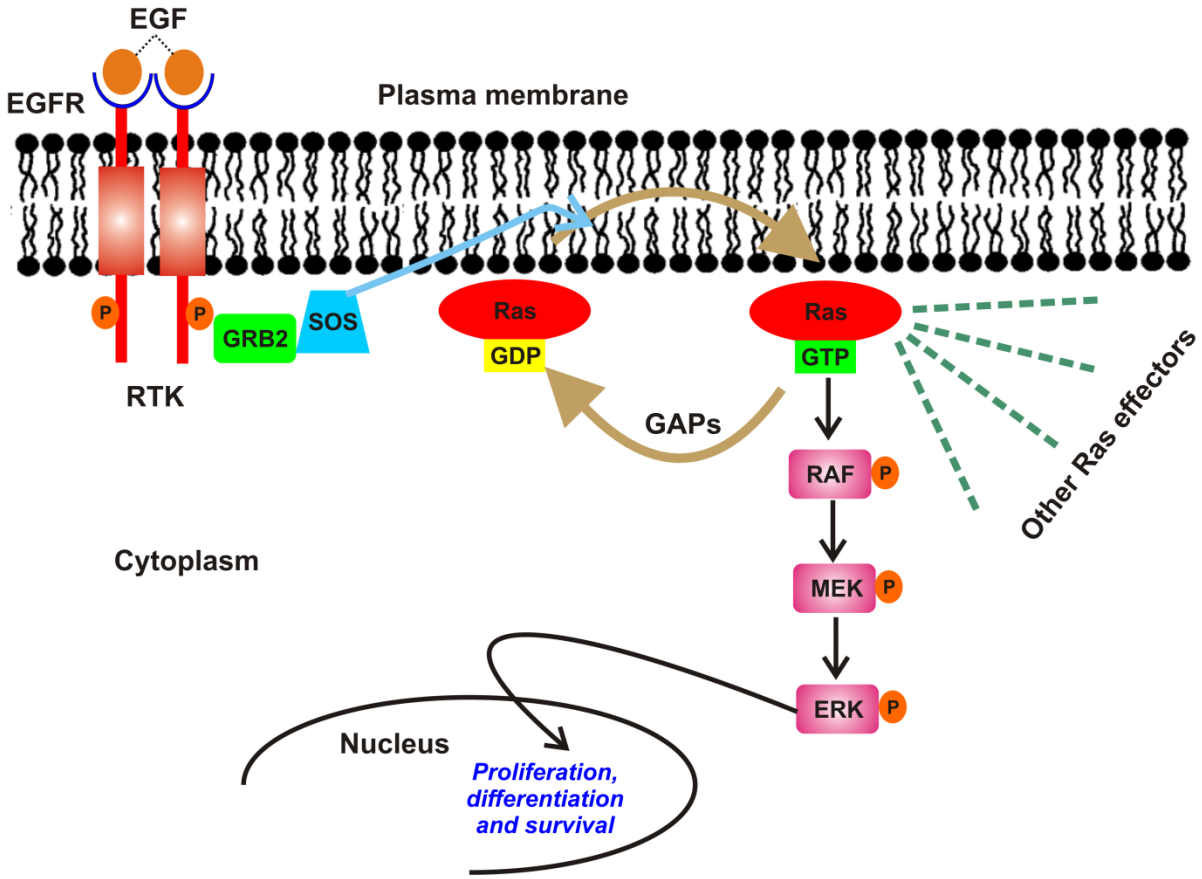

Figure 1.4: Simplified representation of the Ras/MAPK signalling pathway. Ras upon activation by a variety of extracellular stimuli (**signalling convergence**) undergoes a conformational change in its switch regions, which is then recognised by a plethora of other proteins involved in the pathway (**signalling divergence**). This enables the signalling events to get amplified downstream, producing distinct biological outputs ranging from cell growth, differentiation, and vesicle transport to apoptosis. Any kind of alteration in Ras—the key player of the MAPK cascade—along with other components, results in various syndromes. Rasopathies highlight the prominence of the MAPK/Ras cascade in cellular signalling.

1.4 Ras Lipidation and Isoforms

1.4.1 Post Translational Modification (PTM) of Ras

The very fabric of signal transduction pathways (i.e. the Ras proteins) are cytosolic when newly synthesised on free ribosomes (as pro-p21), with a half life of around 24 h.[34] However, delineation of the biochemical basis for their subsequent membrane attachment came from

[34] Ulsh, L.S., and Shih, T.Y. **(1984)**. Metabolic turnover of human c-rasH p21 protein of EJ bladder carcinoma and its normal cellular and viral homologs. *Mol. Cell. Biol. 4*, 1647–1652.

the work of Willumsen, Lowy and colleagues. Using palmitic acid labelling and mutational studies they revealed the C-terminus of Ras protein to be as essential for its PM association[35] as the residue Cys^{186} was critical for lipid binding.[36] This work also speculated Cys^{186} to be the preferred site of palmitoylation (acylation) as palmitate seemed the only lipid relevant to Ras during that time.[37] Further studies elaborated upon such musings, suggesting that acylation was not the foremost step in Ras processing and proclaiming that no more than three C-terminal residues are cleaved during processing,[38] followed by carboxylmethylation of the C-terminus, prior to Ras acylation[39]. These steps compiled together constitute the Posttranslational Modifications (PTMs) of Ras. Our current view of Ras PTMs (Fig. 1.5) to the maximum accuracy can be traced back to the work of Hancock and colleagues. They demonstrated that Ras proteins contain a C-terminal CAAX motif (C= cysteine, A= aliphatic aa, X= terminal aa) and that Cys^{186} is farnesylated instead of palmitoylated.[40-41] Farnesylation is the mandatory first step in the Ras PTM mediated by the cytosolic farnesyltransferase, which catalyses the covalent addition of C15 farnesyl group (a product of cholesterol biosynthesis pathways). This process is followed by proteolytic cleavage of the 3 C-terminal residues (-AAX) upstream of Cys^{186}, acted upon by Rce1 (Ras and a-factor converting enzyme-1). The third step involves carboxylmethylation at the C-terminal farnesylated cysteine (Cys^{186}) by Icmt (isoprenylcysteine carboxylmethyltransferase). The last (but optional) step is the dynamic palmitoylation on the cysteine upstream of C-terminal cysteine via Ras palmitoyltransferase (RPT), an endoplasmic reticulum localised enzyme.[42]

---

[35] Willumsen, B.M., Christensen, A., Hubbert, N.L., Papageorge, A.G., and Lowy, D.R. **(1984a)**. The p21 ras C-terminus is required for transformation and membrane association. *Nature 310*, 583–586.

[36] Willumsen, B.M., Norris, K., Papageorge, A.G., Hubbert, N.L., and Lowy, D.R. **(1984b)**. Harvey murine sarcoma virus p21 ras protein: biological and biochemical significance of the cysteine nearest the carboxy terminus. *EMBO J. 3*, 2581–2585.

[37] Buss, J.E., and Sefton, B.M. **(1986)**. Direct identification of palmitic acid as the lipid attached to p21ras. *Mol. Cell Biol. 6*, 116–122.

[38] Fujiyama, A., and Tamanoi, F. **(1990)**. RAS2 protein of Saccharomyces cerevisiae undergoes removal of methionine at N terminus and removal of three amino acids at C terminus. *J. Biol. Chem. 265*, 3362–3368.

[39] Gutierrez, L., Magee, A.I., Marshall, C.J., and Hancock, J.F. **(1989)**. Post-translational processing of p21ras is two-step and involves carboxyl-methylation and carboxy-terminal proteolysis. *EMBO J. 8*, 1093–1098.

[40] Hancock, J.F., Magee, A.I., Childs, J.E., and Marshall, C.J. **(1989)**. All Ras Proteins Are Polyisoprenylated but Only Some Are Palmitoylated. *Cell 57*, 1167–1177.

[41] Hancock, J.F., Paterson, H., and Marshall, C.J. **(1990)**. A Polybasic Domain or Palmitoylation Is Required in Addition to the Caax Motif to Localize P21ras to the Plasma–Membrane. *Cell 63*, 133–139.

[42] Casey, P.J., Solski, P.A., Der, C.J., and Buss, J.E. **(1989)**. p21ras is modified by a farnesyl isoprenoid. *Proc. Natl. Acad. Sci. U.S.A. 86*, 8323–8327.

"Dynamic" is used here in the sense of being reversed; the half life of palmitate on Ras is shorter than that of Ras itself.[43] These posttranslational modifications bestow upon Ras additional regulatory control to maintain homeostasis and respond to extracellular stimuli.

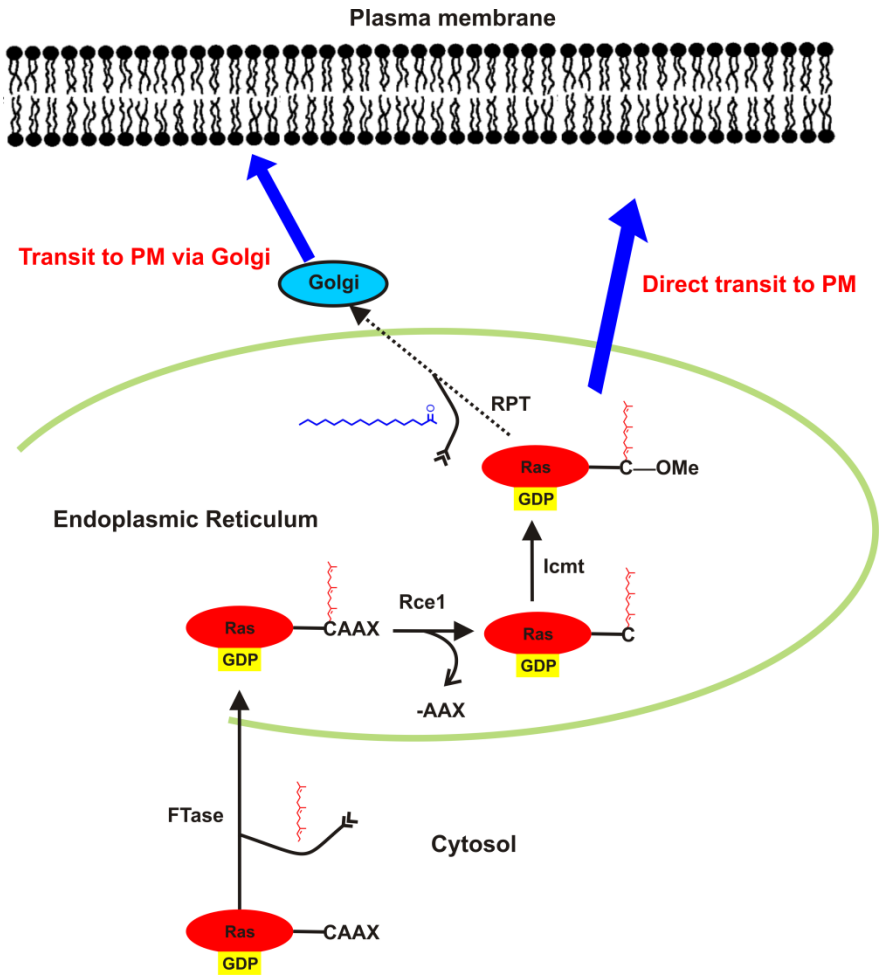

Figure 1.5: CAAX box signalled posttranslational modification of Ras: First, the cysteine of CAAX box is modified by the addition of a farnesyl moiety mediated by FTase, followed by proteolytic cleavage of the -AAX residues via the enzyme Rce1. Processing is completed on the cytosolic leaflet of ER by Icmt catalysed carboxylmethylation of the terminal Far-cysteine. The optional step is the palmitoylation mediated by RPT on the cysteine/s upstream of the terminal cysteine, which enables Ras to enter the classical secretory route to PM via Golgi.

Lipid attachment to Ras represents an essential modification, also found in many other Ras family proteins.[44] The main types of known lipid modifications are:

[43] Magee, A.I., Gutierrez, L., McKay, I.A., Marshall, C.J., and Hall, A. **(1987)**. Dynamic fatty acylation of p21N-ras. *EMBO J. 6*, 3353–3357.

1. **Prenylation**: Irreversible modification involving covalent linkage of either C-15 (farnesyl) or C-20 (geranylgeranyl) isoprenoids to the cysteine residue near the C-terminus of the target proteins via a thioester bond, catalysed by specific prenyltransferases.[45] This modification increases the hydrophobicity of the target proteins, thus imparting membrane affinity, however weak it might be. Prenylation has been largely clarified for Ras and Rab proteins that are farnesylated and geranylgeranylated, respectively, with a preference for specific isoprenyl groups dictated by particular sequences in these proteins.[46]
2. **Palmitoylation:** Either a reversible linkage of the palmitoyl moiety through a labile thioester bond (**S-palmitoylation**), or a stable amide linkage at glycine/cysteine (**N-palmitoylation**). Cases of N-palmitoylation are rather limited, and mainly observed in secreted proteins (e.g. Hedgehog).[47] On the other hand S-palmitoylation has a diverse repertoire of proteins to act on, including peripheral proteins, trans-membrane receptors, and Ras.[48]
3. **Myristoylation:** Cotranslational lipid modification involving the addition of C-14 (myristic fatty acid) to the N-terminal glycine via an amide bond. The addition is catalysed by specific N-myristoyltransferases, dictated by certain conserved protein sequences.[49]

1.4.2 Ras Isoforms

Up till now, Ras has been mentioned only as a single entity, but the three human *ras genes* (H-, N- and K-Ras) encode for four proteins, namely: Harvey (H)-Ras, Kirsten (K)-Ras4A, Kirsten (K)-Ras4B, and Neuroblastoma (N)-Ras. The A and B forms of K-Ras are the

---

[44] Magee, A.I., Newman, C.M.H., Giannakouros, T., Hancock, J.F., Fawell, E., and Armstrong, J. **(1992)**. Lipid Modifications and Function of the Ras Superfamily of Proteins. *Biochem. Soc.Trans. 20*, 497–499.
[45] Casey, P.J., and Seabra, M.C. **(1996).** Protein prenyltransferases. *J. Biol. Chem. 271*, 5289–5292.
[46] Maurer-Stroh, S., and Eisenhaber, F. **(2005)**. Refinement and prediction of protein prenylation motifs. *Genome Biol. 6*, R55.
[47] Pepinsky, R.B., Zeng, C., Wen, D., Rayhorn, P., Baker, D.P., Williams, K.P., Bixler, S.A., Ambrose, C.M., Garber, E.A., Miatkowski, K*., et al.* **(1998)**. Identification of a palmitic acid-modified form of human Sonic hedgehog. *J. Biol. Chem. 273*, 14037–14045.
[48] Resh, M.D. **(2006)**. Palmitoylation of ligands, receptors, and intracellular signaling molecules. *Sci. STKE. 2006*, re14.
[49] Resh, M.D. **(1999)**. Fatty acylation of proteins: new insights into membrane targeting of myristoylated and palmitoylated proteins. *Biochim. Biophys. Acta. 1451*, 1–16.

products of alternate splicing (of the 4th exon) of the K-Ras *gene* and differ considerably in their carboxy-terminus.[50] K-Ras4B is more abundantly expressed in humans (~ 98 %) than its counterpart. *In this document hereafter "K-Ras" will only refer to this form unless stated otherwise.*

These four proteins described above are collectively known as the Ras isoforms. The basic anatomy of the Ras isoforms is divided into two parts (Fig. 1.6): N-terminal (165 aa) and C-terminal residues (24/25 aa, starting at position 165).[51] The N-terminal residues constitute the G-domain, shown in Fig. 1.2, and comprise of all the critical domains required for the GTPase functions (i.e. nucleotide binding and hydrolysis). Based on the primary sequence comparison, the first 86 amino acids are almost 100 % identical among the Ras isoforms and contain the effector binding domain (aa 32-40). *This implies that Ras isoforms should not differ in binding to the effectors or in their GTPase cycle*. The next 80 amino acids show a slight divergence in their sequence, specifically exhibiting 85-90 % homology. In contrast, the C-terminal residues show no sequence similarity among the isoforms, except for the conserved CAAX box (described in Section 1.3). Thus, they are befittingly referred to as the hypervariable region (HVR). The HVR is further divided into two domains: the linker and anchor domains. As the name implies, the linker domain connects the G-domain to the anchor domain, and the latter consists of the membrane trafficking signals. The minimal Ras anchor signal, common to all the isoforms, is the farnesylated C^{186}AAX box (shown in red). The second signal (shown in blue) is highly diverse as follows:

(a) For K-Ras4B, the second signal comprises a polybasic contiguous stretch of six lysines (out of eight) conferring a strong positive charge to its C-terminus. This accounts for the strong electrostatic interactions with the negatively charged phospholipids in the PM coupled with the electrical polarity of the PM. [52-53]

---

[50] McGrath, J.P., Capon, D.J., Smith, D.H., Chen, E.Y., Seeburg, P.H., Goeddel, D.V., and Levinson, A.D. **(1983)**. Structure and organization of the human Ki-ras proto-oncogene and a related processed pseudogene. *Nature 304*, 501–506.

[51] Lowy, D.R., and Willumsen, B.M. **(1993)**. Function and regulation of ras. *Annu. Rev. Biochem. 62*, 851–891.

[52] van Meer, G., Voelker, D.R., and Feigenson, G.W. **(2008)**. Membrane lipids: where they are and how they behave. *Nat. Rev. Mol. Cell. Biol. 9*, 112–124.

[53] Crouthamel, M., Thiyagarajan, M.M., Evanko, D.S., and Wedegaertner, P.B. **(2008)**. N-terminal polybasic motifs are required for plasma membrane localization of Galpha(s) and Galpha(q). *Cell Signal. 20*, 1900-1910.

(b) For K-Ras4A, the second signal is a single palmitoylation site at position 179 (Cys^{179}).

(c) For N-Ras, the second signal also involves a single palmitoylation site (Cys^{181}).

(d) And for H-Ras, it involves two palmitoylation sites (Cys^{181} and Cys^{184}).

Palmitoylation in the isoforms fosters the membrane association by imparting a high membrane affinity to the proteins,[54] which is otherwise weak in the presence of the farnesyl moiety. The targeting signals found in the HVR of Ras proteins are both essential and sufficient to mediate and retain the membrane association,[55] until regulated by additional determinants such as depalmitoylation of N-/H-Ras,[56] and phosphorylation of serine at position 182 in K-Ras[57]. Phosphorylation of serine reduces the net positive charge on the K-Ras HVR, thus weakening the consequent membrane interaction with anionic lipids. More specifically, the *second targeting signal* represents the vital element responsible for differential localisation of all Ras isoforms; all prenylated Ras forms are undistinguishable in their cellular localisations.

Despite exhibiting a high degree of sequence homology, the Ras isoforms are not functionally redundant. They are implicated to share a common spectrum of effector and interaction partners that interact with the same region within the Ras proteins (i.e. the effector binding domain), but still generate distinct signal outputs and diverse biological responses. This has led to the Ras isoform specificity concept, and drives critical scientific research to delineate the determinants imparting this specificity.

---

[54] Rocks, O., Peyker, A., and Bastiaens, P.I. **(2006)**. Spatio-temporal segregation of Ras signals: one ship, three anchors, many harbors. *Curr. Opin. Cell. Biol. 18*, 351–357.

[55] Hancock, J.F., Cadwallader, K., Paterson, H., and Marshall, C.J. **(1991)**. A Caax or a Caal Motif and a 2nd Signal Are Sufficient for Plasma-Membrane Targeting of Ras Proteins. *EMBO J. 10*, 4033–4039.

[56] Rocks, O., Peyker, A., Kahms, M., Verveer, P.J., Koerner, C., Lumbierres, M., Kuhlmann, J., Waldmann, H., Wittinghofer, A., and Bastiaens, P.I. **(2005)**. An acylation cycle regulates localization and activity of palmitoylated Ras isoforms. *Science 307*, 1746–1752.

[57] Bivona, T.G., Quatela, S.E., Bodemann, B.O., Ahearn, I.M., Soskis, M.J., Mor, A., Miura, J., Wiener, H.H., Wright, L., Saba, S.G., *et al.* **(2006)**. PKC regulates a farnesyl-electrostatic switch on K-Ras that promotes its association with Bcl-XL on mitochondria and induces apoptosis. *Mol. Cell. 21*, 481–493.

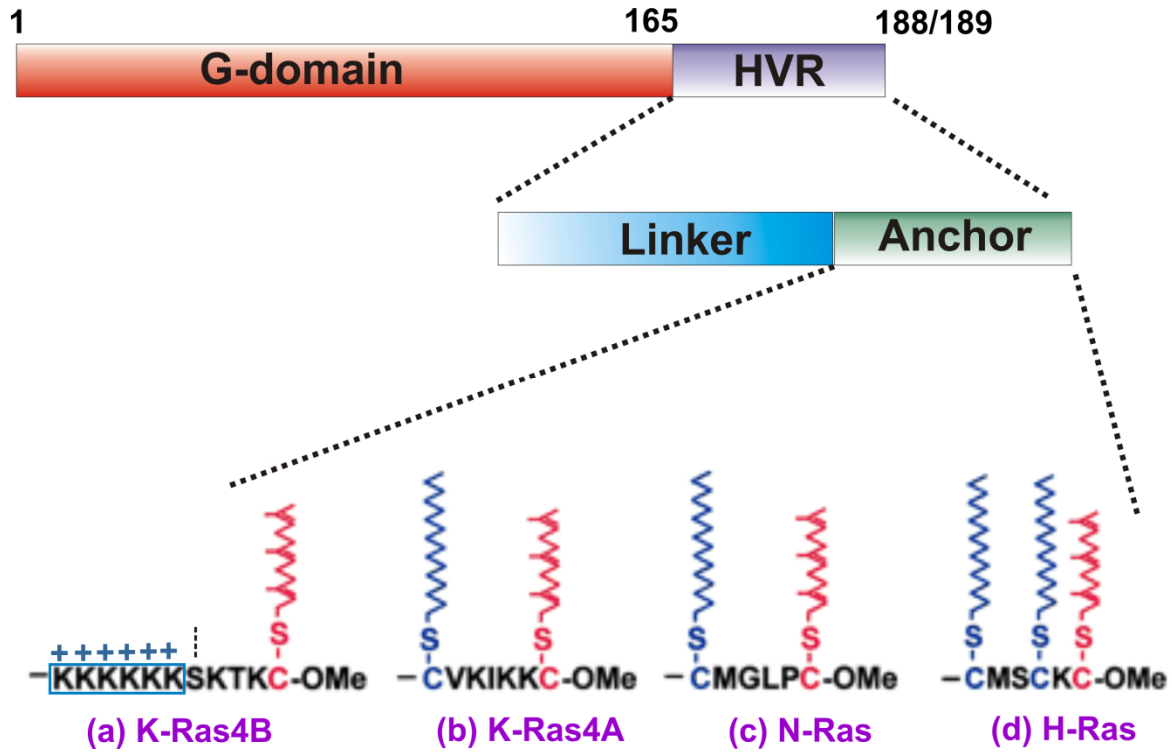

Figure 1.6: Anatomy of Ras proteins. The N-terminal residues form the conserved structural core (G-domain) of the protein, and carry out the basic function of GTP hydrolysis and binding to downstream effectors. The HVR defines the Ras isoforms, and comprises the membrane anchor region, shown with their respective posttranslational modifications. The common CAAX box gets prenylated (shown in red) in all isoforms and the second signal (shown in blue) involves either a polybasic lysine stretch with K-Ras4B (**a**), or a single palmitoylation site in K-Ras4A (**b**), and in N-Ras (**c**) or two palmitoylation sites with H-Ras (**d**). The dashed line in (**a**) indicates the serine residue that is phosphorylated, reducing the net charge in the second signal for K-Ras4B.

(B) AIMS OF THIS WORK

With this perspective, it is clear that Ras proteins are critical nexus points in the cellular signaling pathways mediating diverse biological outputs. Given their role as oncogenes, it is essential to study and understand even the most lucid aspects of Ras proteins and their interactions with lipid membranes, their most complex and ambiguous interaction partner. The goals of the ensuing study utilising diverse biophysical methods were as follows:

1. To establish and characterise a heterogeneous, biomembrane model system with diverse lipid components to closely mimic the highly complex and dynamic biological membranes, which have been implicated as intriguing regulatory controls on cell signalling. Such model membranes would thus serve as ideal platforms to elucidate the role of lipid domains and heterogeneity on the dynamics of Ras, and probably other signalling lipidated proteins.

2. To indentify the possible determinants of Ras isoforms-specific membrane interactions. Probing beyond the most obvious and well-characterised hypervariable regions towards the least obvious catalytic core, the G-domain. To elucidate what role, the common Ras G-domain would impart to its interactions with effector proteins or other interaction partners.

3. To determine whether Ras is part of a complex signalling network requiring the coexistence of multiple functional states, and thereby facilitating transitions to the most suitable spatio-temporal conformation for a given biological event. At present, the conformational equilibria of Ras have been explored in bulk solution, necessitating the explicit role of membranes to be addressed.

4. To study the dynamic interaction of farnesylated Ras isoforms with escort proteins, especially in the presence of heterogeneous membranes of different composition.

5. Adaptation of proteins to external stimulus (chemical and/or physical) is of utmost importance in maintaining the cycle of life. Responding to physical stimulus correlates to the mechanosensitivity of the respective proteins. To this end, Ras proteins have been identified as an early link between mechanotransduction and proceeding signalling events. This aspect of work seeks to study the effects of hydrostatic pressure on membrane-bound Ras proteins. To explore the role of membrane heterogeneities in regulating this effect. To elucidate the type of forces involved or governing Ras–membrane interactions that may be readily extrapolated to other lipidated proteins, taking into account the respective protein's eccentricities.

II

EXPERIMENTAL PROCEDURES & BIOPHYSICAL METHODS*

* In the following chapter, detailed theoretical backgrounds of a few biophysical methods are discussed to facilitate the understanding of the subsequently presented results.

2.1 Materials

2.1.1 Phospholipids and Reagents

PRODUCTS	MANUFACTURER
DPPC	Avanti Polar Lipids, USA
DPPG	Avanti Polar Lipids, USA
DPPC	Avanti Polar Lipids, USA
DOPC	Avanti Polar Lipids, USA
Cholesterol	Avanti Polar Lipids, USA
D_2O	Merck, Germany
Tris	Sigma – Aldrich, Germany
NaCl	Sigma – Aldrich, Germany
DCl	Sigma – Aldrich, Germany
Chloroform	Merck, Germany
$MgCl_2$	Merck, Germany
***N*-Rh DHPE**	Invitrogen, Germany
Dansyl amide	Sigma – Aldrich, Germany
NaOD	Sigma – Aldrich, Germany
N-Ras Far	AG H. Waldman, Max Planck Institute for Molecular Physiology, Dortmund, Germany
N-Ras HD Far	AG H. Waldman, Max Planck Institute for Molecular Physiology, Dortmund, Germany
K-Ras Far	AG H. Waldman, Max Planck Institute for Molecular Physiology, Dortmund, Germany
PDEδ	AG H. Waldman, Max Planck Institute for Molecular Physiology, Dortmund, Germany
Polycarbonate membranes	Avanti Polar Lipids, USA
Syringes	VWR-Hamilton, Germany

Instruments and Software

NAME	MANUFACTURER
Magna 550 IR Spectrometer	Thermo Fisher, USA
Nicolet IR Spectrometer	Thermo Fisher, USA
Vertex 70 IR Spectrometer	Bruker, Germany
A511 External Reflection Unit	Bruker, Germany
Langmuir trough	Prof. H. Reigler, Potsdam, Germany
ATR-FTIR cell	Pike Technologies, USA
ZnSe polarizer	Pike Technologies, USA
ISSK2 Fluorometer	ISS, USA
Origin 7.0	Origin Labs, USA
OPUS	Bruker, Germany
GRAMS 8.0	Thermo Fisher, USA

High pressure FTIR cell	Diamond Optics, USA
High pressure fluorescence cell	ISS, USA
SX. 18MV Stopped-flow apparatus	Applied Photophysics, USA
Chem Draw	Perkin Elmer, USA

2.1.2 Protein Synthesis

The synthesis of all the Ras proteins and their fluorescent analogues has been carried out by the work group of Prof. Dr. H. Waldmann at the Max Planck Institute of Molecular Physiology, Dortmund, Germany. The main synthesis steps of the Ras protein employed for this work have been briefly discussed below. For the active form of Ras proteins, a non-hydroysable GTP analogue (GppNHp) was used. Throughout this document, the active state of Ras refers to the protein complexed with this analogue, unless stated otherwise.

(A) N-Ras Far and HD/Far: Maleimide Ligation Strategy

The synthesis of posttranslationally modified N-Ras proteins was accomplished using the maleimidocaproyl (MIC)-controlled ligation (Scheme 1).[58] First, the N-Ras protein was expressed in a truncated form in *E.coli* with a free C-terminal cysteine which provides a reactive thiol group for the ligation. The cysteine residue is highly exposed to the solvent owing to a high flexibility of the C-terminus, thus making the ligation reaction fast and selective. The truncated protein was then ligated to the C-terminal prenylated peptide sequence, generated via the Fmoc chemistry under argon atmosphere. Purification of the ligated protein was accomplished with Triton X-114 saturated solution that utilises the additional hydrophobicity imparted by the lipid groups. In this synthesis, the *labile acyl thioester* of the palmitoyl lipid group was replaced by a *stable hexadecyl thioether* to prevent spontaneous decomposition of the palmitate group during the course of all measurements.

[58] Brunsveld, L., Kuhlmann, J., Alexandrov, K., Wittinghofer, A., Goody, R.S., and Waldmann, H. **(2006a)**. Lipidated ras and rab peptides and proteins–synthesis, structure, and function. *Angew. Chem. Int. Ed. 45*, 6622–6646, Brunsveld, L., Kuhlmann, J., and Waldmann, H. **(2006b)**. Synthesis of palmitoylated Ras-peptides and -proteins. *Methods 40*, 151–165, Kuhn, K., Owen, D.J., Bader, B., Wittinghofer, A., Kuhlmann, J., and Waldmann, H. **(2001)**. Synthesis of functional Ras lipoproteins and fluorescent derivatives. *J. Am. Chem. Soc. 123*, 1023–1035, Nagele, E., Schelhaas, M., Kuder, N., and Waldmann, H. **(1998)**. Chemoenzymatic synthesis of N-Ras lipopeptides. *J. Am. Chem. Soc. 120*, 6889–6902, Reents, R., Wagner, M., Kuhlmann, J., and Waldmann, H. **(2004).** Synthesis and application of fluorescence-labeled Ras-proteins for live-cell imaging. *Angew. Chem. Int. Ed. 43*, 2711–2714.

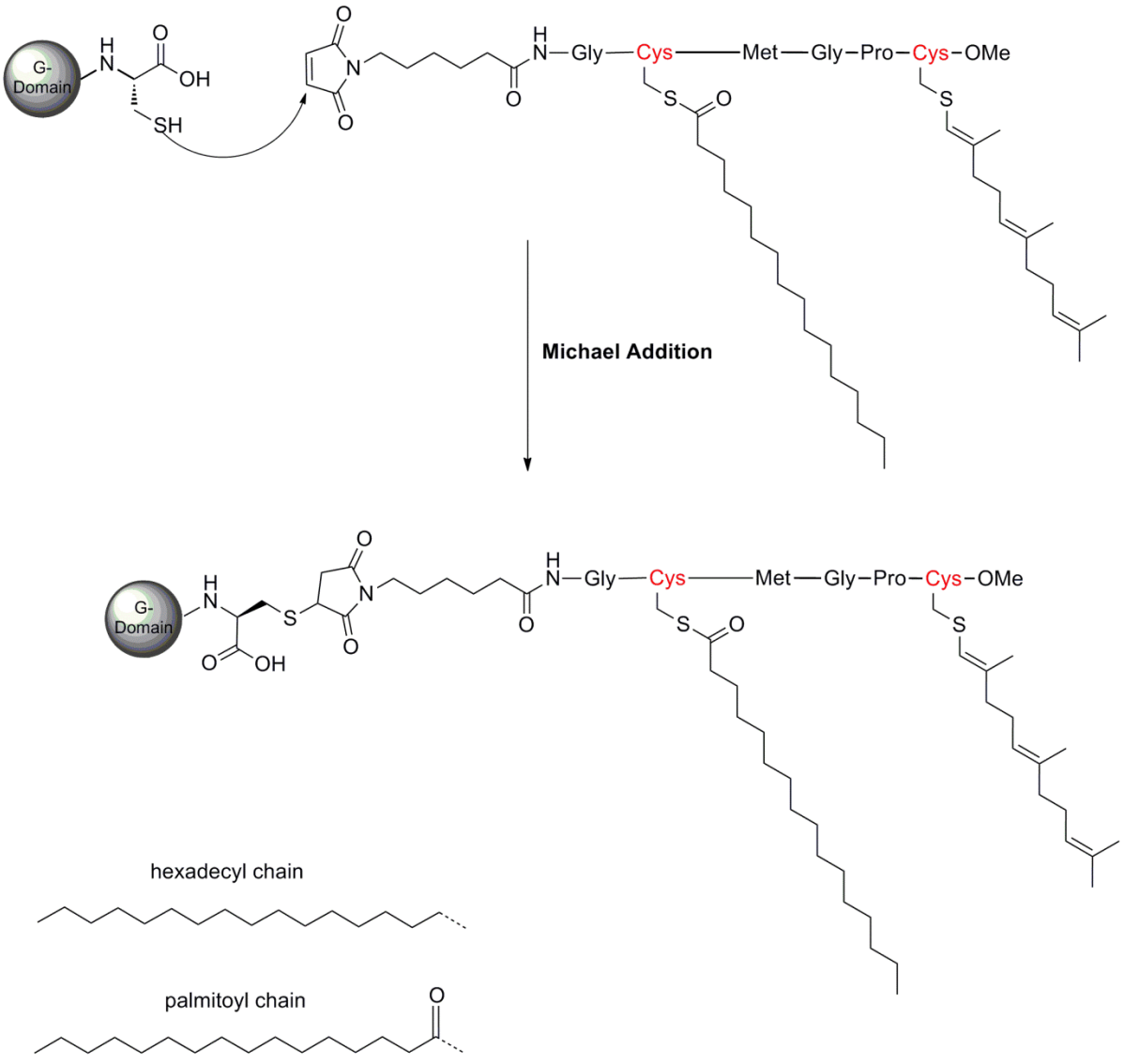

Scheme 2.1: Maleimidocaproyl (MIC) ligation for the synthesis of N-Ras methyl ester. The structural core of N-Ras (G-Domain) expressed in *E.coli* was ligated to the synthesised MIC-peptide sequence (generated via the Fmoc chemistry). For the dually lipidated N-Ras protein, palmitoyl (Pal) group was replaced by a Hexadecyl (HD) group in the peptide sequence, prior to ligation. For the monofarnesylated N-Ras protein, the cysteine at position 182 was attached to S*t*Bu group, prior to ligation. This scheme has been generated in Chem Draw.

(B) K-Ra4B Far: Combination of Expressed Protein Ligation (EPL) and Lipopeptide Synthesis

The approach of EPL connects the lipidated peptide with an N-terminal cysteine to the C-terminus of a thioester-tagged K-Ras protein through a native peptide bond (scheme 2).[59] Since the K-Ras4B peptide does not contain an cysteine at the N-terminus, an additional cysteine was inserted to yield the peptide with the amino acid sequence: H-Cys(S*t*Bu)-Lys_6-Ser-Lys-Thr-Lys-Cys(Far)-OMe. The truncated K-Ras4B protein core thioester was generated via expression in Impact™ [intein - mediated purification with an affinity chitin binding tag] vector pTWIN2. This expression vector allowed the single column isolation of protein thioesters utilising the thiol-induced self-cleavage (thiolysis) activity of the various inteins. First, the target *gene* (in this case, the DNA sequence encoding for the first 174 amino acids of the human K-Ras4B) was cloned into the expression vector at the N-terminus of a modified intein. The C-terminus of the intein was fused to the chitin binding domain (CBD) which enabled the affinity purification of the expressed protein. *E.coli* Bl21(DE3) cells were transformed with the Ras-Intein-CBD plasmid, and protein expression was induced. Finally, after the induction of thiolysis, K-Ras4B MESNA was eluted, and rest of the cell proteins were washed out. As the last step, the ligation between the protein thioester and the lipidated peptide (generated via the Fmoc strategy) yielded the K-Ras4B protein bearing an additional cysteine between Gly^{174} and Lys^{175}. The lipidated protein was purified by cation-exchange chromatography.

[59] Chen, Y.X., Koch, S., Uhlenbrock, K., Weise, K., Das, D., Gremer, L., Brunsveld, L., Wittinghofer, A., Winter, R., Triola, G.*, et al.* **(2010).** Synthesis of the Rheb and K-Ras4B GTPases. *Angew. Chem. Int. Ed. 49*, 6090–6095.

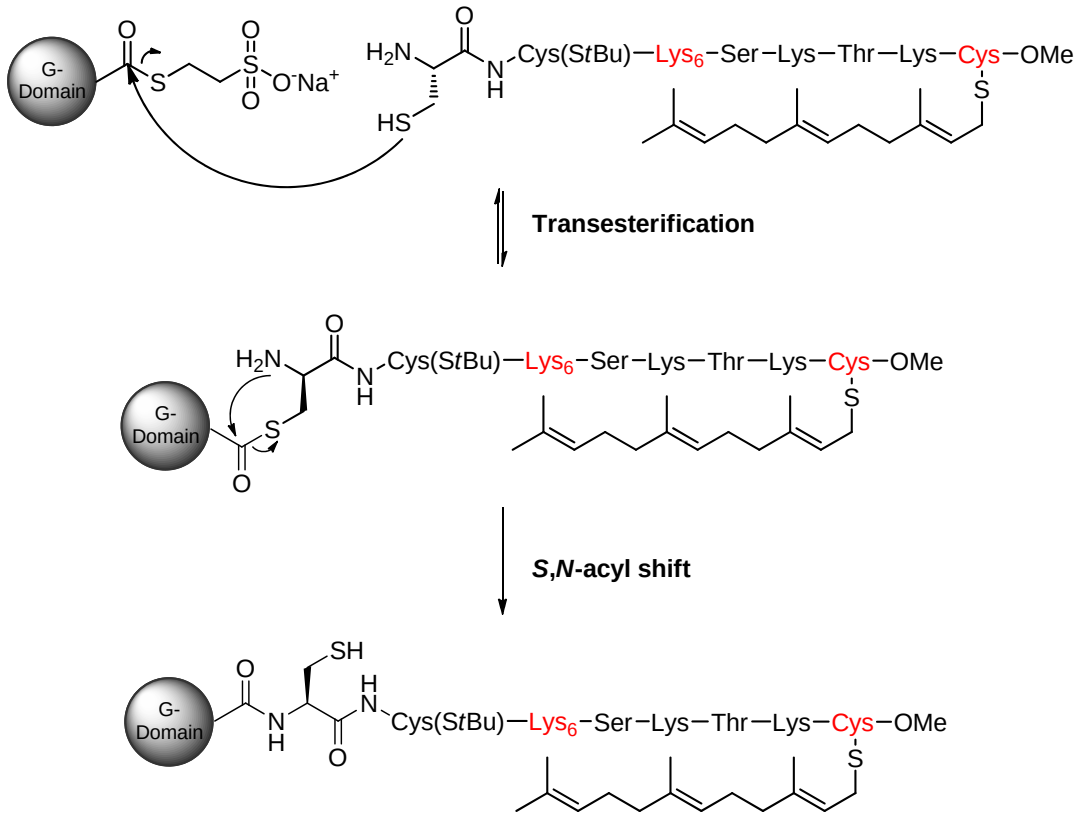

Scheme 2.2: Synthesis of the S-farnesylated K-Ras4B methyl ester. The structural core of K-Ras4B (G-Domain) was expressed in IMPACT vector pTWIN2 and eluted as MESNA thioester (shown on the left). The MESNA-thioester was ligated to the synthesised peptide sequence (generated via the Fmoc chemistry) to yield a native peptide bond. This scheme has been generated in Chem Draw.

BODIPY labelling of the protein core (at the N-terminus of the protein) in both cases was accomplished (before the ligation with lipidated peptide) by mixing with a tenfold excess of BODIPY-NHS. The mixture was shaken for 2 h at 4 ˚C under argon. The labelled protein was purified using a Hi-Trap desalting column and concentrated. The fluorescence/protein ratio was determined by measuring the absorbance at 504 nm and at 280 nm, respectively. Similarly, the nucleotide exchange was performed according to a well established protocol[60] and briefly as follows: unligated proteins were mixed with twofold molar excess of GppNHp in 20 mM Tris-HCl, 100 mM $(NH_4)_2SO_4$, 0.1 mM $ZnC1_2$ (pH 7.6), and alkaline phosphatase

[60] Lenzen, C., Cool, R.H., Prinz, H., Kuhlmann, J., and Wittinghofer, A. **(1998)**. Kinetic analysis by fluorescence of the interaction between Ras and the catalytic domain of the guanine nucleotide exchange factor Cdc25Mm. *Biochemistry 37*, 7420–7430, Lenzen, C., Cool, R.H., and Wittinghofer, A. **(1995)**. Analysis of intrinsic and CDC25-stimulated guanine nucleotide exchange of p21ras-nucleotide complexes by fluorescence measurements. *Methods Enzymol. 255*, 95–109.

at a concentration of 5 units/mg of Ras. Following this, the buffer was exchanged for 20 mM Tris, 5 mM $MgCl_2$ (pH 7.5) using a Hi-Trap desalting column. The sample were analysed by reverse phase HPLC using 100 mM tetrabutylammonium bromide, 100 mM K_2PO_4, and 0.2 mM NaN_3 (pH 6.4) in 7.5% acetonitrile.

All semi synthetic Ras lipoproteins generated were tested for their biological activity, based on the ability of the generated constitutively activated RasG12V mutants to induce differentiation of PC12 cells after microinjection. This was indicative of the functional Ras signalling pathways.[59]

2.1.3 Preparation of Large Unilamellar Vesicles (LUVs)

Stock solutions (10 mg mL^{-1}) of lipids: DOPC, DOPG, DPPC, and Chol in chloroform and DPPG in 3:1 chloroform/methanol solution were prepared and mixed to obtain the desired composition. For the neutral lipid raft-like mixture—DOPC/DPPC/Chol 50:25:50 (molar ratio) and for the anionic lipid raft-like mixture—DOPC/DOPG/DPPC/DPPG/Chol 20:5:45:5:25 (molar ratio). The majority of the chloroform was evaporated with a nitrogen stream; all remaining solvent was subsequently removed by drying under vacuum overnight. The dried lipid mixture was hydrated with 20 mM Tris, 5 mM $MgCl_2$ (for the neutral raft-like mixture) or 7 mM (for the anionic raft-like mixture) in D_2O and pD 7.4. The hydrated lipid mixture was then vortexed, kept in a water bath at 65 ˚C for 15 min, and sonicated for 10 min. After five freeze–thaw–vortex cycles and brief sonication, large multilamellar vesicles were formed and transformed to large unilamellar vesicles of a homogeneous size by use of an extruder with polycarbonate membranes of 100 nm pore size at 65 ˚C. For LUVs composed of pure DOPC lipids, the extrusion was performed at room temperature as the main-chain melting transition temperature is at -18 ˚C, implying that at room temperature the lipids are in the fluid phase. Unless stated otherwise, all the measurements were performed using LUVs (100 nm) of the respective lipid composition.

2.14. Preparation of Solid Supported Lipid Bilayer

Solid supported lipid bilayers were prepared in the ATR flow-through cell with a trapezoidal Ge-crystal (80×10×4 mm^3; angle of incidence 45°). A freshly prepared solution of large

unilamellar vesicles of the desired composition was injected into the ATR flow-cell, which was heated to 60 ˚C. Direct spreading of the sonicated vesicles produced high quality bilayers, especially if the buffer contained ≥ 1 mM of divalent cations, e.g. $MgCl_2$, as used in this study.[61] After adsorption overnight and cooling to 25 ˚C, the membrane was washed with buffer for 1-2 hrs to remove any loosely bound lipid vesicles.

2.1.5 Preparation of Lipid Monolayers

Monolayers composed of DOPC/DPPC/Chol (in the molar ratio of 25:50:25) and DOPC/DOPG/DPPC/DPPG/Chol (in the molar ratio of 20:5:45:5:25) were formed by directly spreading the lipid solution (1 mM) in a mixture of chloroform and methanol on the subphase. Protein adsorption measurements were performed by injection of a concentrated protein solution into the subphase, beneath the monolayers, to yield the required concentration of proteins, needed for the respective experiments.

2.2 Infrared Methods

2.2.1 Fourier Transform Infrared Spectroscopy (FTIR): Transmission Mode

Infrared spectroscopy has a long tradition in providing important contributions to the understanding of proteins.[62-63] Given the vast number of proteins that still await characterisation, IR spectroscopy provides a relatively fast (high time resolution of < μs; short measuring times) and inexpensive (with respect to both the instrument costs and materials required; typically 10-100 μg) means of characterising the protein structure and conformation in its native, aggregated, and denatured state. IR light is absorbed by a molecular vibration when the frequencies of light and the respective vibration coincide. Since, the frequency of vibration and the probability of absorption depend on the strength and polarity of the vibrating bond, they are strongly influenced by inter- and intramolecular environmental effects. As a direct consequence, the effect of environment, e.g. membranes

[61] Papahadjopoulos, D., Vail, W.J., Pangborn, W.A., and Poste, G. **(1976)**. Studies on membrane fusion. II. Induction of fusion in pure phospholipid membranes by calcium ions and other divalent metals. *Biochim. Biophys. Acta. 448*, 265–283.
[62] Timasheff, S.N., Susi, H., and Stevens, L. **(1967)**. Infrared spectra and protein conformations in aqueous solutions. II. Survey of globular proteins. *J. Biol. Chem. 242*, 5467–5473.
[63] Byler, D.M., and Susi, H. **(1986)**. Examination of the Secondary Structure of Proteins by Deconvolved FTIR Spectra. *Biopolymers 25*, 469–487.

on the protein's vibrational frequency is a telltale of how proteins interact with them, and has been used extensively in the present work.

Instrumentation and spectra collection

Time- and temperature-dependent IR measurements were performed on the Nicolet 5700 FTIR spectrometer equipped with a liquid nitrogen cooled MCT (HgCdTe) detector and an IR cell with CaF_2 windows, separated by 50 μm mylar spacers. The spectrometer was purged continuously with dry air to remove water vapour. Typically, FTIR spectra of 128 scans were collected with a resolution of 2 cm^{-1}, apodised with a Happ–Genzel function, and corresponding processing (discussed below) was performed using the GRAMS software. In the studies with proteins under investigation, a concentration (c) of 0.5 wt % was chosen and the protein was lyophilised for 2 h to remove H_2O. For the studies dealing with protein-lipid interactions, a freshly extruded lipid mixture of the required composition was mixed, to give a protein to lipid molar ratio of 1:100. The mixture was shaken for about an hour, prior to the first spectrum collection.

The pressure-dependent FTIR spectra were recorded on the Magna IR 550 spectrometer equipped with a liquid nitrogen cooled MCT (HgCdTe) detector. The infrared light was focussed by a spectral bench onto the pin hole of a diamond anvil cell (Fig. 2.1) with type IIa diamonds; type IIa diamond has no detectable quantity of nitrogen. Powdered barium sulphate, as the calibrant, was placed in the hole of the steel gasket of the diamond anvil cell and changes in pressure were quantified by the shift of the barium sulphate stretching vibration at 983 cm^{-1}.[64]

[64] Wong, P.T.T. and Moffat, D.J. **(1989)**. A new internal pressure calibrant fro high-pressure infrared spectroscopy in aqueous systems. *App. Spectrosc. 43*, 1279–1281.

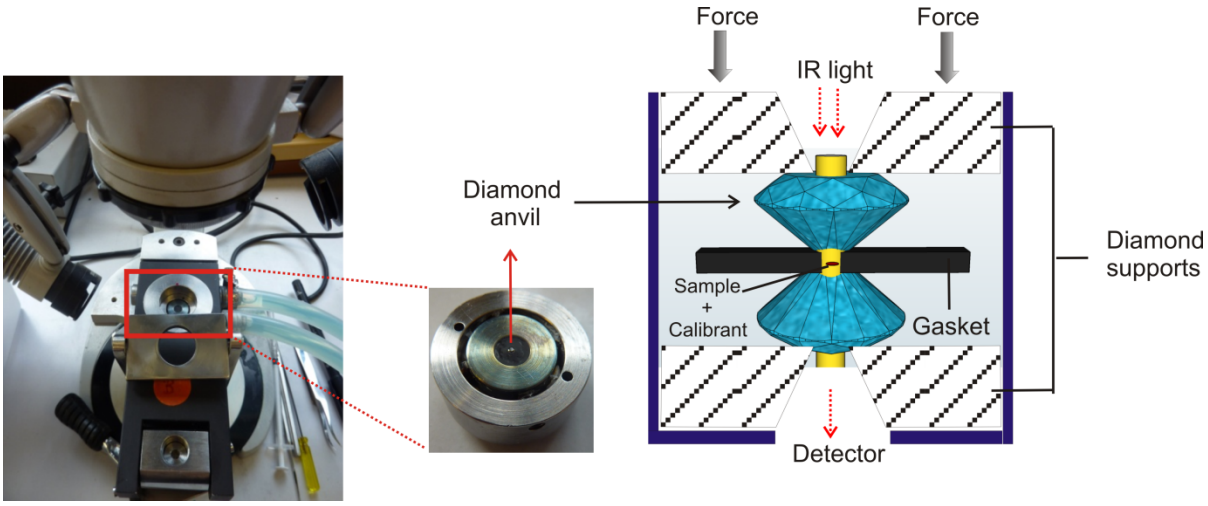

Figure 2.1: Pictorial representation of the high pressure diamond anvil cell. Shown on the left hand side is the HP-DAC unit. A single diamond anvil is highlighted in red. On the right hand, a schematic representation of the setup can be seen with the respective designations.

The basic operating principle of a diamond anvil cell is the application of a moderate force on a small area, thus generating high pressures. Specific details on the design and use of the high pressure diamond anvil cells can be found elsewhere.[65-66] Each spectrum was obtained by co-adding 256 scans at a spectral resolution of 2 cm^{-1}, apodised with a Happ–Genzel function, and the corresponding processing was performed using the GRAMS software. An external, circulating water thermostat controlled the required temperature with an accuracy of ± 0.1 °C. In the studies with proteins as the subject under investigation, a concentration (c) of 3 wt % was chosen and lyophilised for 2 h to remove H_2O. For the studies dealing with protein-lipid interactions, a freshly extruded lipid mixture of the required composition was mixed to give a protein to lipid molar ratio of 1:100. The protein-lipid mixture was shaken for about 1 h, prior to the first spectrum collection.

[65] Dunstan, D.J., and Spain, I.L. **(1989)**. The Technology of Diamond Anvil High-Pressure Cells .1. Principles, Design and Construction. *J. Phys. E-Sci. Inst. 22*, 913–923.
[66] Spain, I.L., and Dunstan, D.J. **(1989)**.The Technology of Diamond Anvil High-Pressure Cells .2. Operation and Use. . *J. Phys. E-Sci. Inst. 22*, 923–933.

Determination of secondary structure of proteins from infrared spectroscopy: Data processing

Following the spectra collection, few processing steps were employed, such as background (buffer) subtraction and spectral baseline correction in the required frequency range of interest [for lipids: 2810-3050 cm^{-1} and for proteins: 1600-1700 cm^{-1} known as the amide-I (in ^1H_2O) or amide-I' (in ^2H_2O)]. The spectra were normalised by setting the area between 1700 and 1600 cm^{-1} to 1 to allow for a quantitative analysis (via curve-fitting, the most common method to resolve overlapping bands in the amide band region of proteins)[63] of the secondary structure of proteins, in the absence and presence of membranes. Second derivative and Fourier self-deconvolution (FSD)[67] manipulations were applied to the normalised spectra to identify the overlapping components of the amide-I′ band region. The normalised FTIR spectra were decomposed using a Levenberg-Marquardt curve-fitting routine[68] with bands of Voigt line shape. All the raw spectra were fitted with a similar set of peaks and parameters. In ambiguous cases (such as the overlap of unordered and α-helical band regions), information from NMR and X-ray diffraction of proteins was taken into account. The band integrals determined the fraction of position-dependently assigned structure, regarding the overall amide integral, assuming similar transition dipole moments for the different conformers. The band positions were assigned to the secondary structures according to Table 9.1. Details on the curve-fitting procedure, applied models and equations can be found in the Appendix Section 9.1.

2.2.2 Polarized Attenuated Total Reflection Fourier Transform Infrared Spectroscopy (Polarized ATR-FTIR)

ATR-FTIR is one of the most powerful techniques to record the infrared spectrum of biomaterials under physiological conditions. More specifically, ATR is an accessory of transmission IR spectrometers that greatly enhances the surface sensitivity. The most distinct advantages of ATR-FTIR over traditional IR spectroscopy are (a) limited path length of the light into the sample, as ATR works on the principle of total internal reflection (discussed in detail below) and (b) a great versatility with respect to conducting *in situ*

[67] Griffiths, P.R., and Pariente, G.L. **(1986)**. Introduction to Spectral Deconvolution. *Trends in Anal. Chem. 5*, 209–215.
[68] Marquardt, D.W. **(1963)**. An Algorithm for Least-Squares Estimation of Nonlinear Parameters. *J. Soc. Indust. and Appl. Math. 11*, 431–441.

experiments, which in most cases are precluded from the normal transmission IR setup. Finally, in conjunction with a high quality polarizer, ATR-FTIR provides unprecedented information about the orientation of lipids, proteins, and membrane-bound proteins.

Instrumentation, spectra collection and processing

Polarized ATR-FTIR spectra were recorded using the Nicolet 6700 infrared spectrometer attached with a wire grid infrared automated ZnSe polarizer and a liquid jacketed ATR flow-through cell with a trapezoidal Ge-crystal. Spectra of 256-512 scans were collected with a spectral resolution of 2 cm^{-1} at both 0° and 90° polarization angles. The ATR flow-cell was maintained at 25 ˚C and a background and buffer spectrum at both polarizations was acquired before the measurement. After establishing a stable lipid bilayer(s) on the Ge-crystal, the protein solutions (c = 4 μM) were injected into the ATR cell. Polarized spectra were collected up to a maximum of 33 h, and obtained after background subtraction, one level of zero filling, and Blackman–Harris three-term apodisation. The spectrum processing was the same as mentioned above. The dichroic spectra (details on the calculations are given in the next section) were smoothened by a nine-point Savitzky–Golay function, where needed.

Theoretical model

A schematic representation of the ATR set-up is shown in Figure 2.2. The infrared beam is directed to an internal reflection element (IRE; phase "a") of a high optical density or refractive index (n_1) in which it propagates, and undergoes total internal reflection at the interface with an adjacent medium; phase "b" of a lower refractive index (n_2).[69] Two planes of polarization indicated by E^{II} (polarization parallel to the incident plane) and $E^{\perp}$ (polarization perpendicular to the incident plane) are generated by using a high quality polarizer.

[69] Born, M., and Wolf, E. **(1965)**. Principles of optics; electromagnetic theory of propagation, interference and diffraction of light, 3d Rev. Ed. (Oxford, New York, Pergamon Press).

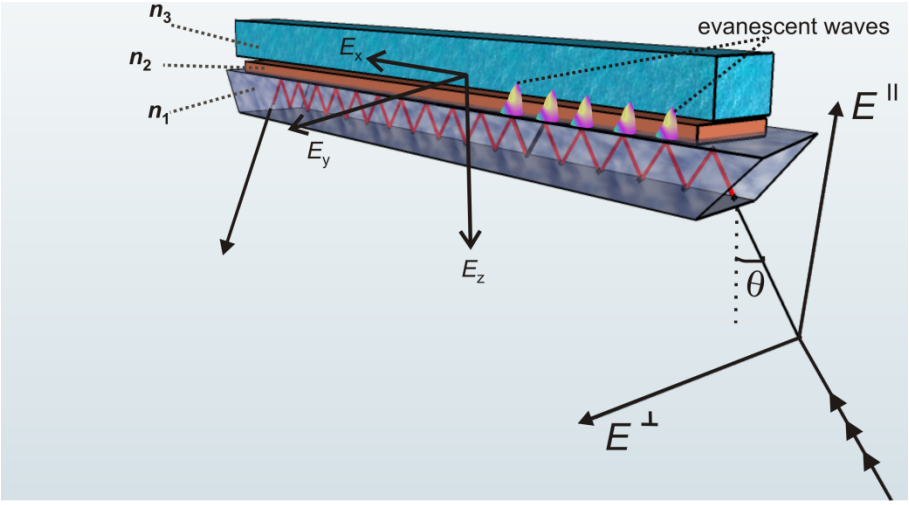

Figure 2.2: Schematic representation of the internal reflection element (IRE) and the light pathway. The Cartesian components of the electric field are shown along the *x*, *y* and *z* axes. Two possible planes of polarization are indicated by E^{II} (polarization parallel to the incidence plane) and $E^{\perp}$ (polarization perpendicular to the incident plane). The incident beam makes an angle, θ, with respect to the normal of the IRE surface. The edges of the IRE are beveled to allow the incident beam to penetrate the IRE (shown in red), through a surface that is perpendicular to its propagation. The electromagnetic disturbance in the rarer medium beyond the IRE creates the evanescent waves. The three distinct phases are denoted by the subscripted refractive indices.

The prerequisite for *total internal reflection* is that the angle of incidence (θ) should be higher than the critical angle (θ_c), which in turn is related to the refractive index of the two phases by Eq. (1).

$$\theta_c = \arcsin\left(\frac{n_2}{n_1}\right) \tag{1}$$

In the present case, θ_c was 21˚ with $n_1 = 4$ (Ge), $n_2 = 1.43/1.45$ (lipid membrane/proteo-lipid), and $\theta_i = 45$˚. Albeit the term "total", substances in phase "b" do absorb some radiation which would otherwise be reflected totally back into the phase "a". This results in *less than total or "attenuated" total internal reflection*. Superposition of the incident and the reflected infrared beam generates a standing wave within the IRE normal to the reflecting surface, given by Eq. (2).

$$E = 2\cos\left(\frac{2\pi z}{\lambda_e} + \phi\right) \tag{2}$$

where, z is the coordinate on an axis normal to the IRE surface; $\lambda_e = \lambda/(n_1\cos\theta)$; and $\varnothing$ is the phase shift.

The electromagnetic disturbance in the rarer medium beyond the IRE creates an evanescent wave with its electric field amplitude decreasing exponentially with the distance from the interface according to Eq. (3).[70-73]

In order to absorb the radiation, the substances in phase "b" must interact with the evanescent wave:

$$E = E_o \cdot \mathrm{e}^{-z/d_\mathrm{p}} \tag{3}$$

where,

E_o and E are the time averaged electric field intensity in the rarer medium and at a distance, z from the interface, respectively, and d_p is the penetration depth of the evanescent filed in the rarer medium of the form:

$$d_\mathrm{p} = \frac{2\pi n_1}{\lambda}\sqrt{\left(\sin^2\theta - n_{21}^2\right)}. \tag{4}$$

For any IR transition, the absorbance is proportional to the effective penetration depth, d_e, given by Eq. (5).

$$d_\mathrm{e} = \frac{n_{21}}{\cos\theta}\int_0^\infty E^2 \mathrm{d}z = \frac{n_{21}E_0^2 d_\mathrm{p}}{2\cos\theta} \tag{5}$$

According to Eq. (5), d_e is related to the depth of penetration, d_p, and includes the strength of interaction with the sample. *The latter generates a complex dependence of the effective penetration depth (for both parallel and perpendicular polarizations) with the sample*

[70] Harrick, N.J. **(1967)**. *Internal Reflection Spectroscopy*. Interscience, New York.
[71] Fahrenfort, J. **(1961)**. Attenuated Total Reflection - a New Principle for the Production of Useful Infra-Red Reflection Spectra of Organic Compounds. *Spect. Acta. 17*, 698–712.
[72] Goos, F., and Hanchen, H. **(1947)**. Ein Neuer Und Fundamentaler Versuch Zur Totalreflexion. *Annal. Der Phys. 1*, 333–346.
[73] Carniglia,C.K, and Mandel, L. **(1971)**. Quantization of Evanescent Electromagnetic Waves. *Phys. Rev. D. 3*, 280–290.

thickness. This is crucial in obtaining the orientational information from ATR-FTIR spectroscopy, as described in detail below.

Determination of Molecular Orientations in ATR-FTIR Spectroscopy

In polarized ATR-FTIR spectroscopy, all the orientational information is contained within the dichroic ratio (R^{ATR}), as defined by Eq. (6):

$$R^{ATR} = \frac{A^{II}}{A^{\perp}}, \tag{6}$$

where, A^{II} and $A^{\perp}$ refer to the integrated absorbance of an IR band measured with parallel and perpendicular polarized light, respectively. The dichroic ratio is further related to the orientational order parameter (S) by Eq. (7):

$$R^{ATR} = \frac{E_x^2}{E_y^2} + \frac{E_z^2\left[1 + S\left(3\cos^2\alpha - 1\right)\right]}{E_y^2\left[1 - 0.5S\left(3\cos^2\alpha - 1\right)\right]}, \tag{7}$$

where, E_x^2, E_y^2, and E_z^2 are the time-averaged square electric field amplitudes of the evanescent wave in the film at the Ge/film interface, and α is the angle between the transition dipole moment and the main axis of symmetry (molecular director) of the structural element under consideration, e.g. the long axis of a helix (depicted in Fig. 2.3). For the thin-film approximation (i.e. films much thinner than the penetration depth of the evanescent wave), the electric field values are described by Eqs. (8) – (10), whereas Eqs. (11) – (13) correspond to the field values for the thick-film model (i.e. films much thicker than the penetration depth of the evanescent wave).[74]

$$E_x = \frac{2\cos\theta\sqrt{\sin^2\theta - n_{31}^2}}{\left(1 - n_{31}^2\right)^{1/2}\sqrt{\left(1 + n_{31}^2\right)\sin^2\theta - n_{31}^2}} \tag{8}$$

$$E_z = \frac{2 \cdot n_{32}^2\cos\theta\sin\theta}{\left(1 - n_{31}^2\right)^{1/2}\sqrt{\left(1 + n_{31}^2\right)\sin^2\theta - n_{31}^2}} \tag{9}$$

[74] Harrick, N.J. **(1971)**. Principles of Internal Reflection Spectroscopy. *Appl. Spect. 25*, 142–170.

$$E_y = \frac{2\cos\theta}{\left(1-n_{31}^2\right)^{1/2}} \tag{10}$$

$$E_x = \frac{2\cos\theta\sqrt{\sin^2\theta - n_{21}^2}}{\left(1-n_{21}^2\right)^{1/2}\sqrt{\left(1+n_{21}^2\right)\sin^2\theta - n_{21}^2}} \tag{11}$$

$$E_z = \frac{2\cos\theta\sin\theta}{\left(1-n_{21}^2\right)^{1/2}\sqrt{\left(1+n_{21}^2\right)\sin^2\theta - n_{21}^2}} \tag{12}$$

$$E_y = \frac{2\cos\theta}{\left(1-n_{21}^2\right)^{1/2}} \tag{13}$$

where $n_{31} = n_3 / n_1, n_{21} = n_2 / n_1,\ n_{32} = n_3 / n_2$, and θ is the angle of incidence. In the current study the refractive index values used were $n_1 = 4.0$ (Ge), $n_2 = 1.43–1.45$ (lipids and proteins), and $n_3 = 1.32$ (D_2O), with $\theta = 45º$.

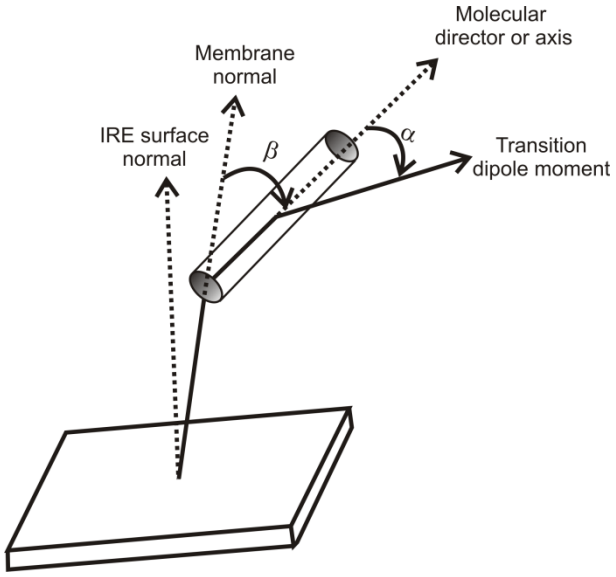

Figure 2.3: Set of nested axially symmetric distributions. The membrane normal is distributed around the IRE surface normal, the molecular director is distributed around the membrane normal (angle, β) and the transition dipole moment is distributed about the molecular director (angle, α).

The order parameter of a molecule can be derived from both the thin- and thick-film approximations from the measured dichroic ratios using Eq. (7). The order parameter, *S*, is a time- and space-averaged function of the angle β between the molecular director and the *z*-axis (the membrane normal or the IRE surface normal; Fig. 2.3) given by:

$$S = 3\langle \cos^2 \beta \rangle - \frac{1}{2} \tag{14}$$

The expressions given in Eq. (7) and (14) are only valid for distributions that are axially symmetric around the *z*-axis. In most cases, it is assumed that molecules exhibit an axially symmetric distribution in a bilayer.[75] For cases dealing with non-axial symmetry issues, explicit details on the derivation of the corresponding expression can be found elsewhere.[76] From Eq. (14), limiting values of *S* (i.e. -0.5 and +1.0) correspond to a fixed orientation of the molecular director perpendicular and parallel to the IRE surface/membrane normal, respectively.

To obtain β-angle values for a molecule (using Eq. (7) and (14)), knowledge of the angle α (between the transition dipole moment and the main axis of symmetry) is required. In this regard, angle α value ranges from 27˚– 39˚ (reviewed in ref. 75) for the α-helix, and implies alignment of the transition dipole moment along the helix long axis. In case of lipids (specifically the CH_2 stretching vibrations), the angle α is taken as 90˚, as the transition dipole of the CH stretching vibration is perpendicular to the acyl chain axis of the lipids.[77] For a special case of $S = 0$, the orientation could be interpreted by either a unique "magic" angle ($\beta = 54.7$˚) or an isotropic distribution, if all angles are equally probable.

In addition to the quantitative order parameter (*S*) and the orientational angle (β), qualitative information on the orientation of molecular constituents can be obtained from the dichroic spectra. For this, the dichroic spectra were obtained by subtracting the perpendicular polarized spectra ($A^{\perp}$) from the parallel polarized spectra ($A^{\parallel}$) by use of

[75] Tatulian, S.A., Jones, L.R., Reddy, L.G., Stokes, D.L., and Tamm, L.K. **(1995)**. Secondary structure and orientation of phospholamban reconstituted in supported bilayers from polarized attenuated total reflection FTIR spectroscopy. *Biochemistry 34*, 4448–4456.
[76] Marsh, D. **(1997)**. Dichroic ratios in polarized Fourier transform infrared for nonaxial symmetry of beta-sheet structures. *Biophys. J. 72*, 2710–2718.
[77] Tamm, L.K., and Tatulian, S.A. **(1997)**. Infrared spectroscopy of proteins and peptides in lipid bilayers. *Q. Rev. Biophys. 30*, 365–429.

Eq. (15). In the absence of any preferred orientation, a straight horizontal line is expected. An upward deviation on the dichroism spectrum indicates a transition dipole moment nearly perpendicular to the membrane plane. Conversely, a downward deviation indicates a preferred alignment of the dipole in the membrane plane. Eq. (7) and (14) have successfully yielded orientations of lipids and purely helical or beta proteins, but have failed to give reasonable results for protein having predominant amounts of both the mentioned secondary structure elements, e.g. the Ras protein. In such circumstances, the qualitative information from the dichroic spectra of such complex proteins molecules gives critical insights into their preferred orientations.

The scaling coefficient required to compute the dichroic spectra, is the dichroic ratio for an isotropic sample (R_{iso}^{ATR}), and is given by Eq. (16). It is the dichroic ratio of a transition dipole that is either spatially disordered or oriented at the magic angle. It takes into account the differences in the relative power of the evanescent field for each polarization and the film thickness.

$$\Delta A = A^{\text{II}} - R_{iso}^{ATR} \cdot A^{\perp} \tag{15}$$

$$R_{iso}^{ATR} = \frac{E_x^2 + E_z^2}{E_y^2} \tag{16}$$

Using the mentioned values of refractive indices and θ, R_{iso}^{ATR} values of 1.712 and 2.0 were obtained for the thin- and thick-films approximations, respectively. This indicates the need to use appropriate models. The difference in the R^{ATR}_{iso} values for the different approximation is due to a remarkable dependence of the electric field amplitude along the *z*-axis (E_z) on n_2, n_3 and the film thickness (Table 2.1).

Table 2.1: Variation of the electric field amplitudes along the z-axis with film thickness. The electric field amplitudes given in the table have been calculated by use of Eqs. (8) – (13) and values of $n_1 = 4.0$ (Ge), $n_2 = 1.43$-1.45 (lipids and proteins), and $n_3 = 1.32$ (D_2O) with $\theta = 45°$.

Electric field amplitudes	Thick-film	Thin-film
E_x^2	1.957	1.969
E_y^2	2.293	2.247
E_z^2	2.629	1.878

Recent studies have revealed that the measured dichroic ratios including $R_{\text{iso}}^{\text{ATR}}$ depend on the amount of sample required to make a film and hence on film thickness.[78] This calls into question, the appropriateness of the thick- and thin-film hypothesis for each sample preparation, and also suggests that there might be an intermediate film thickness. Furthermore, the absorbing substances may be dispersed throughout the phase "b", or distributed at the boundary between the two phases (either sparsely as individual molecules, or layered as a continuous film). For each case, only approximate theories describing the extent to which the absorbing substance perturbs the field are described in detail elsewhere.[79] It seems very likely that the magnitude of this perturbation will depend on the dimension of the absorbing substance compared to the wavelength of the radiation, and on the inhomogeneity and anisotropy in the absorbing substance. Advances in this method have undoubtedly contributed to resolving this uncertainty, which is neither minor nor subtle, regarding the use of a valid model and its associated $R_{\text{iso}}^{\text{ATR}}$ value for calculating the dichroic spectra.[79-81]

[78] Bechinger, B., Ruysschaert, J.M., and Goormaghtigh, E. **(1999)**. Membrane helix orientation from linear dichroism of infrared attenuated total reflection spectra. *Biophys J. 76*, 552–563.
[79] Axelsen, P.H., and Citra, M.J. **(1996)**. Orientational order determination by internal reflection infrared spectroscopy. *Prog. Biophys. Mol. Bio. 66*, 227–253.
[80] Goormaghtigh, E., Raussens, V., and Ruysschaert, J.M. **(1999)**. Attenuated total reflection infrared spectroscopy of proteins and lipids in biological membranes. *Biochim. Biophys. Acta, Biomembr. 1422*, 105–185.
[81] Ausili, A., Corbalan-Garcia, S., Gomez-Fernandez, J.C., and Marsh, D. **(2011)**. Membrane docking of the C2 domain from protein kinase C alpha as seen by polarized ATR-IR. The role of PIP2. *Biochim. Biophys. Acta, Biomembr. 1808*, 684–695.

A well established approximation of R_{iso}^{ATR} can be obtained experimentally by using the lipid ester band ($\nu_{(C=O)}$) between 1762–1700 cm^{-1}. The dichroic spectra were computed by zeroing the area of the lipid ester band near 1738 cm^{-1}.[78] The rationale behind this originates from the fact that the transition dipole of this band is oriented close to the magic angle (54.7º), as supported by ^{13}C and ^{1}H NMR spectroscopies.[82] Furthermore, fast conformational exchange coupled with axial diffusion and molecular motion are in agreement with an apparently isotropic signal of the ester C=O stretching vibration.[83] The suitability of this method was verified by comparing the consistency of the calculated R_{iso}^{ATR} with the dichroism of other lipid bands, discussed in detail in Chapter 4. The advantage of this method is as follows: it takes into account the changes in the relative power of evanescent fields and also the "real" film thickness. Although the lipid ester band provides just an approximation of the R_{iso}^{ATR}, it has been shown to be accurate enough for deriving the orientations of lipid and protein in films of different thickness.[80] In the present study, the results were mainly obtained by using R_{iso}^{ATR} from the lipid ester band; qualitatively similar results were also obtained with corresponding values from the thick- and thin-film approximations.

2.2.3 Infrared Reflection Absorption Spectroscopy (IRRAS)

IRRAS is a biophysical method that combines infrared spectroscopy with the Langmuir-film technique, first introduced by Dluhy et al.[84] Langmuir-films or lipid monolayers at the air/water interface serve as excellent models for studying protein–membrane interactions. For instance, many experimental parameters can be controlled, including but not limited to, the surface pressure of the lipid monolayer, monolayer and subphase compositions, temperature, pH etc. However, a major drawback of the Langmuir method is that the information obtained is mainly limited to the pressure-area isotherms (π/A), and none about the molecular structure and/or conformations of the film constituents. Combination of the Langmuir method with IR spectroscopy has revolutionised our understanding of protein–membrane interactions. The

[82] Wittebort, R.J., Schmidt, C.F., and Griffin, R.G. **(1981)**. Solid-State C-13 Nuclear Magnetic-Resonance of the Lecithin Gel to Liquid-Crystalline Phase-Transition. *Biochemistry 20*, 4223–4228.
[83] Lewis, R.N., and McElhaney, R.N. **(1992)**. Structures of the subgel phases of n-saturated diacyl phosphatidylcholine bilayers: FTIR spectroscopic studies of 13C = O and 2H labeled lipids. *Biophys. J. 61*, 63–77.
[84] Dluhy, R.A., and Cornell, D.G. **(1985)**. Insitu Measurement of the Infrared-Spectra of Insoluble Monolayers at the Air-Water-Interface. *J. Phys. Chem. 89*, 3195–3197.

extremely useful application of IRRAS is the determination of molecular orientations (such as, of lipid chains, protein's helices and sheets). The distinct advantage of IRRAS over polarized ATR-FTIR is in obtaining the orientation of the systems where the applicability of ATR-FTIR levels off.

Instrumentation and spectra collection

Infrared spectra were recorded using the Vertex 70 FTIR spectrometer equipped with a variable angle reflectance accessory, the A511 unit. The accessory is a computer-controlled unit coupled to a custom-designed Langmuir trough, with a Wilhelmy plate as the pressure sensor. Two teflon troughs of different sizes are linked by two small bores to ensure equal heights of the air-D_2O interface. The temperature of the subphase was maintained at 20 ± 0.5 ˚C for all measurements. Unless stated otherwise, all the measurements were carried out in the small (reference) trough at constant surface area with the large trough filled with buffer solution, only. The IR beam was focused by mirrors onto the subphase, and different angles of incidence (from 20˚ – 80˚) could be adjusted. A wire grid polarizer was placed into the optical path just prior to the point where the beam impinges on the aqueous phase. The reflected light was collected at the same angle as the angle of incidence and was directed onto a nitrogen cooled MCT detector. The trough system was positioned on a movable platform to be able to shuttle between the sample and reference trough, thus diminishing the spectral interference due to water vapour absorption in the light beam. The entire experimental setup was enclosed and purged to keep the relative humidity both low and constant. A D_2O-based subphase consisting of 100 mM NaCl, pD 7.4 was used for all the experiments. For each spectrum, 2000 scans were acquired at ~ 8 cm^{-1} resolution, co-added, apodised with the Blackman–Harris three-term function with a zero filling factor of 2 to produce a spectrum encoded at ~ 4 cm^{-1} intervals. Figure 2.4 depicts the IRRAS set-up currently in use at Prof. Dr. R. Winter's laboratory at the Technische Universität Dortmund, Germany.

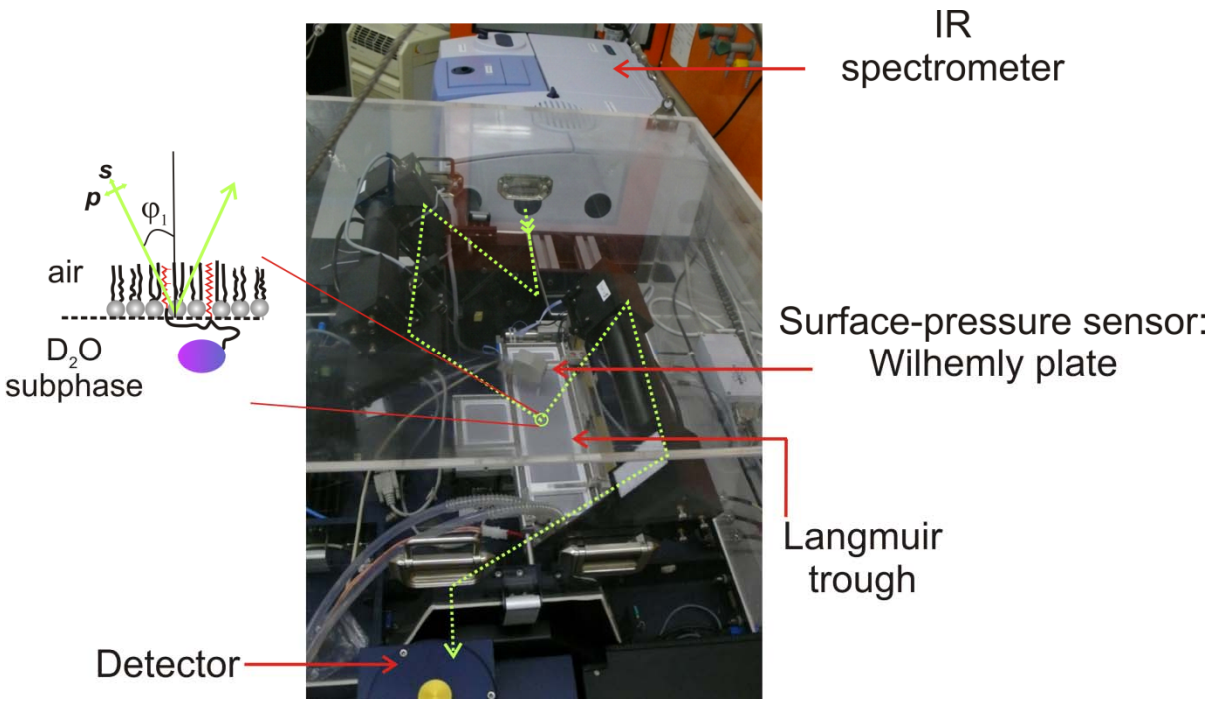

Figure 2.4: Pictorial presentation of the IRRAS setup. The FTIR spectrometer sends out the IR light (dotted green line) which enters into the external reflection (A511 unit) through the incident arm (black motor). This arm directs the light to fall on the Langmuir trough at a particular angle, after passing through a high quality polarizer. The light is then reflected at the same angle as that of incidence and collected by the detector arm. Finally, the reflected light is passed to the MCT detector for processing. The entire setup is enclosed with a plexiglass hood. The Langmuir trough is mounted on a movable motor (in both horizontal and vertical directions) and is connected to a temperature regulating unit.

Theoretical model and definition of optical parameters

The IRRA spectra are depicted as plots of reflectance-absorbance (RA) vs. wavenumber. RA is defined as $-\log[R/R_0]$, where R is the reflectivity of the film-covered trough and R_0 is the reflectivity from the uncovered subphase. The measured IRRA signal can be either positive or negative, depending on the angle of incidence, its proximity to the Brewster angle, polarization state, and the orientation of the transition dipole moment with respect to the interface. At a particular angle of incidence above the Brewster angle, positive intensities imply a transition dipole oriented preferentially in the surface plane, and negative intensities reflect a perpendicular orientation, when measured with p-polarized light.[85] Thus, comparing

[85] Mendelsohn, R., Mao, G.R., and Flach, C.R. **(2010)**. Infrared reflection-absorption spectroscopy: Principles and applications to lipid-protein interaction in Langmuir films. *Biochim. Biophys. Acta, Biomembr. 1798*, 788–800.

the amide-I' band collected with p-polarized light at various angles of incidence furnishes qualitative information on the orientation of the protein at the monolayer interface. The frequency or band position in IRRAS is interpreted in terms of molecular structure similar to the normal transmission IR mode, while the intensities permits determination of the quantitative orientational coordinates of the molecular constituents by performing computer simulations. This in turn, requires detailed consideration of the optical properties of the three layer interface: air–anisotropic film–water. The physical description of such an interface is given in Figure 2.5.

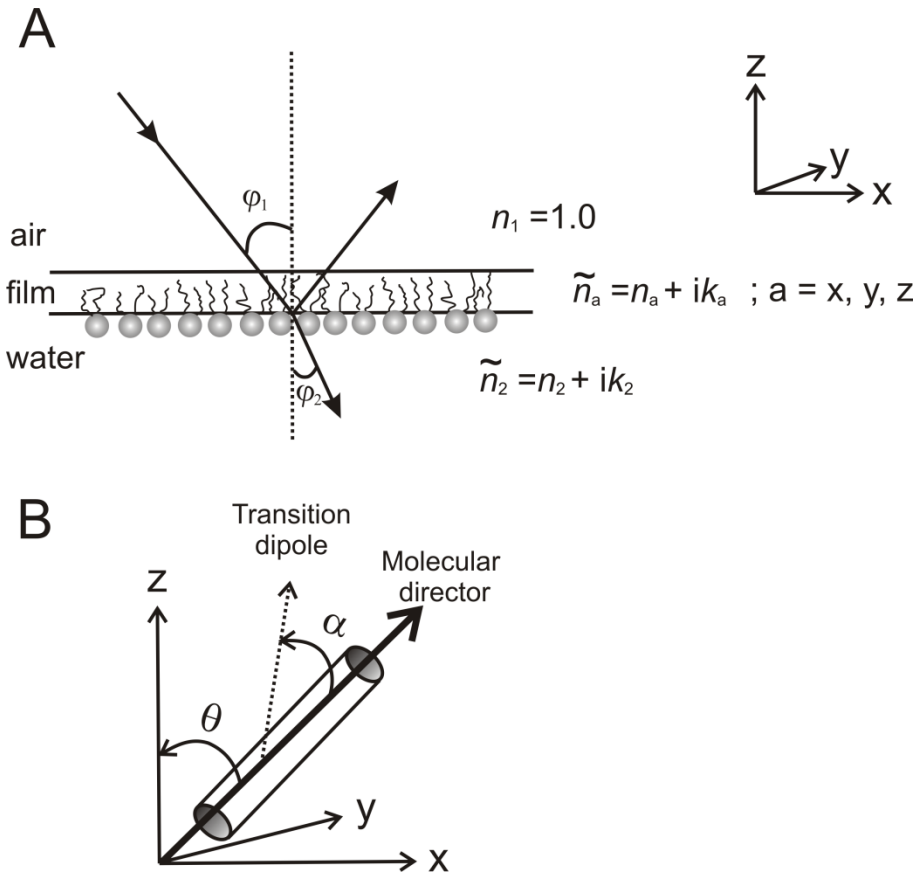

Figure 2.5: Theoretical model for the interaction of light with a three-phase parallel layered system. (**A**) Optical constants for the three phase system: air (homogeneous and non-absorbing), anisotropic monolayer and isotropic subphase. (**B**) Axis system for describing IRRAS geometry with symbols explained in the text.

The Brewster angle, also known as the polarization angle, is defined by $\theta_B = \arctan\left(\frac{n_2}{n_1}\right)$. It is the angle at which the p-polarized light is completely transmitted, or the light that is reflected

from the air-water interface at this angle is entirely polarized perpendicular to the incident plane (i.e. s-polarized). Alternatively, the p-polarized radiation exhibits a minimum in the reflectively at the Brewster angle. In Figure 2.5, the phases separated by a plane boundary, such as an air-water interface, are taken to be semi-infinite (to avoid artificial problems incurring due to multiple reflections). The direction of the incident light ray and the surface normal (*z*-axis) defines the plane of incidence (*x*-*z* plane). Two possible planes of polarizations are defined by E^{II} and $E^{\perp}$ (same as that for ATR-setup).The electric field vector in the p-polarization has *x* and *z* components and the *y* axis is the direction of the electric field vector in the s-polarization. When the light leaves from one phase (non-absorbing) to another (absorbing), the fraction of light reflected depends on the mismatch between the optical constants of the respective phases. The optical properties of the j^{th} (absorbing) phase are characterised by a complex refractive index:

$$\tilde{n}_j = n_j + ik_j \qquad (17)$$

where, n_j is the real refractive index of phase and k_j is the extinction coefficient. The symbol ~ stands for a complex entity. The extinction coefficient is related to the reciprocal of the distance *x* (Λ), in the medium for the intensity to fall to 1/e of its initial value, i.e. $I = I_o e^{-\Lambda x}$ and $k = \Lambda\lambda / 4\pi$, where λ is the vacuum wavelength. The equations describing the interaction of plane-polarized with an N-phase parallel layered system are derived from the Maxwell's equations. The continuity considerations of the electric and magnetic field vectors are taken into account, as described in the classic monograph of Born and Wolf[69] and reviewed elsewhere[86(and refs. within)]. The coefficient of reflection ($\tilde{r}$) at an interface between *two* semi-infinite homogeneous and *isotropic phases* is defined as electric field intensity ratio of the reflected ray to the incident ray.[87] Here, the incident phase (air) is considered to be non-absorbing and the final phase (water) as absorbing. Reflection coefficients for p- and s-polarizations ($\tilde{r}_p$ and $\tilde{r}_s$) are calculated from the Fresnel equations. For p-polarization it is defined as:

---

[86] Mendelsohn, R., Brauner, J.W., and Gericke, A. **(1995)**. External Infrared Reflection-Absorption Spectrometry Monolayer Films at the Air-Water-Interface. *Annu. Rev. Phys. Chem. 46*, 305–334.

[87] Flach, C.R., Gericke, A., and Mendelsohn, R. **(1997)**. Quantitative determination of molecular chain tilt angles in monolayer films at the air/water interface: Infrared reflection/absorption spectroscopy of behenic acid methyl ester. *J. Phys. Chem. B. 101*, 58–65.

$$\tilde{r}_{\mathrm{p}}^{\mathrm{F}} = \frac{\tan(\varphi_1 - \tilde{\varphi}_2)}{\tan(\varphi_1 + \tilde{\varphi}_2)}, \tag{18}$$

and, for s-polarization as:

$$\tilde{r}_{\mathrm{s}}^{\mathrm{F}} = -\frac{\sin(\varphi_1 - \tilde{\varphi}_2)}{\sin(\varphi_1 + \tilde{\varphi}_2)} \tag{19}$$

where, φ_1 is the angle of incidence between the incident ray and the surface normal and $\tilde{\varphi}_2$ is the complex angle of refracted ray (Fig. 2.5). The superscript F denotes a Fresnel interface, i.e. a film-free air-water interface.

$$\sin\tilde{\varphi}_2 = \frac{\sin\varphi_1}{\tilde{n}_2} \tag{20}$$

With the lipid monolayer (film) at the interface between air and water, the expressions need appropriate makeover. To this end, Abelès formulism for calculating the reflection coefficients of a three-layer system with a thin-film between two semi-infinite phases (for both s- and p-polarization) serve as essential starting points in understanding of the light reflection in a typical IRRAS experiment. However, these expressions (mentioned elsewhere)[88] consider the thin-film as *isotropic*, which is far away from reality, especially in cases of lipids and proteins. Following this, two independent approaches were developed taking into account the anisotropy of the thin-film; one by Schopper et al.[89] and the other by Kuzmin et al.[90] In the present work, the latter formulism has been employed to perform IRRAS spectral simulations, with the corresponding reflection coefficients as follows:

$$\tilde{r}_{\mathrm{p}} = -\frac{\sin(\varphi_1 - \tilde{\varphi}_2)\cos(\varphi_1 + \tilde{\varphi}_2) - ik_0\tilde{n}_2^{-1}\sin\varphi_1\left(\tilde{I}_1\cos\varphi_1\cos\tilde{\varphi}_2 - \tilde{I}_2\sin\varphi_1\sin\tilde{\varphi}_2\right)}{\sin(\varphi_1 + \tilde{\varphi}_2)\cos(\varphi_1 - \tilde{\varphi}_2) - ik_0\tilde{n}_2^{-1}\sin\varphi_1\left(\tilde{I}_1\cos\varphi_1\cos\tilde{\varphi}_2 + \tilde{I}_2\sin\varphi_1\sin\tilde{\varphi}_2\right)}, \tag{21}$$

$$\tilde{r}_{\mathrm{s}} = -\frac{\sin(\varphi_1 - \tilde{\varphi}_2) - ik_0\tilde{n}_2^{-1}\sin\varphi_1\tilde{I}_1}{\sin(\varphi_1 + \tilde{\varphi}_2) - ik_0\tilde{n}_2^{-1}\sin\varphi_1\tilde{I}_1} \tag{22}$$

---

[88] Abelès, F. **(1950)**. "Recherches sur la propagation des ondes électromagnétique sinussoïdales dans les milieux stratifiés. Application aux couches minces." *Ann. Phys. 5*, 596–640.

[89] Schopper, H. **(1952)**. Zur Optik Dunner Doppelbrechender Und Dichroitischer Schichten. *Z. Phys. 132*, 146–170.

[90] Kuzmin, V.L., Romanov, V.P., and Mikhailov, A.V. **(1992)**. Light-Reflection on the Boundary of Liquid-Systems and Surface-Layer Structure. *Opt. Spekt. 73*, 3–47.

with

$$k_0 = \frac{2\pi}{\lambda} \tag{23}$$

$$\tilde{I}_1 = \left(\tilde{n}_x^2 - \tilde{n}_2^{\,2}\right) d \tag{24}$$

$$\tilde{I}_2 = \frac{\left(\tilde{n}_z^2 - \tilde{n}_2^{\,2}\right) d}{\tilde{n}_z^2} \tag{25}$$

where, d is the film thickness and $\tilde{n}_x$, $\tilde{n}_z$ represent the complex refractive indices of the thin surface layer. Owing to the uniaxial symmetry of the film, $\tilde{n}_x = \tilde{n}_y$. The product of reflection coefficient and its complex conjugate generates the reflectivity R:

$$R_j = \tilde{r}_j \tilde{r}_j^{*} \tag{26}$$

where, j denotes s- or p-polarization. Finally, the reflectance absorbance (RA) is given by:

$$RA_j = -\log\left[R_j / R_j^F\right], \tag{27}$$

where, R_j^F is the reflectivity from the film-free interface (Fresnel reflectivity), also denoted as R_o.

Computer simulation of the IRRA spectrum

Two different mathematical models are known to calculate the reflectance-absorbance (RA) spectra of a three-phase system, where the film between air and isotropic liquid subphase, is a homogeneous, anisotropic monolayer.[89-90] Both models lead to similar results, although the approaches in their derivations of the reflection coefficients and their final expressions are quite different.[86] In the current work, the mathematical formalism developed by Kuzmin et al. was used and is described in the following.

The first step was the determination of the imaginary part of the refractive index (directional extinction coefficients of the monolayer, k_x, k_y, k_z), according to the previously defined model of Korte et al.[91] The order parameters S and D take into account the tilt (θ) and twist

[91] Korte, E.H. **(1983)**. Influence of the Order Parameter-D on the Linear Dichroism of Nematic Liquid-Crystals. *Mol. Crys. Liq. Crys. 100*, 127–135.

(ψ) angle of the secondary structure elements (shown in Fig. 2.6), and can be written for biaxial molecules ($k_x = k_y$) as:

$$S = 1 - \frac{3}{2}\overline{\sin^2\theta} \tag{28}$$

$$D = \frac{3}{2}\overline{\sin^2\theta\cos 2\psi} \tag{29}$$

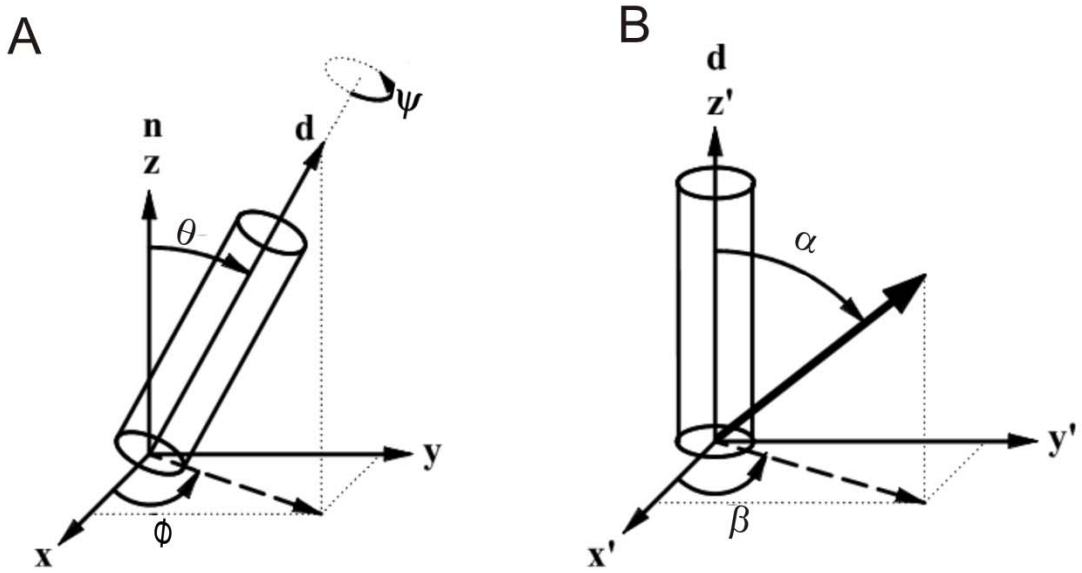

Figure 2.6: Definition of angles for the structural element and its transition dipole moment. The laboratory coordinates $\{x, y, z\}$ are shown in (**A**) with tilt angle (θ), twist angle (ψ), and azimuthal angle (ϕ) for the molecular director, d. **(B)** The molecular coordinates $\{x', y', z'\}$ with the corresponding polar angles α and β defined for the transition dipole moment.

Tilt angles of the α-helices in the Ras protein (as defined in previously)[92] were derived by superimposing a reference helix [program "superpose"][93] and calculating the angle between the vector parallel to the long axis of the reference helix and the normal to the air-water interface (z axis). The twist angle was set to 45° for all α-helical elements due to the

[92] Meister, A., Nicolini, C., Waldmann, H., Kuhlmann, J., Kerth, A., Winter, R., and Blume, A. **(2006)**. Insertion of lipidated Ras proteins into lipid monolayers studied by infrared reflection absorption spectroscopy (IRRAS). *Biophys. J. 91*, 1388–1401.
[93] Bailey, S. **(1994)**. The Ccp4 Suite - Programs for Protein Crystallography. *Acta. Crystall. D. 50*, 760–763.

evidence that the transition dipole moments in an α-helix have a uniaxial distribution around the helix axis. For β-sheets, the orientation of the carbonyl bonds relative to the direction of the individual strands (defined by a vector from the carbonyl C-atom of the neighbouring residue) were used to indicate the orientation of the inter-chain hydrogen bonds and the transition dipole moment of the amide-I mode. Whereas the angle between the strand vector and the *z* axis defines the tilt angle, the angle between the direction vector of a C=O bond and the cross product of the *z* axis with the strand vector defines the twist angle. The values were calculated using a C-program. Implementing order parameters *S* and *D* into the directional extinction coefficients, leads to equation (30) and (31):

$$k_{\mathrm{x\,max}} = k_{\mathrm{y\,max}} = \frac{1}{3}k_{\max}\left[1 - S\left(1 - \frac{3}{2}\sin^2\alpha\right) + \frac{1}{2}D\sin^2\alpha\cos 2\beta\right] \tag{30}$$

$$k_{\mathrm{z\,max}} = \frac{1}{3}k_{\max}\left[1 + 2S\left(1 - \frac{3}{2}\sin^2\alpha\right) - D\sin^2\alpha\cos 2\beta\right] \tag{31}$$

The film extinction coefficient ($k_{\max}$) depends on the oscillation strength and the surface pressure. Normally, $k_{\max}$ is unknown and has to be determined by computer simulation of the reflectance-absorbance. The polar angles α and β define the transition dipole moment (Fig. 2.6). The amide-I band of the α-helix has a major transition with an angle of approximately 36° relative to the helix axis. Perpendicular to the strands, i.e. along the inter-chain hydrogen bonds, the transition dipole moment of the amide-I mode for the β-sheet structure is located.

In the next step, the maximum values for the real part of the directional refraction indices had to be calculated:

$$n_{\mathrm{x\,max}} = n_{\mathrm{y\,max}} = n_{\mathrm{ext}}\,\sin^2\theta + n_{\mathrm{ord}}\cos^2\theta \tag{32}$$

$$n_{\mathrm{z\,max}} = n_{\mathrm{ext}}\,\cos^2\theta + n_{\mathrm{ord}}\sin^2\theta \tag{33}$$

The refractive index is divided into an extraordinary n_{ext} and an ordinary n_{ord} part, which correspond to the directions perpendicular and parallel to the axis direction, respectively.

A wavenumber dependence of the refractive index is required to simulate an entire band with a Lorentzian line shape:

$$k_{\mathrm{x}}(\nu) = \frac{k_{\mathrm{x\,max}}\gamma^2}{4\Delta^2 + \gamma^2} \tag{34}$$

$$k_{\mathrm{z}}(\nu) = \frac{k_{\mathrm{z\ max}}\gamma^2}{4\Delta^2 + \gamma^2} \tag{35}$$

$$n_{\mathrm{z}}(\nu) = n_{\mathrm{z\,max}} - \frac{2\Delta k_{\mathrm{z\,max}}\gamma}{4\Delta^2 + \gamma^2} \tag{36}$$

$$n_{\mathrm{x}}(\nu) = n_{\mathrm{x\ max}} - \frac{2\Delta k_{\mathrm{x\ max}}\gamma}{4\Delta^2 + \gamma^2} \tag{37}$$

where, $\gamma = 2\pi c(\mathrm{FWHH})$, $\Delta = 2\pi c(\nu - \nu_{\mathrm{o}})$, FWHH = Full Width at Half-Height, c = speed of light, ν = frequency for which the calculation was carried out, and ν_{o} = center frequency.

Subsequently, the frequency-dependent refractive index was calculated from its real and imaginary parts:

$$\tilde{n}(\nu) = n(\nu) + \mathrm{i}k(\nu) \tag{38}$$

The starting point for the computation of the RA spectra was the polarisation state dependent reflection coefficients ($\tilde{r}$), which were obtained using Eqs. (18) – (19) for the film-free surface and Eqs. (21) – (22) for the anisotropic film-covered surface, respectively. The complex refractive index of water ($\tilde{n}_2$) was taken from Bertie et al.[94] and interpolated to the desired step width. These were then used to obtain the reflectivity, *R,* by use of Eq. (26). The reflectivity was modified by using a parameter (β) that accounts for non-ideal polarization effects. It describes the ratio of the intensity of s-polarized radiation (I_{s}) to the total intensity of the radiation (I) that passes through the polarizer:[95]

[94] Bertie, J.E., Ahmed, M.K., and Eysel, H.H. **(1989)**. Infrared Intensities of Liquids .5. Optical and Dielectric-Constants, Integrated-Intensities, and Dipole-Moment Derivatives of H_2O and D_2O at 22 ˚C. *J. Phys Chem. 93,* 2210–2218.

[95] Gericke, A., Michailov, A.V., and Huhnerfuss, H. **(1993)**. Polarized External Infrared Reflection Absorption Spectrometry at the Air-Water-Interface - Comparison of Experimental and Theoretical Results for Different Angles of Incidence. *Vib. Spect. 4*, 335–348.

$$R_{\mathrm{p}}^{\mathrm{eff}} = R_{\mathrm{p}} + \beta\left(R_{\mathrm{s}} - R_{\mathrm{p}}\right);\ R_{\mathrm{s}}^{\mathrm{eff}} = R_{\mathrm{s}} + \beta\left(R_{\mathrm{p}} - R_{\mathrm{s}}\right);\ \beta = \frac{I_{\mathrm{s}}}{I} \tag{39}$$

The final equation to calculate the reflectance-absorbance (RA), which is normally plotted versus the wavenumber in IRRAS data, is given by Eq. (27). The RA was normalised to the reflectivity of the Fresnel interface as shown below:

$$RA_{\mathrm{j}}^{\mathrm{eff}} = -\log\left(\frac{R_{\mathrm{j}}^{\mathrm{eff}}}{R_{\mathrm{j}}^{\mathrm{F,\ eff}}}\right) \tag{40}$$

All contributions of the α-helix and β-sheet structural element sections to the respective amide-I bands were weighted by the number of contributing residues in the respective sections. These were then added up for the spectral calculations using a Matlab® implementation of the model described above [This Matlab implementation was performed by Mirko Erlkamp, PhD student in Prof. Dr. R. Winter's laboratory].

To calculate the molecular tilt and twist angles using Eqs. (28) – (31), $k_{\max}$ values were required but were unavailable, as they depend on the surface concentrations of the film-forming species. Thus, IRRAS measurements had to be conducted at different angles of incidences and polarization states, where a non-linear least-square fit can be used to obtain the tilt (θ) and twist (ψ) angles by minimising the difference between the calculated and the measured IRRA intensities (while varying $k_{\max}$, θ, and ψ). However in the present work, the initial estimate of tilt and twist angles were calculated using previously defined orientations for the proteins under investigation using CCP4 suite [These were performed by Dr. Ingrid R. Vetter at the Max Planck Institute of Molecular Physiology, Dortmund, Germany], and subsequently generating simulated spectra using the model described above. The simulated IRRA spectra were compared with the measured spectra enabling the assignment of each defined orientation to a particular state of the protein.

2.3 Fluorescence Methods

2.3.1 Ambient and High Pressure Fluorescence Spectroscopy

All measurements were performed on the ISSK2 multi-frequency phase and modulation spectrofluorometer. High pressure fluorescence experiments were carried out using a stainless steel high pressure vessel coupled with an ISS fluorescence detection system. The required sample solution was injected into a 9 mm round quartz cell (volume 0.8 mL) and sealed with an O-ring. The cell was then placed in the high pressure vessel quipped with three quartz windows and connected to a pump and gauge. High quality (18 MΩ) water was used as the pressurising medium. The high pressure cell was connected to a water bath maintained at 25 ˚C and controlled with an accuracy of ± 0.1 ˚C. Excitation light was provided by a xenon lamp through a monochromator, and the emission spectra collected at 90˚ through another monochromator.

For high pressure studies described in chapter 5:

Excitation wavelength at 275 nm (for tyrosine) was used and the emission spectra were collected between 290–420 nm. First, neutral raft-like lipid vesicles (DOPC:DPPC:Chol::25:50:25; molar ratio) were incubated with GTP-bound N-Ras in 5 mM $MgCl_2$, 20 mM Tris buffer, yielding a protein to lipid molar ratio of 1:100. The emission spectra for the protein bound to lipid vesicles were background corrected for the scattering by the corresponding lipid vesicles alone at the respective pressures.

For ambient pressure studies described in chapter 6:

The PDEδ tryptophan excitation was performed at 282 nm. The emission spectrum of PDEδ (6.8 μM) in 20 mM Tris, 7 mM $MgCl_2$, pH 7.4 was collected, followed by the addition of the Ras proteins (4 μM). Finally, the lipid vesicles (0.25 mM) composed of either anionic raft-like (DOPC:DOPG:DPPC:DPPG:Chol::20:5:45:5:25; molar ratio) or neutral raft-like (DOPC:DPPC:Chol::25:50:25; molar ratio) lipid mixtures were added. The emission spectra for the protein bound to lipid vesicles were background corrected for the scattering by the corresponding lipid vesicles alone.

For high pressure studies described in chapter 7:

The FRET based studies were performed using *N*-Rh-PE labelled neutral raft-like (DOPC:DPPC:Chol 25:50:25 (molar ratio)) or pure fluid lipid vesicles composed of DOPC as the **acceptor**. BODIPY labelled dually lipidated N-Ras proteins were used as the **donor** in 5 mM $MgCl_2$, 20 mM Tris buffer, yielding a ratio of *N*-Rh-PE to BODIPY of 2:1. Excitation was performed at 488 nm (for BODIPY-Ras) and either the emission spectra were collected (between 500–700 nm) or the single point intensity (at 591 nm; em_{max} for *N*-Rh-PE). In each case, the fluorescence intensity was corrected for the scattering by lipid vesicles and the cross excitation of *N*-Rh-PE.

2.3.2 Ambient Stopped-Flow Fluorescence Spectroscopy

Instrumentation and data collection

Fast kinetic measurements were performed using the SX-18MV stopped-flow apparatus by rapid mixing of BODIPY-labelled N-Ras proteins (both, dually- and monolipidated) at a protein concentration of 0.35 μM with liposomes (100 nm diameter) of varying compositions (c = 125 μM). In the standard experimental setup, BODIPY-labelled N-Ras was excited at 488 nm using a slit width of ± 1 nm. Fluorescence emission of liposome-bound *N*-Rh-PE occurring from FRET with Ras was recorded through a 570 nm cutoff filter. Typically, 8 to 10 single injections were accumulated for each experiment. Depending on the association and dissociation kinetics, monitoring times varied from 2 to 500 s. Dissociation experiments were measured with an eightfold excess of unlabelled liposomes over labelled liposomes that were pre-equilibrated with the protein. All measurements were performed at 25 °C in buffer containing 20 mM Tris buffer (pH 7.4) and 5 mM $MgCl_2$. The ratio of BODIPY to *N*-Rh-PE was kept constant at 1:2 in all the measurements.

III

CHARACTERISATION OF AN ANIONIC "RAFT-LIKE" MODEL MEMBRANE LIPID SYSTEM

* The work of the present study has been published and subsequently reprinted in parts (some figures) with permission from Kapoor, S., Werkmuller, A., Denter, C., Zhai, Y., Markgraf, J., Weise, K., Opitz, N., and Winter, R. **(2011)**. Temperature-pressure phase diagram of a heterogeneous anionic model biomembrane system: Results from a combined calorimetry, spectroscopy and microscopy study. *Biochim. Biophys.Acta, Biomembr. 1808*, 1187-1195.

3.1 Background

"It takes a membrane to make sense out of disorder in biology. You have to be able to catch energy and hold it, storing precisely the needed amount and releasing it in measured shares". These were the words of Lewis Thomas in the Lives of a Cell[96] emphasising the complexity encoded by the variety of lipids and their induced structural platforms. Lipid assemblies are much more complicated than other biological constituents; therefore, they self assemble non-covalently and create lipid bilayers, within which lipid molecules can relocate in a variety of ways. Lipids fulfil many critical requirements in the cell, such as, storing energy due to their reduced state and acting as first and second messengers in signal transduction and recognition processes. The matrix of cellular membranes is formed by polar lipids, which consist of a hydrophobic and a hydrophilic portion. The propensity of the hydrophobic moieties to self-associate (entropically driven by water) coupled with the tendency of the hydrophilic moieties to interact with aqueous environments and—in some cases—with each other, forms the physical basis of the spontaneous formation of membranes. With careful cataloguing of lipids (Lipidomics) we are only beginning to comprehend the astounding diversity of lipids in the cellular membranes. The membranes in eukaryotic cells have a wide repertoire of structural lipids. The first one includes glycerophospholipids such as phosphatidylcholine (accounting for > 50% of the phospholipids), phosphatidylethanolamine, phosphatidylserine, phosphatidylinositol, and phosphatidic acid. Sphingolipids constitute another class of structural lipids with their hydrophobic backbone as a ceramide moiety. The major sphingolipids in mammalian cells are sphingomyelin and glycosphingolipids. Sterols are the major non-polar lipids of cell membranes representing a unique class, due to their annealed structures that embody a highly condensed hydrophobic area. Many possible variations in the lipid's hydrophilic headgroups and hydrophobic tails add a high level of complexity to the existing vast pool of lipids. A considerable part of our genome (~5 %) continuously synthesises and regulates this complex array of lipids,[52] leaving some simple yet profound questions. *Why do the cells maintain such a complex diversity of lipids? Could this imply that cells are continuously trying to create heterogeneity in the*

[96] Thomas, L. **(1971)**. Notes of a Biology-Watcher - Lives of a Cell. *N. Engl. J. Med. 284*, 1082–1083.

membrane? Are they aiming at phase coexistence; manifested as the existence of domains of coexisting phase(s)?

In this regard, each kind of cell or membrane type (e.g. plasma membranes vs. endomembranes) has a unique lipid and membrane protein composition[52] that plays an important role in the organisation of the bilayer system. Steric[97] and electrostatic interactions[98] and hydrophobic mismatch[99-100] induce *phase segregation* that forms distinct domains in the bilayer. This ability of lipid membranes to exist in a multitude of phases, characterised by a different spatial arrangement and motional freedom of each lipid with respect to its neighbours, has lead to redefining membrane functionality.[101-102] These phases are influenced by their molecular structure and environmental conditions like pH, ionic strength, water content, temperature, and pressure; they have long fascinated scientists in the field of membrane biophysics.

3.1.1 Lipid Phases in Membranes

Lipid membranes are highly complex entities in which lipid-lipid interactions regulate, in part, the phase behaviour exhibited by them. Hydrated lipid bilayers undergo phase transitions as a function of temperature; the most important is the main (or chain-melting) transition. During the main transition, the bilayer is transformed from a highly ordered quasi-two-dimensional crystalline solid to a quasi-two-dimensional liquid. It involves drastic changes in the order of the systems, i.e. the translational order (related to the lateral diffusion coefficient in the plane of the membrane, D_T) and, the conformational order (related to the *trans/gauche* ratio in the acyl chains, *S*). The lipid structure dominates the phases that are formed. For example, the long saturated hydrocarbon chains in sphingomyelin (SM) are

[97] Roux, M., Auzely-Velty, R., Djedaini-Pilard, F., and Perly, B. **(2002)**. Cyclodextrin-induced lipid lateral separation in DMPC membranes: H-2 nuclear magnetic resonance study. *Biophys. J. 82*, 813–822.
[98] Hartmann, W., and Galla, H.J. **(1978)**. Binding of Polylysine to Charged Bilayer Membranes - Molecular-Organization of a Lipid - Peptide Complex. *Biochim. Biophys. Acta. 509*, 474–490.
[99] Wilkinson, D.A., and Nagle, J.F. **(1979)**. Dilatometric Study of Binary-Mixtures of Phosphatidylcholines. *Biochemistry 18*, 4244–4249.
[100] Knoll, W., Schmidt, G., Rotzer, H., Henkel, T., Pfeiffer, W., Sackmann, E., Mittlerneher, S., and Spinke, J. **(1991)**. Lateral Order in Binary Lipid Alloys and Its Coupling to Membrane Functions. *Chem. Phys. Lipids 57*, 363–374.
[101] Feigenson, G.W. **(2006)**. Phase behavior of lipid mixtures. *Nat. Chem.Biol. 2*, 560–563.
[102] Feigenson, G.W. **(2007)**. Phase boundaries and biological membranes. *Ann. Rev. Biophy. Biomol. Str. 36*, 63–77.

responsible for the solid-like (s_o) phases in SM rich mixtures; unsaturated chains constitute the liquid-disordered phases (l_d). Sterols, on the other hand mix with bilayer forming lipids in varying amounts to induce the liquid-ordered (l_o) phases.[103-105]

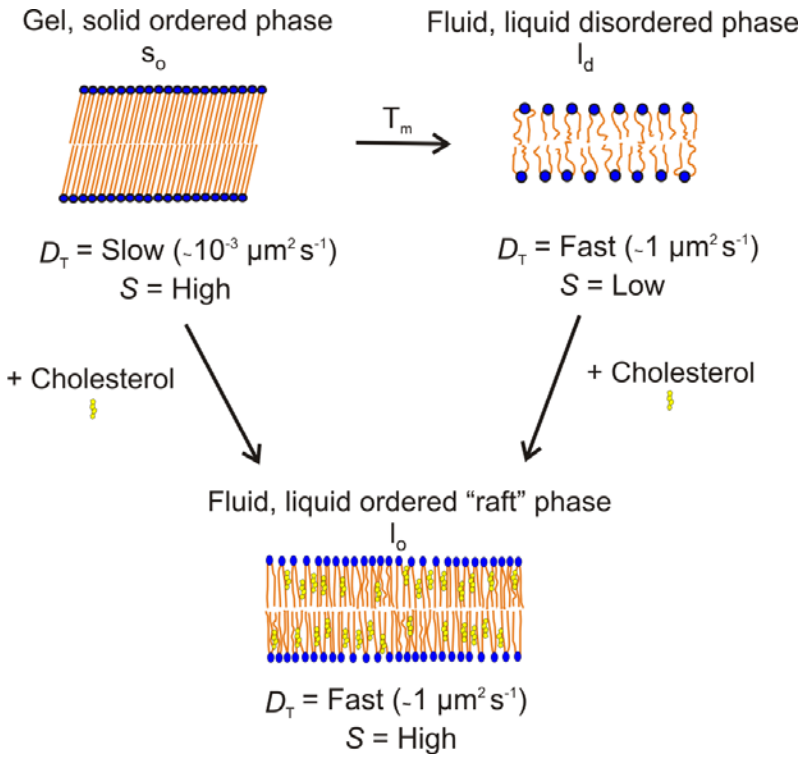

Figure 3.1: Schematic representation of the possible lipid bilayer phases with their physical properties. The phases shown correspond to lamellar bilayer structures. Long, saturated hydrocarbon chains tend to adopt solid-like (s_o) phases; unsaturated chains are found in most biomembranes, so these tend to be enriched in liquid-like, disordered phases (l_d). Sterols by themselves cannot form bilayer phases, but together with bilayer-forming lipids, they generate the liquid-ordered (l_o) phases at high sterol concentrations.

In l_o phases, the flat and rigid structures of sterols impose a conformational ordering upon the neighbouring aliphatic chain,[106] without a corresponding (drastic) reduction in the translational mobility of the lipids.[107]

---

[103] Silvius, J.R., delGiudice, D., and Lafleur, M. **(1996)**. Cholesterol at different bilayer concentrations can promote or antagonize lateral segregation of phospholipids of differing acyl chain length. *Biochemistry 35*, 15198–15208.

[104] Ahmed, S.N., Brown, D.A., and London, E. **(1997)**. On the origin of sphingolipid/cholesterol-rich detergent-insoluble cell membranes: Physiological concentrations of cholesterol and sphingolipid induce formation of a detergent-insoluble, liquid-ordered lipid phase in model membranes. *Biochemistry. 36*, 10944–10953.

[105] Veatch, S.L., and Keller, S.L. **(2002)**. Organization in lipid membranes containing cholesterol. *Phys. Rev. Lett. 89*.

A simple, one-component saturated phospholipid system exhibits two lamellar phase transitions with increasing temperatures: a gel to gel ($L_{\beta'}/P_{\beta'}$) pre-transition, and a gel to liquid-crystalline (L_α or l_d) chain melting (main) transition at a certain temperature, T_m. The fluid-like L_α (or l_d) phase is characterised by a high conformational disorder in the acyl chains of the lipid molecules, where the linear *all-trans* chains present below the T_m undergo rotation and assume diverse *gauche* conformations. Thus, the lipid bilayer undergoes a highly cooperative order-to-disorder transition by expanding laterally and decreasing the bilayer thickness. On the other hand, in the gel phases (P_β, L_β' or L_β) the acyl chains are highly ordered. Whereas the lamellar phase states are more relevant to the biological membranes, non-bilayer lipid phases (e.g. hexagonal and cubic) mainly relate to transient events such as pore formation, fusion and fission, but are nevertheless present in substantial amounts in the biological membranes. In addition to the thermotropic phase transition, lipids also conform to pressure-induced transitions, whereby they adapt to volume restrictions by changing their packing and conformations.[108-109] The variety of complex interactions involved, when considering multiple lipids, induces lipid-lipid immiscibility within the membrane plane. This eventually leads to phase segregation even at ambient conditions of temperature and pressure, e.g. the phase segregation of the model ternary lipid mixture composed of DPPC–DOPC–Chol into l_o and l_d domains.[110] These phase separations precede the formation of domains, with distinct lipid composition, and phase properties. In recent years, considerable research in this field has lead to the concept of *raft domains*.

---

[106] Sankaram, M.B., and Thompson, T.E. **(1990)**. Modulation of Phospholipid Acyl Chain Order by Cholesterol - a Solid-State H-2 Nuclear-Magnetic-Resonance Study. *Biochemistry 29*, 10676–10684.

[107] Nielsen, M., Miao, L., Ipsen, J.H., Zuckermann, M.J., and Mouritsen, O.G. **(1999)**. Off-lattice model for the phase behavior of lipid-cholesterol bilayers. *Phys. Rev. E. 59*, 5790–5803.

[108] Czeslik, C., Reis, O., Winter, R., and Rapp, G. **(1998)**. Effect of high pressure on the structure of dipalmitoylphosphatidylcholine bilayer membranes: a synchrotron x-ray diffraction and FTIR spectroscopy study using the diamond anvil technique. *Chem. Phys. Lipids. 91*, 135–144.

[109] Winter, R., and Jeworrek, C. **(2009)**. Effect of pressure on membranes. *Soft Matter 5*, 3157–3173.

[110] Jeworrek, C., Puhse, M., and Winter, R. **(2008).** X-ray Kinematography of Phase Transformations of Three-Component Lipid Mixtures: A Time-Resolved Synchrotron X-ray Scattering Study Using the Pressure-jump Relaxation Technique. *Langmuir 24*, 11851–11859.

3.1.2 Raft Hypothesis

The raft hypothesis postulated 15 years ago, states that dynamic assemblies of cholesterol and sphingolipids predominantly exist in the *exoplasmic leaflet* of the lipid bilayer, and are connected to the phospholipids and cholesterol in the inner cytoplasmic leaflet of the bilayer.[111-112] Underpinning this concept is the propensity, *in vitro*, of the saturated hydrocarbon chains allowing cholesterol molecules to be tightly intercalated, inducing l_o phases. The membrane surrounding lipid rafts is fluid-like due to the presence of unsaturated phospholipids. Thus, the raft domains can be imagined as platforms of l_o phases dispersed in a l_d matrix of unsaturated glycerolipids (Fig. 3.2). These raft-like assemblies are ordered and tightly packed, but are still fluid due to packing differences. This, in turn, is governed by the saturation level of the hydrocarbon chains in the rafts compared with the unsaturated state of fatty acids of phospholipids in the l_d phase.[111,113] Model biomembranes have been shown to phase segregate into distinct domains of variable composition and biophysical properties. This adds a new level of excitement, as it supports an important tenet of the lipid raft hypothesis: different lipid mixtures *can drive the segregation* of a membrane into distinct domains.[110,114] However, the physiological relevance of this concept remained quite controversial until recently, when improved methodologies have dispelled most of the concerns regarding their existence and definition.[115-118]

---

111 Brown, D.A., and London, E. **(1998)**. Functions of lipid rafts in biological membranes. *Ann. Rev. Cell Dev. Biol. 14*, 111–136.
112 Simons, K., and Ikonen, E. **(1997)**. Functional rafts in cell membranes. *Nature 387*, 569–572.
113 Simons, K., and Ehehalt, R. **(2002)**. Cholesterol, lipid rafts, and disease. *J. Clin. Invest. 110*, 597–603.
114 Nicolini, C., Kraineva, J., Khurana, M., Periasamy, N., Funari, S.S., and Winter, R. **(2006c)**. Temperature and pressure effects on structural and conformational properties of POPC/SM/cholesterol model raft mixtures - a FTIR, SAXS, DSC, PPC and Laurdan fluorescence spectroscopy study. *Biochim. Biophys. Acta, Biomembr. 1758*, 248–258.
115 Varma, R., and Mayor, S. **(1998)**. GPI-anchored proteins are organized in submicron domains at the cell surface. *Nature 394*, 798–801.
116 Pralle, A., Keller, P., Florin, E.L., Simons, K., and Horber, J.K.H. **(2000)**. Sphingolipid-cholesterol rafts diffuse as small entities in the plasma membrane of mammalian cells. *J. Cell Biol. 148*, 997–1007.
117 Wilson, B.S., Pfeiffer, J.R., and Oliver, J.M. **(2000)**.Observing Fc epsilon RI signaling from the inside of the mast cell membrane. *J. Cell Biol 149*, 1131–1142.
118 Levental, I., Grzybek, M., and Simons, K. **(2011)**. Raft domains of variable properties and compositions in plasma membrane vesicles. *Proc. Natl. Acad. Sci. U.S.A. 108*, 11411–11416.

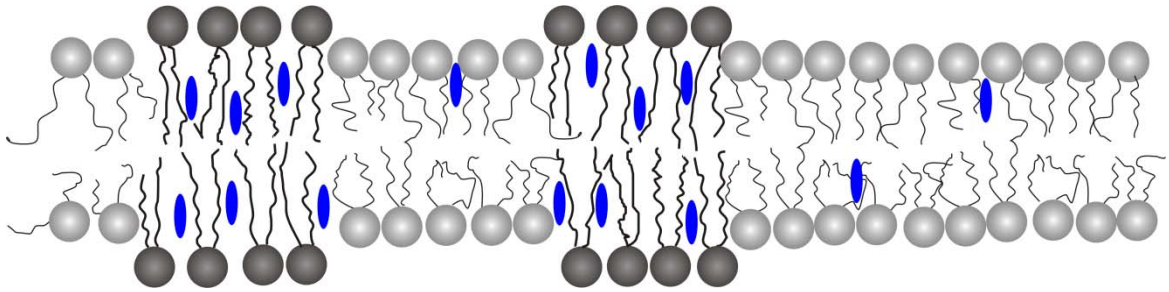

Figure 3.2: Schematic representation of raft and non-raft lipid domains. Unsaturated lipids (non raft) are shown with light grey headgroups, and saturated lipids such as SM are illustrated by dark headgroups (raft). Cholesterol incorporated in both lipid domains is shown by the blue insertions.

The raft domains are involved in a wide range of biological processes, ranging from lateral protein organisation, virus uptake, and signalling to plasma membrane tension regulation. [112,119-121]

Though raft domains *in vivo* are small and transient, the present study was not aimed to support their biological existence, but to explore the following hypothesis: *differential interactions between the various membrane components generate small but definite heterogeneities,* which are likely to influence a plethora of biological processes. These heterogeneities may or may not, be defined as rafts.

[119] Irwin, M.E., Bohin, N., and Boerner, J.L. **(2011)**. Src family kinases mediate epidermal growth factor receptor signaling from lipid rafts in breast cancer cells. *Cancer Biology & Therapy 12*, 718–726.
[120] Parton, R.G., and Hancock, J.F. **(2004)**. Lipid rafts and plasma membrane microorganization: insights from Ras. *Trends Cell Biol. 14*, 141–147.
[121] Lucero, H.A., and Robbins, P.W. **(2004)**. Lipid rafts-protein association and the regulation of protein activity. *Arch. Biochem. Biophys. 426*, 208–224.

3.2 Motivation and Objective: Insights from Ras as a Prototype

The most important biological role of phase segregation or rafts is in cellular signalling including Ras[122], immunoglobulinE,[123] and Hedgehog signalling[124]. Phase separation in general, and specifically induced by rafts, creates a unique compositional phase boundary, where the membrane properties change abruptly. A mismatch of properties at the interface results in a tension—a line tension in two-dimensional systems (e.g. lipid bilayers) and a surface tension in three dimensions—that counteracts to reduce the mismatched interface. A direct consequence of the mismatch reduction is a macroscopic phase separation. In lipid bilayers, the dipole moments of the lipid molecules in each monolayer orient in the same direction (because of the system's geometric constraints) evoking repulsive interactions between the lipid molecules. This repulsion works against the line tension at the phase boundary, so that the domain size and shape is a balance between the two contradictory forces. Additionally, surfactancy (i.e. the ability of surface-active agents to reduce the interfacial surface tension at the interface) adds another intriguing level of complexity. It reduces the interfacial tension to the point that it no longer drives the system to a macroscopic phase separation. Many of the proteins and lipid components in biological membranes might partition into such domain interfaces. In this regard, some Ras isoforms have been revealed to partition preferentially into the interface boundaries of phase segregated model membranes, thus validating the concept of surfactancy.[125] Within the framework of such studies, it may be possible to begin understanding the diversity in the chemical composition of biological membranes, making surfactancy at the domain boundaries a likely possibility. For Ras proteins, the vitality of rafts is highly crucial, as it has been postulated that H-Ras protein signals from raft-like domains, whereas the K-Ras protein

---

[122] Roy, S., Luetterforst, R., Harding, A., Apolloni, A., Etheridge, M., Stang, E., Rolls, B., Hancock, J.F., and Parton, R.G. **(1999)**. Dominant-negative caveolin inhibits H-Ras function by disrupting cholesterol-rich plasma membrane domains. *Nat. Cell. Biol. 1*, 98–105.

[123] Sheets, E.D., Petersen, N.O., Holowka, D., and Baird, B. **(1999)**. Interactions between the high affinity IgE receptor and detergent-resistant membranes measured by image cross-correlation spectroscopy. *Biophys. J. 76*, A391–A391.

[124] Rietveld, A., Neutz, S., Simons, K., and Eaton, S. **(1999)**. Association of sterol- and glycosylphosphatidylinositol-linked proteins with Drosophila raft lipid microdomains. *J. Biol. Chem. 274*, 12049–12054.

[125] Weise, K., Triola, G., Brunsveld, L., Waldmann, H., and Winter, R. **(2009)**. Influence of the Lipidation Motif on the Partitioning and Association of N-Ras in Model Membrane Subdomains. *J. Am. Chem. Soc. 131*, 1557–1564.

from the non-raft domains.[122] Thus, the model biomembrane systems with three or more lipid components, which mimic closely the matrix of the heterogeneous biological membranes, provide an ideal platform for studying the interactions of signalling proteins with lipid membrane. In this regard, Winter and colleagues have explored the phase behaviour of a three component neutral raft-like lipid mixture, revealing the coexistence of l_o and l_d phases over a wide temperature-pressure phase space.[110,114]

What was missing was a corresponding anionic model raft-like membrane system. The motivation for generating such a model membrane system stems from the evidence that the cytoplasmic face of the PM in mammals concentrates anionic phospholipids.[126] Increasing evidence of anionic lipid species enriched in the lateral domains within the cytoplasmic face of the PM, added to the impetus.[127-128] Therefore, in the present study, the structure and phase behaviour of an anionic raft-like membrane system comprising the lipids DOPC, DOPG, DPPC, DPPG and cholesterol were explored. Fourier-transform infrared (FTIR) spectroscopy was employed, since IR parameters like frequency, width, intensity, shape, and band splitting are known to be sensitive to the structural and dynamical properties of membrane lipids.[129-132]

Other biophysical techniques also provided valuable details and are discussed briefly.

---

[126] Williamson, P., and Schlegel, R.A. **(1994)**. Back and Forth - the Regulation and Function of Transbilayer Phospholipid Movement in Eukaryotic Cells. *Mol. Mem. Biol. 11*, 199–216.

[127] Glaser, M., Wanaski, S., Buser, C.A., Boguslavsky, V., Rashidzada, W., Morris, A., Rebecchi, M., Scarlata, S.F., *et al.* **(1996)**. Myristoylated alanine-rich C kinase substrate (MARCKS) produces reversible inhibition of phospholipase C by sequestering phosphatidylinositol 4,5-bisphosphate in lateral domains. *J. Biol. Chem. 271*, 26187–26193.

[128] Pike, L.J., and Casey, L. **(1996)**. Localization and turnover of phosphatidylinositol 4,5-bisphosphate in caveolin-enriched membrane domains. *J. Biol. Chem. 271*, 26453–26456.

[129] Wong, P.T.T., Siminovitch, D.J., and Mantsch, H.H. **(1988)**. Structure and Properties of Model Membranes - New Knowledge from High-Pressure Vibrational Spectroscopy. *Biochim. Biophys. Acta*. *947*, 139–171.

[130] Mendelsohn, R., Davies, M.A., Brauner, J.W., Schuster, H.F., and Dluhy, R.A. **(1989)**. Quantitative-Determination of Conformational Disorder in the Acyl Chains of Phospholipid-Bilayers by Infrared-Spectroscopy. *Biochemistry 28*, 8934–8939.

[131] Davies, M.A., Schuster, H.F., Brauner, J.W., and Mendelsohn, R. **(1990)**. Effects of Cholesterol on Conformational Disorder in Dipalmitoylphosphatidylcholine Bilayers - a Quantitative IR Study of the Depth Dependence. *Biochemistry*. *29*, 4368–4373.

[132] Reis, O., and Winter, R. **(1998)**. Pressure and temperature effects on conformational and hydrational properties of lamellar and bicontinuous cubic phases of the fully hydrated monoacylglyceride monoelaidin - A Fourier transform infrared spectroscopy study using the diamond anvil technique. *Langmuir 14*, 2903–2909.

3.3 Results and Discussion

3.3.1 Temperature- and pressure-dependent FTIR measurements

The assigned internal vibrational modes of lipid acyl chains, giving rise to vibrational bands in the spectral region between 2800 and 3000 cm^{-1}, were used to monitor the conformational order of acyl chains.[133] The CH_2 antisymmetric ($\tilde{\nu}_{asym}(CH_2)$: 2916 - 2925 cm^{-1}) and the symmetric mode ($\tilde{\nu}_{sym}(CH_2)$: 2849 - 2855 cm^{-1}) are the strongest lipid vibrational bands observed in the IR spectrum. These vibrational modes are conformation sensitive and respond to pressure- and temperature-induced changes in the *trans-gauche* ratio and the number of kinks in the acyl chains. [134] Figure 3.3 shows the $\tilde{\nu}_{sym}(CH_2)$ stretching frequency of the five component anionic lipid mixture as a function of temperature. The maximum of the $\tilde{\nu}_{sym}(CH_2)$ vibrational mode increased linearly from 5 °C to 13 °C, and this range was assigned to a solid-ordered phase, s_o. At high temperatures, a change in the slope indicated the formation of a new phase that extended up to about 20 ^oC, and was attributed to a $s_o + l_o$ phase coexistence region.

[133] Senak, L., Davies, M.A., and Mendelsohn, R. **(1991)**. A Quantitative Ir Study of Hydrocarbon Chain Conformation in Alkanes and Phospholipids - CH_2 Wagging Modes in Disordered Bilayer and HII Phases. *J. Phys. Chem. 95*, 2565–2571.
[134] Puehse, M., Jeworrek, C., and Winter, R. **(2008)**. The temperature-pressure phase diagram of a DPPC-ergosterol fungal model membrane - a SAXS and FTIR spectroscopy study. *Chem. Phys. Lipids 152*, 57–63.

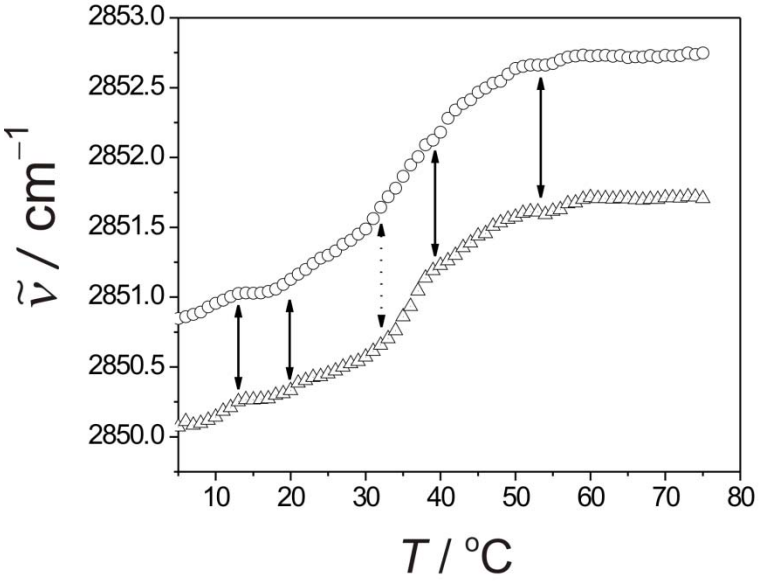

Figure 3.3: Temperature dependence of the symmetric CH_2-stretching vibration in the lipid hydrocarbon chains. FTIR intensity of the CH_2 symmetric stretching vibration in the anionic raft-like membrane (DOPC: DOPG: DPPC: DPPG:Chol 20:5:45:5:25 (molar ratio)) at a concentration of 10 mg / mL and 1 bar**.** Black arrows indicate change in the slopes and were assigned to the onset of phase transformations.

The following phase region exhibited a pronounced sigmoidal shape and was assigned to the liquid-disordered domains. This constituted a three-phase coexistence region, $l_d + l_o + s_o$.[134] The minor change in the slope at ~34 °C (shown by a dashed arrow in Fig. 3.3) was—in agreement with the Gibbs phase rule—assigned to the transition from the three-phase coexistence region ($l_d + l_o + s_o$) to a two-phase coexistence region ($l_d + l_o$). This was accompanied by the disappearance of s_o domains. The decrease in the slope at ~40 °C indicated a transition to a phase region, probably of the type $l_d + l_o'$, where the amount of ordered phase (l_o') was drastically decreased. Distinguishing between the different ordered phases (l_o or l_o') with different lipid compositions was difficult, however. Nevertheless, their existence, or even coexistence, is possible in agreement with the thermodynamics of the five-component lipid mixture. The same was reflected by the minor changes observed in the slopes. When the overall fluid phase was reached, the slope decreased and eventually

levelled off around 55 °C. The assignment of the phases obtained herewith was also substantiated by other techniques (for details, see ref. 135).

Figure 3.4 shows the pressure dependence of the $\tilde{\nu}_{sym}(CH_2)$ stretching vibration at different temperatures. At 5 °C, the $\tilde{\nu}_{sym}(CH_2)$ exhibited a discontinuity at ~7.5 kbar, indicative of a phase transition. Thereafter, it increased linearly with pressure, a behaviour generally observed within one-phase regions.[129-132] This phase transition may be attributed to a transition from one type of s_o phase to another phase, s_o', with different packing and hydration properties. It can probably also be induced by the freezing of bulk D_2O, which occurs in the same pressure-temperature range. At 20 °C, the observed phase changes evident by the discontinuities appearing at about 760 bar and 4 kbar are most likely due to the $l_o + l_d + s_o$ to $l_o + s_o$ to s_o transitions. At 35 °C, the slope changes observed at about 1.5 kbar, 8 kbar, and 10.5 kbar were assigned to the following phase transitions: from a two-phase region ($l_d + l_o$) to a three-phase region ($l_d + l_o + s_o$), a $s_o + l_o$ phase, and finally to a completely solid-ordered phase, respectively. At 45 °C, discontinuities of $\tilde{\nu}_{sym}(CH_2)$observed at ~2.3 kbar, 6 kbar and 15 kbar, were attributed to the transitions to $l_d + l_o$, $l_o + l_d + s_o$ and $l_o + s_o$ phase coexistence regions, respectively. Starting in the all-disordered (l_d) phase at T = 60 °C, phase changes were observed at 4.2 kbar, 7.5 kbar and 15 kbar. They were due to phase transitions to $l_d + l_o'$, $l_d + l_o$, and $l_o + l_d + s_o$ phase regions, respectively. To verify the phase assignment and help establish the tentative pressure-temperature (p, T) phase diagram of the given lipid mixture, complementary thermodynamic, AFM, and fluorescence spectroscopic measurements were also carried out.[135]

[135] Kapoor, S., Werkmuller, A., Denter, C., Zhai, Y., Markgraf, J., Weise, K., Opitz, N., and Winter, R. **(2011)**. Temperature-pressure phase diagram of a heterogeneous anionic model biomembrane system: Results from a combined calorimetry, spectroscopy and microscopy study. *Biochim. Biophys.Acta, Biomembr. 1808*, 1187–1195.

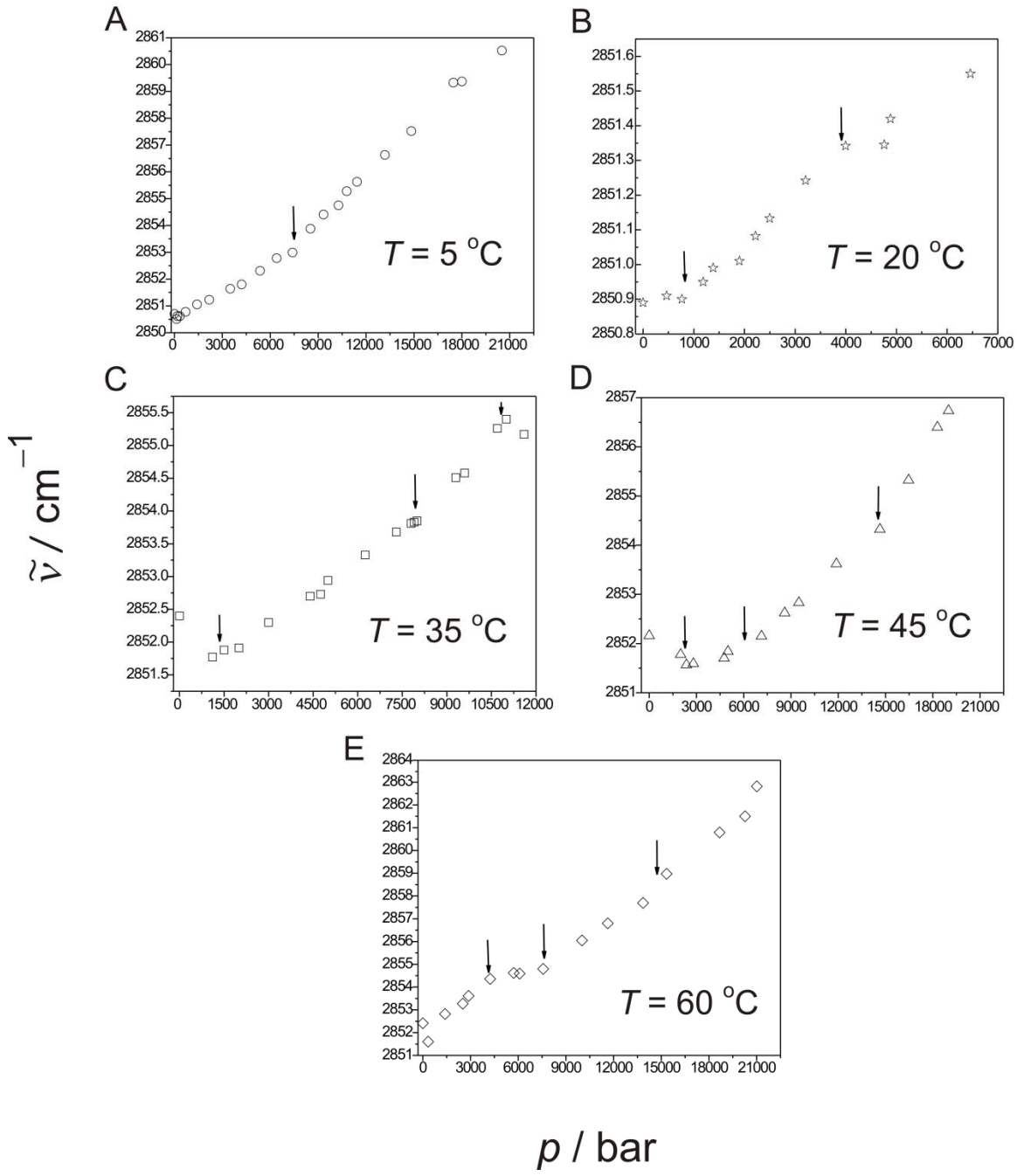

Figure 3.4: Pressure dependence of the symmetric CH_2-stretching vibration in the lipid hydrocarbon chains. FTIR intensity of the CH_2 symmetric stretching vibration in the anionic raft-like membrane (DOPC: DOPG: DPPC: DPPG:Chol 20:5:45:5:25 (molar ratio)) at a concentration of 30 mg / mL and at (A) 5 ˚C, (B) 20 ˚C, (C) 35 ˚C, (D) 45 ˚C and (E) 60 ˚C**.** Black arrows indicate changes in the slopes and were assigned to the onset of phase transformations.

3.3.2 Visualisation of phase coexistence in the anionic raft-like membrane system

To visualise the phase segregation in the anionic raft-like model membrane system and to substantiate the phase assignment, fluorescence microscopy experiments were conducted at varying temperatures in the range of 12 ˚C to 55 ˚C. [These experiments were performed by Christian Denter, Master's Student in the laboratory of Prof. Dr. Roland Winter]. Two model dye markers were used: *N*-Rh-DHPE (red) and BODIPY-Cholesterol (green). *N*-Rh DHPE is known to partition exclusively in the fluid or l_d parts of the lipid membrane whereas BODIPY-Chol (due to the presence of cholesterol modification) typically partitions nearly completely into the raft or l_o regions. As can be seen in Figure 3.4 (**A-C**), incorporation of 10 to 20 mol % PG (a range within the physiological limits) led to the segregation of the lipid mixture into l_o and l_d domains. Furthermore, AFM analysis [carried out by Dr. Katrin Weise, Post-doctoral fellow in the laboratory of Prof. Dr. Roland Winter] on a solid supported homogeneous lipid bilayer on mica revealed isolated islands of fluid l_d domains in a coherent pool of raft-like (l_o) protruding phases, at room temperature (Fig. 3.4 **D**). The thickness of the lipid bilayer was ~ 5.2 nm for the l_o phase and ~ 4.0 nm for the l_d phase. The coexisting phases were clearly distinguishable by a height difference of ~1.0 nm, in agreement with previously published results.[125]

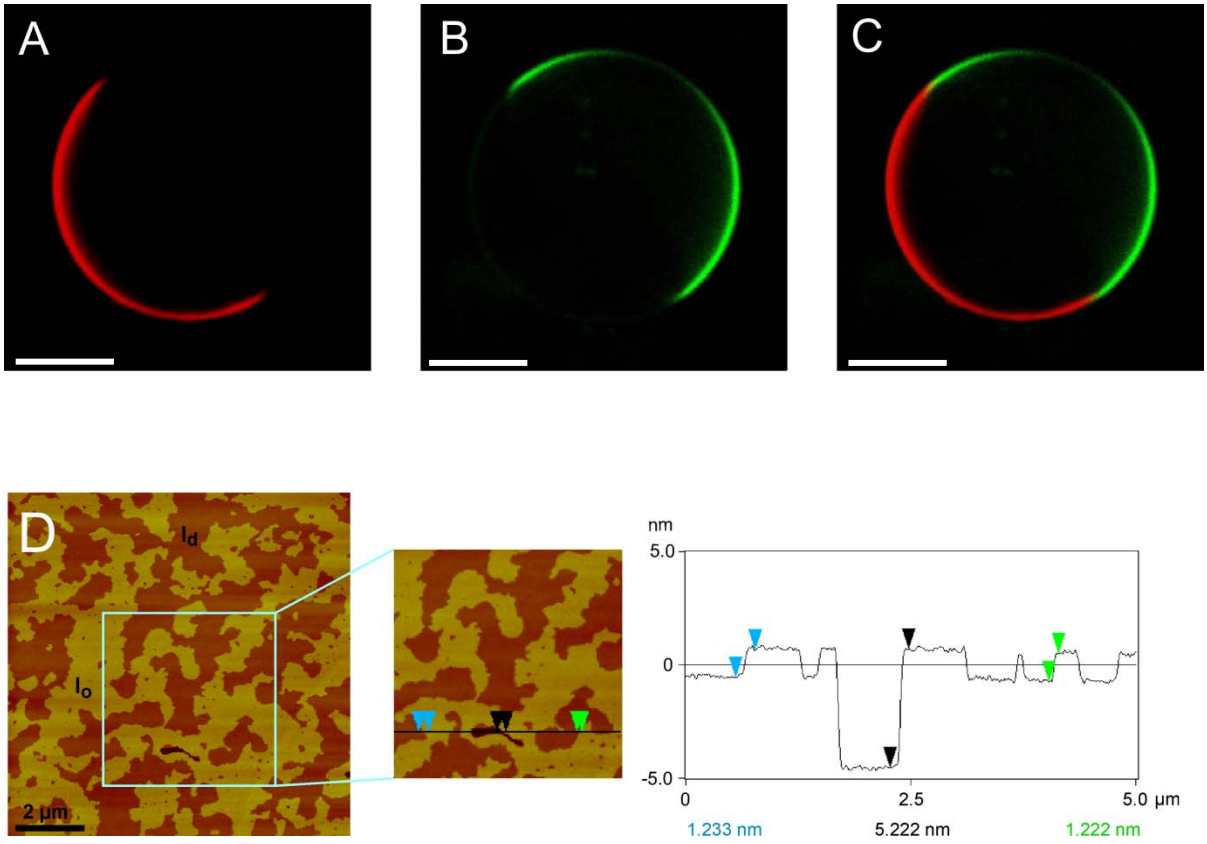

Figure 3.5: Visualisation of raft and non-raft lipid domains. Top panel shows fluorescence microscopy section images of GUVs (DOPC: DOPG: DPPC: DPPG:Chol 15:10:40:10:25 (molar ratio)) at 25 ˚C and 1 bar (**A-C**). Fluorescence intensity was collected in two channels: The red channel detected *N*-Rh-PE (l_d phase marker) and the green channel detected BODIPY-cholesterol (l_o phase marker). The scale bar is 10 µM. The bottom panel is the AFM image of the corresponding lipid membrane on mica at room temperature (D), showing a homogenous lipid bilayer with coexisting domains of l_d and l_o (left-hand side). The concomitant section profile (right-hand side) of the AFM image indicates the vertical distances between a pair of arrows (blue and green: height difference of the l_o/l_d phases, and black: thickness of the l_o domains).

3.3.3 Tentative pressure-temperature phase diagram of the model anionic raft-like membrane system

The (*p, T*) phase diagram of this mixture, based on all the results and with a special emphasis on FTIR spectroscopy, is displayed in Figure 3.5.

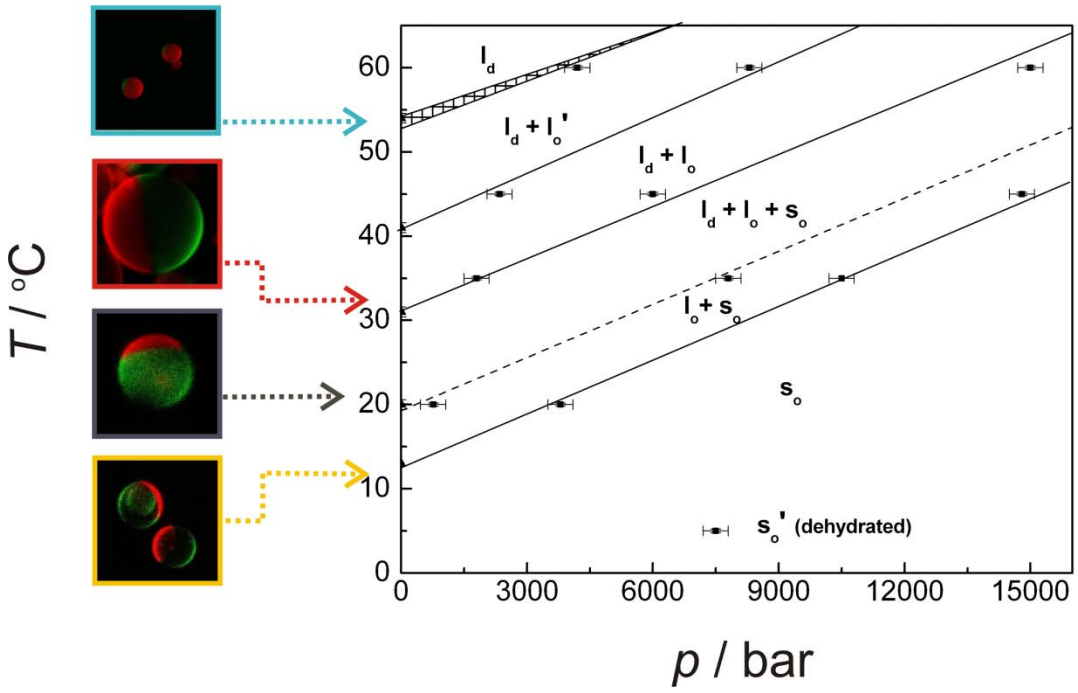

Figure 3.5: Tentative pressure-temperature phase diagram of the anionic raft-like membrane system. The *p*-*T* phase diagram has been compiled by using mainly temperature (■) and pressure (▲) dependent FTIR data, with critical insights from other biophysical techniques. The error bar shows uncertainties in the temperature and pressure determinations.

A series of pressure-induced phase transitions in the temperature range from 5 to 65 °C under pressures ranging from 1 bar up to 16 kbar can be observed. The $l_d \rightarrow l_d + l_o$, $l_d + l_o \rightarrow l_d + l_o + s_o$, $l_d + l_o + s_o \rightarrow l_o + s_o$, and $l_o + s_o \rightarrow s_o$ phase boundaries exhibited transition slopes of ~ 3 °C/kbar. In comparison to the phase transitions of pure one-component lipid systems, these transition slopes are much smaller, which can be explained as follows. From the Clapeyron equation, ($dT/dp = T\Delta V/\Delta H$) the slope of the *p*, *T*-transition is governed by the relative volume and enthalpy (or entropy) changes at the transition. As $\Delta V < 0$ for pressure-induced transitions, ΔH and hence also ΔS ($= \Delta H/T_{tr}$; T_{tr} is the phase transition temperature) are positive. The smaller slope can thus be attributed to smaller ΔV values, which is expected as the ordered-to-fluid transition occurs through various phases with increasing fluidity and conformational disorder. Such rather smooth changes in volumetric and enthalpic properties

are also reflected in the smooth temperature dependence of the differential scanning and pressure perturbation calorimetric data, found elsewhere.[135]

Briefly, the excess heat capacity $C_p(T)$ revealed a broad transition peak between the starting temperature and ~50 °C, with a maximum at 32 °C. The temperature dependence of the coefficient of thermal expansion (α) exhibited a similar shape. Moreover, the integral over the $C_p(T)$ and $\alpha(T)$ curves yielded the overall enthalpy and volume changes respectively, indicating a strong correlation between the thermodynamic properties of the system. Specifically, the system underwent major conformational changes such as *trans-gauche* isomerisation and kink formation in the acyl chains, with increasing temperatures. Thus, the observed broad peak best corresponds to a transition from the $l_o + l_d + s_o$ three-phase region to the $l_o + l_d$ two-phase coexistence region, reaching an overall l_d phase state above 51-53 °C, in agreement with the infrared data. In addition, a similar result was observed by the behaviour of adiabatic compressibility $K_S(T)$ vs. temperature. Furthermore, the fluorescence spectroscopy measurements performed using LAURDAN—a dye that partitions into the hydrocarbon region of the lipid bilayer—as a conformation sensitive probe confirmed the smooth transitional behaviour of the lipid phase transitions. The overall transition is broad due to a continuous increase of the liquid-disordered lipid domains with increasing temperatures, which is connected to a gradual increase in fluidity and conformational disorder. Finally, in a parallel but independent study, raft-like heterogeneity was also deduced within the monolayers of the same anionic lipid mixture, investigated by x-ray reflectivity and grazing incidence x-ray diffraction (GIXD).

3.4 Summary and Outlook

In the present study, thermal and barometric changes in the phase behaviour of the model anionic raft-like lipid mixture comprising of DOPC/DOPG/DPPC/DPPG/Chol (20:5:45:5:25, molar ratio) were delineated. This lipid mixture represents one of the best model systems of natural membranes, representing the anionic features coupled with raft-like heterogeneity in a reasonable fashion. Furthermore, compared with the previously studied neutral raft-like mixture (DOPC/DPPC/Chol), the *p*, *T*-phase diagram is—in accordance with the Gibbs phase rule—more complex.[110] The phase sequence as a function of temperature and pressure

is largely similar, however. It displays the most biologically relevant phase mimicking the raft-like lateral phase separation and heterogeneity of natural membranes, extending over a rather wide temperature and pressure range. Knowledge of the phase diagram of this model biomembrane system not only allows the studies of membrane-associated signalling proteins (as the natural membranes consist of up to ~ 50 % of membrane-associated proteins) implicated with electrostatic contributions, but also biological processes encountered under extreme environmental conditions.

Liquid-liquid immiscibility in lipid bilayers and monolayers has been elucidated by studies on such model membrane systems of complex lipid mixtures. Within the framework of these, it is possible to explore why such a high diversity of lipids is maintained in the natural membranes. The results obtained correlate well with the postulated and experimentally proven existence of sphingolipids–cholesterol rafts, and provide support to the viability of liquid-liquid immiscibility in cell membranes. However, one parameter still requires elaborate attention, if the model membrane systems are to mimic natural membranes in an authentic fashion—the lipid asymmetry. Since the inner and outer leaflet of cellular membranes differ considerably based on lipid composition, it becomes important to generate and study the bilaterally asymmetric model membrane systems. Work towards this end has already been initiated using lipid flipasses (enzymes that catalyse flip-flop of lipids, across the bilayer) to construct asymmetric lipid membranes and has opened up exciting vistas for the future.

IV

RAS ISOFORM-SPECIFIC MEMBRANE INTERACTIONS

ONE GOAL, TWO PLAYERS*

* The work of the present study has been published and subsequently reprinted in parts (some figures) from Kapoor, S., Weise, K., Erlkamp, M., Triola, G., Waldmann, H., and Winter, R. **(2012)**.The role of G-domain orientation and nucleotide state on the Ras isoform-specific membrane interaction. *Eur. Biophys. J.* 41, 801-813, with kind permission from Springer Science and Business Media.

* And from Weise, K., Kapoor, S., Denter, C., Nickolaus, J., Opitz, N., Kock, S., Triola, G., Hermann, A., Waldmann, H., and Winter, R. **(2011)**. Membrane-mediated induction and sorting of K-Ras microdomain signalling platforms. *J. Am. Chem. Soc*. *133*, 880-887. Copyright (2011) American Chemical Society.

4.1 Background

4.1.1 Overlapping or Distinctive Functions of Ras Proteins: The Early View

The functional diversity of the Ras superfamily is highly perplexing. Despite the structurally conserved G-domain allowing the Ras isoforms to maintain common biochemical properties, they show remarkable specificity and affinity to their individual downstream binding partners.[136-137] Due to a strong sequence identity among the Ras isoforms coupled with shared effector utilisation, there has been a common perception that the Ras isoforms are functionally redundant.[138] Many findings have corroborated this general acceptance. For instance, a genetic study on mice showed that N-Ras homozygous mutant mice (i.e. no expression of N-Ras proteins) grow normally. This strongly signified the functions of N-Ras for cell proliferation and survival as dispensable.[139] In another study on yeasts—which harbour two *ras genes* (namely, Ras1 and Ras2)—it was revealed that lack of one of the two *genes* had no effect on spore viability.[140] These and many related studies have reinforced the perception that multiple *ras genes* are indeed functionally redundant. However, the face of functional aspects of Ras proteins changed its shape when another line of evidence suggested otherwise. First, proper credit was given to the evidence that although Ras proteins are ubiquitously expressed in the cells, the mRNA levels vary, depending on the tissue type.[13] The simplest interpretation of this observation is that there is selective expression of N-, H- and K-Ras proteins in different tissues. Second, oncogenic forms of each *ras gene* are associated with specific cell and tissue types; K-Ras mutations account for nearly 50% and 90% of colon and pancreatic cancers, respectively, with N-/H-Ras mutations being extremely uncommon among these cell types. Conversely, in acute leukaemia N-Ras is credited with

136 Colicelli, J. **(2004)**. Human RAS superfamily proteins and related GTPases. *Sci. STKE 2004*, RE13.
137 Wennerberg, K., Rossman, K.L., and Der, C.J. **(2005)**. The Ras superfamily at a glance. *J. Cell. Sci. 118*, 843–846.
138 Rodriguez-Viciana, P., Sabatier, C., and McCormick, F. **(2004)**. Signaling specificity by Ras family GTPases is determined by the full spectrum of effectors they regulate. *Mol. Cell. Biol. 24*, 4943–4954.
139 Umanoff, H., Edelmann, W., Pellicer, A., and Kucherlapati, R. **(1995)**. The murine N-ras gene is not essential for growth and development. *Proc. Natl. Acad. Sci. U.S.A. 92*, 1709–1713.
140 Kataoka, T., Powers, S., Mcgill, C., Fasano, O., Strathern, J., Broach, J., and Wigler, M. **(1984)**. Genetic-Analysis of Yeast Ras1 and Ras2 Genes. *Cell 37*, 437–445.

25 %, without any contributions from the other Ras isoforms.[141] Third, K-Ras, but not N- and H-Ras, functions are indispensable for normal growth and development in mice; absence of K-Ras proteins induces embryonic lethality. No such adverse effects were caused by N-Ras and H-Ras null mutations.[142-143] These contradictory studies left the scientists pondering the complexity encoded by Ras isoforms and have led to a surge in Ras-related research to find the possible key determinants of their functional diversity.

4.1.2 Isoform Specificity in the Context of the Hypervariable Region (HVR) and the G-Domain

4.1.2.1 Role of the hypervariable region: Studies on cells and model systems

Ras proteins harbour a mechanistically preserved G-domain along with a highly divergent HVR, which contains membrane-targeting signals. An important consequence of the HVR divergence is that the lipid anchors of the Ras isoforms are distinct, with only palmitoylation stoichiometric difference in N- and H-Ras. This implies that the PM localisation of each isoform can be different. Thus, the biological differences could arise as a result of the different membrane localisations. The foremost reason for the differential Ras localisation is the alternative trafficking pathways mediated, in part, by the targeting signals in the HVR region exposing Ras to the different pools of effectors and regulators.[144] As mentioned above, all the newly synthesised Ras proteins are farnesylated in the cytosol and subsequently targeted to the endoplasmic reticulum. At the ER, the next steps of posttranslational modification, namely, the AAX proteolysis, carboxymethylation of the farnesylated cysteine, and finally the palmitoylation of H- and N-Ras HVR regions are carried out. Following this, the H- and N-Ras proteins travel by the classical secretory

[141] Bos, J.L. **(1989b)**. ras oncogenes in human cancer: a review. *Cancer Res. 49*, 4682–4689.
[142] Koera, K., Nakamura, K., Nakao, K., Miyoshi, J., Toyoshima, K., Hatta, T., Otani, H., Aiba, A., and Katsuki, M. **(1997)**. K-ras is essential for the development of the mouse embryo. *Oncogene 15*, 1151–1159.
[143] Johnson, L., Greenbaum, D., Cichowski, K., Mercer, K., Murphy, E., Schmitt, E., Bronson, R.T., Umanoff, H., Edelmann, W., Kucherlapati, R*., et al.* **(1997)**. K-ras is an essential gene in the mouse with partial functional overlap with N-ras. *Genes Dev. 11*, 2468–2481.
[144] Casar, B., Arozarena, I., Sanz-Moreno, V., Pinto, A., Agudo-Ibanez, L., Marais, R., Lewis, R.E., Berciano, M.T., and Crespo, P. **(2009)**. Ras Subcellular Localization Defines Extracellular Signal-Regulated Kinase 1 and 2 Substrate Specificity through Distinct Utilization of Scaffold Proteins. *Mol. Cell. Biol. 29*, 1338–1353.

pathways to the PM from the ER *en route* of the Golgi.[145-146] The vesicular pathway is further supported by experiments employing Brefeldin A (BFA), a well-known inhibitor of the secretory pathway, only to observe the ER accumulation of these proteins. On the other hand, K-Ras takes an uncharacterised Golgi independent route to the PM, probably by a simple diffusional mechanism (unaffected by Brefeldin A). Recent studies have further contributed to the diffusion-mediated K-Ras trafficking by shining light on a potential prenyl-binding protein (PDEδ), which increases the kinetics of K-Ras trapping at the PM.[147] Mutations in the second targeting signals in the HVR of Ras isoforms have shown that these proteins accumulate at the ER, undoubtedly implying that the HVR dominates the trafficking pathway Ras isoforms undertake.[145-146] As mentioned before, one possible consequence of the variable trafficking pathways is that the PM localisation of Ras isoforms might be different as well. This hypothesis is now well substantiated by studies providing direct insights into the Ras microlocalisation on the PM, as discussed below.

The plasma membrane is a complex, dynamic, non-equilibrium system with thousands of lipid types and a plethora of membrane-bound proteins. It is not well-mixed at any length and time scale, leading to a non-random distribution of lipids and proteins within the membrane layer generating heterogeneities termed "rafts" (**cf. Ch. 3, section 3.1.2**).[115-118] Disrupting lipid rafts by chemically depleting PM cholesterol selectively inhibits H-Ras, but not K-Ras mediated Raf-1 activation.[122] Thus, K-Ras is targeted to the disordered parts of the PM, whereas H-Ras is confined to the raft domains, where its integrity is maintained by the cholesterol levels. A combination of electron and light microscopy together with biochemical experiments corroborated the above mentioned claims and led to discover a complex behaviour in H-Ras: H-Ras microlocalisation is modulated by the bound nucleotide state.[148] It was demonstrated that H-Ras·GDP is predominantly confined to the raft-like domains in the membrane, and the H-Ras·GTP to the non-raft (bulk) membrane. Mutational analysis of the H-Ras HVR brought to forefront the importance of the HVR domain in maintaining the

[145] Choy, E., Chiu, V.K., Silletti, J., Feoktistov, M., Morimoto, T., Michaelson, D., Ivanov, I.E. and Philips, M.R. **(1999)**. Endomembrane trafficking of Ras: The CAAX motif targets proteins to the ER and Golgi. *Cell 98*, 69–80.

[146] Apolloni, A., Prior, I.A., Lindsay, M., Parton, R.G., and Hancock, J.F. **(2000)**. H-ras but not K-ras traffics to the plasma membrane through the exocytic pathway. *Mol. Cell. Biol. 20*, 2475–2487.

[147] Chandra, A., Grecco, H.E., Pisupati, V., Perera, D., Cassidy, L., Skoulidis, F., Ismail, S.A., Hedberg, C., Hanzal-Bayer, M., Venkitaraman, A.R., *et al.* **(2012)**. The GDI-like solubilizing factor PDE delta sustains the spatial organization and signalling of Ras family proteins. *Nat. Cell Biol. 14*, 148–158.

equilibrium of nucleotide modulated H-Ras localisation between raft and non-raft domains.[148] For N-Ras, the *PM localisation* has not yet been established. Coupling the differential lateral segregation of Ras isoforms to biologically distinct outputs, is the propensity of various effector proteins to be recruited to the distinct PM domains.

Though the *in vivo* studies clearly revealed the localisations of H- and K-Ras, the molecular details on the lateral segregation (especially for N-Ras) still remains an arduous task to observe in cells. In this regard, *in vitro* studies on the partitioning of Ras proteins into heterogeneous model membranes have elucidated a molecular mechanism for the isoform-specific Ras signalling.[125,149] The results have mainly been obtained by time-lapse tapping-mode atomic force (AFM) and confocal fluorescence microscopy on the fully functional and lipidated N-Ras and K-Ras proteins, which were either GDP- or GTP-bound. Both proteins were shown to partition nearly exclusively into the liquid-disordered (l_d) parts of the membranes, independent of the nucleotide state and membrane composition. However, their spatial distribution differed considerably (Fig. 4.1). For N-Ras, a time-dependent diffusion and subsequent clustering in the l_o/l_d phase boundary regions was observed,[125] while formation of new protein-enriched domains inside a fluid environment was detected for K-Ras.[149] This Ras isoform-specific membrane microdomain formation or nanoclustering was attributed to two different determinants. First was the minimisation of the line energy tension at the boundary between the coexisting domains (**cf. Ch. 3, section 3.1.2**), achieved via expulsion of N-Ras proteins to the interfacial region (i.e. the surfactancy effect). Second was the electrostatic-based lipid sorting mechanism, involving interactions between the positively charged lysines of K-Ras and the phospholipid headgroups.

[148] Prior, I.A., Harding, A., Yan, J., Sluimer, J., Parton, R.G., and Hancock, J.F. **(2001)**. GTP-dependent segregation of H-ras from lipid rafts is required for biological activity. *Nat. Cell Biol. 3*, 368–375.

[149] Weise, K., Kapoor, S., Denter, C., Nikolaus, J., Opitz, N., Koch, S., Triola, G., Herrmann, A., Waldmann, H., and Winter, R. **(2011)**. Membrane-Mediated Induction and Sorting of K-Ras Microdomain Signaling Platforms. *J. Am. Chem. Soc. 133*, 880–887.

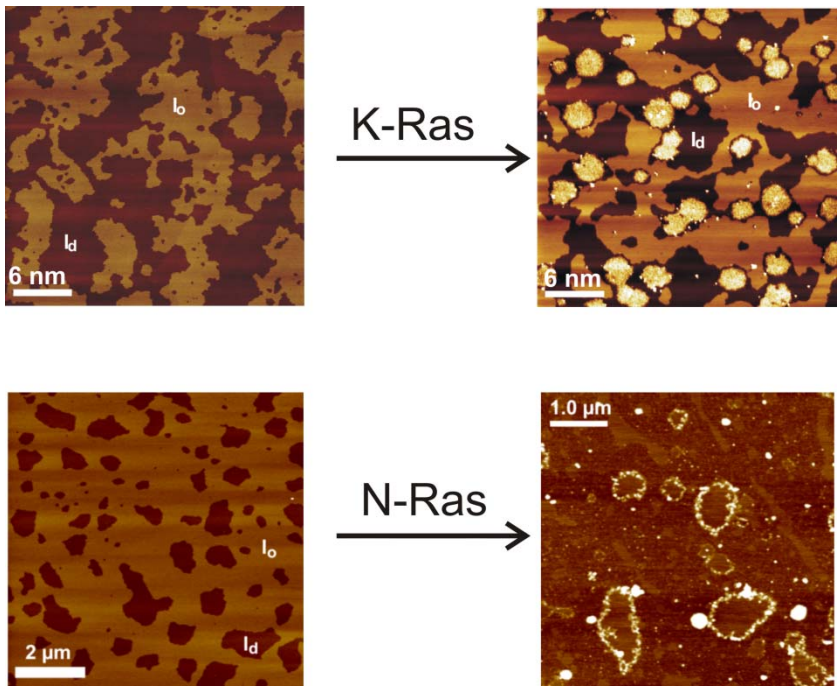

Figure 4.1: Ras isoform-specific distinct signalling platforms. Atomic force microscopy images of a lipid bilayer separated into protruding liquid-ordered (l_o) domains within the background of dark liquid-disordered (l_d) domains, before and after addition of the respective Ras proteins. Modified and reproduced with permission from ref. 125 (Copyright 2011@ American Chemical Society) and ref. 149 (Copyright 2012@ American Chemical Society).

4.1.2.2 Role of the homologous G-domain in the Ras isoform-specific signalling

Ras signalling is heavily influenced by binding to specific effectors, many of which are also membrane-associated. Thus, any minor change in the structure, orientation, localisation, and regulation of these proteins would be reflected in a differential binding to various effectors/regulators inducing diverse biological responses. Earlier studies revealed the Ras isoforms to vary in their ability to activate Raf-1 (a well-known effector protein for Ras) and PI3-K, *in vivo*. Whereas K-Ras4B was found to be a more potent activator of Raf-1, H-Ras dominated the activation of PI3-K.[150-151] At that time, the only reason for such a differential activation of the effector proteins was the different PM localisation of the Ras. Furthermore,

[150] Yan, J., Roy, S., Apolloni, A., Lane, A., and Hancock, J.F. **(1998)**. Ras isoforms vary in their ability to activate Raf-1 and phosphoinositide 3-kinase. *J. Biol. Chem. 273*, 24052–24056.
[151] Voice, J.K., Klemke, R.L., Le, A., and Jackson, J.H. **(1999)**. Four human Ras homologs differ in their abilities to activate Raf-1, induce transformation, and stimulate cell motility. *J. Biol. Chem.. 274*, 17164-17170.

it was postulated that the clusters each Ras isoform generates at the PM vary in their content of membrane-associated factors required for Raf-1 and PI3-K activation. Details regarding Raf-1 activation can be found elsewhere.[152-153] Nevertheless, these studies opened a platform to probe beyond the HVR, and almost 10 years later, work towards it started. Now, there is the general acceptance that the highly homologous G-domain can also contribute to the well-known biological diversity of Ras isoforms. Initial insights were gained through molecular dynamic simulations and validated by Förster resonance energy transfer (FRET) and fluorescence lifetime imaging microscopy (FLIM), combined with an ERK activation and PC12 differentiation cell assay.[154] It was demonstrated that the GDP-bound H-Ras membrane anchorage is predominantly stabilised via two basic residues in the HVR (R161 and R164) in conjunction with the adjacent membrane anchor.[155] GTP-loading triggers structural rearrangements in the classical Switch regions I and II to operate a novel "Switch III" mechanism.[156] Switch III, which consists of a β2–β3 loop and helix α5, pulls the residues R169 and K170 off the membrane, thus enabling the G-domain to rotate. Basic residues in helix-α4 bind to the membrane phospholipids and stabilise the new orientation. The GTP-orientation was shown to be recognised by the cytosolic galectin-1 protein, which upon binding to Ras, provided further stability.[157] An interesting outcome of these studies was the recognition of the Ras G-domain by the Ras-binding-domain of Raf and PI3-K. This provides new insight into studies on the differential activation of Raf-1 and PI3-K by Ras isoforms, suggesting *that the orientations of the respective Ras isoform are indeed different at the membrane interface*.

---

[152] Morrison, D.K., and Cutler, R.E. **(1997)**. The complexity of Raf-1 regulation. *Curr. Opin. Cell Biol*. *9*, 174–179.

[153] Clark, G.J., Drugan, J.K., Rossmann, K.L., Carpenter, J.W., RogersGraham, K., Fu, H., Der, C.J., and Campbell, S.L. **(1997)**. 14-3-3 zeta negatively regulates Raf-1 activity by interactions with the Raf-1 cysteine-rich domain. *J. Biol. Chem. 272*, 20990–20993.

[154] Abankwa, D., Gorfe, A.A., Inder, K., and Hancock, J.F. **(2010)**. Ras membrane orientation and nanodomain localization generate isoform diversity. *Proc. Natl. Acad. Sci. U.S.A. 107*, 1130–1135.

[155] Gorfe, A.A., Hanzal-Bayer, M., Abankwa, D., Hancock, J.F., and McCammon, J.A. **(2007)**. Structure and dynamics of the full-length lipid-modified H-ras protein in a 1,2-dimyristoylglycero-3-phosphocholine bilayer. *J. Med. Chem. 50*, 674–684.

[156] Abankwa, D., Hanzal-Bayer, M., Ariotti, N., Plowman, S.J., Gorfe, A.A., Parton, R.G., McCammon, J.A., and Hancock, J.F. **(2008b)**. A novel switch region regulates H-ras membrane orientation and signal output. *EMBO J. 27*, 727–735.

[157] Abankwa, D., Gorfe, A.A., and Hancock, J.F. **(2008a)**. Mechanisms of Ras membrane organization and signaling: Ras on a rocker. *Cell Cycle 7*, 2667–2673.

4.2 Motivation and Objectives

As all of the Ras isoforms share almost 90-100 % sequence identity in the G-domain, the nucleotide modulated orientation specificity of H-Ras might also apply to N-Ras and K-Ras. However, in all the *in vivo* studies discussed, the observed differences in phenotypic behaviour of RasG12V (constitutively activated Ras form) compared with mutants (alanine substitutions in α4 and HVR) were correlated to differential signalling activities, through plausible changes in the G-domain orientations. Possible conformational changes induced by the mutations themselves make the analysis quite cumbersome, especially when coupled with the potential signalling artefacts associated with tagging and the over-expression of proteins. Thus, the biophysical characterisation of the structural and conformational changes in the Ras proteins, upon incorporation into heterogeneous model membrane systems, was critical. In this regard, direct detection of the conformational and orientational changes in the G-domain of fully lipidated, wild-type Ras isoforms upon membrane binding were hitherto unknown and inspired the present work. For this endeavour, different advanced variants of infrared spectroscopy were employed.

4.3 Results and Discussion

4.3.1 Structural differences between the bulk and membrane-bound Ras proteins

4.3.1.1 Solution structure of the Ras isoforms

Ras proteins belong to the α/β family of proteins, due to the specific arrangement of the helices and sheets (Fig. 1.2, cf. **Ch. 1**). Conformational differences are induced not only by the bound nucleotide states[24,158], but are also expected upon membrane binding. The first step in this study was to explore the structural aspect of Ras proteins in the bulk solution. Figure 4.2 shows the secondary structure contributions of the N- and K-Ras proteins in their different nucleotide-bound states obtained by curve-fitting of the normalised amide-I' FTIR

[158] Brunger, A.T., Milburn, M.V., Tong, L., deVos, A.M., Jancarik, J., Yamaizumi, Z., Nishimura, S., Ohtsuka, E., and Kim, S.H. **(1990)**. Crystal structure of an active form of RAS protein, a complex of a GTP analog and the HRAS p21 catalytic domain. *Proc. Natl. Acad. Sci. U.S.A. 87*, 4849–4853.

band (**explained in detail in Appendix Sections 9.1 and 9.2**). The results revealed on average 25–30 %; α-helices and 35–39 %; β-sheets, and matched reasonably well with the previously determined crystal structures and NMR data.[24,158] Some minor observed differences were expected due to the unknown transition dipole moments of the various conformers and the absence of the HVR in the X-ray or NMR studies. Despite the limitation of IR spectroscopy in generating atomic structural details, it is one of the best methods to study relative secondary structural changes in the system. Temporal changes in the secondary structures showed, within the experimental error of a few percentages, no significant structural changes (i.e. partial unfolding). The case study of the N-Ras protein in the GDP- and GTP-bound forms can be seen in Figure 4.3.

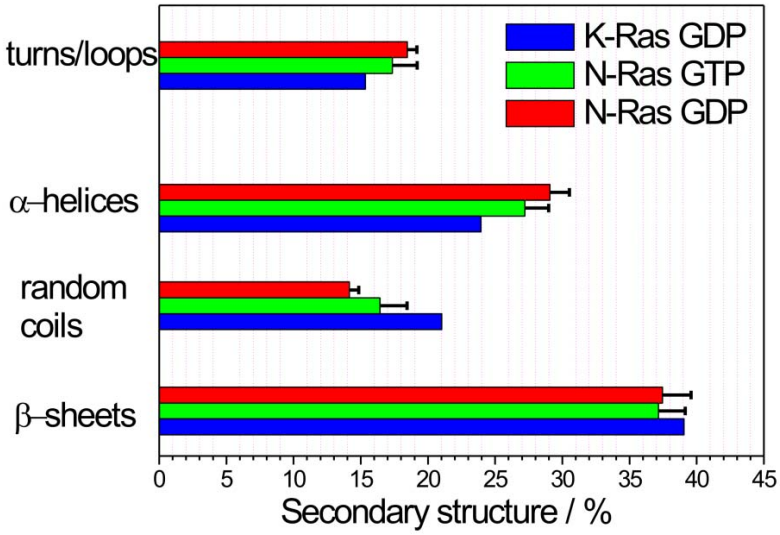

Figure 4.2: Secondary structure of the Ras isoforms in bulk solution. Secondary structure of N- and K-Ras bound to different nucleotide states, at 25 ˚C and 1 atm. These numbers were obtained by curve-fitting of the normalised FTIR amide-I' spectra. The concentration of each protein was 0.233 mM. The results are the average of three experiments, except for K-Ras.

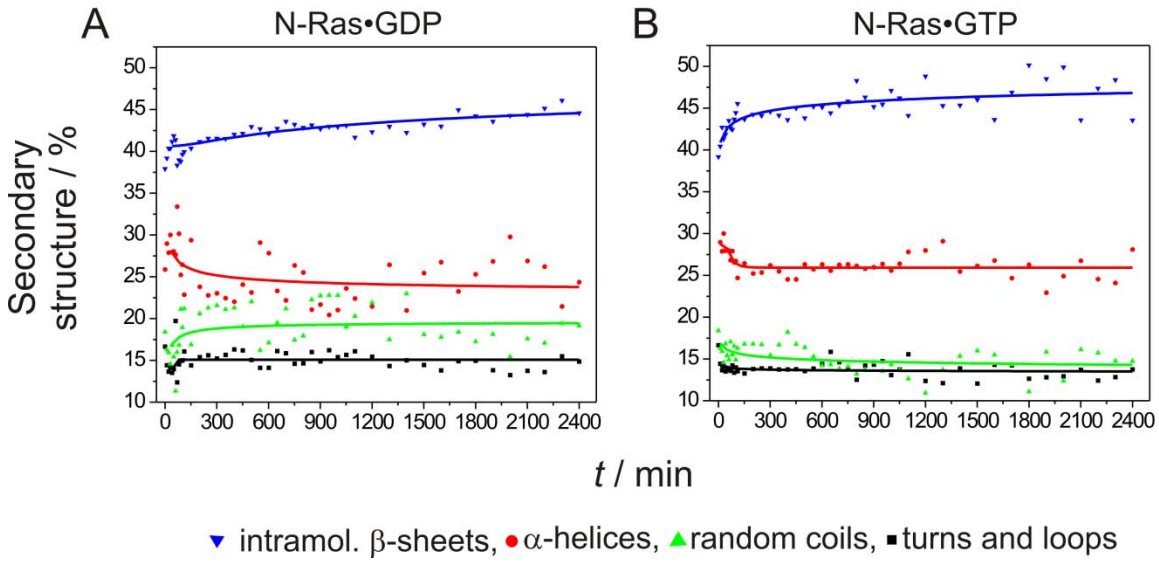

Figure 4.3: Temporal changes in the secondary structure of N-Ras. Secondary structure changes in the (**A**) GDP-bound and (**B**) GTP-bound N-Ras in the bulk solution, at 25 ˚C and 1 atm. These numbers were obtained by curve-fitting of the normalised FTIR amide-I' spectra. The concentration of each protein was 0.233 mM. Within experimental error of a few %, no unfolding or aggregation was observed embarking the high protein stability under the investigated time period. The secondary structure values with time have been fitted with a Sigmoidal distribution function (Weibull-2) using the software, Origin Pro 7.0. The goodness of the fit was in the range of 98.2-99.8 %.

A high structural stability of the Ras proteins under the investigated time frame was demonstrated, making them suitable for techniques probing into the Ras conformational cycles and interactions with membrane/other partners.

4.3.1.2 Ras–membrane interactions: The structural aspects

Following the study in bulk solution, interaction of N-Ras and K-Ras isoforms were also explored upon insertion into neutral and anionic raft-like lipid vesicles, respectively. Figure 4.4 upon comparison with Figure 4.2 revealed no marked structural changes (such as (partial) unfolding or aggregation) in the proteins upon membrane binding, which stands in accordance with the previously published report.[159] Absence of such changes is likely to arise from the evolutionary optimised function and interaction of these signalling proteins with the

[159] Guldenhaupt, J., Adiguzel, Y., Kuhlmann, J., Waldmann, H., Kotting, C., and Gerwert, K. **(2008)**. Secondary structure of lipidated Ras bound to a lipid bilayer. *FEBS J. 275*, 5910–5918.

cell membranes.[160] This interaction is the prerequisite for correct signalling, as Ras is activated only in its membrane-bound form.

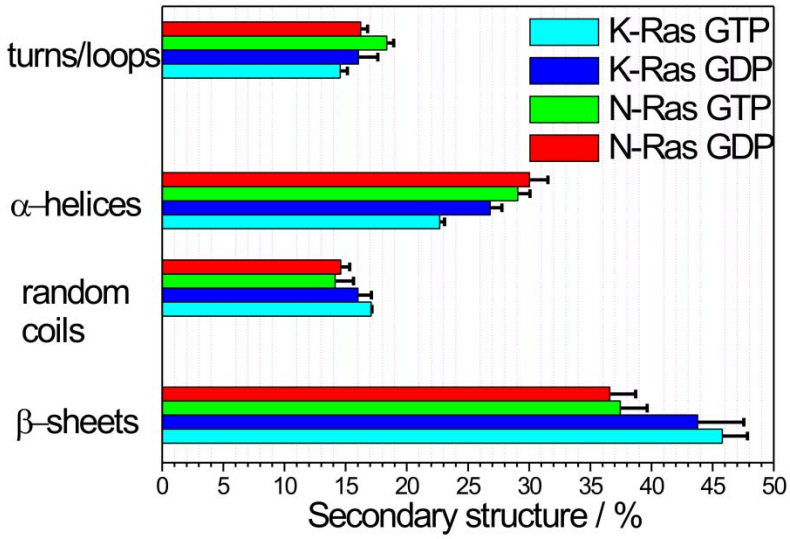

Figure 4.4: Effect of membrane binding on the structural aspect of Ras proteins. Secondary structure of N- and K-Ras bound to the different nucleotide states, upon insertion into and subsequent interaction with the neutral (DOPC:DPPC:Chol::25:50:25; molar ratio) and the anionic (DOPC:DOPG:DPPC:DPPG:Chol::20:5:45:5:25; molar ratio) raft-like lipid vesicles, respectively, at 25 ˚C and 1 atm. The concentration of each protein was 0.233 mM, with a protein to lipid ratio of 1:100. These numbers were obtained by curve-fitting of the normalised FTIR amide-I' spectra. The results are an average of two or three experiments.

The time evolution of the secondary structural changes in the membrane-bound forms of Ras proteins also ruled out dramatic effects such as (partial) unfolding or aggregation upon membrane interaction within the investigated time (Fig. 4.5).

[160] Rojas, A.M., Fuentes, G., Rausell, A., and Valencia, A. **(2012).** The Ras protein superfamily: evolutionary tree and role of conserved amino acids. *J. Cell Biol. 196*, 189–201.

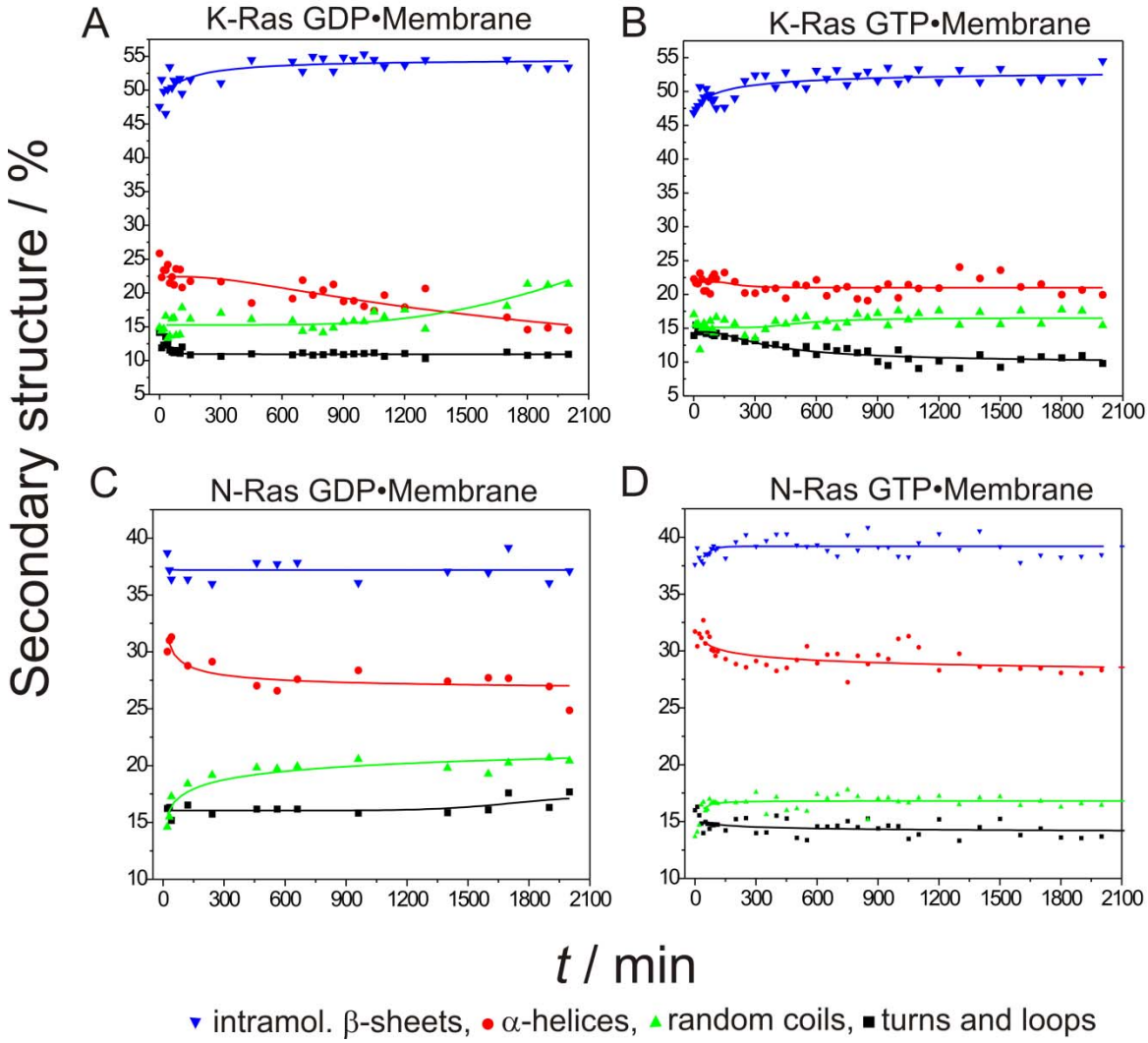

Figure 4.5: Time dependence of the effect of membrane binding on the secondary structure of Ras proteins. Secondary structure of (**A, B**) K-Ras and (**C, D**) N-Ras, bound to the different nucleotide states upon insertion into and subsequent interaction with the anionic (DOPC: DOPG: DPPC: DPPG:Chol 20:5:45:5:25 (molar ratio)) and the neutral (DOPC: DPPC: Chol 25:50:25 (molar ratio)) raft-like lipid vesicles, respectively, at 25 ˚C and 1 atm. The concentration of each protein was 0.233 mM, with a protein to lipid ratio of 1:100. These numbers were obtained by curve-fitting of the normalised FTIR amide-I' spectra. The secondary structure values with time have been fitted with a Sigmoidal distribution function (Weibull-2) using the software, Origin Pro 7.0. The goodness of the fit was in the range of 99.2-99.6 %.

However, closer inspection of the second derivative amide-I' spectra suggested a minor, yet significant effect of membrane-binding. The spectra were obtained by derivatising the normalised FTIR amide-I' band by a second order and 6th degree polynomial. The minima observed represent particular secondary structural elements given by their respective

wavenumbers.[63] The coupling of the secondary structural motif to a particular wavenumber became the basis for studying the interaction of these motifs with the membrane; any interaction that would reduce the electron density on the amide carbonyl bond would shift the band minima towards a lower wavenumber, due to a smaller force constant of the carbonyl bond.

Figure 4.6 shows the time evolution of the second derivative amide-I' spectra (at selected time points) for (**A**) the GDP-bound inactive K-Ras and (**B**) the GTP-bound active K-Ras in the presence of the anionic raft-like lipid vesicles. Infrared subbands (at t = 1.5 min) for the inactive K-Ras protein (**A**) were observed at 1673 (turns/loops), 1661 (helices), 1648 (unordered structures/random coils), 1637 (intramolecular β-sheets) cm^{-1}, and a shoulder at 1626 (intramolecular β-sheets) cm^{-1}. They gradually changed with time to 1671, 1654/1656 (helices), 1648, 1637, and 1626 cm^{-1}. The band at 1661 cm^{-1} and 1654/56 cm^{-1} decreased and increased with time, respectively, as shown in Figure 4.6 (**A**). On the other hand, the active K-Ras protein (at t = 1.5 min) exhibited infrared subbands at 1672 (turns/loops), 1662 (helices), 1651 (helices and unordered structures), 1637 cm^{-1} (intramolecular β-sheets), and a shoulder at 1626 cm^{-1} (intramolecular β-sheets). They remained almost constant with time. In comparison, GDP-bound K-Ras in the bulk solution (**C**) revealed infrared subbands at 1672 (turns/loops), 1659/61 (helices), 1647 (unordered structures), 1637 cm^{-1} (intramolecular β-sheets), and a shoulder at 1626 cm^{-1} (intramolecular β-sheets).

The IR band position for the GTP-bound K-Ras protein observed at 1651 cm^{-1} was at the border line for both the unordered and the helical structures. As such, the assignment of the bands and the subsequent fitting were done in a manner similar to that of the GDP-bound form, both in the bulk solution and in the membrane-bound forms. This minimised errors while dealing with the temporal changes in the secondary structural elements.

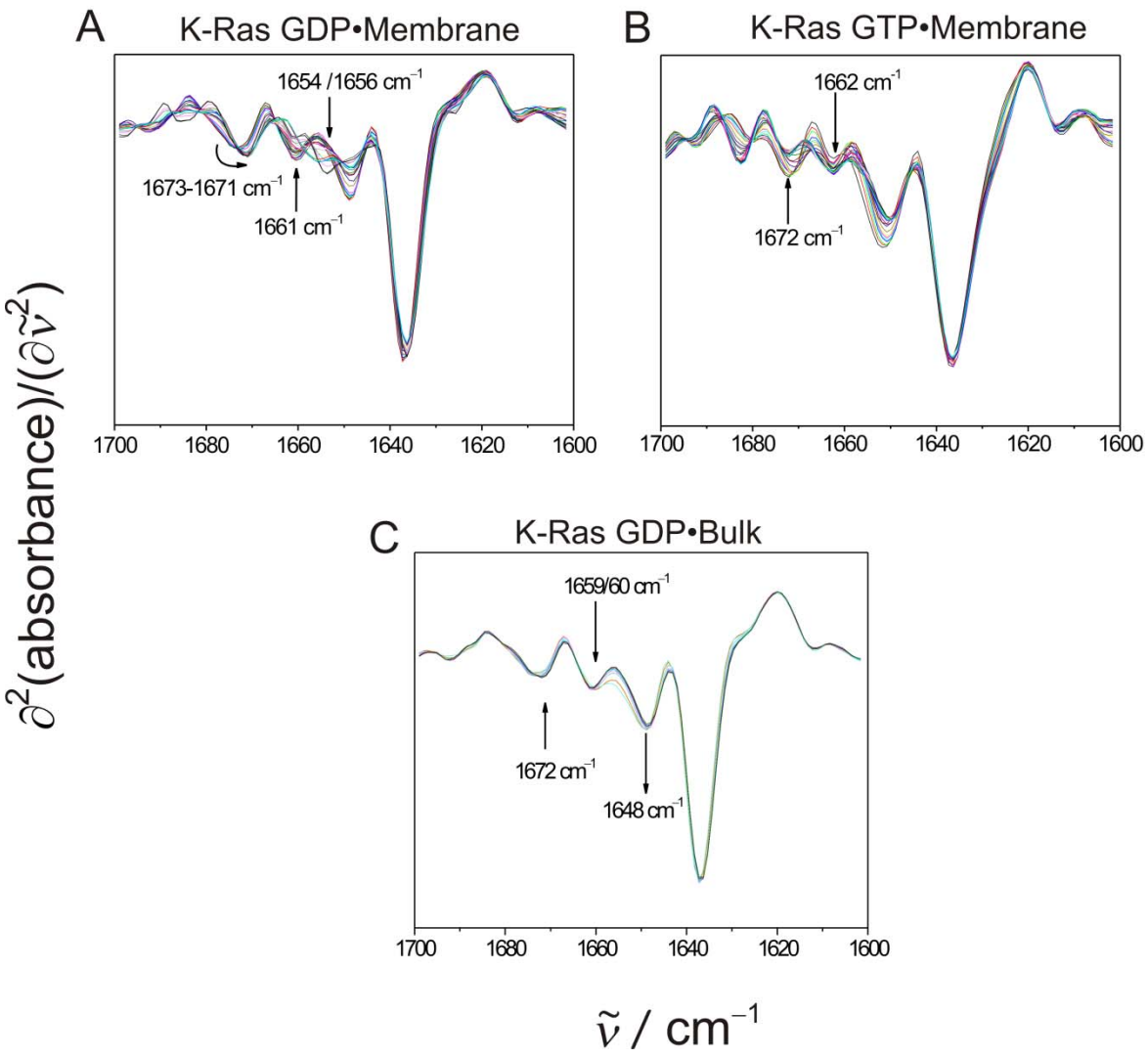

Figure 4.6: Second derivative FTIR analysis of K-Ras–membrane interactions. Second derivative FTIR spectra for the (**A**) GDP-bound and (B) GTP-bound K-Ras in the presence of the anionic raft-like ((DOPC: DOPG: DPPC: DPPG:Chol 20:5:45:5:25 (molar ratio)) lipid vesicles, at 25 ˚C and 1 atm. (**C**.) GDP-bound K-Ras protein in the bulk solution was taken as the control. The concentration of each protein was 0.233 mM, with a protein to lipid ratio of 1:100 in **A** and **B**.

A higher wavenumber for the α-helical subband (1659-1662 cm^{-1}), both in bulk solution and the membrane-bound forms, argues for highly flexible helices.[77] With time, a red shift for the α-helix structures was attained (at 1656 cm^{-1}), but only for the *membrane-bound inactive protein.* This suggests a strong interaction between the membrane and certain motifs in the helical parts of the protein. A similar shift was obtained for the turns and loops (1673 to 1671

cm^{-1}), again signifying a stronger interaction of these distinct protein regions with the membrane. In contrast, no red shifts of the IR bands were observed *for the membrane-bound active K-Ras protein.* Thus, the helices remained flexible and only weakly interacted with the membrane. The nucleotide-dependent differences in the proteins can be explained by the recently proposed "balance model" of Ras–membrane interaction, depicted below in a schematic representation.[154]

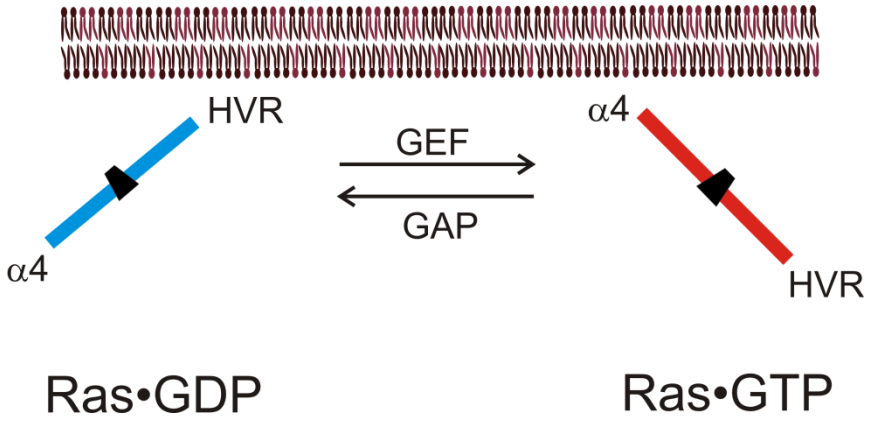

Figure 4.7: Balance model of Ras–membrane interactions. In the inactive (GDP-bound) form, H-Ras interacts with the membrane with its HVR residues and N-terminal residues. Nucleotide exchange induces orientational changes in the Switch III (α-5 and β2-β3 loop), followed by further orientational changes in helix α4. This leads to an interaction of the α4/5 helices with the membrane. K-Ras is proposed to adopt an inverted interaction profile.[154]

According to this model, modulation of the Ras G-domain–PM orientation by the α4-helix and the HVR switches H-Ras in the nucleotide-dependent manner between the two modes of membrane binding. In the same study, MD simulations on the membrane-bound K-Ras4B, along with biochemical experiments on a K-Ras4B-like chimera, suggested an inverted interaction profile for the K-Ras G-domain, compared with H-Ras. Thereby, *K-Ras4B proteins interact with the membrane mainly through their HVR, in both the nucleotide-bound states*.[154] The membrane interaction is further bolstered due to a favourable electrostatic interaction between the positively charged contiguous stretch of six lysines in the HVR of K-Ras and the negatively charged membrane lipids in the PM (and also in the anionic model raft-like system, employed here). As the HVR is located next to the C-terminus α5 helix, the membrane interaction is expected to have a much stronger effect on the α5 helix, compared

with other helices in the K-Ras protein. According to the balance model, the K-Ras–membrane interaction should be nucleotide independent; however, the experimental data from this study connote a nucleotide-dependent membrane interaction (Fig. 4.6). To this end, Abraham et al. illustrated dynamical changes in the K-Ras HVR mediated by the bound nucleotide state.[161] According to their study, the HVR is sequestered by the catalytic G-domain in the GDP-bound form of K-Ras which prevents its interaction with calmodulin (CaM), a highly specific interaction partner for only the K-Ras4B Ras isoform. GTP loading induces a conformational change in the catalytic domain that decouples the HVR from the G-domain and enables it to stably interact with CaM (Fig. 4.8).

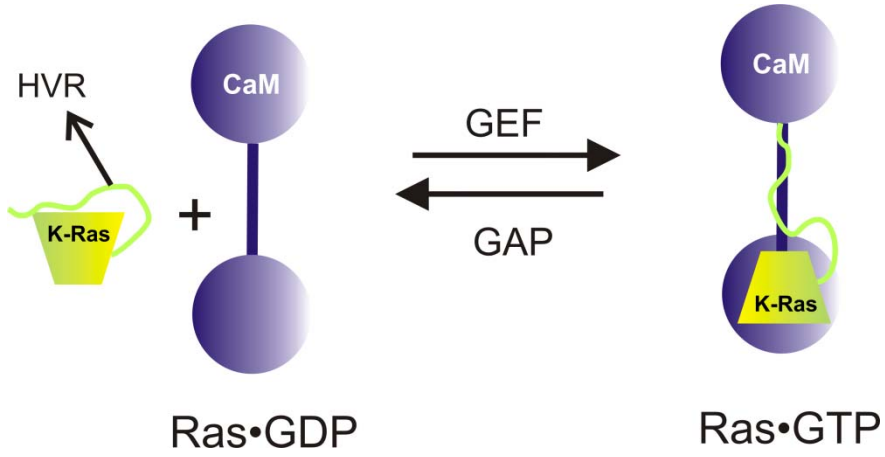

Figure 4.8: Proposed mechanism for the nucleotide-induced sequestering of HVR in K-Ras. The HVR of K-Ras in the inactive state strongly interacts with the protein core, which is decoupled from the G-domain upon nucleotide exchange.

In lieu of this model, coupling of the HVR to the G-domain in the GDP-bound K-Ras would bring the entire catalytic domain closer to the membrane. Thus, a plausible interaction of at least the α5 helix with the membrane could be foreseen. The observed red shifts of the α-helical subbands in the inactive K-Ras protein upon membrane interaction (Fig. 4.6 **A**), bear out this interpretation. On the other hand, GTP binding to K-Ras would release the HVR to interact freely with the membrane through its polylysine residues. As a direct consequence, the rest of the protein would be expected to remain more flexible than the GDP-bound

[161] Abraham, S.J., Nolet, R.P., Calvert, R.J., Anderson, L.M., and Gaponenko, V. **(2009)**. The hypervariable region of K-Ras4B is responsible for its specific interactions with calmodulin. *Biochemistry 48*, 7575–7583.

counterpart. This hypothesis agrees well with the experimental results for the GTP-bound K-Ras: a weaker membrane interaction with no red shifts for the α-helical structures, implying flexible structures (Fig. 4.6 **B**). Furthermore, the high flexibility in the membrane-bound active K-Ras protein, exemplified in this study, is also supported by the recent findings of Lukman et al.[162] They demonstrated via MD simulations, that the wild type 'active' K-Ras protein is more flexible and dynamic than other Ras isoforms. At last, the changes discussed above might very well be the manifestation of the orientational changes modulated by the nucleotide state, a model already verified for H-Ras.[154] Since, the transmission FTIR spectroscopy is unable to provide any information on orientational aspects of the Ras–membrane interaction, this project was followed up by additional IR techniques, which is discussed in the forthcoming sections.

For the membrane-bound N-Ras proteins in both nucleotide states, no such effect in the second derivative FTIR with time was observed, certainly none that fell within the accuracy of the method. But as suggested by the "balance model", the α5 and/or α4 helices in N-Ras in the GTP-bound form might also significantly interact with the membrane. For these reasons, pursuing this system became the option most likely, to reveal any orientational changes that occur upon membrane insertion, thereby supporting or refuting the studies/theories done/proposed before.

4.3.2 Orientational changes modulated by the specific Ras isoform and the nucleotide state

4.3.2.1 Study on a solid supported lipid bilayer

Polarized ATR-FTIR spectroscopy was applied to examine relative changes in the orientations of the Ras isoforms in their different nucleotide states, upon insertion into the heterogeneous raft bilayers. This is a well-established technique for determining the secondary structure and orientation of proteins at lipid interfaces.[80,163] A qualitative orientational analysis was performed by comparing the dichroic spectra, which in turn

[162] Lukman, S., Grant, B.J., Gorfe, A.A., Grant, G.H., and McCammon, J.A. **(2010)**. The Distinct Conformational Dynamics of K-Ras and H-Ras A59G. *PLoS Comput. Biol. 6*.
[163] Marsh, D. **(1999)**. Quantitation of secondary structure in ATR infrared spectroscopy. *Biophys. J. 77*, 2630–2637.

was obtained by use of Eq. (14) of Chapter 2 (**cf. Ch.2, Polarized ATR-FTIR Spectroscopy**). In the absence of any preferred orientation, a straight horizontal line is expected. An upward deviation in the dichroism spectrum indicates the respective transition dipole moment to position nearly perpendicular to the membrane plane. Conversely, a downward deviation indicates a preferred alignment of the dipole in the membrane plane. Since for the α-helix the amide-I transition dipole is along the helix long axis,[164] negative and positive deviations imply a parallel or perpendicular alignment of the α-helix along the membrane plane/interface, respectively.

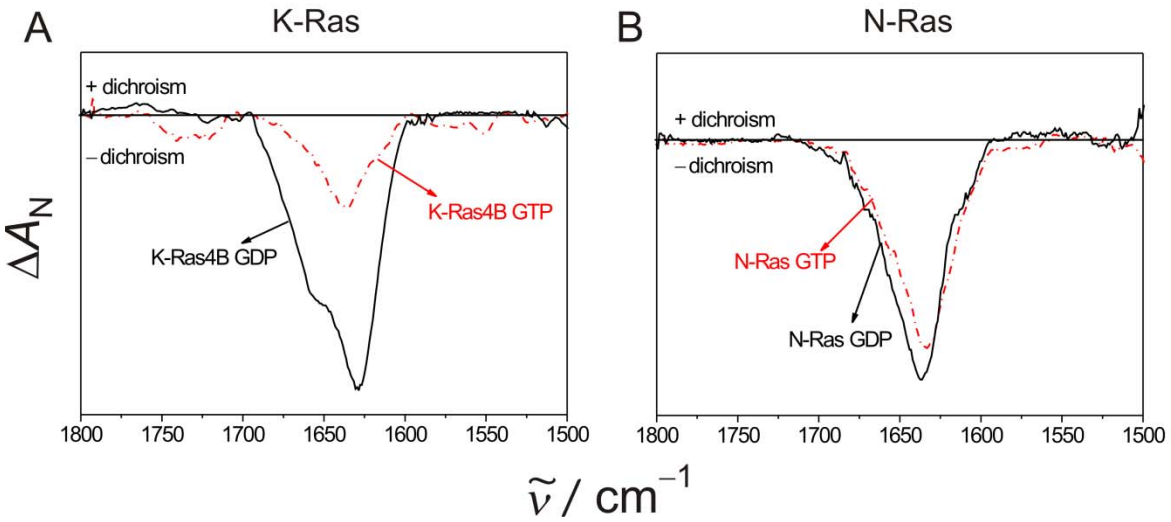

Figure 4.9: Orientational difference among the membrane-bound Ras isoforms. Polarized ATR-FTIR dichroic spectra for (**A**) GDP/GTP-bound K-Ras and (**B**) GDP/GTP-bound N-Ras in the presence of the anionic (DOPC: DOPG: DPPC: DPPG:Chol 20:5:45:5:25 (molar ratio)) and the neutral (DOPC:DPPC:Chol 25:50:25 (molar ratio)) raft-like lipid bilayer, respectively, at 25 ˚C and 1 atm. The protein concentrations were 4 μM each. Δ*A* stands for the difference in the absorbance of the spectra collected with the p- and s-polarized infrared light. The subscript N stands for the Δ*A* normalised to the sum of the amide-I' band area collected with the p- and s-polarized infrared light.

Figure 4.9 (**A**) shows the dichroic spectra for K-Ras proteins in their different nucleotide states, bound to the anionic raft-like lipid bilayer. The observed changes in the magnitude of the dichroism imply the following: Typically, the active K-Ras protein attains a random orientation due to the lower magnitude of dichroism, presumably due to many preferred orientations of the G-domain. Conversly, the inactive form displays a stronger

[164] Marsh, D., Muller, M., and Schmitt, F.J. **(2000)**. Orientation of the infrared transition moments for an alpha-helix. *Biophys. J. 78*, 2499–2510.

dichroism, a fact that presents an argument for a preferred fixed orientation at the membrane interface. Negative deviations in the helix region (1648-1665 cm^{-1}) of the amide-I′ band indicate that the majority of the helices are essentially parallel to the membrane bilayer. Furthermore, the frequency of the amide-I′ band maxima connote the differences in the strength of membrane interaction, being stronger for the GDP-bound K-Ras (maxima at ~ 1629 cm^{-1}) compared with the GTP-bound K-Ras (maxima at ~ 1635 cm^{-1}). These results were validated by the findings of *Lukman et al.*[162], as discussed above. To further enlighten whether the orientational sensitivity is a generic phenomenon in Ras proteins, the dichroic spectra of N-Ras (Fig. 4.9 **B**) in the presence of the neutral raft-like membrane bilayer were recorded. From the negative deviations in the helix region (1648-1665 cm^{-1}) of the amide-I′ band, it can be inferred that N-Ras in both nucleotide-bound states embraces preferred orientations having helices parallel to the membrane interface. Surprisingly, in contrast to the K-Ras proteins, a stronger membrane interaction was demonstrated for the GTP-bound N-Ras (maxima at ~ 1633.5 cm^{-1}) compared with the GDP-bound N-Ras (maxima at ~ 1637 cm^{-1}).

In addition, the dichroic spectra presented in Figure 4.9 were obtained using the R_{iso}^{ATR} value from the lipid ester band. To rule out any possibility of artefact due to improper subtraction, the dichroic spectra were also calculated using R_{iso}^{ATR} values of 1.712 and 2.01 from the thin- and thick-film models, respectively. As can be seen in Figure 4.10, the qualitative results remains the same, i.e. *the negative deviations in the helix region for both proteins in their respective nucleotide-bound forms confirm that the majority of protein helices are lying parallel to the membrane surface, with different magnitudes of negative dichroism, however.* Strikingly, an important observation made at this point dealt with the dichroic spectra for the lipid IR bands. The transition dipole of the lipid CH_2 symmetric/asymmetric stretching is perpendicular to the lipid acyl chains. Thus, a negative deviation in the dichroic spectra would refer to the CH_2 transition dipole lying parallel to the Ge interface. In other words, the lipid acyl chains would be perpendicular to the Ge interface, as expected for a stable and correct bilayer deposition on a solid support. For all the systems used in this study, a negative deviation for the CH_2 band was obtained by using R_{iso}^{ATR} from the lipid ester band. Surprisingly, this was not the case when

the R_{iso}^{ATR} value especially from the thin-film approximation was applied (Fig. 4.11). An observed positive deviation denoted that the lipid acyl chains were parallel to the Ge crystal. Based on this observation, appropriate models should be tested thoroughly before reaching any conclusions regarding the orientation of proteins and lipids under investigation.

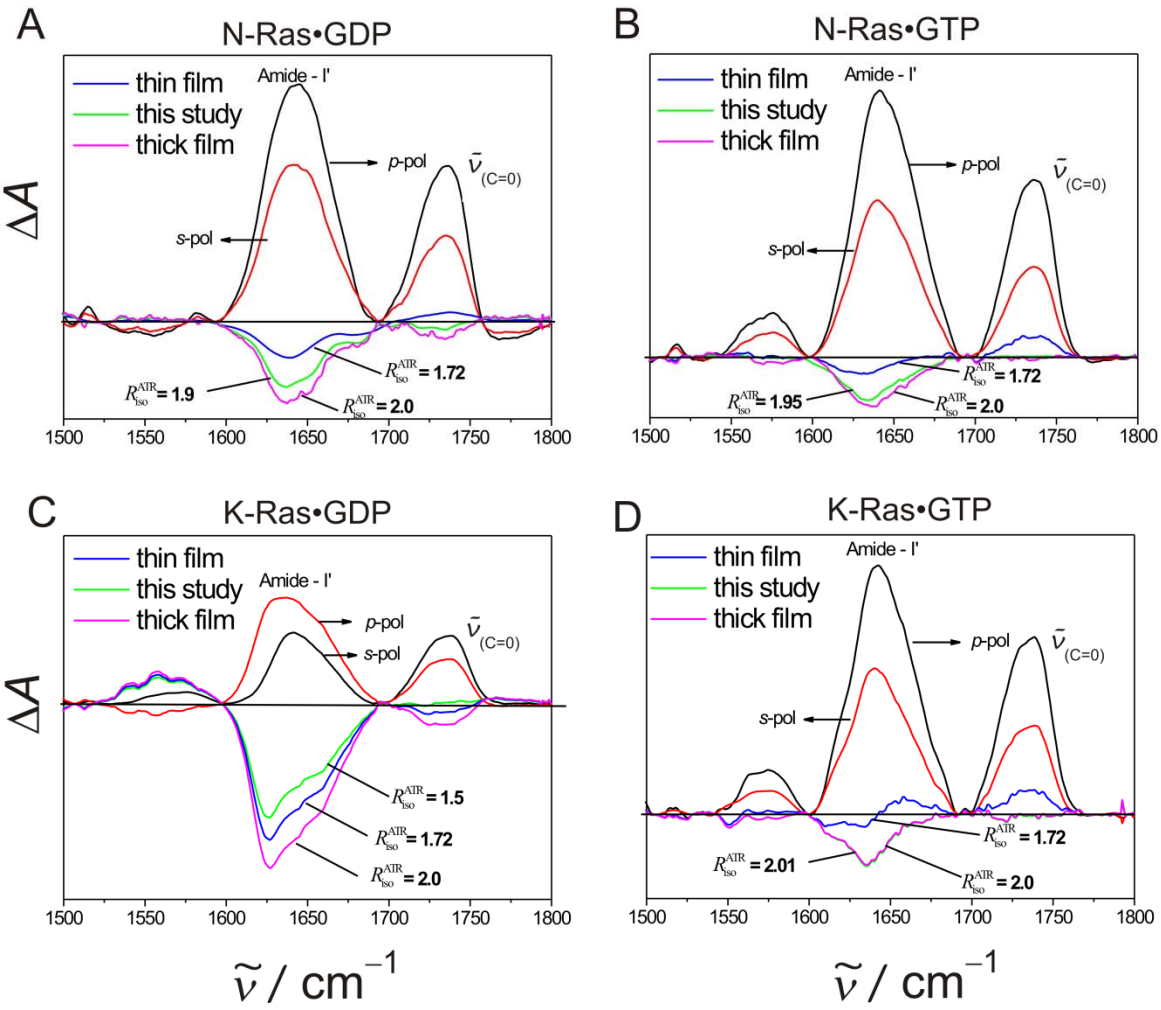

Figure 4.10: Effect of the thin- and thick-film approximation on the orientation of the membrane-bound Ras isoforms. Polarized ATR-FTIR dichroic spectra for (**A, B**) GDP/GTP-bound N-Ras and (**C, D**) GDP/GTP-bound K-Ras in the presence of the neutral (DOPC:DPPC:Chol 25:50:25 (molar ratio)) and the anionic (DOPC:DOPG:DPPC:DPPG:Chol 20:5:45:5:25 (molar ratio)) raft-like lipid bilayer, respectively, at 25 ˚C and 1 atm. The protein concentrations were 4 µM each. Δ*A* stands for the difference in the absorbance of the spectra collected with the p- and s-polarized infrared light.

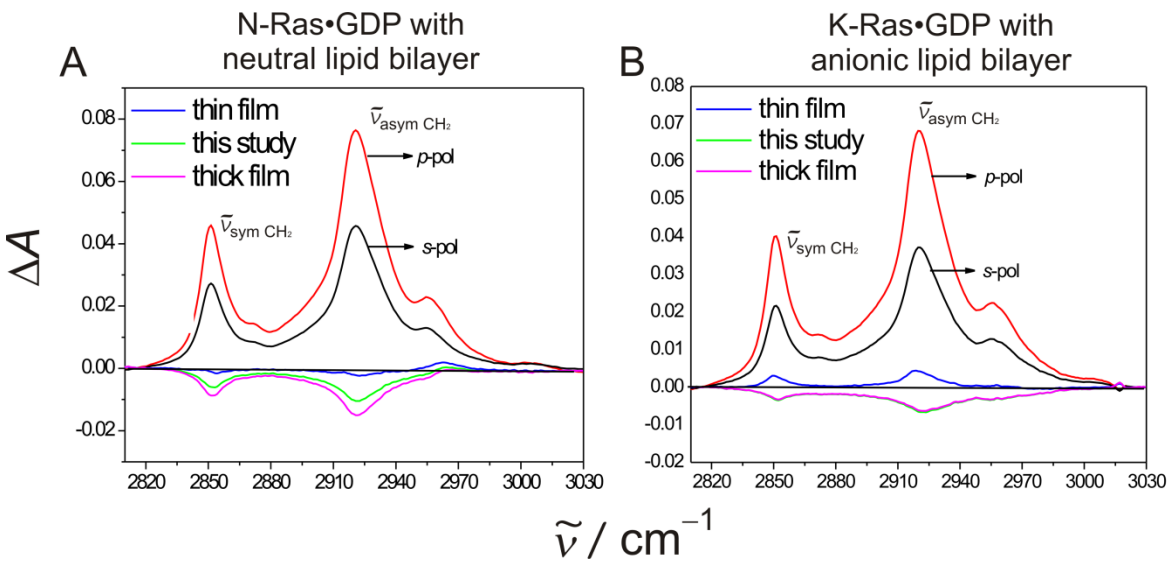

Figure 4.11: Dichroic spectra of the lipids obtained with different film-thickness approximations: Polarized ATR-FTIR dichroic spectra for (**A**) the neutral raft-like lipid bilayer (DOPC:DPPC:Chol 25:50:25 (molar ratio)) with N-Ras and (**B**) the anionic (DOPC:DOPG:DPPC:DPPG:Chol 20:5:45:5:25 (molar ratio)) raft-like lipid bilayer with K-Ras, at 25 ˚C and 1 atm. Δ*A* stands for the difference in the absorbance of the spectra collected with the p and s-polarized infrared light.

Finally, to unequivocally verify the appropriateness of the R_{iso}^{ATR} value from the lipid ester band, its consistency with the dichroism of other lipid bands was crosschecked. A perpendicular orientation of the lipid acyl chains with respect to the Ge surface was confirmed by dichroic ratio values of $\nu_s(CH_2)$ and $\nu_{as}(CH_3)$ lower and higher than R_{iso}^{ATR}, respectively (Table 4.1). Furthermore, the increase in the $R_{CH_2}^{ATR}$ (i.e. the dichroic ratio of the lipid's CH_2 vibration) upon addition of proteins ratifies membrane disordering. This was due to the insertion of the Ras lipid anchor motifs into the acyl chain region of the solid-supported lipid bilayer. In addition, the hydrophobic residues of the HVR might also contribute to this disordering effect, as previously determined by Huster et al.[165]

[165] Huster, D., Vogel, A., Katzka, C., Scheidt, H.A., Binder, H., Dante, S., Gutberlet, T., Zschornig, O., Waldmann, H., and Arnold, K. **(2003)**. Membrane insertion of a lipidated ras peptide studied by FTIR, solid–state NMR, and neutron diffraction spectroscopy. *J. Am. Chem. Soc. 125*, 4070–4079.

Table 4.1: Dichroic ratio of the carbonyl, symmetric CH_2 and asymmetric CH_3 stretching vibrations in lipids. Dichroic values of the respective lipid vibrations for the neutral (DOPC:DPPC:Chol 25:50:25 (molar ratio)) and the anionic (DOPC:DOPG:DPPC:DPPG:Chol 20:5:45:5:25 (molar ratio)) raft-like lipid bilayer deposited on the Ge IRE crystal, at 25 ˚C and 1 atm. The values in parentheses are the average of the time range up to 20 h, and without the parentheses are single spectra values used for plotting Figure 4.9-4.11.

Dichroic Ratio's	**N-Ras•GDP (neutral raft)**	**N-Ras•GTP (neutral raft)**	**K-Ras4B•GDP (anionic raft)**	**K-Ras4B•GTP (anionic raft)**
R_{iso}^{ATR}	1.9	1.95 {1.9155±0.0773}	1.55 {1.5529±0.1202}	2.01 {1.88±0.0503}
$R_{CH_2}^{ATR}$	1.7097	1.8171	1.468	1.8151
	{1.661±0.1022} lipids	{1.6969±0.153} lipids	{1.4496±0.0265} lipids	{1.7405±0.152} lipids
	{1.7769±0.2089} lipids+proteins	{1.7945±0.0221} lipids+proteins	{1.5139±0.0721} lipids+proteins	{1.8067±0.0092} lipids+proteins
$R_{CH_3}^{ATR}$	1.9829 {2.1141±0.359}	2.0335 {1.9950±0.176}	2.0379 {1.9825±0.133}	2.1851 {2.0178±0.11}

In Ras, only three out of five helices are parallel to each other, and the central β-sheet is twisted so that the contributions of the secondary structure elements led to some ambiguity in the calculation of orientational coordinates from ATR-FTIR data. More quantitative data were obtained by IRRA spectroscopy, which, in combination with appropriate simulations, provided a comprehensive orientational analysis of the different structural elements in the Ras protein, relative to the lipid monolayer.

4.3.2.1 Interaction of the Ras isoforms with heterogeneous lipid monolayers: an IRRAS study

Membrane anchors of the Ras proteins (C-14/16) are expected to insert into and span only one leaflet of a lipid bilayer (that is, the inner leaflet of the PM). As the raft-like ordered

domains were recently also detected in neutral and anionic raft-like lipid monolayers of the corresponding lipid compositions,[166] studies on lipid monolayers complement the work done on lipid bilayers. To study the insertion of Ras proteins into lipid monolayers at the air-water interface, infrared reflection absorption (IRRA) spectroscopy was employed. It allowed the inquiry into the combined effects of orientational and structural changes of proteins inserted into lipid monolayers. The protein insertion was followed by measuring the surface pressure profile ($\pi(t)$) simultaneously with the IRRA spectra. Due to the absence of secondary structural changes in the Ras proteins upon membrane contact (Fig. 4.5), the spectral shifts, intensity, and shape changes of the amide-I' band were delineated on account of the protein's orientational changes.

Time scales of the IRRAS measurements were on the order of hours, mainly due to the diffusion control setup, and not comparable with the physiologically relevant scenario. Taking into account the size of Ras proteins and the height of the Langmuir trough used, proteins of these sizes would take at least two to three hours to reach the membrane interface. Thus, the concomitant changes in the conformations or orientations could be spread out in time, requiring the collection of spectra over expanded time scales. For this reason, the stability and integrity of the pure lipid monolayer itself was checked by monitoring its $\pi(t)$ time-dependent profile and concomitant spectral changes associated with the lipid acyl chain region (CH_2 asymmetric and symmetric stretching vibrations at 2923 and 2953 cm^{-1}, respectively) over a time period of 22 h. Both remained essentially constant over the entire period, indicating the long-term stability of the lipid monolayer films (**Appendix, Fig. 9.4**).

[166] Evers, F., Jeworrek, C., Weise, K., Tolan, M., and Winter, R. **(2012)**. Detection of lipid raft domains in neutral and anionic Langmuir monolayers and bilayers of complex lipid composition. *Soft Matter 8*, 2170–2175.

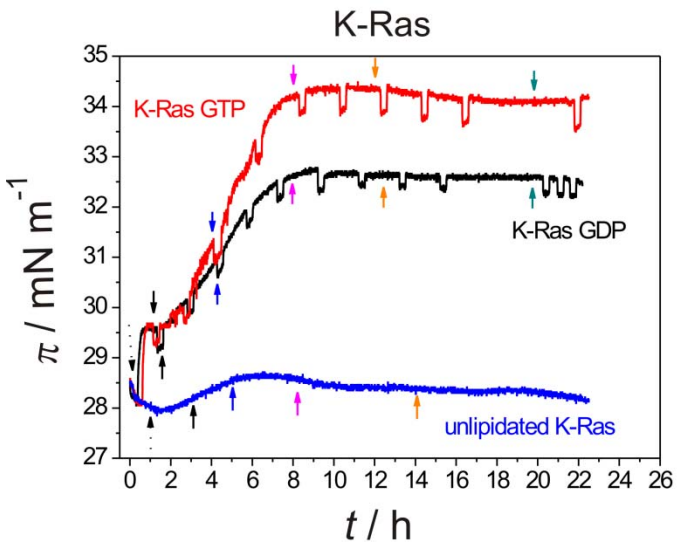

Figure 4.12: Insertion of K-Ras into the anionic raft-like lipid monolayer. Surface pressure profile of (black) GDP- and (red) GTP-bound K-Ras injected (dashed arrow) beneath the anionic (DOPC:DOPG:DPPC:DPPG:Chol 20:5:45:5:25 (molar ratio)) raft-like monolayer, at 20 ˚C and 1 atm. The blue curve is for unlipidated K-Ras protein, and serves as a control. The protein concentrations in the subphase were 200 nM each.

Injection of the K-Ras proteins underneath the lipid monolayer was accomplished at an optimal surface pressure of approximately 28–30 mN m^{-1}, which reflects the physiological lipid packing density found in cellular membranes.[167] A significant increase in the surface pressure ($\Delta\pi \approx 4.5$–6 mN m^{-1}) was indicative of an effective insertion of the farnesyl anchor of K-Ras, in both nucleotide-bound states, into the anionic raft-like lipid monolayer (Fig. 4.12). This was further supported by the corresponding experiments on the unlipidated K-Ras protein, where no insertion (only a slight perturbation of the baseline) was observed (**blue curve**; Fig. 4. 12). A slightly higher initial slope for the GTP-bound protein demonstrated a faster and stronger incorporation into the membrane.

[167] Janmey, P.A., and Kinnunen, P.K. **(2006)**. Biophysical properties of lipids and dynamic membranes. *Trends Cell Biol. 16*, 538–546.

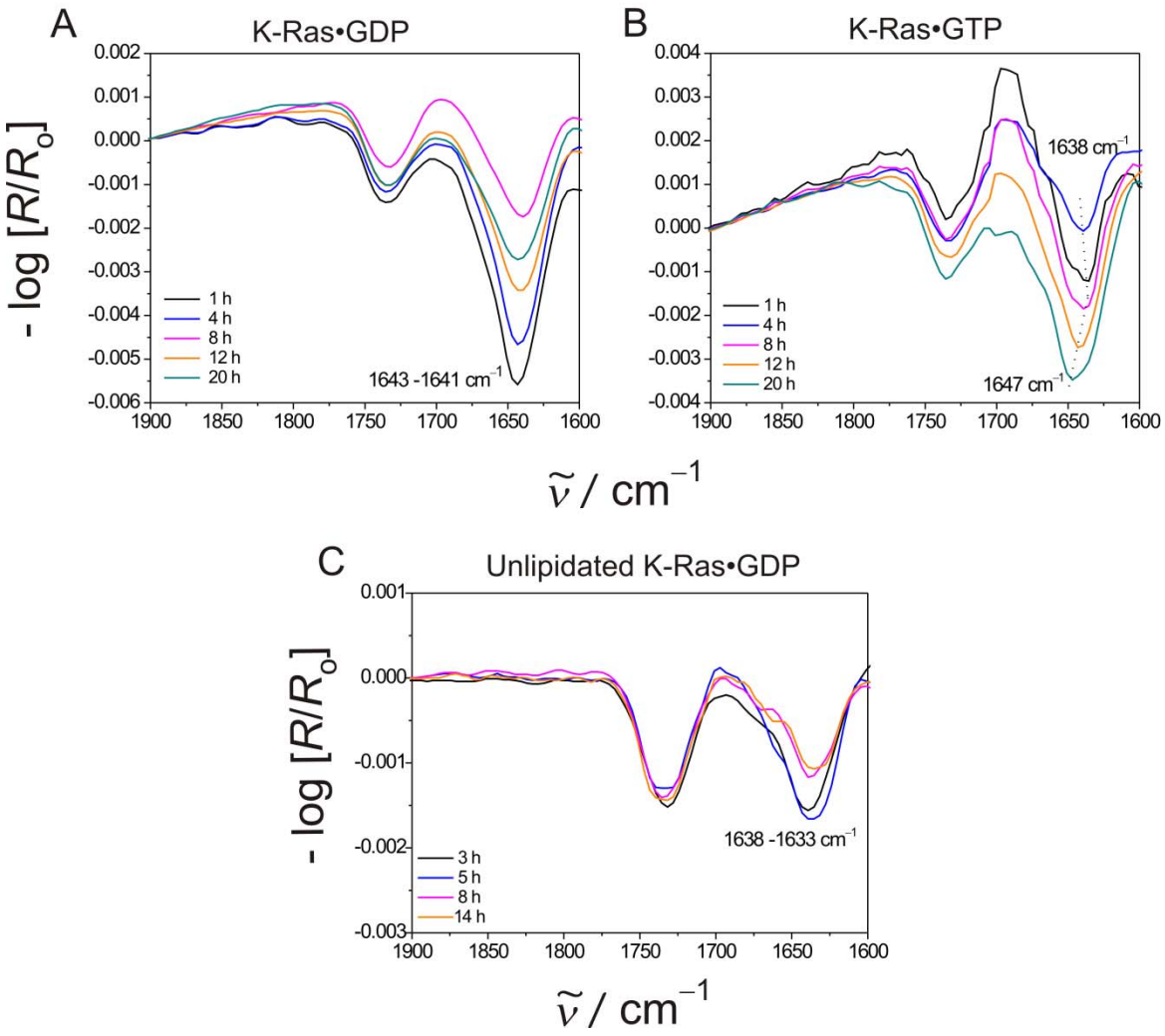

Figure 4.13: IRRA spectra of K-Ras during the membrane insertion process. Infrared reflection absorbance spectra for (**A**) GDP-bound, (**B**) GTP-bound and (**C**) unlipidated K-Ras protein during insertion into the anionic raft-like monolayer (DOPC:DOPG:DPPC:DPPG:Chol 20:5:45:5:25 (molar ratio)), kept at 30 mN m^{-1} at 20 ºC and 1 atm. The concentration of each protein was 200 nM.

The amide-I′ IRRA spectra of the GDP-bound K-Ras protein (Fig. 4.13) displayed a stable maximum between 1641 and 1643 cm^{-1}, indicative of a relatively fixed or less flexible orientation of the protein. On the other hand, fluctuations of the band maximum between 1638 cm^{-1} and 1647 cm^{-1} for the GTP-bound K-Ras protein (Fig. 4.13 **B**) inferred a greater orientational flexibility of the protein at the membrane interface. The absorption intensity for the unlipidated counterpart was lower by almost a factor of three because of the adsorption at—but no insertion into—the lipid monolayer (Fig. 4.13 **C**). The amide-I' band for the

unlipidated K-Ras protein exhibited a comparable orientational flexibility of the G-domain, with that of the lipidated GTP-bound form at the membranes, indicated by the fluctuation of the band maximum between 1633 cm^{-1} and 1638 cm^{-1} (Fig. 4.13 **C**).

For N-Ras proteins (Fig. 4.14), differences were observed in the mode of interaction with the lipid monolayer. The IRRA spectra for the amide-I' region of GDP- and GTP-bound N-Ras exhibited a gradual wavenumber shift from 1639 cm^{-1} to 1632 cm^{-1} and to 1626 cm^{-1}, respectively, within the analysed time. Thus, reorientation of both the proteins upon membrane insertion took place. The temporal evolution of the amide-I' band maxima for K-Ras (Fig. 4.13) and N-Ras (Fig. 4.14) suggest different orientational flexibilities of the respective Ras isoforms at the membrane interface.

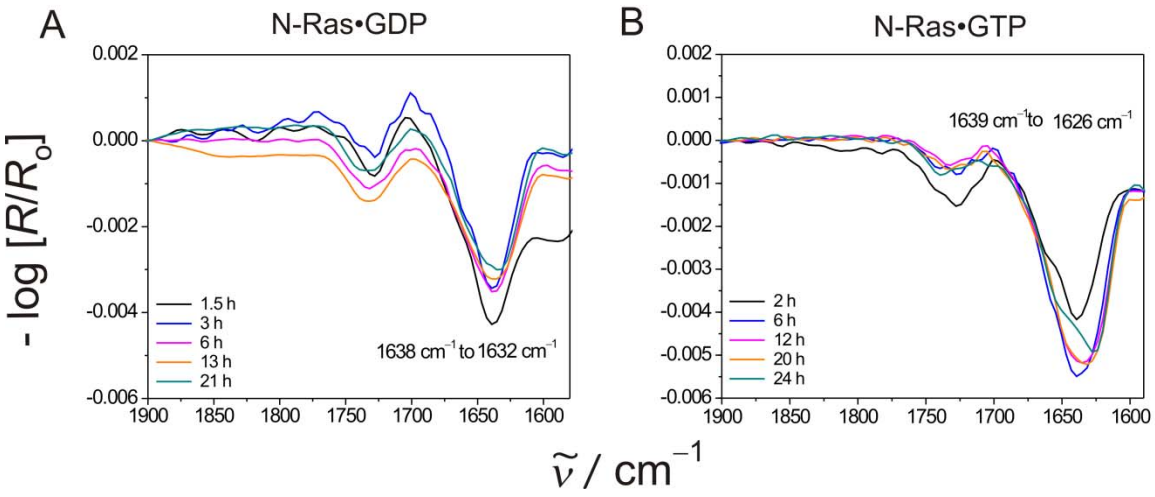

Figure 4.14: IRRA spectra of N-Ras during the membrane insertion process. Infrared reflection absorbance spectra for (**A**) GDP-bound and (**B**) GTP-bound N-Ras during insertion into the neutral raft-like monolayer (DOPC:DPPC:Chol:: 25:50:25; molar ratio), kept at 10 mN m^{-1} at 20 ºC and 1 atm. The concentration of each protein was 200 nM.

The corresponding $\pi(t)$ isotherms (Fig. 4.15) show a persuasive insertion of the two lipid anchors of N-Ras in both nucleotide-bound states into the lipid monolayer, evident by the marked increase in the surface pressure ($\Delta\pi \approx 15.5–17$ m N m^{-1}).

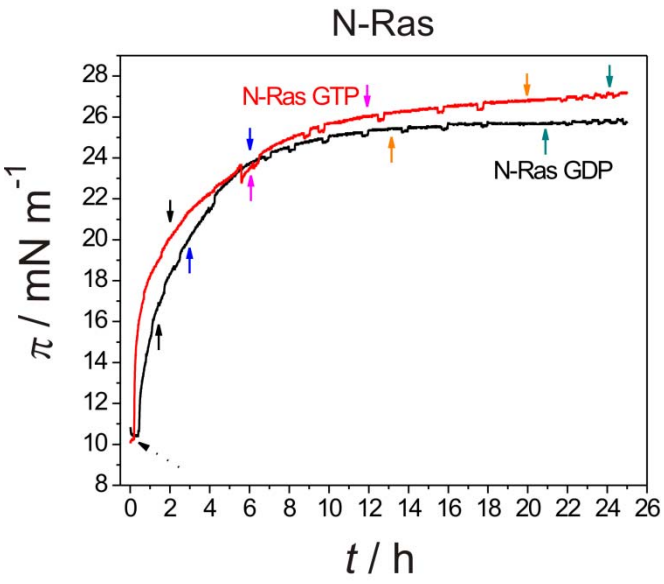

Figure 4.15: Insertion of N-Ras into the neutral raft-like lipid monolayer. Surface pressure profile of N-Ras protein in the GDP-(black) and GTP-bound (red) forms, injected beneath the neutral raft-like lipid monolayer (DOPC:DPPC:Chol 25:50:25 (molar ratio)), at 20 ˚C and 1 atm. The concentration of each protein in the subphase was 200 nM.

A lower initial surface pressure of the lipid monolayer (i.e. 10 mN m^{-1}) was chosen for the following reason. N-Ras proteins having two lipid anchors (HD and Far) seemed to produce a non-significant increase in surface pressure following their insertion underneath a lipid monolayer kept at 30 mN m^{-1} (Fig. 4.16; **brown curve in the inset**), also reported elsewhere.[92]

Although insertion of the dually lipidated proteins at physiological surface pressures (i.e. 30 mN m^{-1}) cannot be ruled out, rather the small increase in the surface pressure obtained in this study is beyond the detection limit of the instrument. Indeed, the insertion behaviour was similar to that of the unlipidated N-Ras protein (Fig. 4.16; **blue curve** in the inset). However, both cases can be differentiated by the visibility of the IRRA amide-I' band, which was observed only for the dually lipidated protein (Fig. 4.16). Similar wavenumber shifts of the IRRA band maxima for the GDP-bound N-Ras proteins were observed, irrespective of the membrane surface pressure (Figs. 4.14 **A** and 4.16).

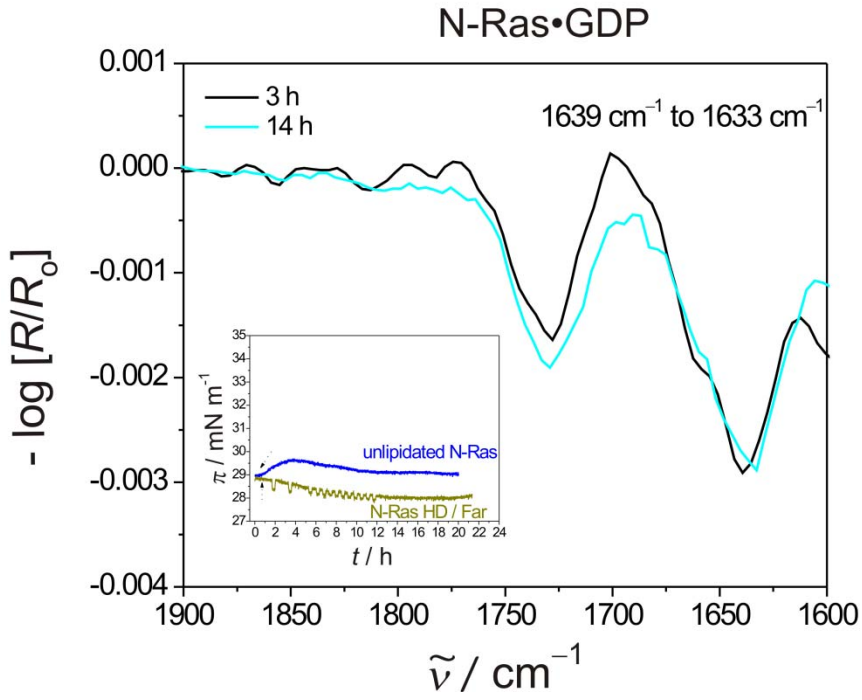

Figure 4.16: IRRA spectra of N-Ras under the physiological lipid density. IRRA spectra for the GDP-bound N-Ras protein during insertion into the neutral raft-like lipid monolayer (DOPC:DPPC:Chol 25:50:25 (molar ratio)), kept at 30 mN m^{-1} at 20 ºC and 1 atm. **Inset**: Surface pressure profile of the dually lipidated HD/Far (**brown**) and unlipidated (**blue**) N-Ras protein, injected beneath the monolayer, yielding a concentration of 200 nM each for both the proteins.

This result showed that the membrane interaction of N-Ras proteins is independent of the surface pressure, thus making the comparison to the K-Ras study reasonable. One thing to notice is the presence and absence of the IRRA amide-I' for the unlipidated K-Ras (Fig. 4.13 **C**) and the unlipidated N-Ras proteins, respectively. This most likely arises from a stronger membrane interaction or adsorption of the unlipidated K-Ras protein, mediated by its preserved polybasic lysine stretch in the HVR.

Minor changes in the $\pi(t)$ profiles for the unlipidated Ras proteins (Fig. 4.12 and 4.16, **inset**) were attributed to the perturbation of the lipid monolayer, due to the adsorption of the proteins. No stable insertion was demonstrated, however. Insertion of the hydrophobic side chains of the protein into the hydrophobic region of the membrane, thus stabilising the protein at the membrane interface, is likely to produce such a perturbation. This hypothesis was in agreement with X-ray diffraction (GIXD) and specular reflectivity (XR) studies

probing the adsorption of lipidated N-Ras protein at lipid monolayers.[168] Furthermore, studies on lipid bilayers also revealed that the backbone of the C-terminus of the lipidated Ras peptide is preferentially localised at the lipid-water interface. Due to the realities that the lipid modification and the hydrophobic side chains of the lipidated Ras peptide insert into the membrane,[165] the membrane perturbation is very likely.

4.3.3 Orientations of the Ras isoforms revealed by simulations of the IRRA spectra

Besides demonstrating the HVR and nucleotide-modulated binding of Ras isoforms to lipid bilayers and monolayers as outlined above, the orientation of the Ras G-domain with respect to the membrane was quantitatively determined. This involved a detailed simulation of the amide-I contour at various angles of incidence with p- and s-polarized light using the formulism defined in Chapter 2 (**Ch. 2, Section 2.1.2**), and the subsequent calculation of the simulated IRRA intensity. For this purpose, the experimental IRRA spectra were acquired at different angles of incidence ranging from 32˚ to 68˚ with different polarizations, upon equilibration of the insertion process (i.e. at the end of approximately 20 h in Figs. 4.12 and 4.14). For all the Ras isoforms: K-Ras GDP/GTP (Fig. 4. 17) and N-Ras GDP/GTP (Figure. 4.18), a switch in the sign of the IRRA amide-I' band at an angle of incidence above the Brewster angle was obtained with the p-polarized light, though it varied in intensity. This switch indicates a parallel alignment of most of the protein helices relative to the lipid monolayer interface,[85] and corroborates the concomitant polarized ATR-FTIR studies on the lipid bilayers.

[168] Bringezu, F., Majerowicz, M., Wen, S.Y., Reuther, G., Tan, K.T., Kuhlmann, J., Waldmann, H., and Huster, D. **(2007)**. Membrane binding of a lipidated N-Ras protein studied in lipid monolayers. *Eur. Biophys. J. Biophys. Lett. 36*, 491–498.

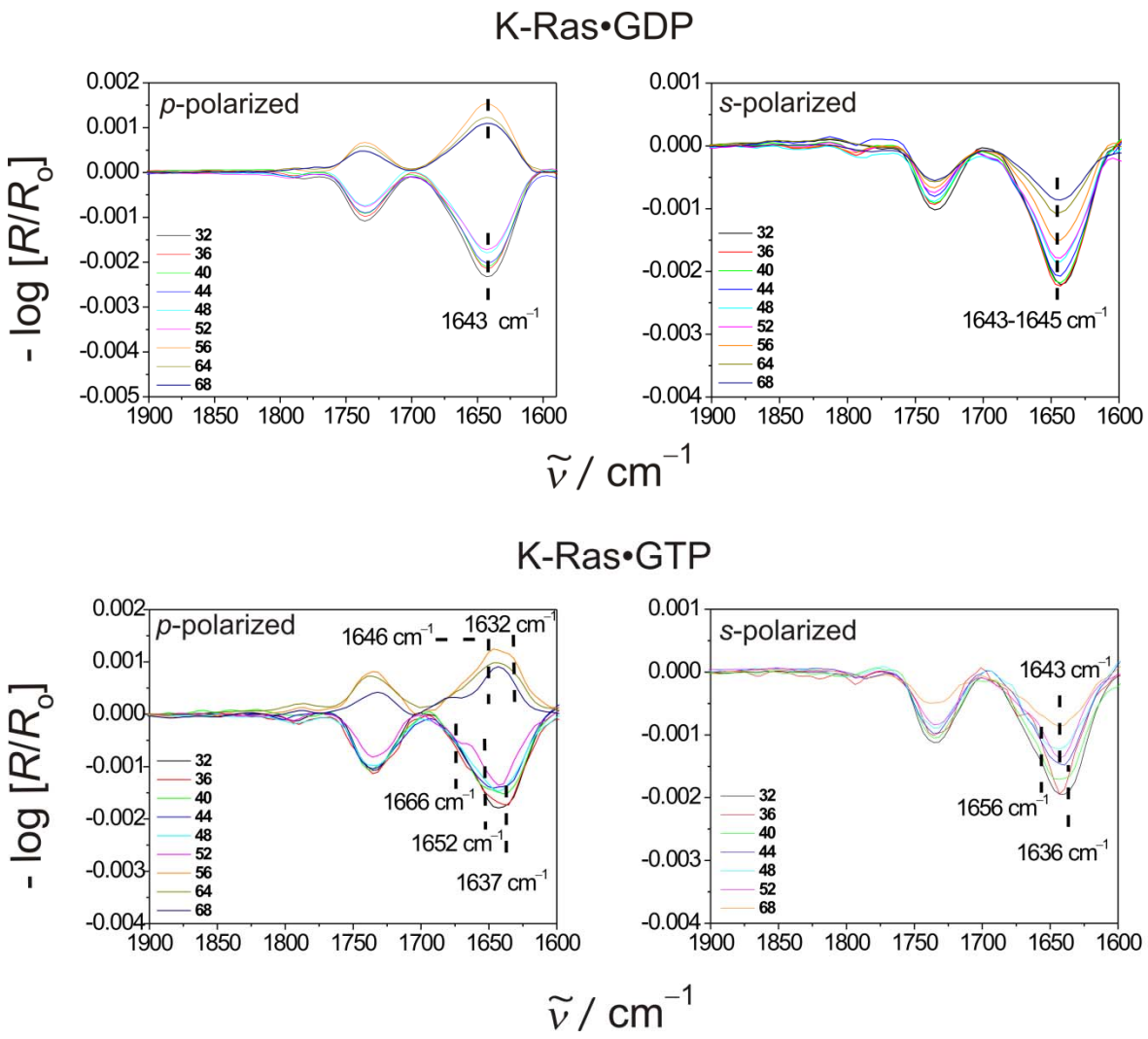

Figure 4.17: Angle-dependent IRRA spectra for membrane-bound K-Ras. Infrared reflection absorption spectra of GDP-bound and GTP-bound K-Ras at varying angles of incidence from 32º to 68º, collected with the p-and s-polarized light, approximately 20 h after injection (equilibration) underneath the anionic lipid raft-like monolayer (DOPC:DOPG:DPPC:DPPG:Chol 20:5:45:5:25 (molar ratio)) at 20 ºC and 1 atm.

Within the bounds of experimental resolution and reproducibility, no significant changes were detected between the GDP- and GTP-bound K-Ras proteins in the presence of the anionic raft-like lipid monolayers. This hampered a detailed comparison with the simulated spectra. An additional hurdle was manifested due to the ambiguity inherent in the calculation of the simulated IRRA spectra for the *highly flexible* active state of K-Ras, and thus restricted further detailed orientational insights for the K-Ras G-domain. However, it is most likely that the inactive K-Ras would orient with the majority of its helices parallel to the membrane

interface. The α5-helix would strongly interact with the membrane, thus moving the G-domain closer to the membrane. The reason for such a preferred orientation is based on the corresponding FTIR spectroscopic results, showing a red shift of the α-helical subband (indicative of stronger helix–membrane interaction) upon membrane insertion, but only in the inactive form. For the active K-Ras, a highly flexible conformation of the G-domain at the membranes was expected due to (a) a less pronounced dichroism in polarized ATR-FTIR, together with larger spectral shifts in IRRAS and (b) no red shifts of the α-helical subband in the corresponding FTIR measurements. A weaker helix–membrane interaction was elucidated in this form. The flexible conformation of the GTP-bound K-Ras was further supported by similar membrane interaction behaviour of the unlipidated K-Ras protein, i.e. comparable IRRA spectral shifts due to an unstable interaction with the membrane.

On the other hand, for the N-Ras proteins, the angle dependent amide-I' band IRRA spectra displayed significant differences between the active and inactive forms (Fig. 4.18), and enabled comparison with the simulated IRRA spectra. Spectra were simulated for the p-polarized light at different angles of incidence ranging from 32˚ to 68˚ (**Appendix**, Fig. 9.4), for the α-helical and β-sheet structures in the N-Ras protein with PDB code-3CON. This was done taking into account the different relative orientations of the secondary structure elements from the *two models proposed by Gorfe et al.*[155] The first model was designated as *Model 1* (for H-Ras GDP), in which the protein interacts with the membrane through its HVR region and N-terminal residues. The second was designated as *Model 2* (for H-Ras GTP), where the protein contacts the membrane mainly via its α4 and α5 helices. Owing to thermal effects and hence orientation fluctuations, the widths of the experimental spectra were larger than the calculated ones. Within the experimental resolution, the simulated spectra for Model 1 (GDP-form) fitted well with the experimental spectra for inactive GDP-bound N-Ras, and the simulated spectra for Model 2 (GTP-form) matched to the active GTP-bound N-Ras measured spectra (Fig. 4.18). The intensity distribution over the entire amide-I vibrational wavenumber region was comparable for the experimental and simulated IRRA spectra.

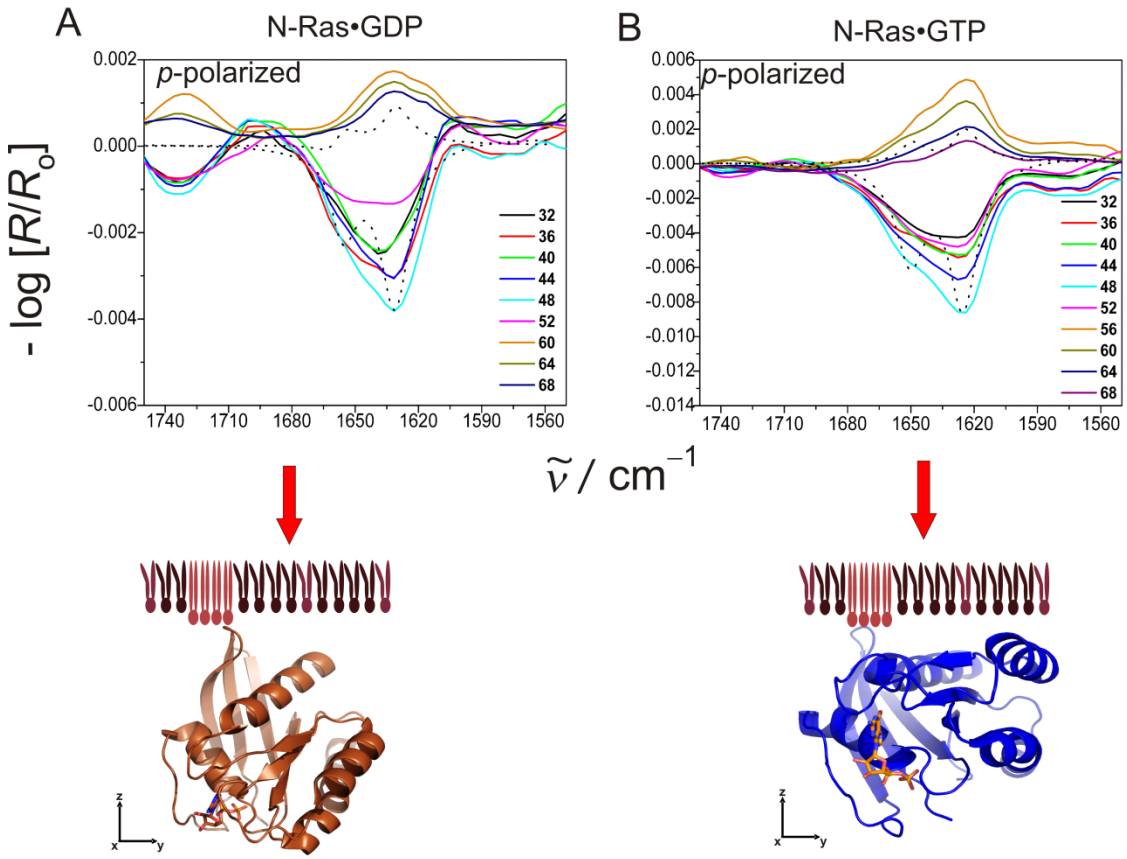

Figure 4.18: Angle-dependent IRRA spectra for membrane-bound N-Ras. Infrared reflection absorption spectra of (**A**) GDP- and (**B**) GTP-bound N-Ras at varying angles of incidence from 32º to 68º, collected with p-polarized light approximately 20 h after injection (in equilibrium) underneath the neutral lipid raft-like monolayer (DOPC:DPPC:Chol 25:50:25 (molar ratio)) at 20 ºC and 1 atm. Dotted lines show the p-polarized simulated spectra for (**A**) N-Ras GDP (angles 48º and 60º, model 1) and (**B**) N-Ras GTP (angles 48˚ and 56˚, model 2) using PDB entry 3CON. **Respective red arrows show the proposed orientations of N-Ras in the different nucleotide-bound states.**

The above results were consistent with the hypothesis that in addition to H-Ras, N-Ras also shows a dynamic modulation of its G-domain orientation by the bound nucleotide state. GDP-bound N-Ras protein adopts an orientation (depicted by Fig. 4.18 **A),** where it interacts with the membrane through the HVR region and N-terminal residues. On the other hand, GTP-bound N-Ras exhibits an orientation (depicted by Fig. 4.18 **B),** where the nucleotide exchange triggers a reorientation of the G-domain, leading to a more pronounced interaction of the helices α4 and α5 with the lipid interface.

Furthermore, the time scales of the IRRAS data correlate well with the AFM data on the lateral partitioning of Ras proteins in the different membrane systems (Fig. 4.1). Thus, a hypothesis is introduced at this stage: The orientational changes observed might be attributed to the conformational constraints imposed by the clustering of Ras isoforms in the lipid bilayer plane. Hence, all the spectral changes might be linked to orientational substates the Ras proteins are likely to adopt in the membrane-bound state.

4.3 Summary and Outlook

Signalling in general, and Ras mediated signalling in particular are strongly influenced by binding to specific effectors, many of which are also membrane-associated. Therefore, any change in the conformation, orientation, and localisation of membrane-bound signalling proteins is reflected in a modified binding to different effectors/regulators/modulators and, consequently regulated cell signalling. In recent years, exuberant research has revealed distinct functionality/signal outputs of the Ras isoforms, despite utilising a shared set of effectors and regulators. As such, this leads to activate the common signalling pathways to various degrees. Thus, one of the questions most investigated in Ras signalling is: ***What are the determinants of these specific interactions?*** One of the structural components of Ras that is expected to contribute to the observed biological differences is the C-terminal HVR. Previous *in vitro* and *in vivo* studies have revealed that the HVR is associated with isoform-specific localisation and lateral segregation of Ras proteins in membranes, forming specific nanoclusters, generating high fidelity signalling platforms.[125,149,169-170] In addition to the HVR, members of the Ras superfamily also harbour a structurally and mechanistically preserved GTP-binding core: the G-domain, which can also play an essential role in generating variable signalling outputs. This led to the idea that the Ras diversity may not be limited to the obvious distinct HVR.

The same idea was extensively exploited in the present study using a combination of different biophysical techniques. It was demonstrated that no dramatic structural changes like

[169] Hancock, J.F. **(2003)**. Ras proteins: Different signals from different locations. *Nat. Rev. Mol. Cell Biol. 4*, 373–384.
[170] Prior, I.A., Muncke, C., Parton, R.G., and Hancock, J.F. **(2003)**. Direct visualization of Ras proteins in spatially distinct cell surface microdomains. *J. Cell Biol. 160*, 165–170.

partial unfolding or secondary structural rearrangements take place in the N- and K-Ras proteins upon membrane interaction; however, significant G-domain orientational changes were observed. The bound nucleotide state and the HVR together attune the orientational flexibility of each Ras isoform at the membrane interface. The main conclusions drawn from all the data presented here, along with previous studies on the lateral segregation behaviour of Ras proteins, are summarised in Fig. 4.19. It can be convincingly stated that the Ras isoform specificity extends beyond the hypervariable region to the highly conserved G-domain.[171]

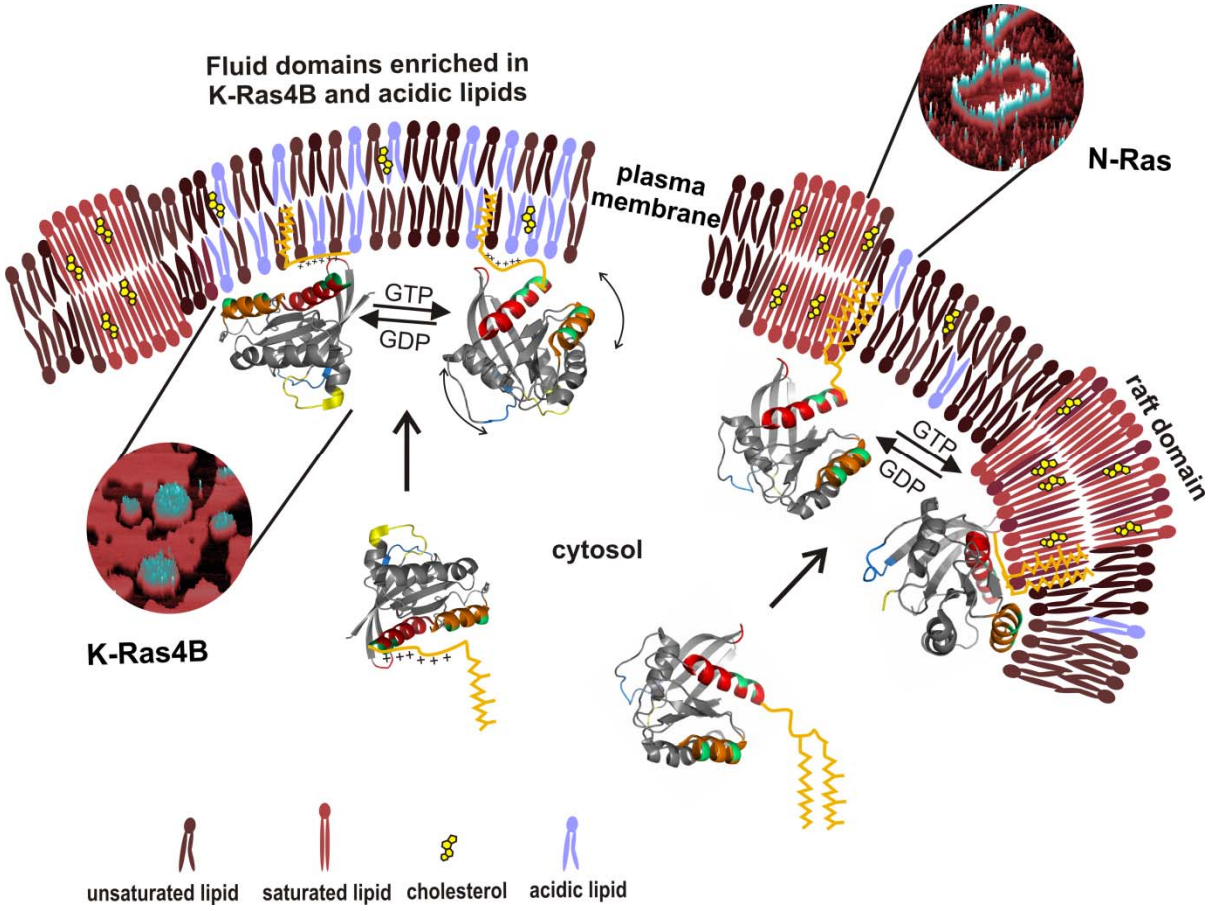

Figure 4.19: Schematic representation of the Ras isoform-specific membrane interactions. The figure summarises the G-domain orientational results obtained in this study and the schematic AFM results adapted from ref. 125 and 149. Ras proteins cluster in separate membrane microdomains subsequently forming isoform-specific signalling platforms (depicted by AFM data in *blue-white*). In addition, the G-domain mediates the Ras–membrane interactions by inducing different sets of preferred orientations in the active and inactive states

[171] Kapoor, S., Weise, K., Erlkamp, M., Triola, G., Waldmann, H., and Winter, R. **(2012)**. The role of G-domain orientation and nucleotide state on the Ras isoform-specific membrane interaction. *Eur. Biophys. J. 41*, 801–813.

of the protein. Due to membrane-associated clustering and the dynamics of lateral organisation, no starkly fixed orientations are envisioned; rather the proteins are bestowed with variable degrees of flexibility in each nucleotide-bound state, dependent on the isoform. Reproduced with permission from ref. 171.

This study adds to the steady accumulation of evidence regarding Ras isoforms being functionally distinct, contrary to the earlier perceptions. The distinct localisation of the isoforms mediated by *HVR*, coupled with the potential role of the homologous *G-domain* suggests a synergy between these types of recognition motifs, thus justifying the concept of isoform specificity in Ras. At last, given that the understanding of Ras signalling has increased significantly in recent years, the ability to selectively inhibit Ras isoforms has not yet kept pace. The search for the elusive "anti-Ras" drug is still growing. As exemplified by this and previous studies focussed on the Ras–membrane interactions, an intriguing level of complexity is evoked in the Ras conformational cycle. It is tempting to propose that this might also apply to the oncogenic Ras conformations. There is a copious evidence regarding the ability of effector proteins (such as Raf-1 and PI3-K) to sense and interact with specific orientations of Ras isoforms, in perspective of which this study might be useful. Designing isoform-specific drugs and targeting the conformational heterogeneity inherent to Ras proteins could inhibit Ras–effector interactions, thereby blocking oncogenic Ras signalling, with limited side effects.

Finally, the limitation of IRRA spectroscopy to quantitatively elucidate the orientations of K-Ras can be overcome by using a superior variant of IRRA spectroscopy, namely polarization modulation infrared reflection absorption spectroscopy PM-IRRAS. PM-IRRAS with a higher resolution and better signal to noise ratio would be able to resolve the differences likely to exist between the active and inactive K-Ras IRRA spectra, and thus would enable comparison with the simulations. Furthermore, in the future, nuclear magnetic resonance (NMR) spectroscopy can ostensibly provide atomistic details of Ras–membrane interactions, and edify a more comprehensive picture of the conformational heterogeneity existing among membrane-bound Ras isoforms.

V

PRESSURE PERTURBATION OF THE RAS CONFORMATIONAL SUB-SPACE*

* The work of the present study has been published and subsequently reprinted in parts (some figures) with permission from Kapoor, S., Triola, G., Vetter, I.R., Erlkamp, M., Waldmann, H., and Winter, R. **(2012)** Revealing conformational substates of lipidated N-Ras protein by pressure modulation. *Proc. Natl. Acad. Sci. U.S.A.* 109, 460-465.

5.1 Background

5.1.1 Conformational Substates (CS) and Selection in Proteins

"...a protein cannot be said to have 'a' secondary structure but exists mainly as a group of structures not too different from one another in free energy, but frequently differing considerably in energy and entropy. In fact the molecule must be conceived as trying out every possible structure..."[172] were the phenomenal words of Linderstrøm-Lang and Schellman as they described the bewildering dynamic nature of proteins. More specifically, proteins tend to harbour an intrinsic capability to exist in a multitude of slightly different overall structures, but nearly isoenergetic, referred to as conformational substates (CS). CS, for the most part, have their own hierarchy and are endowed with conformational fluctuations.[173] Alternatively, the multidimensional conformational Gibbs (free) energy surface of a protein *in a given state,* exhibits many energy valleys or *substates* separated by small energy barriers. Figure 5.1 **A** provides a clearer picture of the coexistence of the native and the non-native (higher energy) conformations of proteins. The two types of motions inherently taking place due to the existence of protein *states* and *substates* are equilibrium fluctuations (EM) and functionally important motions (FIM). EF are motions between CS in equilibrium in a given protein state, and FIM, also known as non-equilibrium transitions, are the motions leading from one protein state to another (Fig. 5.1 **B**). There is an exuberant body of experimental evidence supporting the existence of CS in proteins,[174] with myoglobin being the opening member. Elegant flash photolysis experiments coupled with X-ray diffraction and the Mössbauer effect, revealed at least up to four tiers of CS in a given state of myoglobin (i.e. MbCO - Mb bound to carbon monoxide). The furcation in each tier constitutes the substates of the next level tier, with smaller barriers, forming a well defined hierarchical arrangement (Fig. 5.1 **B**).[175] In addition, by using FTIR spectroscopy, detectable substates of Mb binding to carbon monoxide with different rates were observed. This

[172] Linderstrøm-Lang, K. U. & Schellman, J. A. **(1959)** Protein Structure and Enzyme Activity in *"The Enzymes" Vol 1*, Second Ed. 443–510 Boyer, Lardy, Myrbäk Eds. Academic Press, New York.
[173] Ansari, A., Berendzen, J., Bowne, S.F., Frauenfelder, H., Iben, I.E. Sauke, T.B., Shyamsunder, E., and Young, R.D. **(1985)**. Protein states and proteinquakes. *Proc. Natl. Acad. Sci. U.S.A. 82*, 5000–5004.
[174] Frauenfelder, H., Parak, F., and Young, R.D. **(1988)**. Conformational substates in proteins. *Annu. Rev. Biophys. Biophys. Chem. 17*, 451–479.
[175] Frauenfelder, H., Sligar, S.G., and Wolynes, P.G. **(1991)**. The energy landscapes and motions of proteins. *Science 254*, 1598–1603.

generates a high level of precision in the statistical ensemble of conformations that gives rise to complex protein kinetics.[176]

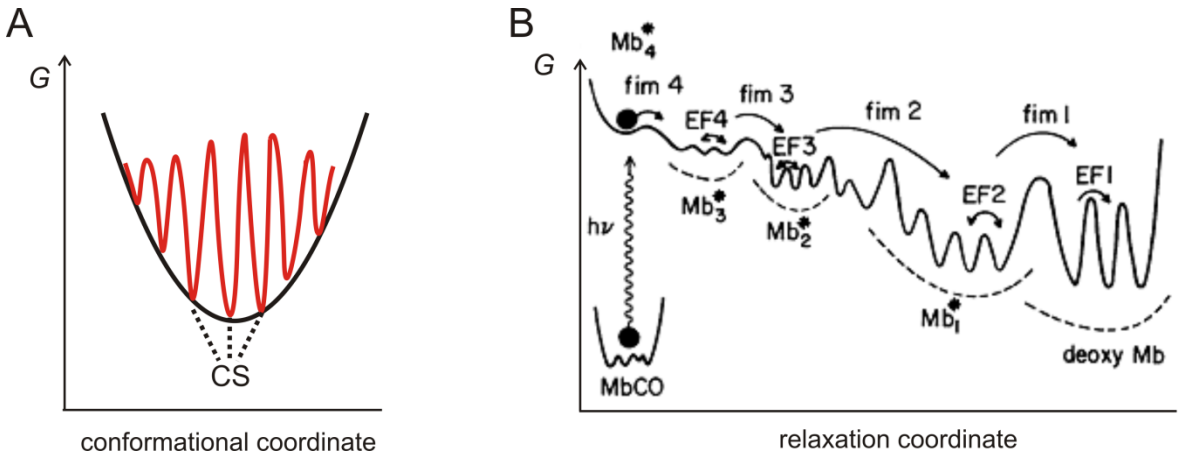

Figure 5.1: Conformational substates and related motions in protein. (**A**) Schematic illustration of the finer energy landscape (minima) within the native state of the protein where these finer minima represent the CS of that state. (**B**) Hierarchical CS assembly of the MbCO state of myoglobin and its related changes upon flash photolysis (reproduced from ref. 174). $Mb^*_{1\text{-}4,}$ designate the four distinct states of Mb, where inter-conversion among these states represent FIM, and fluctuations within each of these states (i.e. between different CS) represents EM.

The conformational selection model has emerged as an alternative to the "induced fit model" and is derived from the funnel-like energy landscape theory of protein folding.[175,177] This concept, implicit in the renowned Monod-Wyman-Changeux (MWC) theory of allostery,[178] envisions no single conformation of the native state of a protein but rather an ensemble of closely related coexisting conformations with different functional characteristics. The most suitable conformation for biological events, such as binding to ligands, nucleic acids or other proteins, produces a population/equilibrium shift redistributing the conformations. Intriguingly, this concept was foreseen long ago, as exemplified in the following excerpt by Francis Bacon in 1620, long before any experimental verification was available.

[176] Frauenfelder, H., Alberding, N.A., Ansari, A., Braunstein, D., Cowen, B.R., Hong, M.K., Iben, I.E.T., *et al.* **(1990)**. Proteins and Pressure. *J. Phys. Chem. 94*, 1024–1037.
[177] Dill, K.A., and Chan, H.S. **(1997)**. From Levinthal to pathways to funnels. *Nat. Struct. Biol. 4*, 10–19.
[178] Monod, J., Wyman, J., and Changeux, J.P. **(1965)**. On the Nature of Allosteric Transitions: A Plausible Model. *J. Mol. Biol. 12*, 88–118.

"It is certain that all bodies whatsoever, though they have no sense, yet they have perception; for when one body is applied to another, there is a kind of election to embrace that which is agreeable, and to exclude or expel that which is ingrate; and whether the body be alterant or altered, evermore perception precedeth operation; for else all bodies would be like one to another."[178]

A plethora of studies now lend support that proteins in their native state or conformation are predisposed to undergo conformational fluctuations, forming a generic mechanism for their biological functions.[179] Functional relevance of the higher energy, non-native protein conformations has been extensively explored and reviewed elsewhere.[180] There exist many striking examples of their role in processes ranging from protein regulation, catalysis, and molecular recognition to signalling, emphasising the urgency of the need to study the non-native conformation thoroughly. For example, the higher energy conformer of the oncoprotein Vav1 shows a linear correlation between its catalytic activity (i.e. phosphorylation) and population. [181] The same study provided unambiguous structural and functional evidence for the involvement of a high energy conformer in biological function. Another remarkable example is that of hamster prion protein, where the weakly populated higher energy conformer is the "active" conformer turning into the contagious scrapie type.[182] All of these examples highlight the reality that it is not always the most obvious *native* conformation of the protein, as revealed by crystallography, but rather the non-native, high energy (low-lying) conformations that are primarily responsible (in most cases) for the biological functions (see ref. within 179). In this regard, an arduous task is the identification of the functionally relevant non-native conformational substates of proteins. Specifically, the low fractional populations of these conformers at ambient conditions are not easily detectable by any spectroscopic means. As a direct consequence, many events in the protein

[179] Boehr, D.D., Nussinov, R., and Wright, P.E. **(2009)**. The role of dynamic conformational ensembles in biomolecular recognition. *Nat. Chem. Biol. 5*, 789–796.
[180] Akasaka, K. **(2003)**. Exploring the entire conformational space of proteins by high-pressure NMR. *Pure Appl. Chem. 75*, 927–936.
[181] Li, P., Martins, I.R., Amarasinghe, G.K., and Rosen, M.K. **(2008)**. Internal dynamics control activation and activity of the autoinhibited Vav DH domain. *Nat. Struct. Mol. Biol. 15*, 613–618.
[182] Kuwata, K., Li, H., Yamada, H., Legname, G., Prusiner, S.B., Akasaka, K., and James, T.L. **(2002)**. Locally disordered conformer of the hamster prion protein: a crucial intermediate to PrPSc? *Biochemistry 41*, 12277–12283.

conformational dynamics go unnoticed that might be decisively important in protein function.

5.1.2 Pressure Induced Conformational Selection in Proteins

To gain insight into the protein conformational subspace, biological, chemical and physical perturbations are employed to shift the population equilibrium and characterise the otherwise rare conformational substates. The thermodynamic aspect of temperature perturbation is exhaustive,[183-184] wherein temperature produces simultaneous changes in the total energy and volume. On the other hand, the effects of a denaturant (chemical perturbation) depend on its binding properties. However, when the conformational substates vary only in terms of very small energy differences, separation by temperature or chemical perturbations are often difficult to achieve. Under such circumstances, pressure, as a further fundamental thermodynamic variable, provides a clean and efficient mean to redistribute the conformational equilibrium through volume differences. Pressure favours protein states with smaller partial volumes which exhibit a lower degree of order, and thus are more solvated than the native state.[184-188]

Electrostriction[189], hydration of newly exposed polar or non polar residues, and the loss of free volume or cavities[190] (arising due to the packing defects in the folded ensemble of proteins) are some of the effects observed upon pressurisation of proteins in solution. The volume decrease upon unfolding is of the order of 0.5–1.0 % of the total specific protein

[183] Privalov, P.L., and Gill, S.J. **(1988)**. Stability of protein structure and hydrophobic interaction. *Adv. Prot. Chem. 39*, 191–234.
[184] Ravindra, R., and Winter, R. **(2003)**. On the temperature–pressure free-energy landscape of proteins. *Chemphyschem 4*, 359–365.
[185] Winter, R., and Dzwolak, W. **(2005)**. Temperature-pressure configurational landscape of lipid bilayers and proteins. *Phil. Trans. R. Soc. A 363,* 537–563
[186] Akasaka, K. **(2006)**. Probing conformational fluctuation of proteins by pressure perturbation. *Chem. Rev, 106*, 1814–1835.
[187] McCoy, J., and Hubbell, W.L. **(2011)**. High-pressure EPR reveals conformational equilibria and volumetric properties of spin-labeled proteins. *Proc. Natl. Acad. Sci. U.S.A. 108*, 1331–1336.
[188] Collins, M.D., Kim, C.U., and Gruner, S.M. **(2011)** High-pressure protein crystallography and NMR to explore protein conformations. *Annu. Rev. Biophys. 40*, 81–98.
[189] Silva, J.L., Foguel, D., and Royer, C.A. **(2001)**. Pressure provides new insights into protein folding, dynamics and structure. *Trends Biochem. Sci. 26*, 612–618.
[190] Roche, J., Caro, J.A., Norberto, D.R., Barthe, P., Roumestand, C., Schlessman, J.L., Garcia, A.E., Garcia-Moreno, B.E., and Royer, C.A. **(2012)**Cavities determine the pressure unfolding of proteins. *Proc. Natl. Acad. Sci. U.S.A. 109*, 6945–6950.

volume. The volume changes accompanying population shifts are even smaller, such that the application of pressure substantially populates the low-lying excited substates, thus providing elegant means to study them by spectroscopic techniques. Readers interested in basic rules governing the response of proteins to pressure are directed to the review by K. Akasaka.[186] Briefly, pressure can affect proteins in two ways. First, it can induce a linear compression, i.e. reduce the inter-atomic distances in the protein, without changing its topology. During this, the protein remains in the same substate, and these changes fall in the category known as the elastic effects. Most of the information for this category has been obtained from the measurements of isothermal compressibility coefficient (β_T) of proteins. It is correlated to the relative volume fluctuation ($\partial V/V$) through Eq. (1), thus providing information concerning structural dynamics.

$$\beta_T = -(1/V)\cdot(\partial V/\partial p)_T \qquad (1)$$

The second category constitutes conformational effects, wherein pressure induces a change in the local or global arrangement/topology of the atoms. Under this effect, proteins move from one CS to another, thereby influencing protein's structure, dynamics, and function. Under pressure, the decrease in the partial molar volume of the protein may involve a combination of these two effects. However, in reality, a clear cut distinction between them may not always be possible. Most importantly, the pressure effects on proteins are fully reversible unlike in temperature or chemical perturbation.

5.1.3 Relevance of Conformational Selection to Ras

The binding of guanine nucleotides to Ras contributes to a growing repertoire of interactions that underpins biomolecular recognition. In fact, Ras operates through a nucleotide-induced conformational shift mechanism, predicted by MD simulation[191] and later on experimentally proven.[192] Distinct chemical species in the nucleotide binding site—such as GTP, GDP and GTP analogues—correlate with distinct global conformations. Thus, conformational

[191] Grant, B.J., McCammon, J.A., and Gorfe, A.A. **(2010)**. Conformational Selection in G-Proteins Lessons from Ras and Rho. *Biophys. J. 99*, L87–L89.

[192] Meierhofer, T., Rosnizeck, I.C., Graf, T., Reiss, K., Konig, B., Kalbitzer, H.R., and Spoerner, M. **(2011)**. Cu2+-cyclen as probe to identify conformational states in guanine nucleotide binding proteins. *J. Am. Chem. Soc. 133*, 2048–2051.

selection is expected to be the predominant mechanism for the regulation and function of Ras, and other small GTPases.

In addition, within the same nucleotide-bound state, Ras samples multiple conformations among which two main conformers (relating to the Switch I) have been characterised[193]: denoted as substate 1 (CS^1) and substate 2 (CS^2), hereafter. The conformational equilibrium between CS^1 and CS^2 has been observed for both, the wild type and the mutated Ras proteins with the natural GTP ligand[194] and its analogues[195]. However in each scenario, different relative populations of CS^2/CS^1 were obtained. This suggests a fine tuning mechanism of the Ras CS, not only by the bound-nucleotide, but also by mutations[196]–an important consideration for the anti-Ras therapy. The native conformer detectable at ambient conditions (CS^2) was immediately assigned as the effector binding state,[193-197] whereas the non-native higher energy conformer (CS^1) was found to interact with GEFs [for instance: SOS]. CS^1 exhibits a reduced affinity for the effector proteins.[198] High pressure ^{31}P-NMR was employed to elucidate the structural and functional relevance of CS^1 in the unlipidated wild type Ras.GppNHp. The consequences of these studies are far reaching, as the stabilisation of CS^1 could weaken Ras–effector interactions, and thereby curb oncogenic Ras signalling.

---

193 Geyer, M., Schweins, T., Herrmann, C., Prisner, T., Wittinghofer, A., and Kalbitzer, H.R. **(1996)**. Conformational transitions in p21ras and in its complexes with the effector protein Raf-RBD and the GTPase activating protein GAP. *Biochemistry 35*, 10308–10320.

194 Spoerner, M., Hozsa, C., Poetzl, J.A., Reiss, K., Ganser, P., Geyer, M., and Kalbitzer, H.R. **(2010)**. Conformational states of human rat sarcoma (Ras) protein complexed with its natural ligand GTP and their role for effector interaction and GTP hydrolysis. *J. Biol. Chem. 285*, 39768–39778.

195 Spoerner, M., Nuehs, A., Ganser, P., Herrmann, C., Wittinghofer, A., and Kalbitzer, H.R. **(2005)**. Conformational states of Ras complexed with the GTP analogue GppNHp or GppCH2p: implications for the interaction with effector proteins. *Biochemistry 44*, 2225–2236.

196 Spoerner, M., Wittinghofer, A., and Kalbitzer, H.R. **(2004)**. Perturbation of the conformational equilibria in Ras by selective mutations as studied by ^{31}P-NMR spectroscopy. *FEBS Lett. 578*, 305–310.

197 Spoerner, M., Herrmann, C., Vetter, I.R., Kalbitzer, H.R., and Wittinghofer, A. **(2001)**. Dynamic properties of the Ras switch I region and its importance for binding to effectors. *Proc. Natl. Acad. Sci. U.S.A. 98*, 4944–4949.

198 Kalbitzer, H.R., Spoerner, M., Ganser, P., Hozsa, C., and Kremer, W. **(2009)**. Fundamental link between folding states and functional states of proteins. *J. Am. Chem. Soc. 131*, 16714–16719.

5.2 Motivation and Objectives

Ras fulfils its biological roles in the membrane-bound form, a fact that yet remains unexplored, as all of the research mentioned above on CS of Ras has been performed exclusively in bulk solution. Hence, a major goal of this study was to explore the conformational sub-space of membrane-bound Ras. For this purpose, the fully lipidated N-Ras protein was chosen with two lipid anchors: farnesyl and hexadecyl (a non-hydrolysable analogue of the palmitoyl group). The existence of CS[1 and 2] has been reported mainly for the active, GTP-bound protein, whereas this equilibrium can also exist in the inactive, GDP-bound protein. Thus, in the present work, the Ras CS were explored both in the active and inactive membrane-bound forms. Moreover, to decouple the effects of membrane binding on the CS of Ras, experiments were also performed with the corresponding proteins in bulk solution (i.e. in the absence of membranes). The motivation for this work comes from the nucleotide-modulated Ras–membrane partitioning behaviour[125,149] and orientations[171] at the lipid interface. These are expected to have a marked effect on the Ras conformational substates, and probably other membrane-associated signalling proteins. Finally, the protein conformational dynamics is linked to signalling pathways, for which many functional states crucial for signalling may not have a population large enough to be easily studied. Thus, a population shift was induced using high hydrostatic pressure. Appropriate methodology had to be adopted, as experimental techniques monitoring such effects, especially in the presence of lipid membrane, are rather limited. For example, the (limited) applicability of high pressure circular dichroism spectroscopy is twofold. First, there is pressure-induced birefringence of the windows, and second a high scattering signal from lipid vesicles. Similarly, high pressure NMR can only be preformed up to a pressure range of approximately 2-3 kbar, while the use of lipid systems is rather restricted. Though the superiority of NMR is providing atomistic details even at high pressure remains unmatched, other limitations can be suitably overcome by using other techniques. In this regard, high pressure infrared (HP-FTIR) and fluorescence spectroscopy (FS) were chosen. In HP-FTIR, each CS is expected to give rise to a slightly different peak wavenumber, and the overall band is the superimposition of Gaussian or Lorentzian (or Voigtian) functions. A pressure-induced shift in the population not only shifts the line, but also changes its

shape. On the other hand fluorescence spectroscopy provides an overview of the pressure-induced effects on the protein with respective to the fluorophore's environmental changes.

5.3 Results and Discussion

5.3.1 Effect of pressure on the conformational substates of N-Ras modulated by the bound nucleotide state

HP-FTIR spectra of N-Ras in its different nucleotide-bound states in bulk solution and in the pressure range from 1 bar to 10 kbar (Fig. 5.2) exhibits an asymmetric amide-I′ band with predominant contributions from α-helix and β-sheet structural elements; this is in good agreement with the X-ray crystal structure and previous studies.[159,171] The presence of sharp features in the Fourier self-deconvoluted amide-I' spectra even at a pressure of 10 kbar demonstrates a remarkably *high pressure stability of the Ras protein, retaining its compact tertiary structure in both the nucleotide-bound forms*.

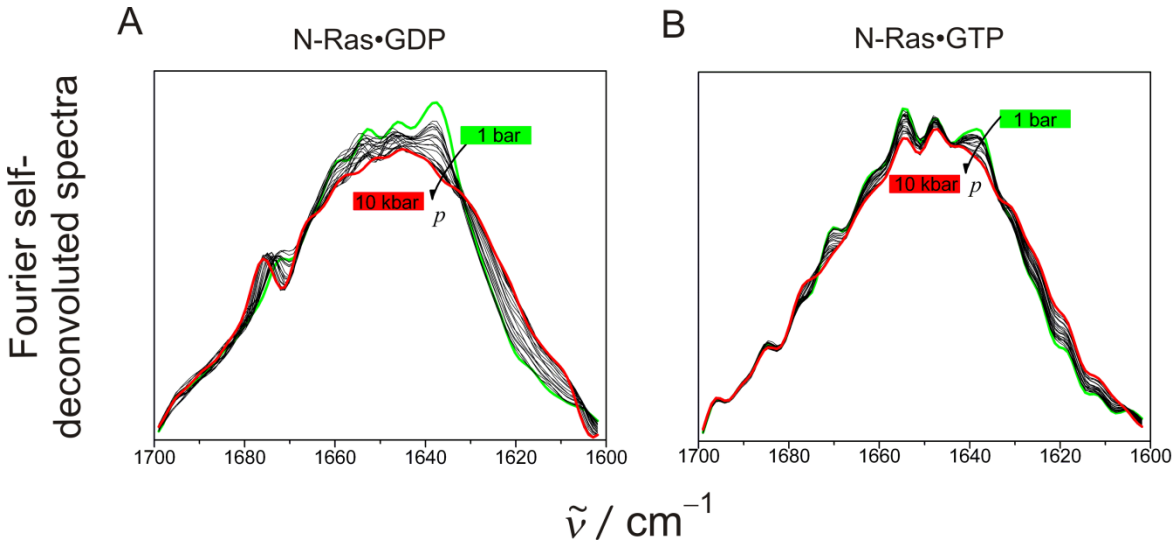

Figure 5.2: Conformational changes in N-Ras upon pressurisation in bulk solution. Fourier self-deconvoluted amide-I' spectra for (**A**) GDP- and (**B**) GTP-bound N-Ras at 25 ˚C, in the pressure range of 1 bar to 10 kbar.

Only small changes in the spectral shape were observed upon pressurisation, which are better visualised in the second derivative spectra of the amide-I′ band (Fig. 5.3 **A**, **B**). For GDP-

bound N-Ras, the α-helical subband (at 1658 cm^{-1} in the ambient pressure native state) showed a splitting at around 3.5 kbar suggesting pressure-induced changes in the α-helical/turn region of the protein. Appearance of peak positions at 1663 cm^{-1} and 1654 cm^{-1} indicated formation of solvent exposed turns/loops and solvated α-helices, respectively.[199-200] Concomitantly, a slight decrease of the intensity of intramolecular β-sheets (at 1637 cm^{-1}), with a parallel increase of a band at the lower wavenumber side, typical for exposed β-sheets, was observed. For the active form of the protein, a similar scenario was observed, but the exposed β-sheets appeared at much higher pressures (at > 5 kbar compared with that of the GDP form at 3.5 kbar), *indicating a higher pressure stability of this form*.

The pressure-induced changes in secondary structural elements were monitored by a quantitative fit analysis of the amide-I′ band (Fig. 5.3 **C**, **D**). As already mentioned above, even at high pressures N-Ras still retained its compact structures in both forms, with only minor changes observed, particularly with respect to an increase or decrease of certain secondary structures. For GDP-bound N-Ras, decreases were observed in the helix content by about 4 %, in turns by 5 %, and for intramolecular β-sheets by about 6 %. Increases were observed for random structures by 3 % and for exposed β-sheets by 10 %. Similarly, GTP-bound N-Ras also displayed minor changes, such as a decrease in helices by 2 %, in turns by 3 %, and in intramolecular β-sheets by 3 %, and increases were observed for random structures by 3 % and for exposed β-sheets by 4 %.

[199] Heremans, K., and Smeller, L. **(1998)**. Protein structure and dynamics at high pressure. *Biochim. Biophys. Acta 1386*, 353–370.
[200] Dzwolak, W., Kato, M., and Taniguchi, Y. **(2002)**. Fourier transform infrared spectroscopy in high-pressure studies on proteins. *Biochim. Biophys. Acta*. *1595*, 131–144.

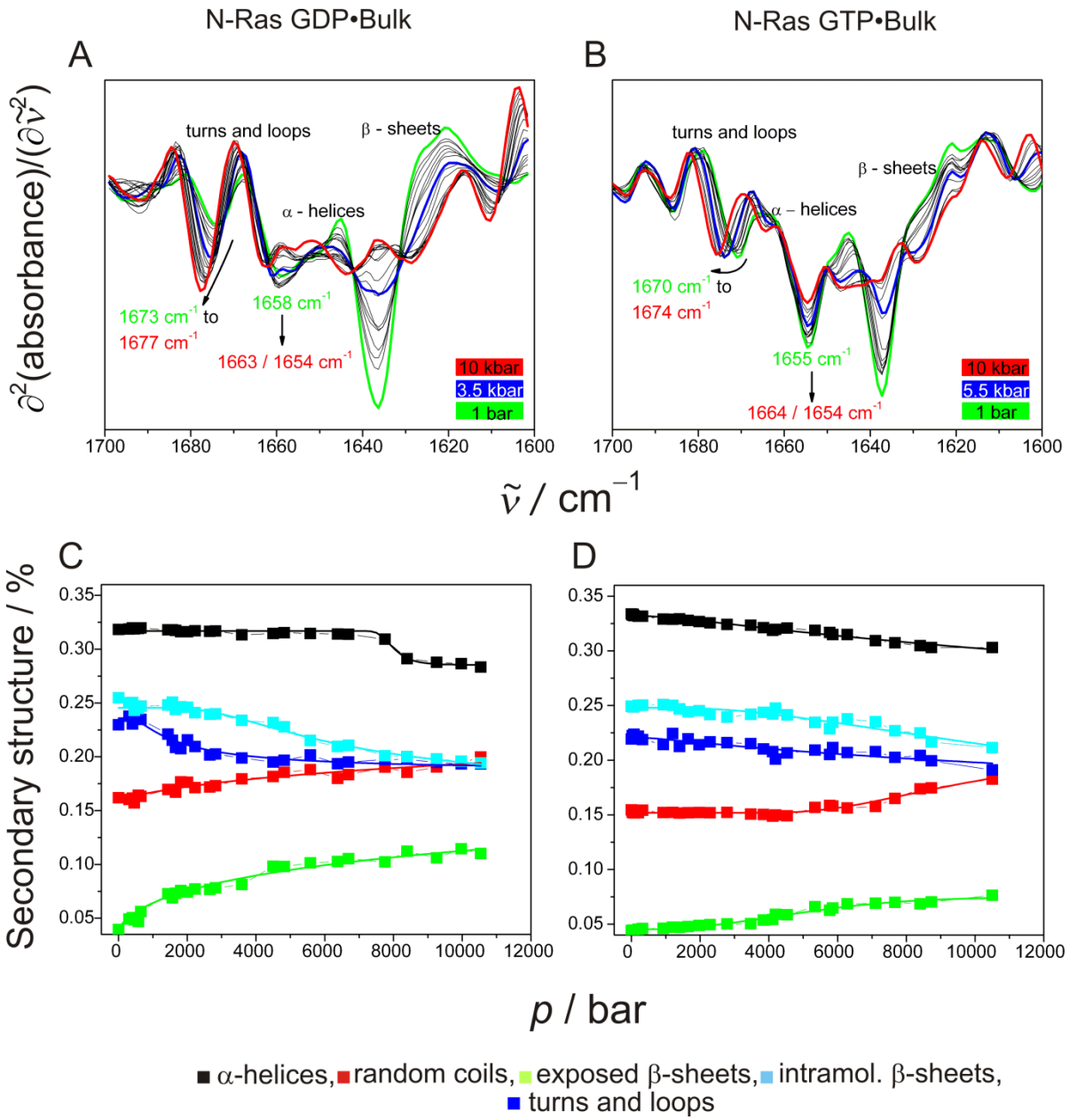

Figure 5.3: Conformational and secondary structural changes in N-Ras upon pressurisation in bulk solution. Second derivative amide-I' spectra for the (**A**) GDP- and (**B**) GTP-bound N-Ras, at 25 ˚C in the pressure range of 1 bar to 10 kbar. Change in the secondary structure elements of the (**C**) GDP- and (**D**) GTP-bound N-Ras, at 25 ˚C in the pressure range of 1 bar to 10 kbar. The concentration of each protein was 3 wt %. The secondary structure values were obtained by curve-fitting of the normalised FTIR amide-I' spectra. The secondary structure values with pressure have been fitted with a Sigmoidal distribution function (Weibull-2) distribution function using the software, Origin Pro 7.0. The goodness of the fit was in the range of 99.7-99.9 %.

These data indicate a pressure-induced shift towards a more solvent exposed β-sheet/disordered structure. This is achieved by weakening the hydrophobic interactions, allowing water to penetrate the protein interior, in particular at places where voids and cavities are present. It is known—by analysing the protein structure database—that β-strand residues have a higher propensity to line such cavities[201], thus accounting for the observed pressure-induced increase in the exposed β-sheets content. The (albeit small) differences observed between the two forms apparently connote the influence of the bound nucleotide on the packing mode of the protein, which determines the amplitude of pressure-dependent conformational changes.

The volume change, ΔV^0 accompanying the conformational change (from 1 bar till 10 kbar) was determined as follows. The standard volume change upon a conformational change in the protein (e.g. from state 1 to state 2) is given by, $\Delta V^0 = V^0_2 - V^o_1$, at temperature T, and can be determined from Eq. (2).

$$\Delta V^0 = \left(\frac{\partial \Delta G^0(p)}{\partial p} \right)_T \tag{2}$$

where, $\Delta G^0(p)$ is the standard Gibbs (free) energy change at pressure p, which in turn is determined from the equilibrium constant, $K_{eq}(p) = x_2(p)/x_1(p)$, using the IR band intensity/area profiles of the conformers in the two states (Fig. 5.3)[202]:

$$\Delta G^0(p) = -\mathrm{R}T \ln K_{\mathrm{eq}}(p) = -RT \ln \frac{I_1 - I(p)}{I(p) - I_2}, \tag{3}$$

where, $I(p)$ is the intensity/area at the pressure p, and I_1 and I_2 are the asymptotic intensity/area values of state 1 and state 2, respectively. The standard Gibbs energy change, ΔG^0 at 1 bar is obtained by extrapolation to 1 bar:

$$\Delta G^0 = \lim_{p \to 1\,\mathrm{bar}} \Delta G^0(p) \tag{4}$$

---

[201] Sonavane, S., and Chakrabarti, P. **(2008)**. Cavities and atomic packing in protein structures and interfaces. *PLoS Comput. Biol. 4*, e1000188.

[202] Panick, G., Malessa, R., Winter, R., Rapp, G., Frye, K.J., and Royer, C.A. **(1998)**. Structural characterization of the pressure-denatured state and unfolding/refolding kinetics of staphylococcal nuclease by synchrotron small-angle X-ray scattering and Fourier-transform infrared spectroscopy. *J. Mol. Biol. 275*, 389–402.

By this a volume change of $\Delta V^0 = -24 \pm 6$ mL/mol was obtained for the GDP-bound N-Ras from the pressure-dependent changes of the turns/loops, random, and exposed β-sheet structures. The pressure-induced changes were similar, but of lesser magnitude, in the GTP-bound N-Ras. For the GTP-bound form, ΔV^0 of about –14.7 mL/mol was obtained. Such volume changes are a factor of 3-5 smaller than those observed upon the pressure-induced unfolding of proteins,[202] thus corroborating the high pressure stability of Ras in the measured pressure range.

A well-known effect of pressure is to populate low volume conformers that are more solvated, thus decreasing the total volume of the protein system. Likewise, here the application of pressure to the conformational ensemble of N-Ras shifted the equilibrium existing between the distinct substates towards the more solvent exposed and open conformations, which could correspond to CS^1, in accordance with previous reports.[198] The GEF interacting state, CS^1 is known to have an enlarged protein surface, and is more open and solvated due to the opening of the nucleotide binding pocket, thus stabilising its interaction with GEFs. Such a structural characteristic for CS^1 implies that this state should be easily populated under pressure perturbation. By comparing the corresponding volume changes driving the conformational transition from CS^2 (heavily populated at ambient pressure) to CS^1 (weakly populated conformer) for N-Ras, as obtained by this and other studies (e.g. ^{31}P NMR on the unlipidated Ras GTP)[198], we can confirm that the increasing pressures shifts the Ras conformational equilibrium from CS^2 to CS^1.

An important finding in this study was the existence of the conformational equilibrium of CS^2/CS^1 in the GDP-bound, inactive N-Ras as well. Pressure stability for the GTP-bound N-Ras was higher compared to the GDP-bound form, deduced by lower amounts of exposed β-sheets, along with the splitting of the α-helical subband at high pressures. The first plausible reason for such a difference was estimated by comparing the free volume or cavities in both the forms (Fig. 5.4) from the available X-ray structures, using the software package msms and a probe radius of 1.4 Å [This calculation was performed by Dr. I. R. Vetter, at the Max Planck Institute of Molecular Physiology, Dortmund, Germany].[203] Cavities were found to

[203]Sanner, M.F., Olson, A.J., and Spehner, J.C. **(1996)**. Reduced surface: an efficient way to compute molecular surfaces. *Biopolymers 38*, 305–320.

account for less than 1% of the total protein volume, probably not significant enough to explain the differences. Moreover, qualitatively GTP-bound N-Ras seemed to have a slightly higher cavity volume, so that a higher pressure sensitivity (or lower pressure stability) could be foreseen for this form. Clearly this was not observed in the experimental data, and the higher predisposition to form open and solvent exposed conformations in the GDP-bound N-Ras should have arisen from other reasons, as discussed below.

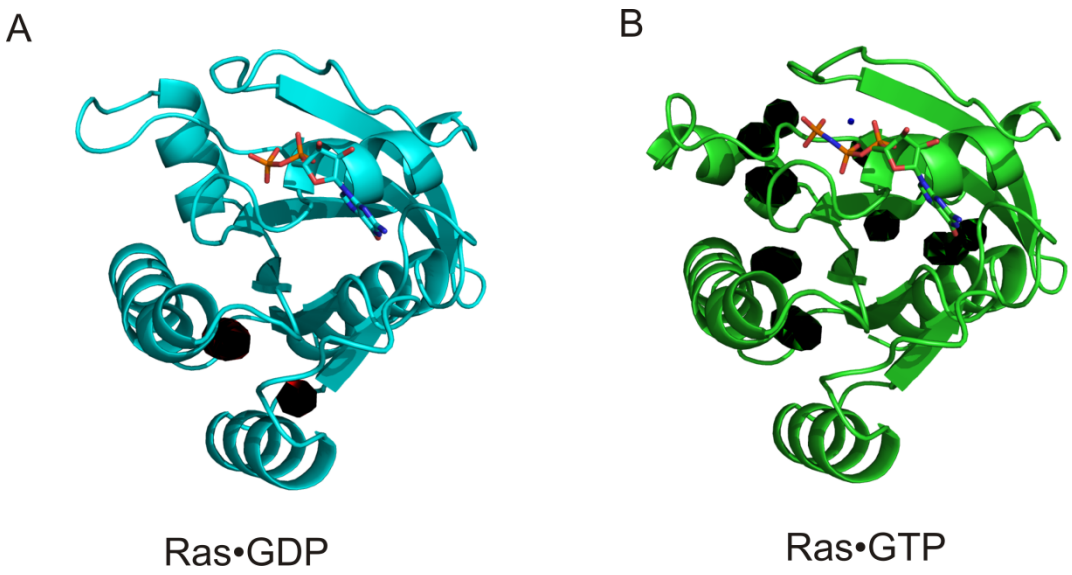

Figure 5.4: Schematic representation of the cavities (in black) in Ras·GDP (A) and Ras·GTP (B). The structure of the G-domain for the GDP- and GTP-bound form was adopted from the PDB 4q21 and 5q21, respectively. The two switch regions are on the top of the images. For Ras·GTP, there are 10 cavities calculated among which only three are large enough to capture a water molecule, and one of these cavities overlaps with a cavity found in Ras·GDP.

Since, the $CS^{1 \text{ and } 2}$ in Ras are assigned to the different conformations of the Switch I region, differences in the pressure dependence of the GDP and GTP forms is possibly linked to the flexibility of the switch regions, which is much greater in the GDP-bound Ras (**cf. Fig. 1.3 A**). The existence of a potentially easier opening of the highly flexible Switch I region in the GDP-bound N-Ras was proven by comparing the initial slopes in Fig. 5.3 **C-D**, for the increase of the exposed β-sheets (Δ[exposed sheets]/Δp) up to 2 kbar. It was found to be higher in the GDP-bound N-Ras (1.84×10^{-5}) compared with the GTP-bound N-Ras (2.09×10^{-6}). The slopes were compared only up to 2 kbar, keeping in mind that in the previously published report[198] a maximum pressure of about 2 kbar changed the ratio of CS^2:CS^1 from

2:1 to 1:2 in the GTP-bound Ras. Therefore, under the pressure of approximately 10 kbar, the shift to state 1 is probably (almost) complete, and thus the corresponding changes in the observables should exhibit the most significant changes only up to 2 kbar, with minor changes at pressures beyond 2 kbar. This explanation is further supported by ultrasound velocimetry studies providing insights into the flexibility–compressibility relationship of proteins,[204] and suggests a higher compressibility of the more flexible regions in proteins. *Finally, high pressure induces substate 1 in both the GTP- and GDP-bound N-Ras protein, but due to a higher flexibility of the GDP-form, the substate 1 is populated more easily*.

5.3.2. Effect of membrane binding on the conformational substates of N-Ras

Membrane interaction of Ras proteins is crucial for their signalling properties; as such, the effect of membrane binding on the pressure-induced conformational sub-space were explored, and compared to the bulk solution behaviour. Upon insertion into the neutral raft-like membranes consisting of DOPC:DPPC:Chol (1:2:1, molar ratio) at 1 bar, no major secondary structural changes were observed in the GDP- and GTP-bound N-Ras (in agreement with studies documented in Ch. 4). Moreover, upon pressurisation, no unfolding was observed in the membrane-bound proteins, evident from the asymmetric shape of the amide-I' spectra (Figs. 5.5 **A** and **B**). However, significant changes were identified in the second derivative amide-I' spectra (Figs. 5.5 **C** and **D**). Changes were observed mainly in the α-helical, loop, and β-sheet regions. First, the α-helical subbands were broader in the membrane-bound proteins, suggesting the existence of different spatial orientations of helices (mainly α4 and α5) and the hypervariable region (HVR), and their subsequent involvement in membrane binding. Pronounced splitting for the α-helical band for the membrane-bound inactive N-Ras was observed above 7 kbar (in the bulk solution, the splitting was observed at lower pressures of 3.5 kbar), and thereafter both the band shoulders were distinguishable up to 10 kbar. For the membrane-bound active N-Ras, definite splitting of the α-helical band was observed at low pressures (clearly visible above 600 bar), forming a shoulder at 1664 cm^{-1} (solvated turns and loops) and at 1653 cm^{-1} (solvated helices). The splitting at such low pressures could possibly be due to a significant involvement of the α-helical region of the G-

[204] Gekko, K., Kamiyama, T., Ohmae, E., and Katayanagi, K. **(2000)**. Single amino acid substitutions in flexible loops can induce large compressibility changes in dihydrofolate reductase. *J. Biochem. 128*, 21–27.

domain upon membrane insertion in the GTP-bound state. This was finally proven and shown to arise from a different overall orientation of the G-domain with respect to the membrane, leading to a pronounced membrane interaction of the helical counterparts, as deduced from the polarized ATR-FTIR and IRRAS studies described in Chapter 4 (**cf. Ch. 4, Fig. 4. 18**)

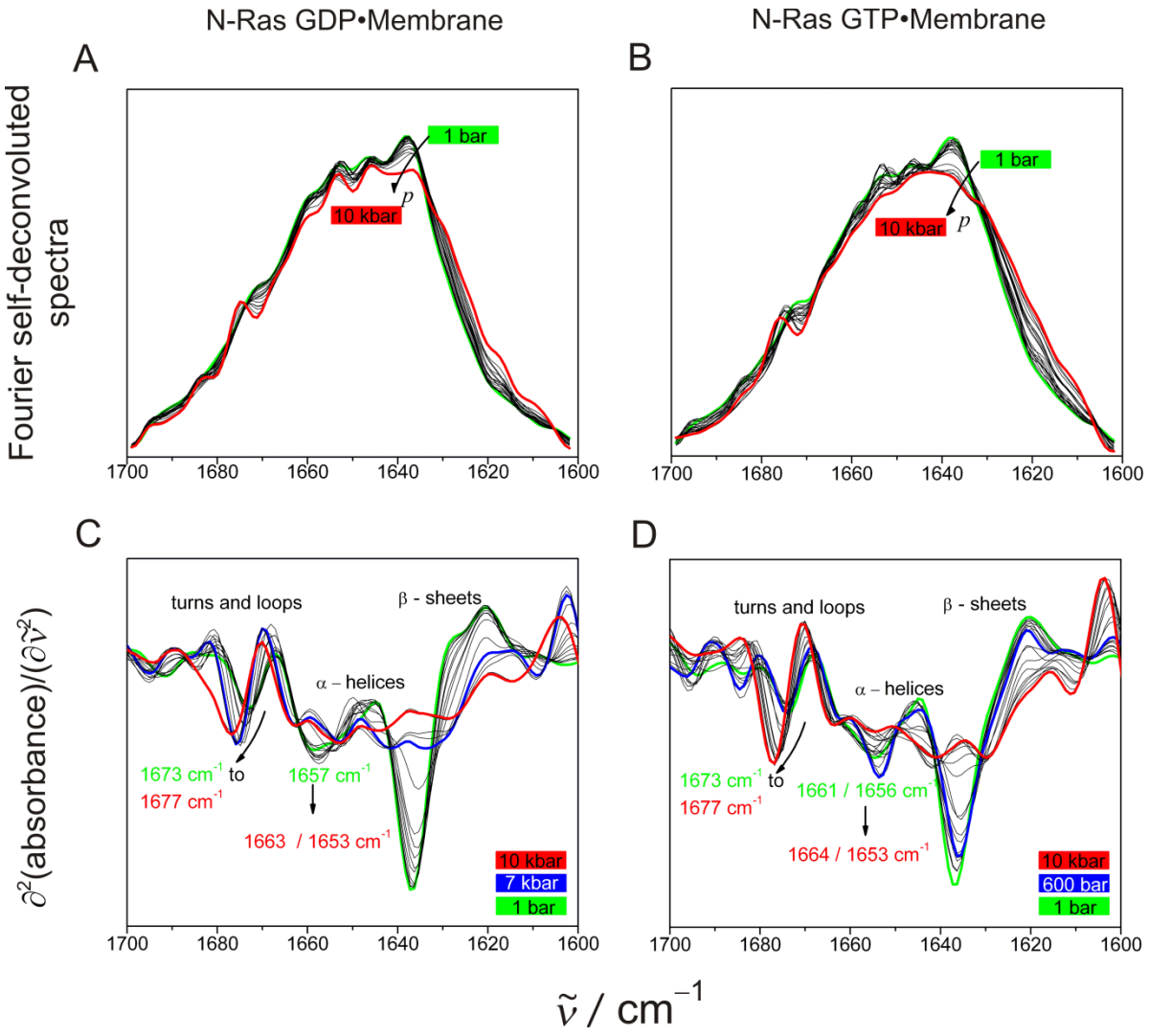

Figure 5.5: Conformational changes in membrane-bound N-Ras upon pressurisation. Fourier self-deconvoluted amide-I' spectra for (**A**) GDP- and (**B**) GTP-bound N-Ras inserted into the neutral raft-like lipid vesicles (DOPC:DPPC:Chol 25:50:25 (molar ratio)), at 25 ˚C in the pressure range of 1 bar to 10 kbar. Corresponding changes in the second derivative amide-I' spectra for (**C**) GDP- and (**D**) GTP-bound N-Ras. The concentration of each protein was 3 wt%, with a protein to lipid molar ratio of 1:100.

Analysing the variations in the secondary structure contents of membrane-bound N-Ras in the different nucleotide states with pressure (Fig. 5.6), revealed a decrease in the helix

content of GDP-bound N-Ras by about 3 %, and turns by 6.0 %. Increases were observed for random coils by 2 % and exposed β-sheets by 6 %. Similarly, GTP-bound N-Ras also showed minor changes, such as a decrease in helices by 3 %, turns by 6 % and increases in random coils and exposed β-sheets by 3 % and 6 %, respectively. Most remarkably, the pressure dependence for the intramolecular β-sheets structures was strikingly different for both the membrane-bound N-Ras forms when compared with the bulk solution. Increasing pressures first stabilised the intramolecular β-sheets, and finally at even higher pressures (> 4 kbar), a trend reversal was observed, where the intramolecular β-sheet contribution slightly decreased. The occurrence of the intensity maximum of this band indicates the existence of an additional conformational equilibrium, i.e. the population of a further, membrane-induced conformational substate of the protein (denoted as substate 3: CS^3 hereafter).

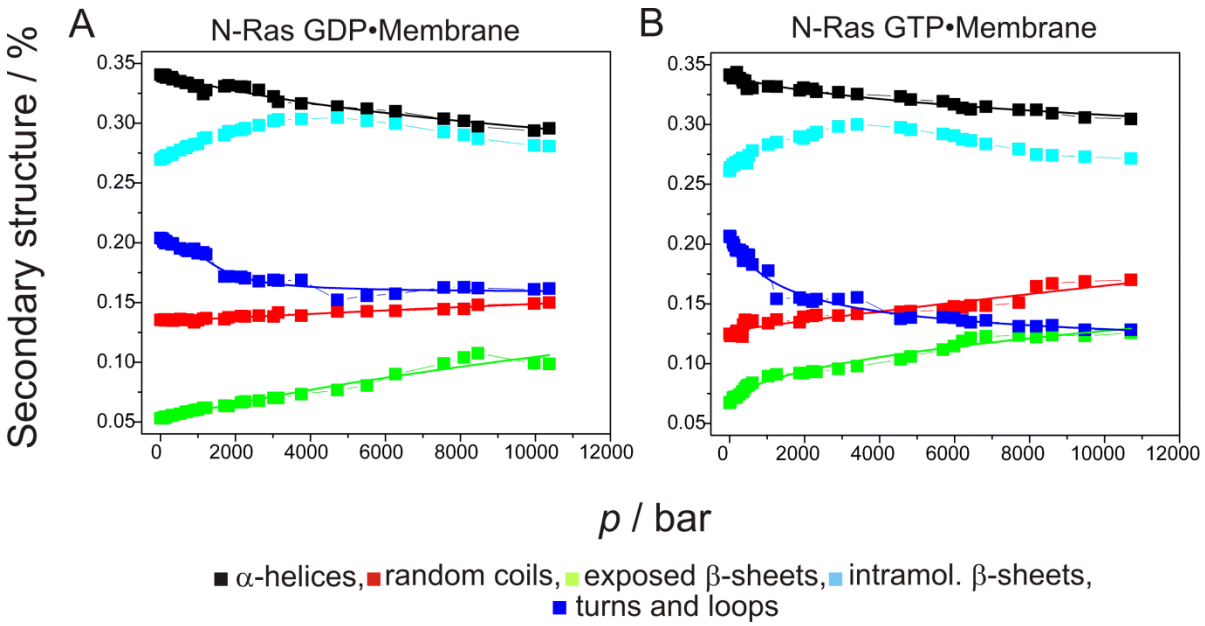

Figure 5.6: Secondary structure changes in the membrane-bound N-Ras upon pressurisation. Change in the secondary structure elements in the (**A**) GDP- and (**B**) GTP-bound N-Ras protein inserted into the neutral raft-like lipid vesicles (DOPC:DPPC:Chol 25:50:25 (molar ratio)), at 25 ˚C in the pressure range of 1 bar to 10 kbar. The concentration of each protein was 3 wt %, with a protein to lipid molar ratio of 1:100. The secondary structure values were obtained by curve-fitting of the normalised FTIR amide-I' spectra. The secondary structure values with pressure have been fitted with a Sigmoidal distribution function (Weibull-2) using the software, Origin Pro 7.0. The goodness of the fit was in the range of 99.5-99.8 %.

As demonstrated, not only the nucleotide binding, but also the membrane binding modulates the conformational dynamics of N-Ras markedly, and interestingly, brings about new and opposite changes in the conformational properties of the membrane-bound N-Ras GDP and GTP, respectively. Upon membrane binding, the pressure sensitivity of the two nucleotide-bound states of N-Ras was reversed. This is attributed to the two different preferred orientations of the proteins at the membrane interface (**cf.** Fig, 4.18). Occurrence of the CS^3 was found to be faster and at lower pressures (~ 600 bars) in the GTP-bound state. The volume change driving the conformational transition from CS^2 to CS^3 for the GTP-bound N-Ras was estimated to be approximately ~ –41 ± 2 mL/mol. This enabled the CS^3 (the lowest volume conformer) to get substantially populated than the CS^1 up to intermediate pressures only. The conformational transition from CS^2 to CS^1 occurred in parallel and dominated only at higher pressures (evident by the non-linear change of intramolecular β-sheets with pressure). Efficient interaction with GEFs and effectors requires selection of CS^1 and CS^2 respectively, shifting the equilibrium towards these states. This study indicates that upon membrane binding, such conformational selection is additionally modulated, preselecting CS^3 with significant structural rearrangements. Through these conformational changes, the interaction with membrane-associated interaction partners, such as effectors and activity modulators (e.g. galectins), may be influenced. In fact, recent *in vivo* studies have revealed high affinity of galectins for the GTP-bound Ras. This could also be due to the interaction with CS^3, as the GTP-bound N-Ras shows a higher favourable predisposition to shift its conformational equilibrium towards CS^3.

5.3.3. Mapping the intrinsic fluorescence of N-Ras as a function of pressure

The effect of membrane binding on the Ras CS was further studied by employing high pressure fluorescence spectroscopy. In this respect, N-Ras protein shows intrinsic fluorescence due to the presence of tyrosine and phenylalanine amino acids. In the absence of tryptophan (present case), tyrosine dominates the absorption spectra to the exclusion of phenylalanine and other non-aromatic absorptions designated to cysteine, histidine, or the peptide bonds. The intrinsic fluorescence of proteins containing tryptophan or—to a lesser

extent—tyrosine is a valuable tool to study the insertion of proteins into lipid membranes.[205] As a result of its sensitivity to the microenvironment that lead to observable changes in the spectral characteristics (such as lifetime, anisotropy or intensity), the intrinsic tyrosine fluorescence has also been employed to study the stages of aggregation pathways in amyloidal proteins.[206-207] The tyrosine emission maximum of GTP-bound N-Ras in the bulk solution (at 302 nm) revealed no observable changes (Fig. 5.7), supporting the corresponding HP-FTIR results.

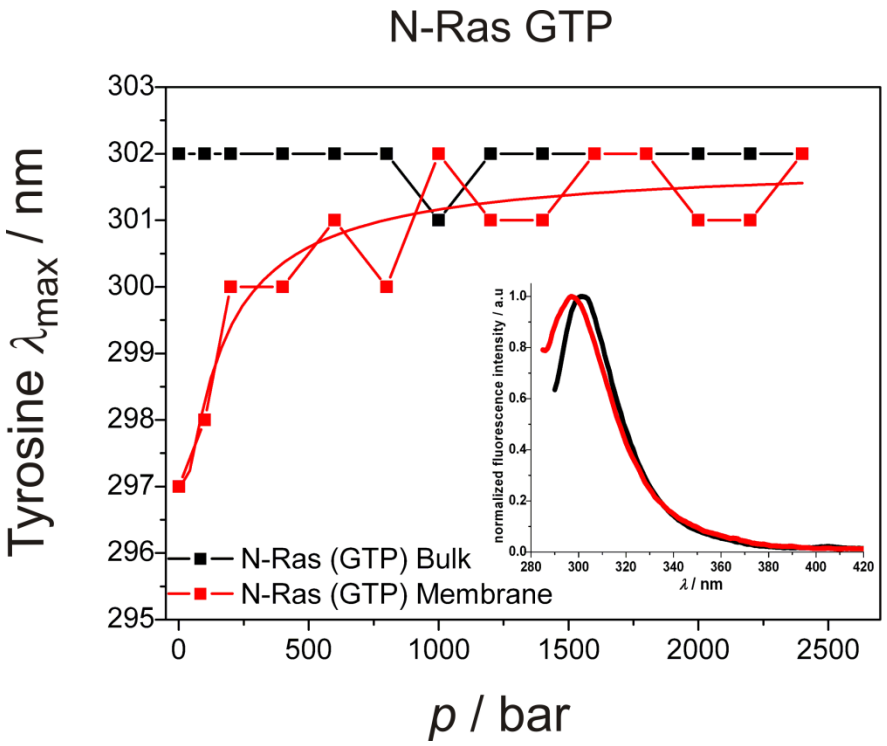

Figure 5.7: Tyrosine fluorescence changes in N-Ras upon pressurisation Fluorescence emission spectra showing the variation of the tyrosine emission maximum as a function of pressure for the GTP-bound N-Ras in bulk solution and bound to the neutral raft-like lipid membrane (DOPC:DPPC:Chol 25:50:25 (molar ratio)), at 25 ˚C in the pressure range 1 bar to 2.5 kbar. Inset: Emission spectra of the GTP-bound N-Ras in the two different environments at ambient pressure. The protein concentration was 4.58 µM, with a protein to lipid molar ratio of 1:100.

[205] Matos, P.M., Franquelim, H.G., Castanho, M.A., and Santos, N.C. **(2010)**. Quantitative assessment of peptide-lipid interactions. Ubiquitous fluorescence methodologies. *Biochim. Biophys. Acta 1798*, 1999–2012.
[206] Bekard, I.B., and Dunstan, D.E. **(2009)**. Tyrosine autofluorescence as a measure of bovine insulin fibrillation. *Biophys. J. 97*, 2521–2531.
[207] Amaro, M., Birch, D.J., and Rolinski, O.J. **(2011)**. Beta-amyloid oligomerisation monitored by intrinsic tyrosine fluorescence. *Phys. Chem. Chem. Phys. 13*, 6434–6441.

In the membrane-bound form, the tyrosine emission maxima initially shifted towards a lower wavelength at 1 bar (from 302 nm to 297 nm), due to a less hydrophilic environment rendered by the lipid interface (Fig. 5.7 **inset**). Upon pressurisation, a red shift in the emission maxima was observed at pressures as low as 200 bar due to the solvent exposure of the tyrosine residues upon pressurisation. The non-linear pressure dependence of the emission maximum is due to the conformational changes occurring in the protein bound to lipid vesicles which, again, could arise due to the different orientations of the G-domain with respect to the membrane interface. Taken together, these results provide additional support in showing that membrane binding substantially affects the pressure-induced changes in the conformational substates of N-Ras proteins.

5.3.4. Temperature modulation of the Ras conformational equilibrium

To ascertain whether temperature modulation could also serve as a tool in revealing the low-lying excited N-Ras substates, changes occurring in the GDP- and GTP-bound N-Ras with temperature were explored. As expected, the temperature-induced structural changes were more pronounced and strikingly different from the pressure-induced changes. The spectrum of the native proteins acquired in the temperature cell was not distinguishable from that measured in the high pressure cell. No significant changes were observed below 55 ˚C, and above this temperature, the intensity for the ordered structures, like α-helices, β-sheets and turns, started to decrease significantly. This was followed by a concomitant increase of the intensity at around 1619 cm^{-1} and 1683 cm^{-1}, characteristic hallmarks of the intermolecular antiparallel β-sheet structures due to protein aggregation (Fig. 5.8 **A**-**B**).

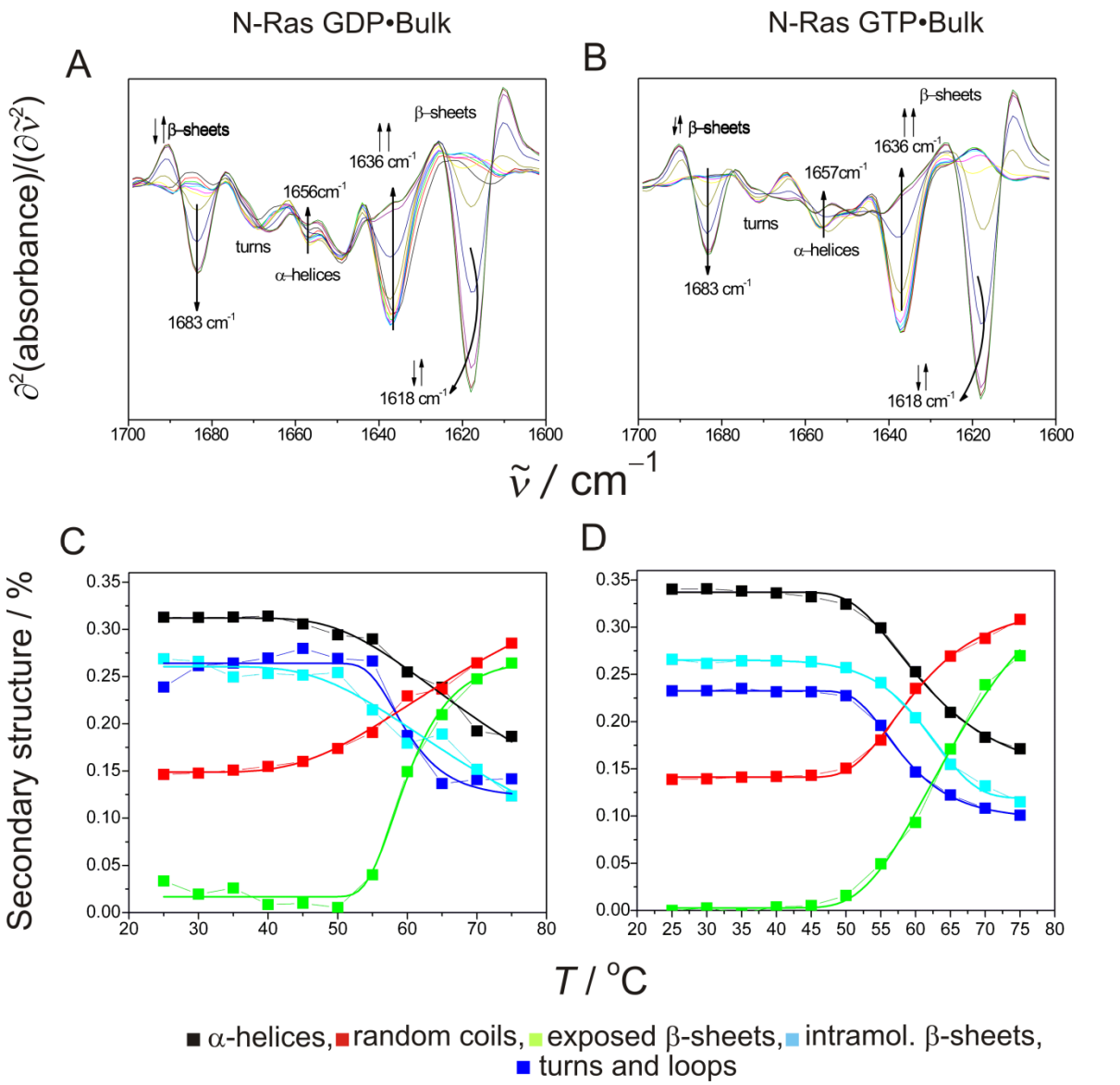

Figure 5.8: Temperature modulation of the conformational sub-space of N-Ras. Second derivative amide-I' spectra for the (**A**) GDP- and (**B**) GTP-bound N-Ras protein in the bulk solution at 1 bar, in the temperature range 25 ˚C to 75 ˚C. The corresponding change in the secondary structure elements of the (**C**) GDP- and (**D**) GTP-bound N-Ras protein at 1 bar in in the temperature range of 25 ˚C to 75 ˚C. The secondary structure values were obtained by curve-fitting of the normalised FTIR amide-I' spectra. The secondary structure values with temperature have been fitted with a Sigmoidal distribution function (Weibull-2) using the software, Origin Pro 7.0. The goodness of the fit was in the range of 99.5-99.8 %. The concentration of each protein was 0.233 mM, with a protein to lipid molar ratio of 1:100.

The thermal aggregation that sets in after the temperature-induced unfolding of N-Ras was found to be irreversible upon returning to ambient temperatures. The same message was

deduced from the variation of secondary structure changes (Fig. 5.8 **C-D**). The temperature-induced decrease of the structural contents linked to intramolecular β-sheets, turns and α-helices was accompanied by an increase in conformations originating from unordered structures. Within the experimental error, no marked differences in the thermal behaviour of the GTP- and GDP-bound N-Ras both in the bulk and in the membrane-bound forms were obtained. Only minor changes were observed with respect to the onset of thermal aggregation, with significant amounts of intermolecular β-sheets formed at a slightly higher (~ 2.5 ˚C) temperature (Fig. 5.8 **C-D**), in the GTP-bound form. This could be due to the different packing modes of the structural elements. Similar effects were observed for the membrane-bound N-Ras GDP and GTP, respectively. These studies demonstrate the viable use of pressure as a mild perturbant, resulting in fully reversible changes; a prerequisite for determination of thermodynamic properties of the system. Alternatively, temperature modulation was less successful, resulting in irreversible unfolding and aggregation of the proteins.

5.4 Summary and Outlook

In an attempt to fully understand the structure, dynamics, and function of signalling proteins and their signalling networks, the vast conformational space exhibited by them needs to be explored. For this endeavour, pressure modulation was applied to explore the conformational substates of Ras that might be linked to the various signalling outputs. This was accomplished by using the ability of pressure to populate low volume-high energy conformers. Pressure perturbation shifted the Ras conformational equilibrium in bulk solution from CS^2 (native state), towards the more open and solvent exposed CS^1 (non native high energy), for both the nucleotide-bound states of the N-Ras protein. This transition exhibited faster kinetics in the inactive N-Ras protein, due to a higher flexibility of its switch regions. In addition, next to the nucleotide state, the membrane also played an important role in the conformational selection and dynamics, by inducing a marked population of another substate, CS^3. The membrane-induced substate became clearly detectable at high pressures (up to 4 kbar), and was accompanied by a significant structural reorientation of the G-domain

at the lipid interface, particularly in the GTP-bound N-Ras protein.[208] At higher pressures only (i.e. beyond 4 kbar), the transition to CS^1 is fostered, since it corresponds to the substate with the lowest free energy.

CS^3 is expected to foster the interactions with membrane-associated interaction partners involved in the Ras signal transduction pathway.

A schematic representation of the pressure modulation of the Ras conformational substates is depicted in Figure 5.9. Owing to the high intrinsic flexibility of the switch loops in the GDP-bound N-Ras protein, a rapid inter-conversion between the different conformers is expected. Thus, the energy funnels of the substates in the GDP-bound N-Ras are expected to be broader.

[208] Kapoor, S., Triola, G., Vetter, I.R., Erlkamp, M., Waldmann, H., and Winter, R. **(2012)**. Revealing conformational substates of lipidated N-Ras protein by pressure modulation. *Proc. Natl. Acad. Sci. U.S.A. 109*, 460–465.

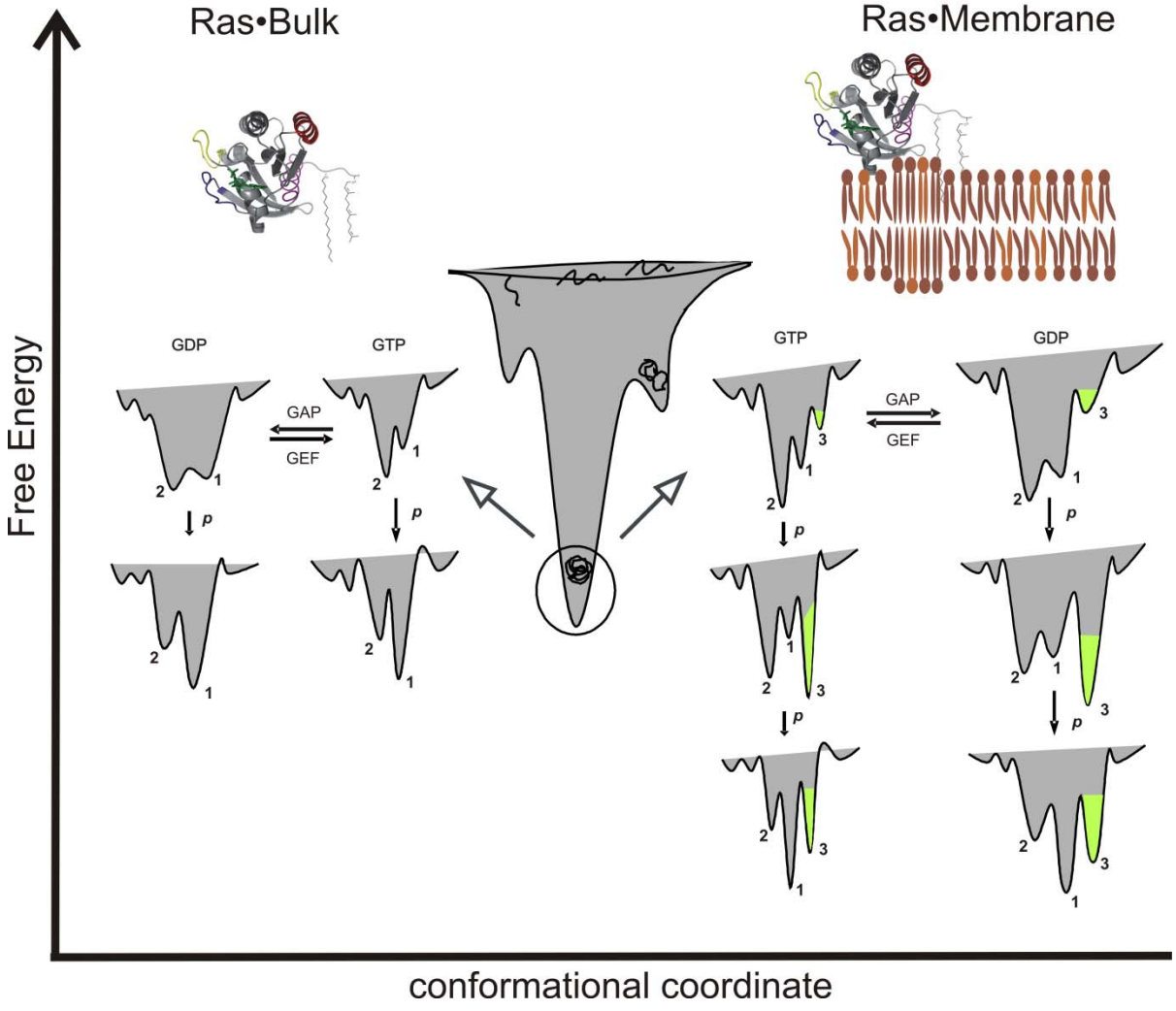

Figure 5.9: Pressure modulation of the Ras conformational substates. Schematic representation of the pressure modulation of conformational substates of active GTP- and inactive GDP-bound N-Ras in bulk solution and in the presence of membranes. Small arrows indicate changes at low pressure values, and longer arrows indicate changes occurring after application of higher pressures. The membrane-associated substate is marked in green.

Finally, these results also shed some light on the effect of high pressure on membrane-associated Ras-controlled signalling events under extreme environmental conditions. Although pressure is an important environmental parameter, such as in the deep sea where organisms have to cope with pressures as high as 1 kbar, the fundamental understanding of its effects remain largely fragmentary. The effects of pressure on gene expression or on biomolecules such as lipid membranes, proteins, and DNA have been studied in recent years.

However, the effects of pressure on the dynamics of metabolic events and signalling processes have been largely unexplored.

Considering the functional aspect of the higher energy conformers in general, and their relevance to Ras, this study has numerous practical implications in areas such as drug design and protein engineering. Designing small molecule inhibitors against the high energy conformer would weaken the interactions with effectors, and curb oncogenic Ras signalling. In this regard, this study discloses one problem (and opportunity) not yet discussed in detail, i.e. the evaluation of the functional aspect of CS^3. Future studies into the effect of pressure on the membrane-bound Ras proteins, in the presence of their putative interaction partners, would help in understanding not only the accurate functional relevance of CS^3, but also the conformational dynamics, free energy landscape and function of Ras in its membrane-associated state. Along a similar line, enhanced exploration of the conformational sub-space of mutated membrane-bound Ras is also required. Moreover, this study was conducted only on one of the Ras isoforms (N-Ras) and should be conducted on others as well, since the recent studies have revealed different ratios of the high energy conformers in different Ras isoforms, though only in the bulk solution.[192] Fine-tuning of the conformational equilibrium of each Ras isoform, to gain structural insights into their high energy conformers (isoform-specific?), might aid in designing Ras isoform-specific drugs, a dream that has not been realised to date. To this end, such studies have another advantage not considered before, i.e. biasing the docking approaches towards the high energy and functional protein conformations would considerably reduce the computational time, thus making application of the energy landscape theory to drug design more viable.

VI

INTERACTION OF PRENYL-BINDING PROTEIN (PDEδ) WITH RAS*

* The majority of the work in the present study has been published and subsequently reprinted in parts (some figures) with permission from Weise, K., Kapoor, S., Werkmüller, A., Möbitz, S., Zimmermann, G., Triola, G., Waldmann, H., Winter, R. **(2012)**. Dissociation of the K-Ras4B/PDEδ complex upon contact with lipid membranes: Membrane delivery instead of extraction. *J. Am. Chem. Soc*., *134*, 11503-11510. Copyright (2012) American Chemical Society.

6.1 Background

6.1.1 Cyclic Nucleotide Phosphodiesterase 6 Regulatory Binding Protein: PDEδ

Cyclic nucleotide phosphodiesterases (PDEs) form a large family of enzymes[209] that regulate the cellular levels of second messengers, cAMP and cGMP, which, in turn, are involved in the signal transduction and regulation of physiologic responses. Of the 11 PDE families (PDE1-11), PDE6 is an integral part of the vertebrate visual transduction cascade serving as an effector enzyme for the trimeric G protein transducin, in the photoreceptor cells (i.e. rods and cones). The rod photoreceptor PDE6 core is a heterodimer composed of two catalytic subunits–PDE6α and PDE6β,[210] and two identical inhibitory subunits–PDE6γ.[211] Each catalytic subunit is posttranslationally modified at its C terminus with an isoprenyl group (farnesyl or geranylgeranyl), responsible for anchorage to the outer segment disk membrane.[212] A putative fourth subunit of PDE6 was isolated and later termed as the "δ-subunit of PDE6"—PDEδ.[213] PDEδ was demonstrated to directly bind to the prenylated C-terminus of the catalytic subunits of PDE,[214] resulting in its solubilisation and translocation from the rod outer segment disk membrane to the cytoplasm.[215] PDEδ allosterically regulates PDE6, reducing the efficacy of phototransduction and light-activated cGMP hydrolysis.[216]

---

[209] Beavo, J.A. **(1995)**. Cyclic nucleotide phosphodiesterases: functional implications of multiple isoforms. *Physiol. Rev. 75*, 725–748.

[210] Baehr, W., Devlin, M.J., and Applebury, M.L. **(1979)**. Isolation and characterization of cGMP phosphodiesterase from bovine rod outer segments. *J. Biol. Chem. 254*, 11669–11677.

[211] Deterre, P., Bigay, J., Forquet, F., Robert, M., and Chabre, M. **(1988)**. cGMP phosphodiesterase of retinal rods is regulated by two inhibitory subunits. *Proc. Natl. Acad. Sci. U.S.A. 85*, 2424–2428.

[212] Qin, N., Pittler, S.J., and Baehr, W. **(1992)**. In vitro isoprenylation and membrane association of mouse rod photoreceptor cGMP phosphodiesterase alpha and beta subunits expressed in bacteria. *J. Biol. Chem. 267*, 8458–8463.

[213] Gillespie, P.G., Prusti, R.K., Apel, E.D., and Beavo, J.A. **(1989)**. A soluble form of bovine rod photoreceptor phosphodiesterase has a novel 15-kDa subunit. *J. Biol. Chem.. 264*, 12187–12193.

[214] Cook, T.A., Ghomashchi, F., Gelb, M.H., Florio, S.K., and Beavo, J.A. **(2000)**. Binding of the delta subunit to rod phosphodiesterase catalytic subunits requires methylated, prenylated C-termini of the catalytic subunits. *Biochemistry 39*, 13516–13523.

[215] Florio, S.K., Prusti, R.K., and Beavo, J.A. **(1996)**. Solubilization of membrane-bound rod phosphodiesterase by the rod phosphodiesterase recombinant delta subunit. *J. Biol. Chem. 271*, 24036–24047.

[216] Cook, T.A., Ghomashchi, F., Gelb, M.H., Florio, S.K., and Beavo, J.A. **(2001)**. The delta subunit of type 6 phosphodiesterase reduces light-induced cGMP hydrolysis in rod outer segments. *J. Biol. Chem*. *276*, 5248–5255.

However, the role of PDEδ extends beyond the photo-transduction cascade. This protein is ubiquitously expressed in a variety of non-retinal tissue, including heart, placenta, lung, brain, liver, and skeletal muscles. Furthermore, it interacts with proteins unrelated to known photo-transduction processes, such as Rab13[217] and the Arf-like proteins: Arl2 /Arl3.[218] This clearly suggests versatile biological activities of PDEδ.

6.1.2 PDEδ as a Prenyl-binding Protein: Significance for Ras

The crystal structure of PDEδ[219] (Fig. 6.1 **A**) displays a hydrophobic pocket packed by two β-sheet structures. The overall β-sandwich fold is identical to that of RhoGDI (a guanine-nucleotide dissociation inhibitor that binds to prenylated GDP-bound small G-proteins, and thus generates a cytoplasmic pool of inactive G-proteins). The structure-based sequence alignment reveals that the residues lining the inner surface of the hydrophobic pocket are in identical or similar positions in both the proteins, suggesting that not only the fold, but also the lipid-binding pocket are common features in both PDEδ and RhoGDI. Based on the similarity of their three-dimensional structures (implying that PDEδ might have analogous functions), this family of proteins (which also includes the PDEδ-homologues UNC119/RG4) seems to define a novel class that interacts with prenylated proteins and regulates their association with lipid membranes. However, in terms of prenylated ligand's specificity, PDEδ is less restricted than RhoGDI. Whereas only GTPases of the Rho family can interact with RhoGDI, PDEδ solubilises various prenylated proteins including kinases, PDE subunits, Ras, and Rheb.[59,220-221] In addition, binding is specific for farnesylated versus geranylgeranylated G proteins, both *in vivo* and *in vitro*.[220] Surprisingly, PDEδ also binds to other small G proteins–Arl2 and Arl3 in a prenyl-chain independent manner, where the

[217] Marzesco, A.M., Galli, T., Louvard, D., and Zahraoui, A. **(1998)**. The rod cGMP phosphodiesterase delta subunit dissociates the small GTPase Rab13 from membranes. *J. Biol. Chem.. 273*, 22340–22345.
[218] Linari, M., Hanzal-Bayer, M., and Becker, J. **(1999)**. The delta subunit of rod specific cyclic GMP phosphodiesterase, PDE delta, interacts with the Arf-like protein Arl3 in a GTP specific manner. *FEBS Lett. 458*, 55–59.
[219] Hanzal-Bayer, M., Renault, L., Roversi, P., Wittinghofer, A., and Hillig, R.C. **(2002)**. The complex of Arl2-GTP and PDE delta: from structure to function. *EMBO J. 21*, 2095–2106.
[220] Zhang, H., Liu, X.H., Zhang, K., Chen, C.K., Frederick, J.M., Prestwich, G.D., and Baehr, W. **(2004)**. Photoreceptor cGMP phosphodiesterase delta subunit (PDEdelta) functions as a prenyl-binding protein. *J. Biol. Chem. 279*, 407–413.
[221] Nancy, V., Callebaut, I., El Marjou, A., and de Gunzburg, J. **(2002)**. The delta subunit of retinal rod cGMP phosphodiesterase regulates the membrane association of Ras and Rap GTPases. *J. Biol. Chem. 277*, 15076–15084.

binding is highly specific for the GTP-bound form, thus classifying PDEδ as a bonafide effector of the Arl2/3 proteins.[218] This leads to two important conclusions: PDEδ can interact with proteins in two ways-(1) through a lipid binding pocket (Fig. 6.1 **A**) and, (2) through β-sheet/β-sheet interactions (Fig. 6.1 **B**).

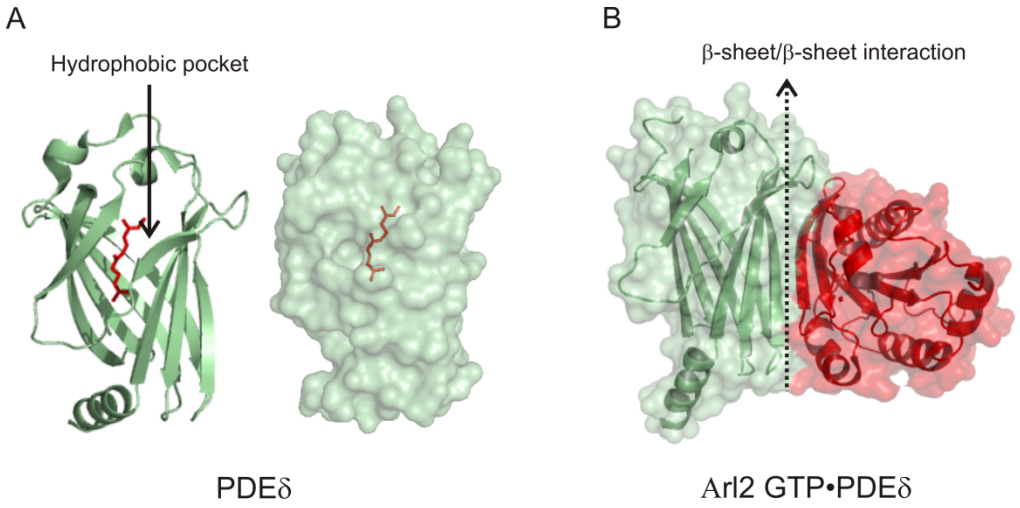

Figure 6.1: Structure of PDEδ and its interaction modes with a protein. (**A**) Ribbon representation of PDEδ in green (PBD: 3T5G) showing the immunoglobulin-like fold. In red "stick representation" is the farnesyl lipid moiety modelled from PDB: 3T5I. Next to it is the surface representation of PDEδ, with transparency set at 40 %, showing the farnesyl deeply penetrating PDEδ. (**B**) The ribbon diagram of the complex of Arl2·GTP with PDEδ (PDB: 1KSJ) showing the inter-protein β-sheet interactions involving β2 of the Arl2 and β7 of PDEδ. All the images were generated using PyMOl.

Recently, it has been shown that the cytoplasmic prenyl-binding factor PDEδ assists in H/N/K-Ras trafficking. Specifically, it shields the Ras hydrophobic anchor from the cytosol, facilitating intracellular Ras diffusion, and augments signalling by enriching Ras at the PM.[147,221] On the contrary, a PDEδ-mediated extraction of membrane-anchored Ras protein from cellular membranes was proposed, but no molecular level details of such an interaction were provided.[221-222] In either case it *is proposed* that this interaction occurs mainly via the insertion of the Ras lipid anchor into the PDEδ hydrophobic pocket, and the absence in PDEδ of a RhoGDI "regulatory arm"—known to contact the switch regions of the G-domain—implies a nucleotide-independent binding of Ras to PDEδ. In contrast, some reports *propose*

[222] Bhagatji, P., Leventis, R., Rich, R., Lin, C.J., and Silvius, J.R. **(2010)**. Multiple Cellular Proteins Modulate the Dynamics of K-ras Association with the Plasma Membrane. *Biophys. J. 99*, 3327–3335.

that the solvent (though short) exposed N-terminal helix of PDEδ could, in analogy to RhoGDI, be involved in interaction with the G-domain. But the lack of crystal structure for the PDEδ•Ras complex makes such statements highly speculative.

If PDEδ indeed sustains the dynamic distribution of Ras in cellular membranes, then how is this interaction regulated? It has been shown that PDEδ undergoes a profound conformational change upon binding to (a) farnesylated cargo designated as the *open conformation* with cavity of ~581 $Å^3$, and (b) interaction with Arl2/Arl3, resulting in the closure of the hydrophobic pocket with accessible volume of <200 $Å^3$, designated as the *closed conformation*. This closure is mediated by the β-sheet/β-sheet interactions between the two proteins causing the β-sheets 6, 7, and 4 of PDEδ to come closer. As a result, the pocket closes and the cargo is released from the carrier.[223]

6.2 Motivation and Objectives

Much is known about the spatial and biological regulation of Ras proteins that are tackled by their lipid modification and GEFs/GAPs, respectively, but there is little information detailing the dynamic interactions of Ras with escort proteins (enabling them to reach appropriate membrane microenvironments (like raft or non-raft domains) for signalling). However, it is clear that PDEδ binds prenylated Ras protein both *in vitro* (in the absence of membrane) and *in vivo* solubilising them, and thereby imposes implications on the Ras intracellular diffusion. Moreover, as most of the studies dealing with PDEδ have either been done in bulk solution without any lipid membranes[59,220,223] or in cellular systems,[147,217,221,222] the mechanistic details of this interaction have been rendered largely obscure. To this end, model systems provide ideal platforms to unambiguously study the interaction of farnesylated Ras isoforms (in this study: K-Ras and monofarnesylated N-Ras) with PDEδ, in the presence of heterogeneous raft-like membranes of different compositions. In this study, different biophysical techniques were employed to answer the following questions:

Can the Ras proteins show isoforms-specific and nucleotide-modulated interactions with PDEδ?

[223] Ismail, S.A., Chen, Y.X., Rusinova, A., Chandra, A., Bierbaum, M., Gremer, L., Triola, G., Waldmann, H., Bastiaens, P.I.H., and Wittinghofer, A. **(2011)**. Arl2-GTP and Arl3-GTP regulate a GDI-like transport system for farnesylated cargo. *Nat. Chem. Biol. 7*, 942–949.

How does PDEδ interact with monofarnesylated Ras in the presence of lipid membranes?

Does PDEδ itself shows any preferential interaction with lipid membranes?

What role does the PDEδ-membrane interaction play in Ras biology: extraction or delivery?

What is the mechanism that accounts for the release of Ras from PDEδ in the presence of membranes?

6.3 Results and Discussion

6.3.1 Effect of PDEδ on membrane-bound monofarnesylated Ras

A FRET-based assay was established to ascertain whether PDEδ would extract the membrane-bound Ras. For this, BODIPY-labelled K-Ras or N-Ras was used as the donor, with *N*-Rh-PE (a dye that preferentially partitions into the fluid phase of phase segregated membranes) labelled anionic raft-like lipid membranes, as the acceptor. As the protein partitions into the membrane, the labelled protein transfers energy to the labelled lipid, that was monitored. BODIPY and *N*-Rh-PE have a Föster radius of approximately 56 Å, and have been widely used as an ideal RET pair. Upon equilibration of the protein–membrane association process, a stable fluorescence intensity baseline was obtained. With the addition of PDEδ, a decrease in the intensity would imply that Ras has been extracted from the membrane, thereby disabling Ras to transfer energy to the membrane-bound acceptor. If the intensity remains unaltered, no effect of PDEδ on the membrane-bound Ras is suggested. Figure 6.2 **A** shows the change in the fluorescence intensity at 591 nm (acceptor emission maximum), following association of BODIPY-K-Ras to the labelled anionic raft-like membranes. Upon addition of PDEδ, the fluorescence intensity decreased, which would have confirmed the extraction of K-Ras by PDEδ (by sequestering the farnesyl group of K-Ras within its hydrophobic pocket), if the corresponding experiments monitoring the effect of PDEδ on the labelled lipid vesicles (without any Ras protein) would have shown a different result from that depicted in Figure 6.2 **B**. It shows that PDEδ itself interacted with the membrane, leading to possible quenching of *N*-Rh, thus masking the said effect of extraction,

if any. Whether PDEδ was inserting within the lipid membrane or only strongly adsorbing at the membrane interface is altogether a different issue, which is dealt with in the Section 6.3.2.

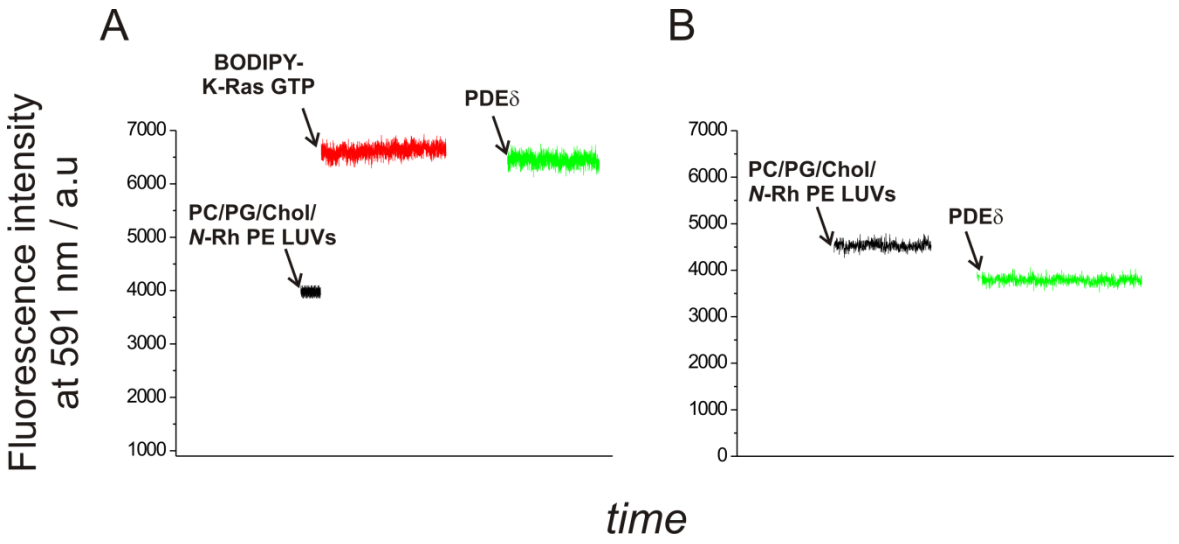

Figure 6.2: Interaction of PDEδ with membrane-bound active K-Ras. The abscissa in both cases is time which progresses from left to right. (**A**) LUVs (0.125 mM) containing *N*-Rh (0.25 μM) were added to the buffer (20 mM Tris, 7 mM $Mgcl_2$ and pH 7.4) at the first arrow. At the second arrow BODIPY-K-Ras GTP (2.73 μM) was added, which resulted in the increase in fluorescence intensity due to energy transfer, and finally PDEδ (4.64 μM) was added at the third arrow. The gap in time between arrows corresponds to ~ 1-2 min. The excitation was performed at BODIPY-donor excitation of 488 nm. (**B**) Same as (**A**) except that the second arrow corresponds to the addition of PDEδ (4.64 μM) only. All experiments were performed at 25 ˚C and 1 bar.

At this stage, in a collaborative study with Dr. Katrin Weise [Post-doctoral fellow in the laboratory of Prof. Dr. Roland Winter] and Simone Möbitz [Scientific worker in the laboratory of Prof. Dr. Roland Winter], the hypothesis—PDEδ extracts Ras from lipid membranes—was directly tested using a further biophysical technique: Surface Plasmon Resonance (SPR).[224] The exhaustive details on this method can be found elsewhere.[225-226]

[224] Weise, K., Kapoor, S., Wekmüller, A., Möbitz, S., Zimmermann, G., Triola, G., Waldmann, H., and Winter, R. **(2012)**. Dissociation of the K-Ras4B/PDEδ complex upon contact with lipid membranes: Membrane delivery instead of extraction. *134*, 11503–11510.

[225] Myszka, D.G. **(1997)**. Kinetic analysis of macromolecular interactions using surface plasmon resonance biosensors. *Curr. Opin. Biotechnol. 8*, 50–57.

Briefly, SPR detects the binding and dissociation kinetics of proteins to and from a membrane surface in real time by measuring the changes in the resonance angle. The resulting sensogram is comprised of a plot of the SPR signal in resonance units (1 RU = 1 pg mm^{-2}, i.e. surface coverage with protein in terms of mass protein/mm^2 surface area) against time. The lipid bilayer is immobilised onto a lipophillic modified dextran matrix of a L1 sensor chip, and the protein solution is injected across the surface. From the SPR sensograms, the membrane interaction of the proteins can be quantified by determining several representative parameters: the initial slope of the association phase that allows a comparison of the protein's incipient affinities to lipid membranes and the relative amount of quasi-irreversibly bound proteins at the end of each dissociation phase, which reflects the ability of the protein to stably insert into the lipid membrane.

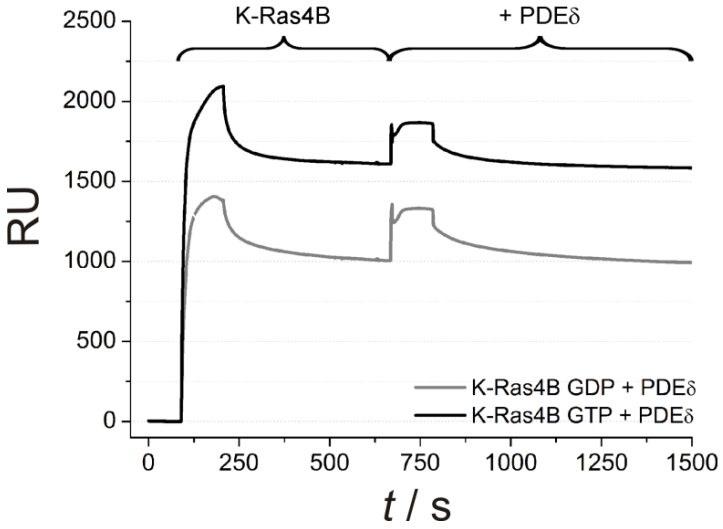

Figure 6.3: No PDEδ-mediated extraction of membrane-bound active K-Ras. SPR sensograms of the binding of (gray) GDP- and (black) GTP-bound K-Ras (2 μM) to the anionic raft-like membranes (DOPC:DOPG:DPPC:DPPG:Chol 20:5:45:5:25 (molar ratio)) and subsequent addition of PDEδ (3.4 μM) at 25 ˚C and 1 bar. Modified and reproduced with permission from ref. 224. Copyright (2012). American Chemical Society.

The sensograms in Figure 6.3 show that independent of the Ras nucleotide loading, PDEδ was not able to extract K-Ras from anionic raft-like membranes, since the amount of membrane-bound K-Ras (given by the plateau at the end of the dissociation phase) was not

[226] Myszka, D.G. **(2000)**. Kinetic, equilibrium, and thermodynamic analysis of macromolecular interactions with BIACORE. *Methods Enzymol. 323*, 325–340.

reduced by PDEδ. Although a similar behaviour was observed for the K-Ras protein bound to neutral raft-like membranes, for the membrane-bound monofarnesylated/depalmitoylated N-Ras, a partial extraction could be insinuated (unpublished results). This can be attributed to a loose or weaker membrane interaction of depalmitoylated N-Ras, thereby facilitating its solubilisation by PDEδ. *Thus, a loose association of Ras proteins with membranes is a crucial prerequisite for the interaction with PDEδ, also demonstrated in vivo lately.*[147] The inability of PDEδ to sequester membrane-bound K-Ras, that exhibits a high affinity binding to the PM,[227] can be rationalised by the plausible binding model of PDEδ to Ras. When the lipid anchor of membrane-bound Ras is stably inserted into the lipid membrane (in case of K-Ras: supported by strong electrostatic interactions between the Lys stretch in its HVR and the anionic lipid interface), there is no exposed binding site available for PDEδ to interact and extract Ras, since it has been postulated that there are no additional contact sites between PDEδ and the Ras G-domain.[223] Moreover, recent *in vivo* studies also demonstrated that PDEδ can mostly solubilise the loosely bound K-Ras from endomembranes (as the Ras binding to endomembranes is highly dynamic and independent of the HVR)[145], but not actively extract K-Ras from the PM.[147] This suggests that K-Ras must desorb from the PM in order to get solubilised by PDEδ, which can be realised by decreasing the net charge on the K-Ras HVR and/or the PM.[147,228] Finally, analysis of the initial slopes in SPR revealed that the relative affinities of the protein to lipid membranes varies in the following order: PDEδ ≥ K-Ras > monofarnesylated N-Ras. Furthermore, a minor increase in the response unit measured upon addition of PDEδ (Fig. 6.3) indicated that PDEδ is bound to the membrane, even in the presence of K-Ras. These SPR observations corroborated the fluorescence results (Fig. 6.2), in showing a strong membrane interaction capability of PDEδ itself, and objective reasoning suggests that this interaction should not exist without a defined biological function. This fuelled the necessity to study the PDEδ•Ras complex in the presence of lipid membranes. Thus, all the subsequent experiments discussed in the forthcoming sections were

[227] Heo, W.D., Inoue, T., Park, W.S., Kim, M.L., Park, B.O., Wandless, T.J., and Meyer, T. **(2006)**. PI(3,4,5)P3 and PI(4,5)P2 lipids target proteins with polybasic clusters to the plasma membrane. *Science 314*, 1458–1461.

[228] McLaughlin, S., and Aderem, A. **(1995)**. The myristoyl-electrostatic switch: a modulator of reversible protein-membrane interactions. *Trends Biochem. Sci. 20*, 272–276.

performed by allowing complexation of the two proteins in bulk solution, and by observing the effect of membranes on this preformed complex.

6.3.2 Interaction of PDEδ with lipid membranes

To study the interaction of PDEδ with raft-like heterogeneous membranes, infrared reflection absorption spectroscopy was employed to study the orientational and structural changes of PDEδ at lipid monolayers. From the surface-pressure profile, π (t), of PDEδ (Fig. 6.4 **A**), it can be clearly seen that the protein does not insert within the acyl chain region of the lipid monolayer. However, it does seem to interact with the headgroup region, as evident by minor changes in the $\pi(t)$ profile. The strong amide-I' IRRA band intensity was also indicative of an effective adsorption of PDEδ at the lipid interface (Fig. 6.4 **B**). The band maximum at 1622-24 cm^{-1} characteristically stands for predominantly β-sheet structures, in accord with the three dimensional crystal structure of PDEδ (**cf.** Fig. 6.1 **A**). In addition, no further changes in the amide band maxima were observed over time, suggesting a rather stable interaction with the membrane.

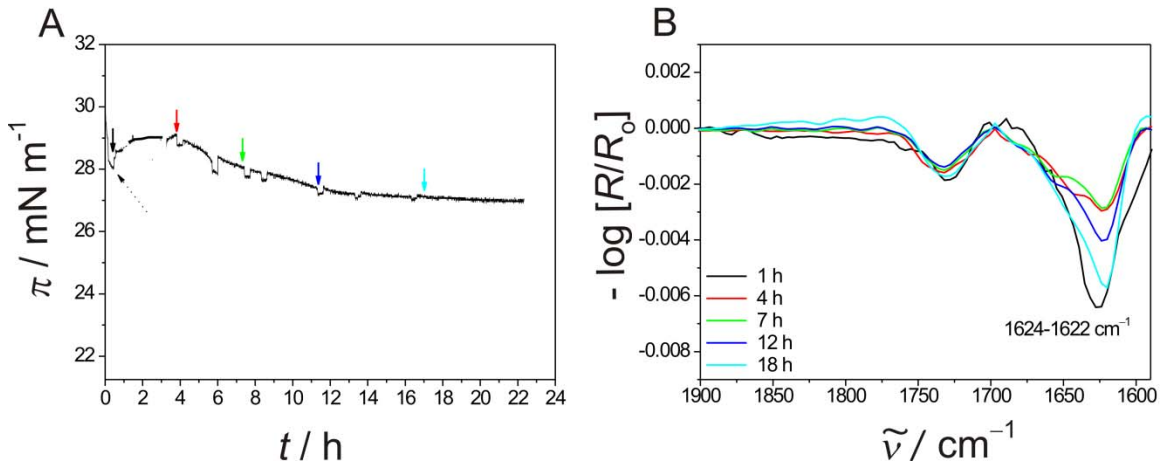

Figure 6.4: Interaction of PDEδ with lipid membranes. (**A**) Surface pressure profile of PDEδ (340 nM) upon injection (dashed arrow) underneath the anionic raft-like (DOPC:DOPG:DPPC:DPPG:Chol 20:5:45:5:25 (molar ratio)) monolayer, kept at ~ 28 m N m^{-1} at 20 ˚C and 1 bar. (**B**) IRRA spectra of PDEδ at selected time points during the interaction process acquired with p-polarized light at an angle of incidence of 35˚. The D_20 subphase beneath the lipid monolayer contained 100 mM NaCl.

Corresponding transmission Fourier-transform infrared spectroscopy experiments ruled out any structural changes such as unfolding or aggregation of the protein upon interaction with anionic lipid membranes, which would have otherwise resulted in a substantial increase of disordered or aggregated intermolecular β-sheet structures (Table 6.1).

Table 6.1: X-ray secondary structure of PDEδ in comparison with FTIR spectroscopy data obtained in this study (column 3). The values given were obtained by performing curve-fits of the normalised FTIR spectra. In the table, the mean values ± standard deviation are given, (n = 2).

Secondary structure Element	PDEδ from X-ray (PDB: 3T5G)	PDEδ in the presence of anionic membrane (this study)
α-helices	14 %	18.4 ± 0.9 %
β-sheets	57 %	49.1 ± 2.2 %
disordered structure (turns/loops and random coils)	29 %	32.5 ± 1.8 %

In order to explore the preferred conformation/orientation of PDEδ at the membrane interface, IRRA spectra were acquired at different angles of incidence using p-polarized light. From the switch in the sign of the amide-I' band from negative below to positive above the Brewster angle, it can be concluded that the protein adopts an orientation with its β-sheet fold lying parallel to the membrane interface or perpendicular to the lipid acyl chains (Fig. 6.5).

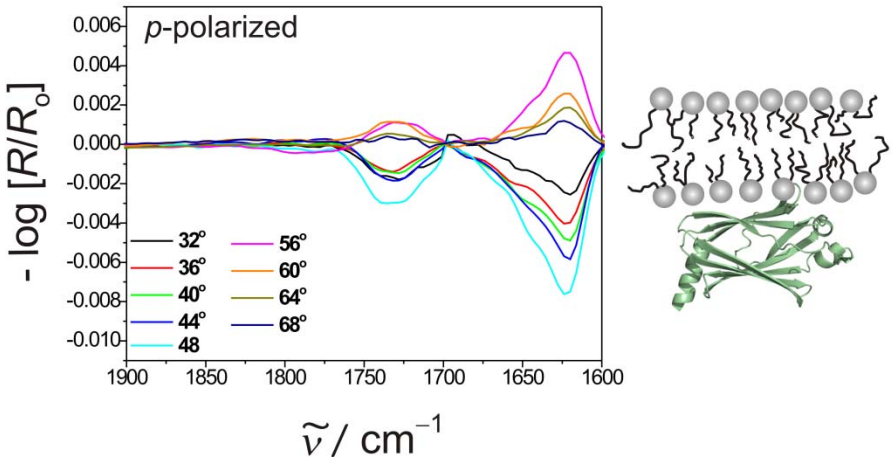

Figure 6.5: Orientation of PDEδ at the membrane interface. IRRA spectra for PDEδ (340 nM) upon adsorption at the anionic raft-like monolayer with varying angles of incidence from 32 to 68˚ acquired with p-polarized light at 20 ˚C and 1 bar.

This conformation of the protein at the membrane interface was also indirectly supported by the corresponding AFM experiments, demonstrating the mean height of PDEδ at the membranes to be approximately 1.1 ± 0.2 nm.[224] For monomeric Ras the mean height at the membrane interface was found to be approx. 2.5 nm (assuming a spherical shape), and since PDEδ and Ras have almost the same molecular weight, in which case, a mean height of < 2 nm would suggest that PDEδ is aligned flat (with respect to its immunoglobulin-like β-fold) at the membrane interface. To ascertain more explicitly the conformation of PDEδ at the membrane interface, as to see what regions of the protein might be involved in the interaction with the lipid headgroup region, an *in situ* salt gradient IRRAS experiment was performed. Concerning this, the PDEδ surface at the opening of the hydrophobic pocket is negatively charged, which might facilitate binding of the polycationic C-terminus containing Ras proteins, for instance K-Ras4B (Fig. 6.6 **A**). Furthermore, this C-terminus region of PDEδ also encompasses a highly flexible loop (aa: 111-117), which adopts diverse "defined" conformations in complex with different prenylated cargo providing a broad specificity to PDEδ. But in the absence of any cargo, it remains highly disordered and unstable (Fig. 6.6 **B**), thus requiring a "missing" lipid ligand to stabilise this section of the protein.[219]

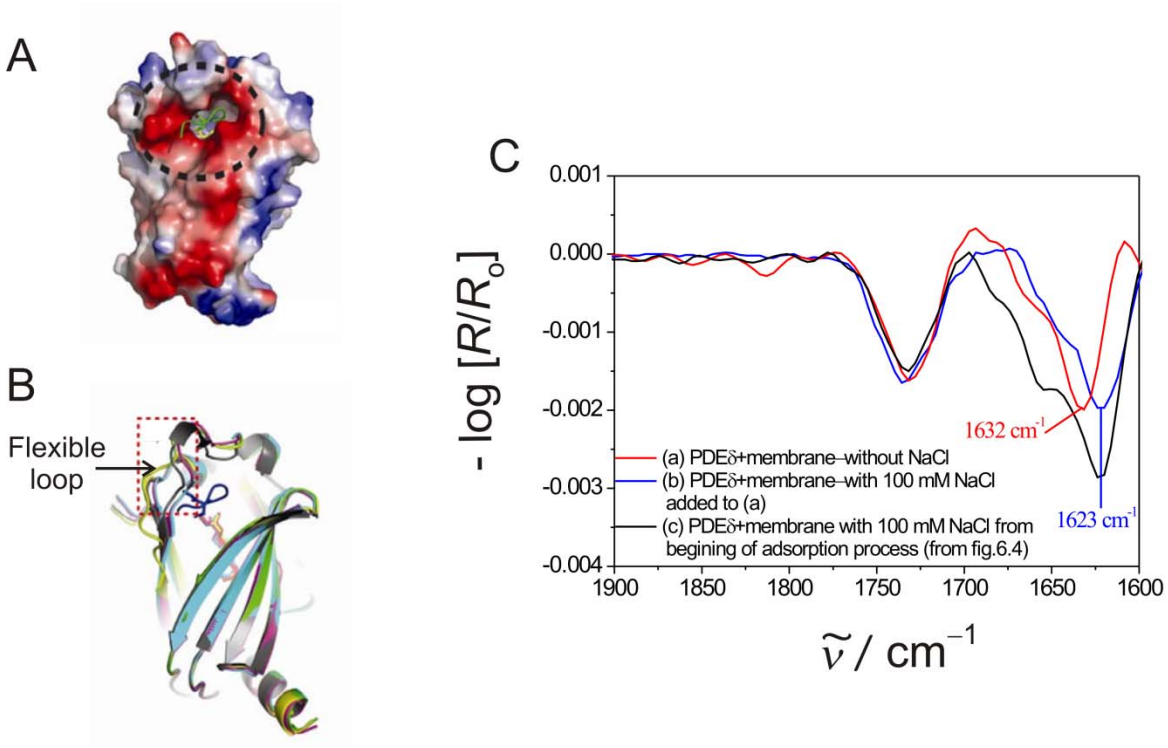

Figure 6.6: Proposed PDEδ–membrane interaction motifs. (**A**) Electrostatic surface charge of PDEδ showing the negative charge surrounding the opening of the farnesyl binding pocket (encircled by a dashed line and the polycationic C-terminus peptide of Rheb in green). (**B**) Superimposition of different molecules of the F–octapeptide–PDEδ complex showing the diverse conformations of the flexible PDEδ loop (residues 111-117). Figures (**A**) and (**B**) have been reprinted with permission from ref. 223. Macmillan Publishers Ltd: Nature Chemical Biology, Copyright (2012) (**C**) IRRA spectra for PDEδ (340 nM) upon adsorption at the anionic raft-like monolayer in the absence and upon subsequent addition of salt (NaCl) at 20 ˚C and 1 bar, acquired with p-polarized light at an angle of incidence of 35˚.

Under charge screening conditions i.e. in the presence of salt (NaCl), PDEδ exhibits the amide-I' band maximum at 1622-24 cm^{-1} (Fig. 6.4). Without any salt in the subphase (a different experiment), the PDEδ amide-I' band maximum was observed at 1632 cm^{-1} (Fig. 6.6 **C**) and remained stable over time (~12 h). After addition of a concentrated salt solution into the subphase (giving a total concentration of 100 mM NaCl), the band maximum shifted back to 1622 cm^{-1}. This shift in the amide-I' band can be attributed to a reversible change in the protein conformation, coupled with a stronger interaction of the protein with the lipid interface, especially in the presence of salt. However, since under both the conditions, the angle-dependent IRRAS measurements revealed a parallel orientation of the protein's β-sheets with respect to the membrane interface, these observations suggests that PDEδ most

probably interacts with the lipid interface in a flat configuration through its acidic surface. The flexible loop and the opening side of the hydrophobic pocket, under non-charge screening conditions, most likely experience electrostatic repulsion from the negatively charged headgroup region of the lipid membrane, thus exhibiting a weak membrane-interaction profile and a concomitant higher wavenumber (at 1632 cm^{-1}) of the amide-I' band. This leads to a speculative suggestion: the disordered and unstable flexible loop in the PDEδ cannot only be stabilised by a "prenylated" cargo, but also by interaction with lipid membranes.

6.3.3 Interaction of the PDEδ•Ras complex with lipid membranes

Interaction of PDEδ itself with the lipid membranes hinted that this interaction should not exist without a defined biological function. Thus, the PDEδ•Ras complex preformed in bulk solution was exposed to heterogeneous membranes. From the corresponding SPR measurements also monitoring this interaction, a higher affinity of the complex to the membrane was affirmed[224] that raised several important questions:

Does the PDEδ•Ras complex remains intact upon contact with lipid membranes?

If not, then can Ras partition into the membranes or is it still (loosely) bound to PDEδ?

What functional significance can be assigned to such a scenario?

These aspects were studied as follows.

6.3.3.1 Fluorescence based observations: Dissociation of the complex upon membrane contact

In order to monitor the complex formation between PDEδ and prenylated Ras, and the subsequent effect of lipid membranes, two independent fluorescence approaches were followed. In the first one, a tryptophan-based fluorescence assay was employed keeping in mind that PDEδ harbours four tryptophans (Trp^{19}, Trp^{32}, Trp^{90}, and Trp^{105}) uniformly distributed along its hydrophobic pocket, and two tyrosines (Tyr^{81} and Tyr^{149}). One of each is directly involved in (Trp^{32}) or closely related to (Tyr^{149}) mediating the interaction with the

prenyl moiety.[229] While monitoring the emission from PDEδ in the absence and presence of Ras (that has nine tyrosines but no tryptophan), and after the addition of the raft-like lipid membrane, changes in the band maximum and shape could be correlated to the structural changes in the environment of the fluorophore. In the second approach, a FRET-based assay was employed using tryptophan in PDEδ as the donor and Dansyl-labelled K-Ras or N-Ras as the acceptor. Tryptophan and Dansyl have been widely used as an RET pair to study protein–protein interactions.

(A) Tryptophan assay to study PDEδ•Ras complex formation and the effect of membrane contact

A rather asymmetric emission band of PDEδ was obtained, indicating different locations of the fluorescent residues, i.e. fluorescent residues buried in the non-polar regions of the protein as well as at the protein surface (Fig. 6.7 **D**). Upon addition of GTP-bound K-Ras to PDEδ, a blue shift was observed in the fluorescence spectra, indicative of a decrease in the polarity of the fluorophore surroundings. This is due to the insertion of the K-Ras lipid farnesyl anchor into the hydrophobic binding pocket of PDEδ (Fig. 6.7 **A**). The same behaviour was observed for the interaction of PDEδ with the GDP-bound K-Ras, pointing towards a *nucleotide-independent* process (Fig. 6.7 **B**). Surprisingly, the blue shift was reversible and the initial fluorescence spectrum of PDEδ was recovered upon addition of anionic raft-like lipid vesicles to the GTP- or GDP-bound-K-Ras•PDEδ complex (Fig. 6.7 **A - B**).

[229] Alexander, M., Gerauer, M., Pechlivanis, M., Popkirova, B., Dvorsky, R., Brunsveld, L., Waldmann, H., and Kuhlmann, J. **(2009)**. Mapping the Isoprenoid Binding Pocket of PDE delta by a Semisynthetic, Photoactivatable N-Ras Lipoprotein. *Chembiochem 10*, 98–108.

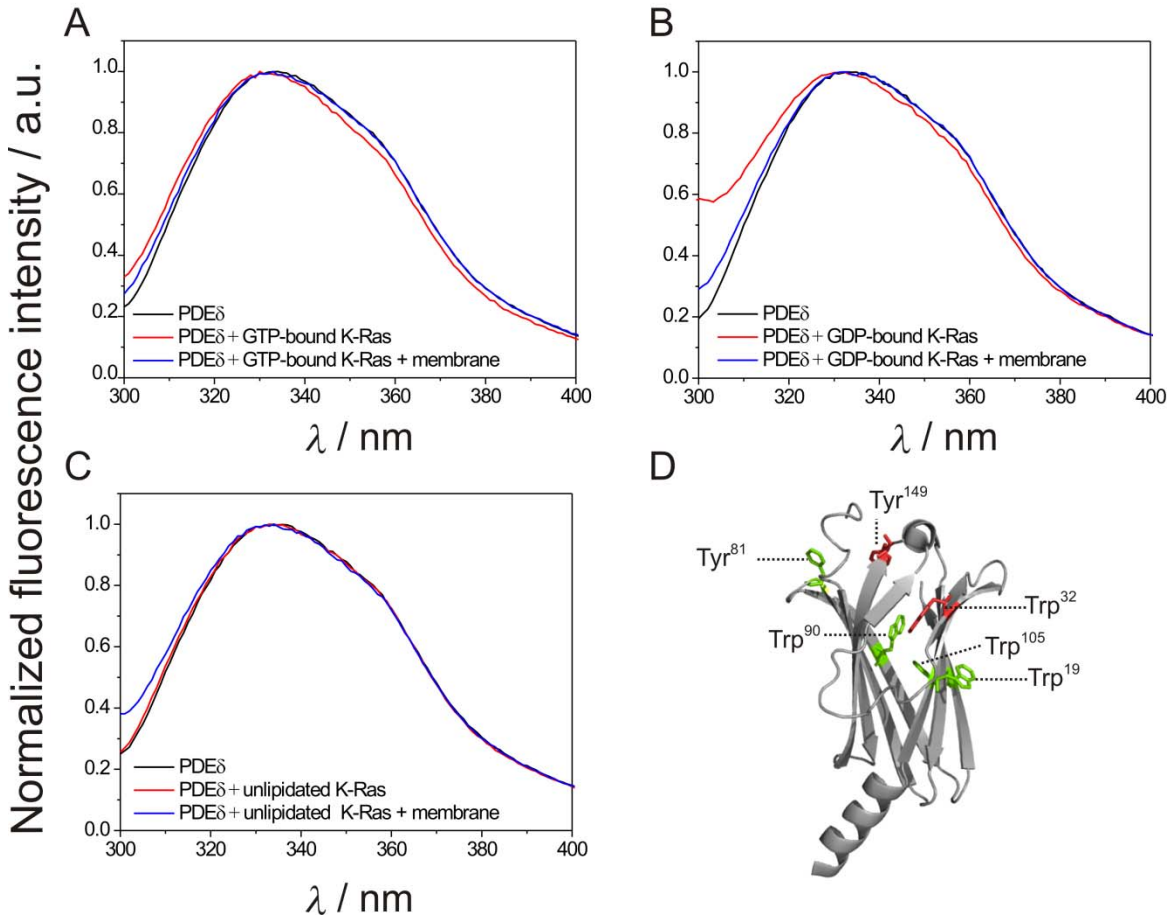

Figure 6.7: Changes in the binding pocket of PDEδ reflect the PDEδ•K-Ras complex dissociation upon membrane contact. Fluorescence emission spectra of PDEδ (6.8 µM) in the absence (black) and presence (red) of (**A**) GTP-bound K-Ras (4 µM), (**B**) GDP-bound K-Ras (4 µM) and (**C**) unlipidated K-Ras (4 µM) at 25 ˚C and 1 bar. Finally, the anionic raft-like membrane (0.25 mM) was added in each case and the emission spectra (blue) collected. The spectra show the change of the PDEδ tryptophan emission maximum and band shape upon complexation (in **A, B**) and membrane-mediated dissociation (in **A, B**) of the PDEδ•K-Ras complex. In contrast, no blue shift of the PDEδ fluorescence spectrum could be detected upon addition of unlipidated K-Ras protein (**C**). (**D**) Ribbon presentation of PDEδ (PDB: 3T5G; generated using PyMol) showing the different fluorophors (green) with the two fluorophors Trp^{32} and Tyr^{149} (red) that are directly involved in the interaction with the lipid ligand.

This observation hints towards the PDEδ•Ras•membrane interaction being *nucleotide-independent*. In either case, a dissociation of the K-Ras farnesyl moiety from the binding pocket of PDEδ (Figs. 6.8 **A-B**), when the complex contacted the membrane was demonstrated. Conversely, when the experiment was carried out with an unlipidated K-Ras protein, no blue shift of the PDEδ fluorescence spectrum could be detected implying that the

complex formation mainly involves the farnesylated C-terminus of K-Ras (Fig. 6.8 **C**). Owing to the evidence that K-Ras (in both nucleotide-bound states) shows the same partitioning process in the neutral raft membranes,[149] and that the affinity to the *anionic* raft-like lipid mixture is only one order of magnitude higher, a similar behaviour was expected in the tryptophan assay with the *neutral* raft-like lipid mixture.

Similar PDEδ-tryptophan spectroscopic changes were observed upon mixing PDEδ with monofarnesylated N-Ras (Fig. 6.8), pointing towards a *Ras isoform-independent binding to PDEδ.* This is in accordance with the notion of PDEδ not interacting with the G-domain, and thus being unable to recognise the specific Ras isoform. However, upon addition of membranes composed of the neutral raft-like lipid mixture, no (complete) reversible changes were observed in the PDEδ-tryptophan emission spectra (Fig. 6.8).

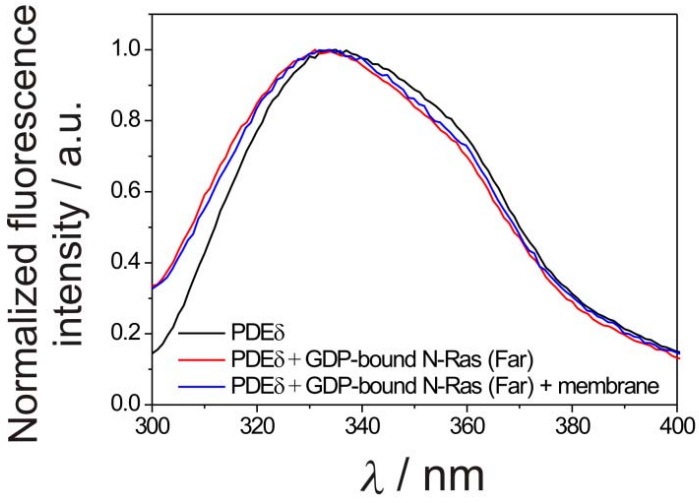

Figure 6.8: Changes in the binding pocket of PDEδ reflecting PDEδ•N-Ras(Far)•membrane interaction. Fluorescence emission spectra of PDEδ (6.8 µM) in the absence (black) and presence (red) of monofarnesylated N-Ras (4 µM) at 25 ˚C and 1 bar (excitation at 282 nm). Finally, the neutral raft-like membrane (0.25 mM) was added and the emission spectra (blue) collected.

The finding for N-Ras Far can be attributed to the nature of this Ras-isoform, which is twofold. First monofarnesylated N-Ras lacks a second membrane targeting signal (such as a palmitoyl moiety or a polybasic stretch in its HVR), thereby it exhibits a highly dynamic interaction with membranes. Second, the lack of positive charges near the N-Ras C-terminus

might also abrogate a high affinity binding to PDEδ, which itself contains a negatively charged surface close to its binding pocket. In this regard, a parallel *in vitro* study elucidated that a farnesylated C-terminus is required, but not sufficient, for a *high binding affinity* to PDEδ, and that the C-terminal residues significantly influence this binding event [for instance: whereas the polycationic C-termini of Rheb or K-Ras4B have a higher binding affinity (K_D ~100 nM) to PDEδ, the farnesylated neutral peptide exhibits a much lower affinity (K_D ~600 nM)].[59] As a result, monofarnesylated N-Ras is expected to shuttle between the membrane-bound and PDEδ-complexed state, thus likely to produce an averaged outcome in the observables, as obtained. But as the previous mentioned studies were performed in the absence of membranes, it is clear that the affinity or interaction of PDEδ itself with the membrane (shown in Section 6.3.2) might have a role in regulating the interaction of Ras with PDEδ (as shown in the present study). However, the incomplete dissociation of the Far-N-Ras GDP•PDEδ complex upon contact with the *neutral* raft-like membrane was not explicitly ruled out, which, if ruled in, would point towards the membrane composition adding another tier of complexity in regulating the interaction of PDEδ with Ras.

(B) FRET-based assay to study the PDEδ-Ras complex formation and the subsequent effect of interaction with membranes

To confirm the dissociation of the PDEδ•Ras complex upon membrane contact, a FRET-based assay was conducted with PDEδ-tryptophan as the donor and Dansyl-labelled and GDP-bound N-/K-Ras as the acceptors. As it has been ascertained in the previous sections that the Ras-PDEδ interaction is nucleotide-independent, so only the GDP-bound proteins were used for this assay. PDEδ in the presence and absence of Dansyl-labelled Ras was excited at λ = 282 nm, and the fluorescence spectrum was measured from 300 to 550 nm. The fluorescence spectrum of the mixture of PDEδ and Dansyl-Ras was corrected for the cross excitation signal from the pure Dansyl-Ras.

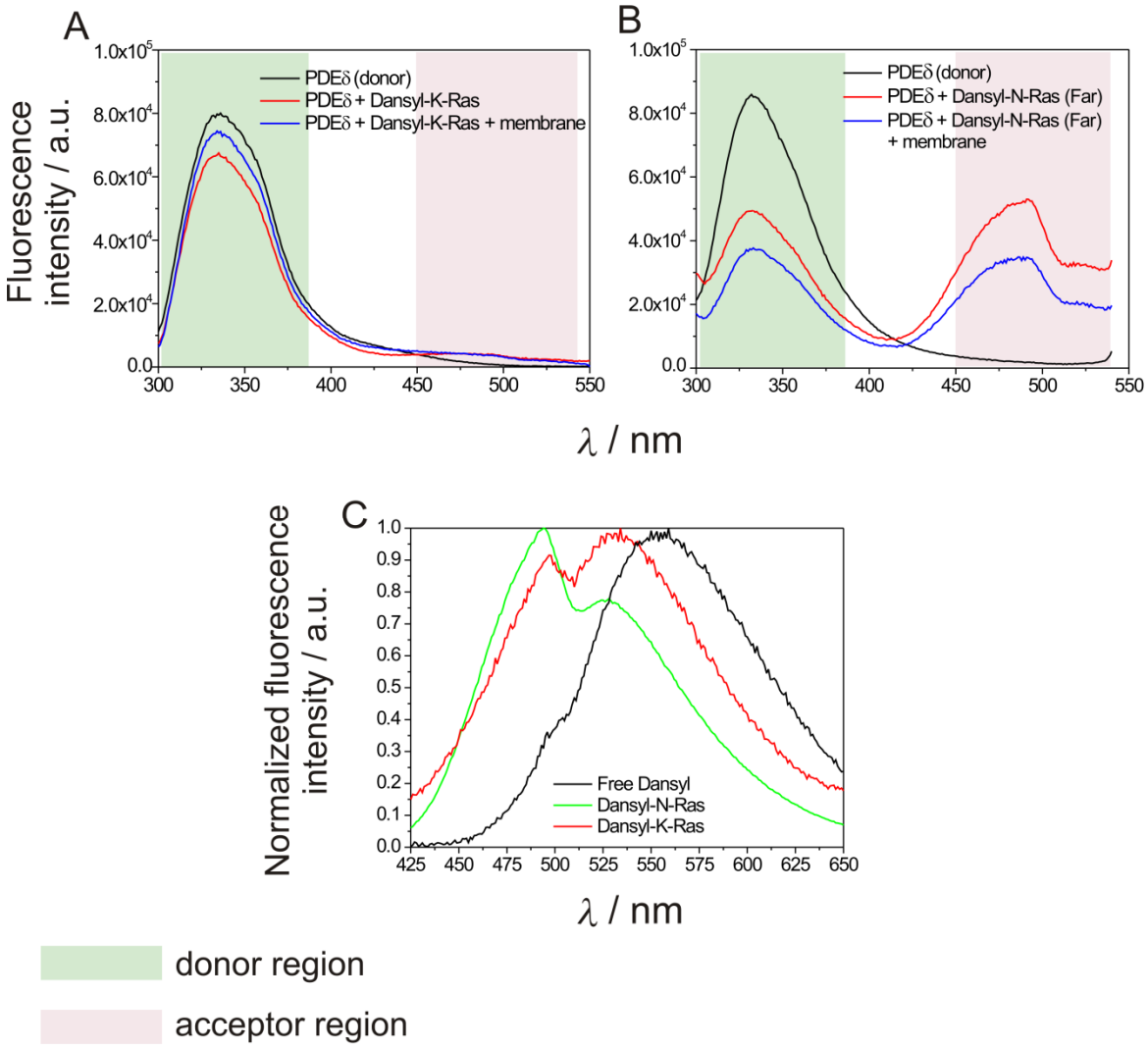

Figure 6.9: FRET-based assay to probe the PDEδ•Ras•membrane interactions. FRET assay of PDEδ (6.8 µM) binding to Dansyl-labelled (**A**) K-Ras (6.8 µM) and (**B**) monofarnesylated N-Ras (6.8 µM) in solution, and subsequent dissociation upon addition of (**A**) the anionic and (**B**) the neutral lipid membranes at 25 ˚C and 1 bar. Excitation was performed at 282 nm. (**C**) Comparison of the normalised emission spectra of free Dansyl in solution (Dansyl amide) with Dansyl-labelled K-/N-Ras, with direct excitation of the Dansyl fluorophore at 340 nm.

The marked RET-induced changes in the donor emission, i.e. quenching of the intrinsic Trp fluorescence, demonstrates the binding of PDEδ to K-Ras (Fig. 6.9 **A**) and to N-Ras (Fig. 6.9 **B**) in solution. As expected, the energy transfer also increases the fluorescence intensity in the acceptor region (425-550 nm, with a broad maximum around 494 nm). Comparison of the fluorescence spectrum of the free Dansyl group in solution (Dansyl amide) and in complex

with K-Ras and N-Ras, showed a strong blue shift with two overlapping emission maxima centred on 494 nm and 530 nm, with different relative intensities of the two bands in protein-bound form, however (Fig. 6.9 **C**). Such a broad peak of Dansyl, when conjugated with K-Ras, coupled with the limitation to monitor the emission spectra beyond 550 nm (due to effects of the second-order monochromator excitation), prevented analysing the changes in Dansyl-K-Ras fluorescence. Moreover, the inherent low labelling efficiency of the K-Ras proteins also rendered the analysis in the acceptor region quite ambiguous. For these reasons, only the RET-induced changes in the donor region were commented upon. Contrarily, a sharp peak for the Dansyl group, when conjugated to N-Ras (Fig. 6.9 **B**) (most likely due to a relatively easier preparation and purification of Dansylated-N-Ras), enabled clear visualisation of the complexation-induced changes in the acceptor emission region.

Upon addition of the lipid vesicles composed of neutral and anionic raft-like mixture to PDEδ•N-Ras and PDEδ•K-Ras complexes, respectively, an increase in the intrinsic tryptophan fluorescence of PDEδ (after background subtraction of the scattering signal by lipids and cross excitation by pure Dansyl-Ras) was observed only in the case of K-Ras proteins. This argues for the dissociation of the PDEδ•K-Ras complex upon membrane contact, leading to a reduced FRET, thereby increasing the donor signal as observed (Fig. 6.9 **A**). The absence of such an effect for PDEδ•N-Ras is attributed to the reasons mentioned in Section 6.3.3.1 (**A**).

6.3.3.2 Infrared-based observations: Membrane insertion of Ras following complex dissociation

By monitoring the changes happening explicitly in the binding pocket of PDEδ (Section 6.2.31), it can be safely stated that the farnesyl moiety of Ras dissociates from PDEδ once the complex contacts the membrane. In this section, IRRAS was used to ascertain if the Ras proteins could then stably insert with its lipid anchor (that was once shielded by PDEδ) into the membrane or are still loosely bound to PDEδ.

Figures 6.10 (**A** and **C**) shows the $\pi(t)$ profile upon addition of the preformed GDP-/GTP-bound-K-Ras•PDEδ complex beneath the anionic raft-like lipid monolayers. The increases in the surface pressure for K-Ras GTP•PDEδ and K-Ras GDP•PDEδ with time resembles that

of the pure GTP-bound and GDP-bound K-Ras proteins, respectively, and are indicative of an effective insertion of the K-Ras proteins into the lipid monolayer.

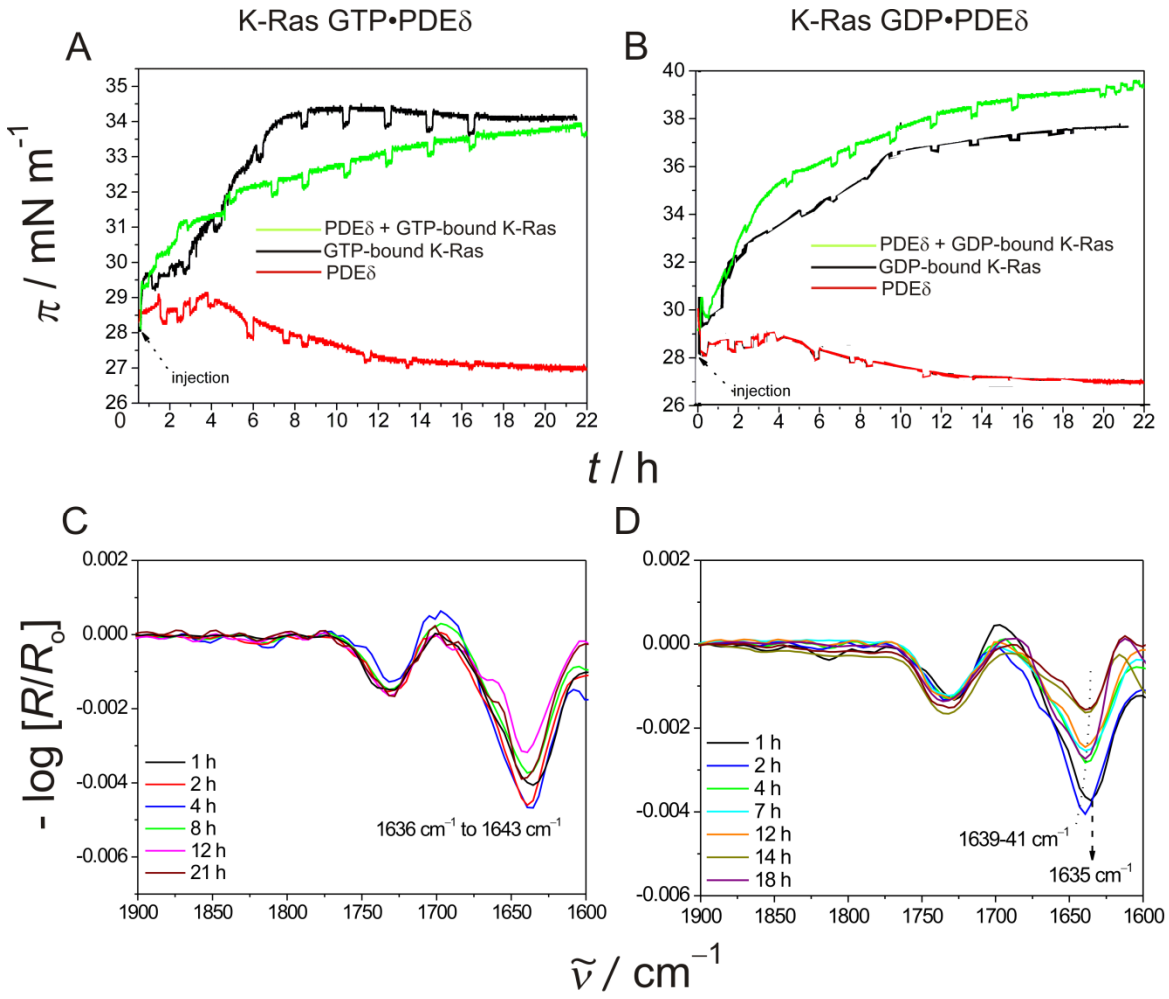

Figure 6.10: Membrane insertion of K-Ras following dissociation from PDEδ. Surface pressure profile of preformed (**A**) GTP-bound K-Ras•PDEδ complex (green), GTP-bound K-Ras alone (black) (**B**) GDP-bound K-Ras•PDEδ complex(green), GDP-bound K-Ras alone (black) upon interaction with the anionic lipid raft-like (DOPC:DOPG:DPPC:DPPG:Chol 20:5:45:5:25 (molar ratio)) monolayer kept at ~ 28 mN m^{-1} at 20 ˚C and 1 bar. PDEδ in both cases is shown in red. IRRA spectra of (**C**) GTP-bound K-Ras•PDEδ, and (**D**) GDP-bound K-Ras•PDEδ complexes at selected time points during the interaction process. IRRA spectra were acquired with p-polarized light at an angle of incidence of 35˚.

For the K-Ras GTP•PDEδ complex, the amide-I' band maximum fluctuated between 1636 and 1643 cm^{-1} (Fig. 6.10 **C**), and reflected the characteristic band fluctuations of the pure GTP-bound K-Ras at the membrane (**cf. Fig. 4.13 A, Ch. 4**). Likewise for the K-Ras

GDP•PDEδ complex, the amide-I' band maximum remained stable at 1639-1641 cm^{-1} (Fig, 6.10 **D**) and mimicked the behaviour of pure GDP-bound K-Ras–membrane interaction (**cf. Fig. 4.13 B, Ch. 4**). The same conclusions were drawn from the comparative experiments performed with Far-N-Ras GDP•PDEδ, pointing toward a membrane interaction process that is independent of the Ras isoform specificity (Fig 6.11).

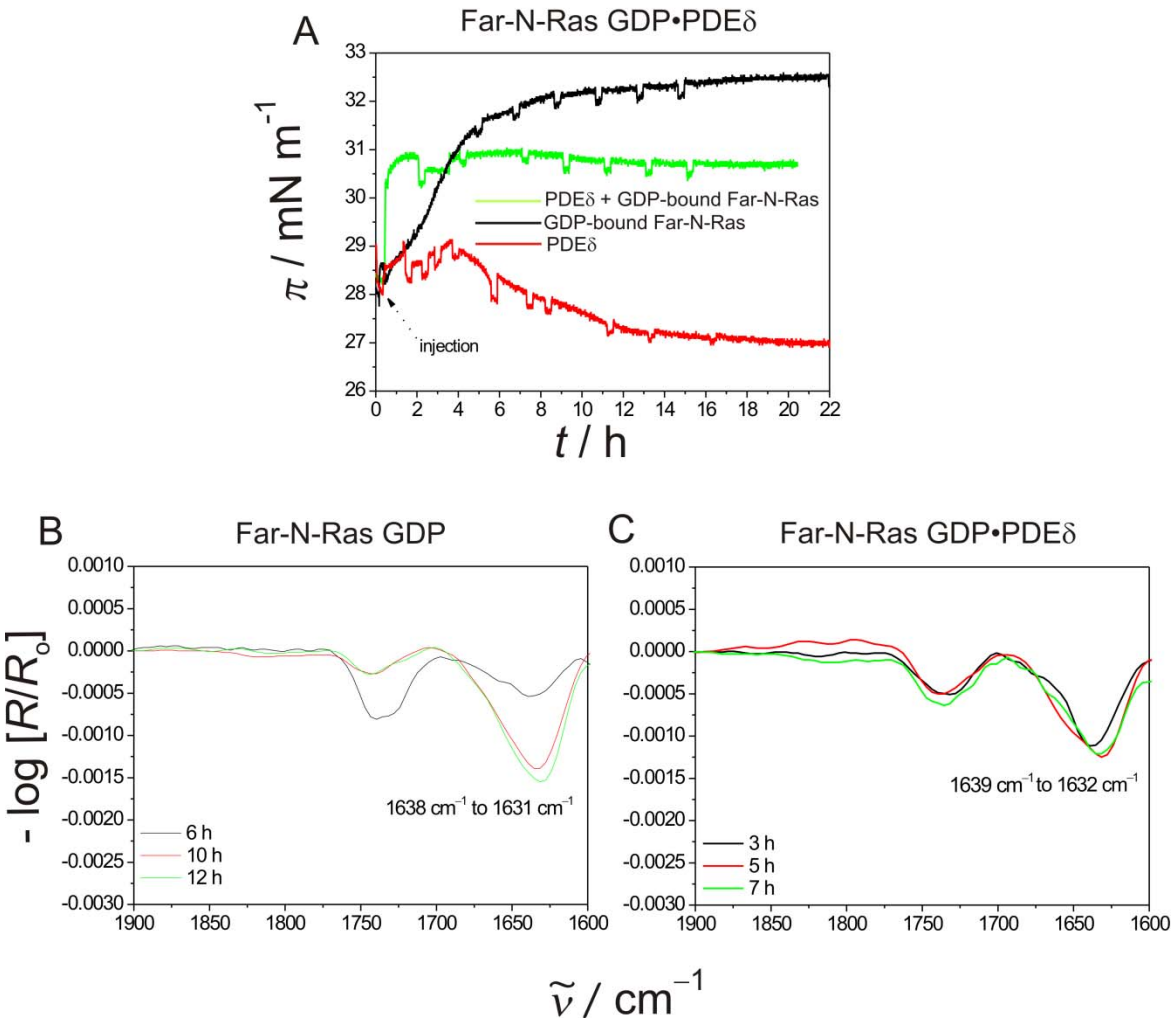

Figure 6.11: Membrane insertion of N-Ras following (partial) dissociation from PDEδ. (**A**) Surface pressure profile of the preformed GDP-bound N-Ras (Far)•PDEδ complex (green), GDP-bound N-Ras (Far) alone (black) and PDEδ(red) upon interaction with the neutral lipid raft-like (DOPC:DPPC:Chol 25:50:25 (molar ratio)) monolayer kept at ~ 28 mN m^{-1} at 20 ˚C and 1 bar. IRRA spectra of GDP-bound N-Ras alone (**B**) and in complex with PDEδ (**C**) at selected time points during the interaction process acquired with p-polarized light at an angle of incidence of 35˚.

However, the absence of the characteristic IR band for PDEδ in each case (Fig. 6.10 and 6.11) does not imply that PDEδ is no longer able to interact with the membrane, but that adsorption at the membrane interface of PDEδ is possibly suppressed by the dominant Ras−membrane interactions. Hence, the contribution of PDEδ to the IRRA intensity seems to be alleviated by the membrane-bound Ras. In this regard, the corresponding AFM measurements provided visual details at the molecular level of the PDEδ•Ras•Membrane interaction.[224] Not only was PDEδ visualised solitarily bound to the fluid-disordered membrane domains, but remarkably, the Ras proteins were also observed to exhibit their respective isoforms-specific lateral segregation within the membrane. Whereas time-dependent diffusion and subsequent clustering in the l_o/l_d phase-boundary of heterogeneous membranes were observed for monofarnesylated N-Ras, formation of new protein-enriched domains inside the fluid environment was detected for K-Ras.[224] This clearly implies membrane partitioning of the single components of the complex, thus supporting the PDEδ•Ras complex dissociation upon contact to the membrane.

6.3.4 A plausible mechanism for the release of Ras from PDEδ in the presence of lipid membranes

The following can be concluded from the results above: *PDEδ binds and solubilises farnesylated Ras protein in the bulk (complex formation), and delivers them to the membrane (complex dissociation)*. One-to-one correlation to the natural biological systems would be: PDEδ solubilising (any) cytosolic or (mis)-localised depalmitoylated or dephosphorylated Ras, and relocating them to their respective membrane compartments (PM in case of polycationic Ras, Golgi in case of depalmitoylated Ras) to restore equilibrium.[147] However, if the binding between the two proteins is mediated by only the Ras C-terminus, then release of the Ras-farnesyl lipid anchor from the PDEδ pocket is thermodynamically unfavourable. This generates a genuine need of an additional interaction partner that can facilitate the release of Ras from PDEδ. One such proposed interaction partner is a member of the Arf subfamily of G-proteins: Arl. Specifically, Arl2/3 interact allosterically with PDEδ (the interaction of PDEδ to Arl and Ras is mutually exclusive due to the non-overlapping

interaction site, mentioned in Section 6.1), and mediate the release of farnesylated-Rheb by inducing conformational changes in PDEδ. This helps in recruiting Rheb onto the membranes and modulating the G-protein activation, spatially and temporally (Fig. 6.12). Although we can only speculate as to the nature of the Ras binding site on PDEδ (due to lack of any crystal structure), a generic role of Arl in mediating Ras release from PDEδ can be envisioned.

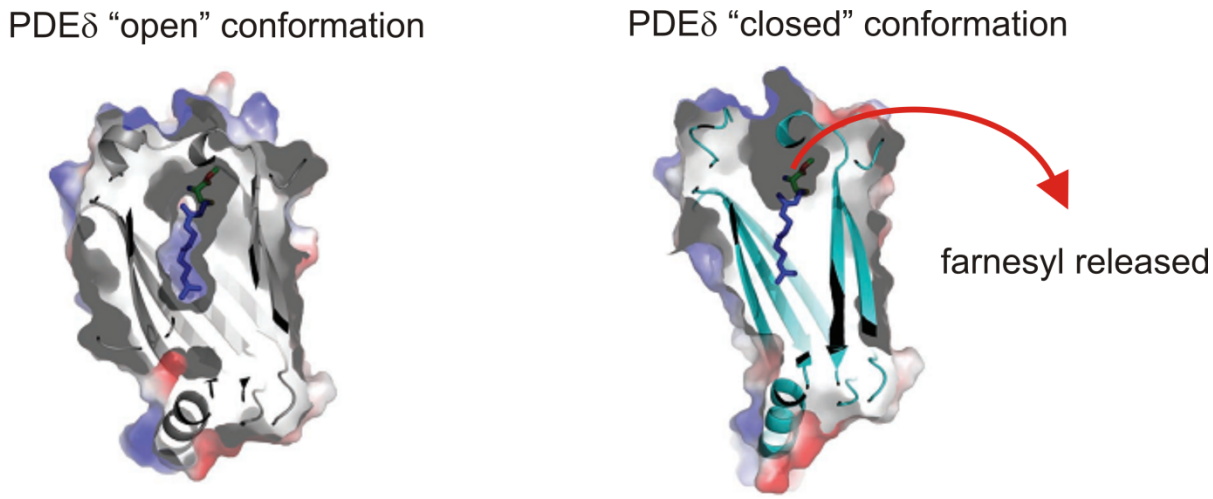

Figure 6.12: Conformational changes in PDEδ dictating cargo loading and unloading. Electrostatic surface presentation of PDEδ sliced through, to show the hydrophobic pocket and farnesylated cysteine in open (right side) and closed (left side) conformations. The transformation from the open to closed conformation in PDEδ is brought by the movement of the two β-sheets (highlighted in cyan) upon interaction with GTP-bound Arl 2/3. Modified and reprinted with permission from Macmillan Publishers Ltd: Nature Chemical Biology, ref. 223, copyright (2012).

However, the detachment of Ras proteins from PDEδ, and their subsequent membrane insertion in the present study, surprisingly in the absence of Arl, hints towards other conceivable determinants. First, the preferable orientation of PDEδ with its immunoglobulin-like β-fold parallel to the lipid interface (showing a relatively strong membrane-interaction) leads to the postulation of a hypothesis. This includes a conformational change in the PDEδ's hydrophobic pocket upon interaction of its β-sheets with the membrane, which lies, at least to some extent, in a direction similar to that already postulated for the Arl-PDEδ interaction. Although this is just a speculative suggestion that demands further critical investigation, if/when proven, it would revolutionise the accepted thoughts regarding the crucial role of lipids in regulating membrane-associated cellular process. This presumably Arl-free

membrane-mediated (partial) release of Ras from PDEδ would also contribute to construing the *in vivo* relocations of the depalmitoylated Ras to endomembranes (Golgi); the endomembranes are likely to have a lower, if any, fraction or accumulation of the Arl proteins. This is accounted for by the very nature of the Arl proteins (i.e, a polybasic protein with *possible* N-myristoylation) that belong to the polycationic Ras superfamily of proteins. Thus, Arl should get accumulated largely at the negatively charged PM, which serves as a thermodynamically favoured trapping structure for most of the polycationic Ras family members.[227]

Another plausible reason for the cargo release in the absence of Arl could be the comparable binding affinities of Ras to the membrane and PDEδ as reported[224]. But, this would imply a very transient or unstable PDEδ•Ras complex, which directly contradicts other *in vitro*[59] and *in vivo*[223] reports. Future studies will have to be carried out to study the two different alternatives proposed here.

6.4 Summary and Outlook

Spatial regulation of Ras proteins is dominated by their lipid modifications, but the transport of Ras proteins to the PM remains a major conundrum in the field. Understanding the mechanisms that counter both, the entropy-driven randomisation of Ras over all the intracellular membranes and the otherwise slow Ras diffusion, might improve our knowledge regarding its transport in cellular systems. In this regard, involvement of a chaperone or escort protein- PDEδ, as a solubilisation-based diffusion system for Ras transport, has been recently proposed.[147] PDEδ has long been implicated as a prenyl-binding protein, due to its structural similarity with RhoGDI (that sequesters and buries its cognate partner's hydrophobic lipid moiety). Despite this structural similarity, there are marked differences in their binding to G-proteins. For example, the relatively longer N-terminal regulatory arm in RhoGDI contacts the switch regions of its cargo, thus exhibiting nucleotide-dependent binding.

In this study, the interaction of PDEδ with Ras in the presence and absence of heterogeneous raft-like membranes of different compositions was studied. Taken together, the findings

revealed that PDEδ exhibits a generic binding to Ras protein, i.e, independent of the nucleotide loading and isoform specificity. This affirms that the most likely interaction site is the C-terminal farnesylated region (common among all the Ras isoforms). However, studies stating the otherwise have also been reported, and it is only a matter of time until further examination of the PDEδ•Ras complex will shed light on their possible interaction sites. No PDEδ-mediated extraction of Ras (especially in the case of K-Ras) could be observed. The PDEδ•Ras complex preformed in bulk solution dissociated upon contact with heterogeneous membranes; the results confirmed a stable membrane insertion of the Ras proteins mediated by their freed farnesyl anchor in both the isoforms. However, what has not been mentioned till now is the eminence of PDEδ in transporting prenylated Ras to the respective membranes. Unfortunately the techniques discussed in the present work fail to give any kinetic account of such interactions. In this regard, inter-membrane transfer experiments of the *different Ras proteins with different membrane compositions, and in the presence and absence of PDEδ,* would delineate the proposed role of PDEδ as a diffusion facilitator,[147] enabling the delivery of Ras proteins to their specific, cognate membrane compartments by enhancing the kinetics of membrane trapping. Furthermore, the proposed role of the membranes in mediating the release of the farnesyl moiety from PDEδ can be put to test by performing NMR experiments, to obtain residue-specific details of PDEδ in the presence and absence of lipid membranes.

Finally, signalling from Ras proteins critically depends on their PM enrichment and subcellular distribution, which in turn is at the mercy of accelerated diffusion by PDEδ. This implicates the PDEδ•Ras complex as an attractive target for cancer therapeutics, tempering with which can lower the oncogenic Ras dose at the PM below a particular threshold. This could either help re-instate the endogenous level of signalling required for normal cell growth or fully activate the wild-type Ras via highly complex feedback mechanisms.

VII

PRESSURE MODULATED MEMBRANE ASSOCIATION AND INTERVESICLE TRANSFER OF RAS

7.1 Background

7.1.1 Pressure-Induced Cellular Signalling: Mechanotransduction

High hydrostatic pressure has been extensively used to study the structural and functional aspects of biological macromolecules such as proteins, lipid membranes and nucleic acids, but the application of this tool to explore bioprocesses—especially membrane-associated cellular processes—has only gained attention recently. Interactions in the biological macromolecular assembly are mainly stabilised by non-covalent forces such as hydrophobic and electrostatic, and the alteration of these weak bonds by pressure (due to the low energy it imparts) provide subtle insights into the mechanism of these stabilisation forces. Mechanical forces are also important modulators of cellular processes, and research along those lines has revealed trans-membrane signalling processing as important loci of pressure perturbation.[230-231] In addition, many mechanosensitive biomolecules such as mechanically gated channels,[232] receptors,[233] G-proteins,[234] and cytoskeletons mediating this response have emerged. Although in the majority of these studies, the mechanical stimulus was shear stress—a directional pressure induced by the frictional flow of blood or other fluids—mechanosensitivity towards hydrostatic pressure (a non directional stress) has also been implicated in many cell types.[230,235] A common key discovery amongst them was the activation of the MAPK/ERK signalling pathway, of which Ras is a crucial nodal point.[231,236-237] Moreover, it has also been demonstrated that mechanochemical signalling

[230] Wu, H.J., Zhang, Z.Q., Yu, B., Liu, S., Qin, K.R., and Zhu, L. **(2010)**. Pressure activates Src-dependent FAK-Akt and ERK1/2 signaling pathways in rat hepatic stellate cells. *Cell Physiol. Biochem. 26*, 273–280.
[231] Salvador-Silva, M., Aoi, S., Parker, A., Yang, P., Pecen, P., and Hernandez, M.R. **(2004)**. Responses and signaling pathways in human optic nerve head astrocytes exposed to hydrostatic pressure in vitro. *Glia 45*, 364–377.
[232] Sukharev, S.I., Blount, P., Martinac, B., Blattner, F.R., and Kung, C. **(1994)**. A large-conductance mechanosensitive channel in E. coli encoded by mscL alone. *Nature 368*, 265–268.
[233] Paoletti, P., and Ascher, P. **(1994)**. Mechanosensitivity of NMDA receptors in cultured mouse central neurons. *Neuron 13*, 645–655.
[234] Gudi, S., Nolan, J.P., and Frangos, J.A. **(1998)**. Modulation of GTPase activity of G proteins by fluid shear stress and phospholipid composition. *Proc. Natl. Acad. Sci. U.S.A. 95*, 2515–2519.
[235] Ferraro, J.T., Daneshmand, M., Bizios, R., and Rizzo, V. **(2004)**. Depletion of plasma membrane cholesterol dampens hydrostatic pressure and shear stress–induced mechanotransduction pathways in osteoblast cultures. *Am. J. Physiol. Cell. Physiol. 286*, C831–839.
[236] Li, Y.S., Shyy, J.Y., Li, S., Lee, J., Su, B., Karin, M., and Chien, S. **(1996)**. The Ras-JNK pathway is involved in shear-induced gene expression. *Mol. Cell Biol. 16*, 5947–5954.
[237] Tzima, E. **(2006)**. Role of small GTPases in endothelial cytoskeletal dynamics and the shear stress response. *Circ. Res. 98*, 176–185.

originates at the cell membrane, where the lipid bilayer itself plays a major role in mediating it. Thus, it is critical to study in detail the thermodynamic and kinetic aspects of pressure-induced *membrane*-associated processes via appropriate tools. The effects of pressure-induced stimulation of signalling is now a relatively well documented field of research, though the basic mechanisms by which barometric forces are detected and translated into biological signals are not clearly defined; theories postulating such mechanisms are vague and limited.

7.1.2 Protein–Membrane Interactions under Pressure: A Theoretical View

7.1.2.1 Pressure effects on the protein–membrane association

A priori, pressure influences membrane-associated processes most that are accompanied by large volume changes. When the reaction volume is positive or negative, high hydrostatic pressure will stunt or foster the association, respectively. The main contributors to volume changes, naming a few, are release of the void volumes (due to imperfect packing of two macromolecular surfaces), electrostriction, and lipid condensation. Volume changes accompanying protein–protein associations have been widely explored in solution, but studies on those accompanying protein–membrane interactions are scarce. In this regard, membrane properties such as charge, hydration, curvature, and packing density are some of the most prominent features that influence the volume changes. Pressure effects on these membrane properties (also related to the present study) are briefly discussed below:

(a) Surface charges: Cellular membranes contain a significant amount of negatively charged lipids[52], and many proteins are known to bind to membranes with strong electrostatic contributions, e.g. K-Ras4B. Explicit theoretical aspects on the role of this contribution can be found elsewhere.[238-239] The ionisation of the lipid headgroups is pressure sensitive, due to the volume reduction accompanying electrostriction. However, in the case of lipid bilayers, this effect is less pronounced due to the

[238] McLaughlin, S. **(1989)**. The electrostatic properties of membranes. *Annu. Rev. Biophys. Biophys. Chem. 18*, 113–136.
[239] Weise, K., Huster, D., Kapoor, S., Triola, G., Waldmann, H., and Winter, R. **(2012)**. Gibbs energy determinants of lipoprotein insertion into lipid membranes: The case study of Ras proteins. *Faraday Discussions*. DOI: 10.1039/C2FD20100C

counter-effect of energy needed to expand and hydrate the lipid interface.[240] If binding of proteins to membranes is driven by electrostatic interactions, it could be reversed under pressure (because of the volume decrease as a result of electrostriction of water near ions), but such an effect has never been experimentally observed.[241] This reflects the fact that the binding event does not significantly dehydrate the charges involved. Moreover, for the electrically neutral lipid PC (used in the present study) and even charged PG, no changes in the surface charge and hydration have been observed.[240]

(b) Packing density: The lipid headgroup is rather incompressible compared to the interior of the bilayer, where the application of pressure increases the packing density of lipid chains. Thereby, the thickness of the membrane increases along the lipid chain. This is accompanied by a concomitant decrease in the cross sectional lipid chain area. For example, in the DMPC lipid bilayer using ^{2}H NMR, an increase in the membrane thickness by 1.3 Å/kbar was obtained. The pressure effect on the partitioning of proteins—especially lipidated protein—remains unexplored; however it is expected to modulate the binding of lipidated proteins. This is due to the evidence that the post-synthetic lipid modifications in proteins play a major role in the membrane partitioning and stabilisation of proteins, via the classical hydrophobic effect,[239] which has been shown to be weakened upon pressurisation.

(c) Lateral surface structure: Throughout this document, the lateral heterogeneity or the phase segregation in model/biological membranes has been repetitively mentioned, and the physiological implications on Ras protein–membrane interactions have been discussed. Thus, considering their importance, it is logical to examine the effects of high pressure upon them. As stated above, high pressure promotes chain ordering and—in accordance with the Gibbs phase rule—would be expected to steadily reduce the amount of l_d phases in the membranes. The physical properties of the l_o/l_d phases are likely to become increasingly similar upon pressurisation, finally ending in all-ordered phase regions. Owing to the different packing properties of cholesterol,

[240] Scarlata, S.F., and Rosenberg, M. **(1990)**. Effect of increased lipid packing on the surface charge of micelles and membranes. *Biochemistry 29*, 10233–10240.

[241] Montich, G., Scarlata, S., McLaughlin, S., Lehrmann, R., and Seelig, J. **(1993)**. Thermodynamic characterization of the association of small basic peptides with membranes containing acidic lipids. *Biochim. Biophys. Acta 1146*, 17–24.

saturated and unsaturated chains, phase separation into different l_o or gel-like phases might take place, but at high pressures values, only.

7.1.2.2 Pressure effects on membrane-bound proteins

The pressure stability of a membrane-bound protein is primarily governed by its packing efficiency with the membrane surface, and its ability to deform under pressure.[242] The effects of hydrostatic pressure on the stability of membrane-bound peripheral and integral proteins are variable (reported elsewhere[243]), and have established a few well-accepted guidelines. First, under efficient protein–membrane packing, high pressure is not expected to destabilise the system. Second, if the packing is inefficient resulting in void volumes (often observed for multimeric membrane-associated protein, such as Na, K-ATPase), then the stability will depend on two factors, which tend to reduce the overall volume of the proteo-lipid system. Either the protein dissociates from the membrane allowing water to fill in the void volumes, or the protein itself (or certain regions of the protein) deforms under pressure, i.e. undergoes conformational changes, to fill the void volume.

7.2 Model Studies: Motivation and Objectives

Pressure may affect cellular signalling in various ways, such as by alteration of the signalling protein's conformational substates (thereby, modifying the rate of nucleotide binding), affecting the coupling of proteins to the membrane receptors, or by modulation of the protein–membrane association/dissociation reactions. Hence, the study of protein–membrane interactions using high pressure perturbation has also the potential to provide novel information regarding molecular interactions that cause the proteins to bind to membranes. To assess the pressure-induced effects on the signalling processes, model systems provide exemplary platforms to study the discrete steps that might be mechanosensitive. Furthermore, considering the evidence that small GTPases (i.e. Ras) were found as an early link between mechanotransduction and proceeding signalling events[237], it is crucial to obtain detailed insights into the pressure-induced effect on

[242] Teng, Q., and Scarlata, S. **(1993)**. Effect of high pressure on the association of melittin to membranes. *J. Biol. Chem. 268*, 12434–12442.
[243] Plager, D.A., and Nelsestuen, G.L. **(1992)**. Dissociation of peripheral protein–membrane complexes by high pressure. *Protein Sci. 1*, 530–539.

Ras proteins. In the present study, a FRET-based assay was employed to explore the effects of hydrostatic pressure on the membrane association and dissociation of the fully lipidated N-Ras proteins, and to obtain the associated kinetics and volumetric changes. Different membrane compositions (pure fluid versus ordered raft-like) were used to reveal the role of lipid bilayer packing and heterogeneity.

7.3 Description of the Transfer Model

There are two principally distinct mechanisms conceivable for the transfer of (lipidated) protein between lipid vesicles: (1) diffusion through the aqueous phase separating the lipid membranes (aqueous diffusion model), and (2) transfer mediated by vesicle-vesicle collisions (collision-mediated model). At the relatively low lipid concentrations employed here, and in agreement with previous observations, the collision-mediated model is not expected to play a significant role.[244,245,246] Thus, rate equations describing the diffusion pathway (Fig. 7.1) for the Ras–membrane interactions have been formulated. The corresponding equations for the collision-mediated pathway can be found elsewhere.[247]

[244] Pagano, R.E., Martin, O.C., Schroit, A.J., and Struck, D.K. **(1981)**. Formation of asymmetric phospholipid membranes via spontaneous transfer of fluorescent lipid analogues between vesicle populations. *Biochemistry 20*, 4920–4927.
[245] Nichols, J.W., and Pagano, R.E. **(1982)**. Use of resonance energy transfer to study the kinetics of amphiphile transfer between vesicles. *Biochemistry*. *21*, 1720–1726.
[246] Wimley, W.C., and Thompson, T.E. **(1991)**. Transbilayer and interbilayer phospholipid exchange in dimyristoylphosphatidylcholine/dimyristoylphosphatidylethanolamine large unilamellar vesicles. *Biochemistry*. *30*, 1702–1709.
[247] Nichols, J.W. **(1988)**. Kinetics of Fluorescent-Labeled Phosphatidylcholine Transfer between Nonspecific Lipid Transfer Protein and Phospholipid-Vesicles. *Biochemistry*. *27*, 1889–1896.

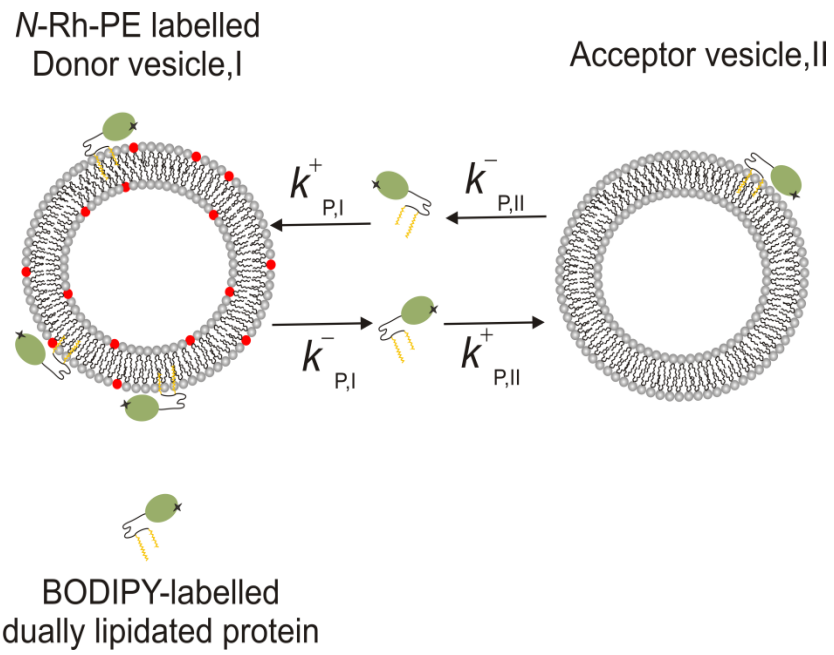

Figure 7.1: Schematic diagram of the diffusion-mediated transfer process and definition of rate constants.

The rate equations for the BODIPY-labelled lipidated N-Ras proteins (serving as the FRET donor) interacting with the *N*-Rh-PE doped lipid vesicles (serving as the FRET acceptor) can be easily written by assuming the following prerequisites:

(a) The rate at which a protein molecule (protein, P) dissociates from the surface of the lipid vesicle (off-rate) is proportional to its surface concentration on that vesicle.

(b) The association rate (on-rate) is proportional to the product of its concentration in the bulk solution and the external (outer) surface area of the lipid vesicle (vesicle, V).

The initial rate equations describing the transfer kinetics of the BODIPY-lipidated protein (P) from *N*-Rh doped donor lipid vesicles (I) to the unlabelled acceptor lipid vesicles (II) of the same size and composition (Fig. 7.1) are then as follows:

$$\frac{\partial c_{P,I}}{\partial t} = k^+_{P,I} \cdot c_{P,free} \cdot \left(s_P \cdot c_{P,I} + s_{V,I} \cdot c_{V,I}\right) - k^-_{P,I} \cdot c_{P,I} \qquad (1)$$

$$\frac{\partial c_{P,II}}{\partial t} = k^+_{P,II} \cdot c_{P,free} \cdot \left(s_P \cdot c_{P,II} + s_{V,II} \cdot c_{V,II}\right) - k^-_{P,II} \cdot c_{P,II} \qquad (2)$$

where, $k_{\mathrm{P,I}}^{-}$, $k_{\mathrm{P,II}}^{-}$, $k_{\mathrm{P,I}}^{+}$, and $k_{\mathrm{P,II}}^{+}$ are the dissociation or off-rate and association or on-rate constants of the BODIPY-labelled lipidated protein in vesicle populations I and II, respectively; $c_{\mathrm{P,free}}$ is the molar concentration of the free protein in bulk solution, and $c_{\mathrm{P,I}}$, $c_{\mathrm{P,II}}$, $c_{\mathrm{V,I}}$, and $c_{\mathrm{V,II}}$ are the concentrations of the protein (P) and lipid molecules (V) in the external monolayer of the lipid vesicles I and II; s_{P}, $s_{\mathrm{V,I}}$ and $s_{\mathrm{V,II}}$ are the external surface areas per mole of the protein and lipid molecules within the subscripted lipid layers, respectively. The affinity constant of protein molecules (P) for lipid membranes, $K_{\mathrm{P,ass}}$, is defined as the ratio:

$$K_{\mathrm{P,ass}} = \frac{k_{\mathrm{P}}^{+}}{k_{\mathrm{P}}^{-}} \tag{3}$$

At steady-state equilibrium we have,

$$\frac{\partial c_{\mathrm{P,I}}}{\partial t} + \frac{\partial c_{\mathrm{P,II}}}{\partial t} = 0. \tag{4}$$

When the donor (I) and acceptor (II) vesicles are of the same composition, and the acceptor vesicle concentration is largely in access of the donor, as realised in our experiments, then by substituting Eqs. (1) and (2) into (4) one obtains

$$-\frac{\partial c_{\mathrm{P,I}}}{\partial t} = \frac{\partial c_{\mathrm{P,II}}}{\partial t} \approx k_{\mathrm{P,I}}^{-} \cdot c_{\mathrm{P,I}} \tag{5}$$

which is proportional to the initial slope of the measured fluorescence intensity with time (scaled to the maximum fluorescence intensity change expected upon complete redistribution of the lipidated protein at equilibrium).

Integration of Eq. (5) for the cases where the protein P transfers more rapidly than the phospholipids (which is a safe approximation), and if initially only vesicles of population I bind to the protein, yields Eq. (6), accounting for the time-dependent decay of the protein molecules.

$$c_{\mathrm{P,I}}(t) = c_{\mathrm{P,I}}(0) \cdot \mathrm{e}^{-k_{\mathrm{P,I}}^{-} \cdot t} \text{ or } c_{\mathrm{P,II}}(t) = c_{\mathrm{P,I}}(0) \cdot (1 - \mathrm{e}^{-k_{\mathrm{P,I}}^{-} \cdot t}) \tag{6}$$

Hence, from the decay of the fluorescence intensity with time, $F(t)$, the dissociation or off-rate $k_{\mathrm{P,I}}^{-}$ can be calculated. The corresponding halt-time for $c_{\mathrm{P,II}}$ to reach equilibrium amounts to:

$$t_{1/2} = \frac{\ln 2}{k_{P,I}^{-}} \tag{7}$$

Under these boundary conditions, the rate of dissociation $k_{\mathrm{P,I}}^{-}$, or in general terms k_{diss}, is directly related to the rate k_{trans} at which the BODIPY-labelled lipidated N-Ras protein transfers from the *N*-Rh-PE labelled donor vesicles to the unlabelled acceptor vesicles. This is because, in the absence of any collision-mediated transfer, the rate of dissociation from donor vesicles is the rate-determining step for the intervesicle transfer process.

The association or on-rate $k_{\mathrm{P,I}}^{+}$ can be measured by adding protein molecules P at concentration $c_{\mathrm{P,free}}$ to the bulk solution containing fluorescent labelled lipid vesicles (population I). If $c_{\mathrm{P,I}} = 0$ for $t = 0$, one obtains for the decrease of the protein molecules in the bulk and initial association process,

$$c_{\mathrm{P,I}}(t) = c_{\mathrm{P,free}}(0) \cdot (1 - \mathrm{e}^{-k_{\mathrm{P,I}}^{+} \cdot (s_{\mathrm{P}} \cdot c_{\mathrm{P,I}} + s_{\mathrm{V}} \cdot c_{\mathrm{V,I}}) \cdot t}) \qquad \text{and} \tag{8}$$

$$c_{\mathrm{P,free}}(t) = c_{\mathrm{P,free}}(0) \cdot \mathrm{e}^{-k_{\mathrm{P,I}}^{+} \cdot (s_{\mathrm{P}} \cdot c_{\mathrm{P,I}} + s_{\mathrm{V}} \cdot c_{\mathrm{V,I}}) \cdot t} \tag{9}$$

respectively, where $k_{\mathrm{P,I}}^{+} \cdot (s_{\mathrm{P}} \cdot c_{\mathrm{P,I}} + s_{\mathrm{V}} \cdot c_{\mathrm{V,I}})$ can be treated as an observed effective association rate constant, k_{eff}^{+} (with units of inverse time), which can be determined from the time-dependent increase of the fluorescence intensity upon incorporation of BODIPY-labelled protein into the *N*-Rh-PE doped lipid vesicles due to the FRET between the respective fluorophores.

Moreover, the true on-rate constant, k_{P}^{+}, or in general terms k_{on}, can also be approximated with certain assumptions. In a simplest case, the partitioning of the lipidated protein (P) with

the vesicle (i.e. population, I) occurs in a single step, and the association is a pseudo first-order process (due to $c_V \gg c_P$). This leads to

$$c_{P,I}(t) = c_{P,I}(\infty) \cdot (1 - e^{-t/\tau}) \quad (10)$$

where $c_{P,V}(\infty)$ is the protein concentration partitioned into the vesicles at equilibrium, and τ is the relaxation time of the process, where the reciprocal of the relaxation time is given by:

$$\frac{1}{\tau} = k_{on} \cdot c_V + k_{off} \quad (11)$$

When the experimental data are plotted as $1/\tau$ *versus* c_V, the on-rate can be obtained from the slope of this curve, which equals, k_{on}/n, where n is the number of lipid molecules comprising the binding sites on the vesicle. In a very oversimplified scenario, it can be equated to the total number of lipid molecules residing in the external leaflet of the vesicles exposed to the bulk, a calculable quantity. We can only speculate about the number of binding sites and lipid molecules within such sites on the vesicles, required for the interaction with lipidated proteins, which till now has appeared to be an arbitrary number. In such circumstances, given the fact that we are only interested in relative changes of the protein–membrane interaction, subjected to different conditions, the use of an effective association rate constant, k_{eff}^{+}, seems justifiable.

7.4 Results and Discussion

7.4.1 A FRET-based system for studying Ras–membrane interactions

In this work, the dually lipidated N-Ras (i.e. N-Ras HD/Far) labelled with BODIPY-FL (ex_{max}: 501 nm, em_{max}: 515 nm) at its N-terminus served as the donor, and the large unilamellar vesicles (100 nm) composed of either DOPC or DOPC:DPPC:Chol (1:2:1; molar ratio) symmetrically doped with 0.2 mol % *N*-Rh-PE (a dye that serves as a fluid lipid-phase marker with ex_{max}: 568 nm, em_{max}: 591 nm) was used as the acceptor. Unless otherwise stated, the ratio between BODIPY-Fl and *N*-Rh-PE was kept constant at 1: 2. The labelling yield of N-Ras protein was approximately 37 %, obtained by comparing the absorbance of BODIPY-FL at 505 nm and the protein at 280 nm. Low levels of the lipid marker were

chosen (0.2 mol %) to maintain the integrity and phase state of the lipid vesicles, as it has been observed that ratios higher than 0.5 mol % may induce disorganisation of the lipid bilayer.[248] BODIPY and *N*-Rh-PE have been used as an ideal FRET pair in many studies.[249] A significant spectral overlap between the emission spectrum of BODIPY and the absorption spectrum of *N*-Rh-PE was obtained (Fig. 7.2). When both the fluorophores were embedded within the same bilayer, excitation of BODIPY-N-Ras (at 488 nm) resulted in significant energy transfer between the two fluorophores, and an increased emission from *N*-Rh-PE was followed at 591 nm (Fig. 7.3); the fluorescence signal from the labelled N-Ras at this wavelength was negligible. The association studies were monitored by measuring the increase in acceptor fluorescence and the dissociation process (initiated by adding an eightfold access of unlabelled lipid vesicles to the protein-bound labelled vesicles) was followed by the concomitantly decreased acceptor fluorescence, due to the transfer of BODIPY-labelled protein from labelled to unlabelled lipid vesicles.

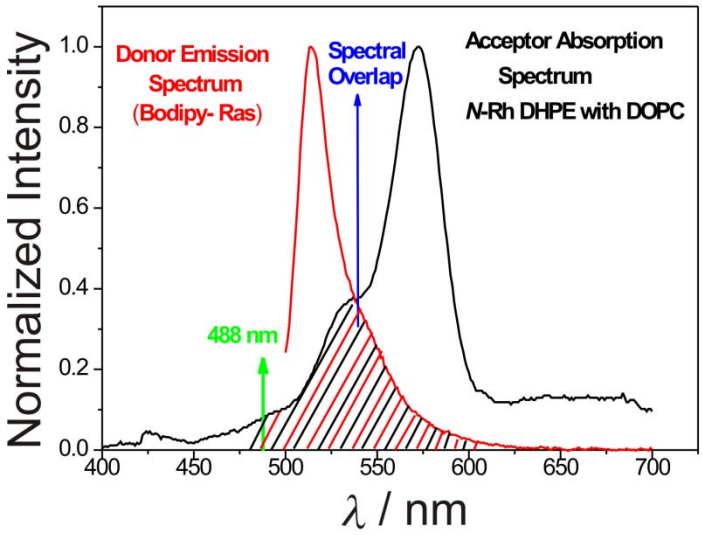

Figure 7.2: Spectral overlap between BODIPY-labelled N-Ras and N*-Rh-PE *doped lipid vesicles. The overlap between the emission spectrum of BODIPY-labelled Ras and the absorption spectrum of *N*-Rh-PE labelled lipid vesicles upon excitation of the BODIPY fluorophore at 488 nm.

[248] Lapinski, M.M., and Blanchard, G.J. **(2007)**. The role of phospholipid headgroups in mediating bilayer organization. Perturbations induced by the presence of a tethered chromophore. *Chem. Phys. Lipids 150*, 12–21.

[249] Yang, J., Chen, H., Vlahov, I.R., Cheng, J.X., and Low, P.S. **(2006)**. Evaluation of disulfide reduction during receptor-mediated endocytosis by using FRET imaging. *Proc. Natl. Acad. Sci. U.S.A. 103*, 13872–13877.

The FRET efficiency can be determined by measuring the donor quenching according to

$$E_{\text{eff}} = 1 - \frac{F_{\text{da}}}{F_{\text{d}}} \tag{12}$$

where F_{da} and F_{d} are the donor fluorescence intensities in the presence and absence of the acceptor, respectively. However, this only holds true for FRET pairs separated by fixed distances. Under the conditions when a FRET pair exhibits a distribution of distances—as in the case of externally labelled proteins—the observed E_{eff} is directly related to the distance distribution.[250]

7.4.2 Membrane association of N-Ras under ambient and high pressure conditions: Time-resolved fluorescence spectroscopy results

7.4.2.1 Association to pure fluid and heterogeneous membranes at ambient pressure

The association could be observed either by a decrease or an increase in the donor or acceptor intensity, respectively. However, in the present case, it has been characterised by following the acceptor fluorescence over time, mainly for two reasons. First, it was found that the fluorescence of BODIPY-N-Ras showed a time-dependent increase upon insertion to the lipid vesicles (Fig. 7.3 **A**), whereas a completely opposite behaviour is expected due to energy transfer. Second, *N*-Rh DHPE served as a non-exchangeable probe, which reduced errors in the data analysis, especially while performing the intervesicle transfer experiments.

The increase in the donor intensity (Fig. 7.3 **A**) was attributed to the increased effective concentration of proteins on the membrane, compared with the bulk. In addition, the more hydrophobic environment provided by the lipid interfacial region also contributed to the donor intensity, in accordance with other studies on partitioning of labelled lipidated peptides.[251] Thus, the increase in the donor fluorescence upon insertion of the protein into the membrane was expected to occur in parallel to the energy transfer process, thereby restricting the use of the donor as an association marker. In order to cross check if the two processes

[250] Haas, E., Wilchek, M., Katchalski-Katzir, E., and Steinberg, I.Z. **(1975)**. Distribution of end-to-end distances of oligopeptides in solution as estimated by energy transfer. *Proc. Natl. Acad. Sci. U.S.A.. 72*, 1807–1811.

[251] Silvius, J.R., and l'Heureux, F. **(1994)**. Fluorimetric evaluation of the affinities of isoprenylated peptides for lipid bilayers. *Biochemistry 33*, 3014–3022.

were happening in conjunction, another lipid vesicle sample (with a fourfold increase in the *N*-Rh-PE concentration) was employed. A decreased donor fluorescence was obtained (Fig. 7.3 A), due to a higher energy transfer as a result of the increased D:A ratio (from 1:2 to 1:8).

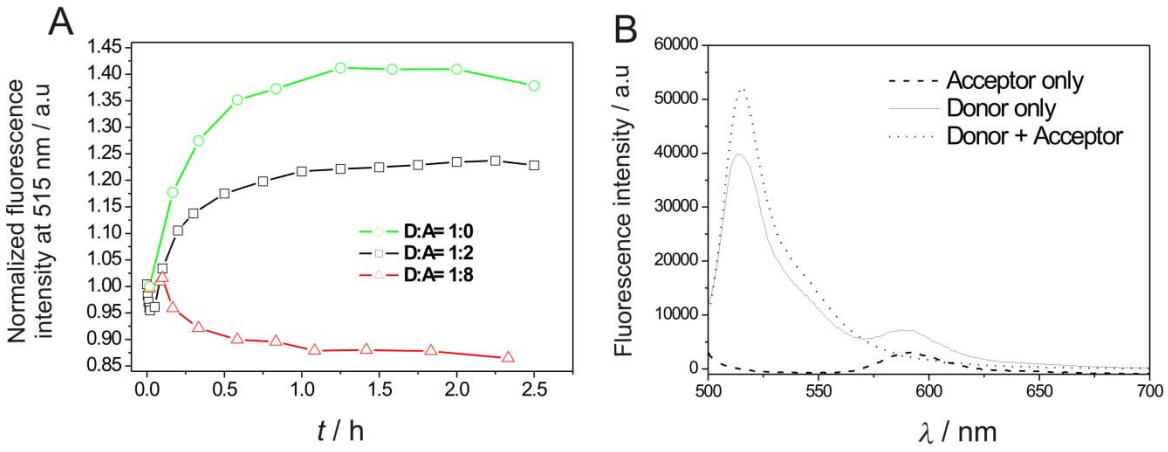

Figure 7.3: FRET between BODIPY-labelled dually lipidated N-Ras and N-Rh-PE labelled lipid membrane. **(A)** Time-dependent **e**nergy transfer from the BODIPY-labelled N-Ras ($c_{protein}$ = 0.35 µM, c_{BODIPY} = 0.125 µM) to the *N*-Rh labelled DOPC vesicles ($c_{vesicles}$ = 0.125 mM, $c_{N\text{-}Rh}$ = 0.25 µM) at 1 bar and 25 ˚C. Excitation of the donor was performed at 488 nm and acceptor fluorescence was measured at 591 nm. (**B**) Emission spectra of the donor with and without the acceptor, and the cross excitation of the acceptor only. Excitation was performed at 488 nm.

Figure 7.3 **B** shows the emission spectra for the donor only, the acceptor only and the donor in the presence of the acceptor. The observed efficiency of transfer (calculated using Eq. 12) was estimated to be approximately 22 ± 3 %. The rather low efficiency observed was due to the distance distributions between the flexible donor and the acceptor. As the N-Ras protein partitions only into the outer leaflet of the lipid vesicle, it is expected to transfer the maximum of energy to *N*-Rh-PE molecules in the outer vesicle leaflet, and to a much lesser extent to the *N*-Rh-PE molecules in the inner leaflet (the overall lipid bilayer thickness is ~ 5 nm). The fraction of the surface-exposed lipids (and also the fraction of surface-exposed *N*-Rh-PE) was estimated to be ~0.42 ± 0.3 and ~0.46 ± 0.2 for pure DOPC and the neutral raft-

like lipid vesicles, respectively, using the TNBS-accessibility assay of Nordlund et al.[252] This implied that approximately half of the acceptors (*N*-Rh-PE) were present in the outer leaflet.

Figure 7.4 **A** shows the time-dependent increase in the acceptor fluorescence (F_{corr}) due to the insertion of BODIPY- N-Ras into the *N*-Rh doped DOPC vesicles, after correction of the signal intensities from donor only and acceptor only, respectively (i.e. $F_{corr} = F_{obs}-F_d-F_a$). The association reached equilibrium after approx. 1.0 h, observed by the stable fluorescence intensity plateau.

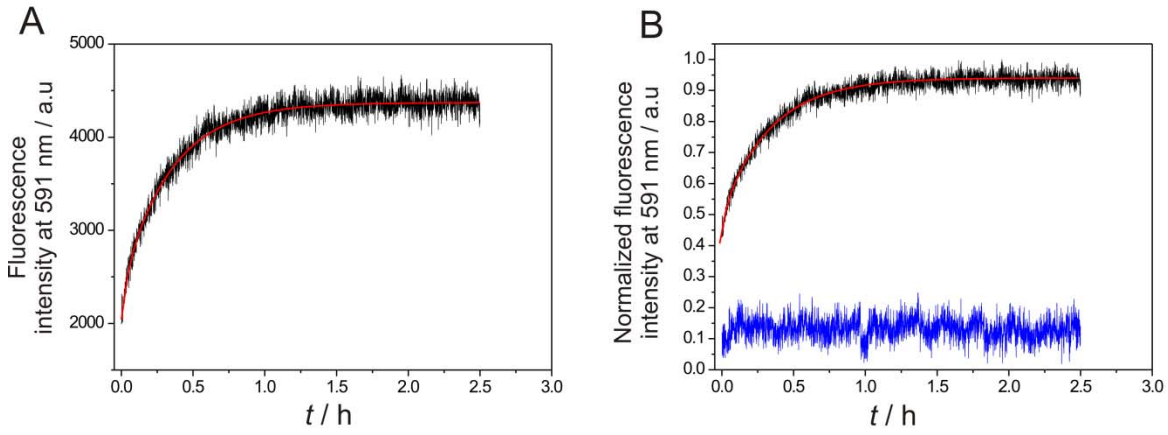

Figure 7.4: ***Monitoring membrane insertion of dually lipidated N-Ras via the FRET-based assay.*** (**A**) Energy transfer from the BODIPY-labelled N-Ras ($c_{protein}$ = 0.35 µM, c_{BODIPY} = 0.125 µM) to the *N*-Rh labelled DOPC vesicles ($c_{vesicles}$ = 0.125 mM, $c_{N\text{-}Rh}$ = 0.25 µM) at 1 bar and 25 ˚C, measured at 591 nm (ex: 488 nm). The red curve represents the best fit to the experimental data. (**B**) Fluorescence intensity normalised to the maximum of the Fig. 7.3 **A** at ~ 2.5 h (black). The blue curve represents the FRET signal from BODIPY-labelled unlipidated N-Ras to the *N*-Rh doped DOPC lipid vesicles.

After normalisation of the fluorescence intensity by the equilibrium value in Figure 7.4 **A,** the surprisingly quite high fluorescence intensity observed at initial times ~ 5 min (in Fig. 7.4 **B**) suggests the following. First, a *"proximity"* FRET due to a rapid non-specific localisation of the Ras proteins near the membranes. However, this effect was ruled out by performing a control experiment using labelled unlipidated N-Ras protein, which had almost no fluorescence signal intensity compared with its lipidated counterpart (Fig. 7.4 **B**, **blue curve**).

[252] Nordlund, J.R., Schmidt, C.F., Dicken, S.N., and Thompson, T.E. **(1981)**. Transbilayer distribution of phosphatidylethanolamine in large and small unilamellar vesicles. *Biochemistry*. *20*, 3237–3241.

The other plausible reason could be the initial docking of the protein followed by reorientation and subsequent insertion of the Ras lipid anchors into the membrane. This was confirmed by performing Stopped-Flow measurements with a dead time of sub-500 μs (See Appendix, Fig. 9.7), with a similar concentration of donor and acceptor labelled biomolecules. These measurements revealed significant insertion of the dually lipidated N-Ras protein into the membrane already within the dead time (of a few minutes) of the current set-up. Though the non-exponentiality of the association curve reflects a complex interaction behaviour of N-Ras with the membrane, the best fits to the time-dependent changes were obtained with a bi-exponential curve (Fig. 7.4, **red line**), given by Eq. (13).

$$F_{\text{corr}} = F_{\text{min}} + A_1 \cdot \left(1 - \mathrm{e}^{-k^{+}_{\text{eff},1} \cdot t}\right) + A_2 \cdot \left(1 - \mathrm{e}^{-k^{+}_{\text{eff},2} \cdot t}\right) \tag{13}$$

The two steps representing the membrane insertion were assigned to:

(1) An initial docking, reorientation, and subsequently high affinity insertion into the lipid membrane mediated by its lipid anchors as the first step.
(2) The lateral reorganisation of the proteins within the plane of the membrane leading to clustering, as shown by the AFM studies (**cf. Fig. 4.1, Ch. 4**).

A similar insertion process was observed for the neutral raft-like lipid mixture. Its particular lipid composition was chosen to study the effects of raft-like heterogeneities on the partitioning behaviour and stability of the membrane association. Figure 7.5 **A** shows the bi-exponentential fits for the N-Ras association to DOPC and the raft-like lipid mixture, from an average of 11 experiments. To improve visual comparison, the intensity data have also been normalised (Fig. 7.5 **B**). This normalisation did not affect the curve-fitting module and resulted in similar kinetic rate constants (Table 7.1).

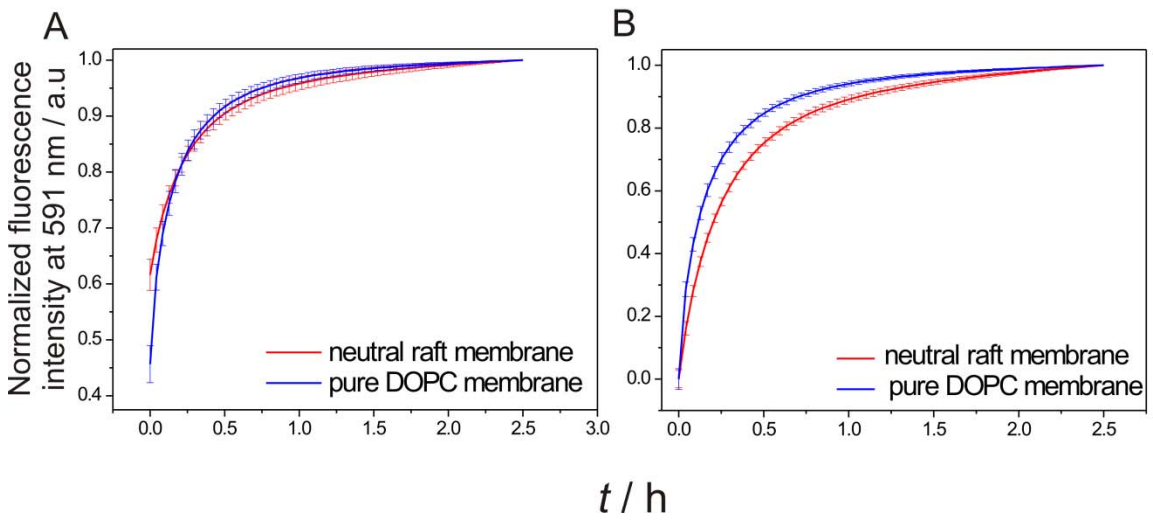

Figure 7.5: Kinetic delineation of the Ras-membrane insertion process and the influence of membrane composition on the insertion. **(A)** Time-dependent increase in the normalised fluorescence intensity due to energy transfer from the BODIPY-labelled N-Ras ($c_{protein}$ = 0.35 µM, c_{BODIPY} = 0.125 µM) to the *N*-Rh labelled DOPC or the neutral raft-like (DOPC:DPPC:Chol 25:50:25 (molar ratio)) lipid vesicles ($c_{vesicles}$ = 0.125 mM, $c_{N\text{-}Rh}$ = 0.25 µM) at 1 bar and 25 ˚C. (**B**) Intensity normalisation of Fig. 7.5 **A** to the range 0-1.

Table 7.1: Kinetic rate constant for the association of the dually lipidated N-Ras to lipid membranes of different composition at 1 bar. The effective association rate constants for the curves presented in Fig. 7.5 were obtained Eq. (13). In the table, mean values ± standard deviation (n = 10-11) are given.

N-Ras HD/Far to the	$k^{+}_{eff,1}$ / **h^{-1}**	$k^{+}_{eff,2}$ / **h^{-1}**
DOPC membrane	10.16 ± 1.47	2.48 ± 0.53
Neutral raft-like membrane	4.81 ± 0.70	1.97 ± 0.35

The initial, linear slopes in the association curves are of similar magnitude, suggesting a preferable partitioning of N-Ras into the fluid-like phase of the heterogeneous membranes. However, meagre changes in the initial (effective) association rate constants, $k^{+}_{eff,1}$, between the two lipid compositions (i.e. $k^{+}_{eff,1}$ (DOPC) > $k^{+}_{eff,1}$ (raft-like)), demonstrate a minor slowing down of the association process in the heterogeneous membranes. This could arise from an overall larger lipid order parameter in the fluid phase of the heterogeneous

membrane, owing to the presence of saturated lipids and cholesterol. This effect is most likely dominated by the bulky nature of the farnesyl (Far) group, coupled with its higher hydrophobic mismatch with lipid acyl chains in the heterogeneous membrane. In this regard, an independent NMR study revealed that the lipid anchors of membrane-associated Ras are able to undergo remarkable adaptations with respect to the hydrophobic thickness of the host membranes, rendering the Gibbs free energy for hydrophobic mismatch, ΔG^{o}_{mism} (given by Eq. 14)[239] almost negligible:

$$\Delta G^{o}_{mism,chain} = \frac{1}{2} K_{th} A_L \frac{(l_L - l_0)^2}{l_0}, \quad (14)$$

where A_L is the membrane surface area per lipid molecule, l_L is the length of the Ras lipid anchor, and l_0 is the length of the undistorted lipid molecule in the free lipid bilayer. Specifically, the saturated 16:0 chain of N-Ras can easily bisect its length by introducing up to six additional *gauche* defects, thus allowing adaptation to both the l_o, s_o as well as to l_d phases in the heterogeneous membrane. However, no such effect is possible for the Far group implying that its mismatch with the l_o phase would be higher than in the l_d phase. Such an effect, if significant at all, would still have a minor contribution though.

The second association rate constant, $k^{+}_{eff,2}$, was found to be similar in both the lipid membrane systems, suggesting that the lateral reorganisation and clustering of the proteins are of similar magnitudes, the stability of which depends on the associated values of k_{off}, however. Although clustering of the dually lipidated N-Ras has only been observed in the heterogeneous lipid membranes,[125] there is no reason to rule out its occurrence in the pure fluid membranes as well, but this still requires verification. The clustering of proteins into distinct membrane domains is not biologically redundant, as it is expected to increase the association rates (due to an increase in the effective concentration (reaction cross-section) in particular regions of the membranes) to other downstream proteins in the signalling pathways, thus causing massive signal amplification.[120]

7.4.2.2 Association to pure fluid and heterogeneous membranes under high pressure

Measurements of the association kinetics of N-Ras to the different lipid membranes were carried out at a pressure of 2.0 kbar. This pressure did not unfold the Ras protein, as was shown recently.[208] As a control, pressure effects on the fluorescence of pure BODIPY-FL and *N*-Rh labelled DOPC/raft-like lipid vesicles in solution were also measured (**Appendix Fig. 9.4**) and were found to contribute less than 5 % of the observed signal. As such, they were accounted for in the final data analysis. The data analysis was the same as undertaken for the ambient pressure studies, mentioned above. The association of N-Ras to both membrane systems was fostered under pressure (Fig. 7.6), with higher association rate constants, as given in Table 7.2.

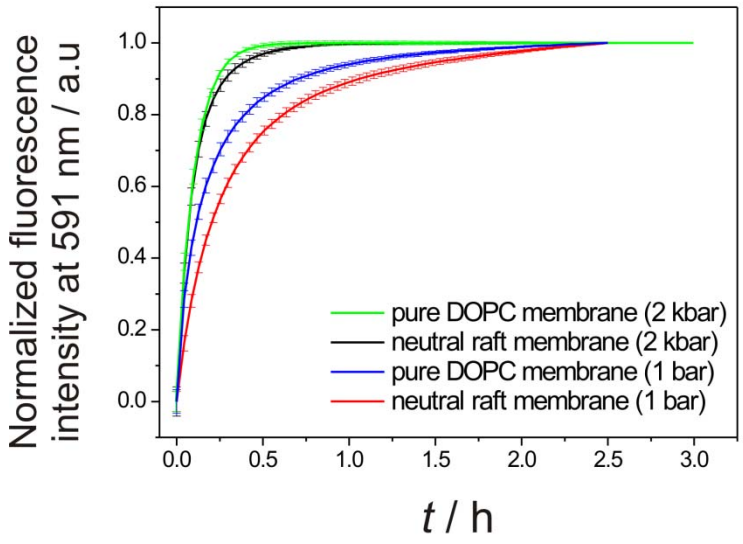

Figure 7.6: Influence of HHP on the kinetics of the dually lipidated N-Ras–membrane insertion process. Time-dependent increase in the normalised fluorescence intensity due to energy transfer from the BODIPY-N-Ras ($c_{protein}$ = 0.35 µM, c_{BODIPY} = 0.125 µM) to the *N*-Rh labelled DOPC or the neutral raft-like (DOPC:DPPC:Chol 25:50:25 (molar ratio)) lipid vesicles ($c_{vesicles}$ = 0.125 mM, $c_{N\text{-}Rh}$ = 0.25 µM). The measurements were done at 1 bar and 2 kbar and at 25 ˚C.

Table 7.2: Kinetic rate constants for the association of the dually lipidated N-Ras to lipid membranes of different composition at 2 kbar. The effective association rate constants for the curves presented in Fig. 7.6 were obtained by use of Eq. (13). In the table, mean values ± standard deviation (n = 3-4) are given.

N-Ras HD/Far to the	$k^{+}_{\mathrm{eff},1}$ / **h^{-1}**	$k^{+}_{\mathrm{eff},2}$ / **h^{-1}**
DOPC membrane (2 kbar)	18.05 ± 2.14	6.04 ± 1.30
Neutral raft-like membrane (2 kbar)	18.91 ± 1.17	4.43 ± 0.97

The foremost reason for the higher observed association rates was first thought to be the dissociation of the N-Ras dimer, as it has been shown that the dually lipidated N-Ras exists essentially as a dimer in solution (measured using fluorescence anisotropy; A. Werkmüller, unpublished results). Dimers are formed mainly through the HVR or lipid anchors, which could dissociate under pressure, thus increasing the association rate to the membranes. However, this possibility was ruled out based on the results indicating no changes in the anisotropy with increasing pressures. Thus, the Ras HVR or lipid anchors are expected to remain fully hydrated even in the dimeric state, which causes a potential (negative) volume change to be almost negligible.

Another plausible reason considered was the back/re-folding of the Ras HVR onto the protein core. In this respect, some studies have revealed that the HVR in Ras proteins does make contacts (or are sequestered) to the G-domain (referred to as back/refolding).[161,253] Application of high pressures could eventually reverse this effect, and hence contribute to the higher association rates. However, the expected volume change would still be negligible, because of the weak interactions between the HVR and the G-domain, permitting it to still remain fully hydrated. Other factors such as increases in number density and curvature of the membrane surface towards the proteins (arising from fissions upon a vesicle shape change) were also considered, but were carefully ruled out. At this stage it was realised that the basic properties of the membrane itself needed careful inspection. These were pressure-induced changes in the lipid chain packing density, a steady reduction in the amount of l_d phase and

[253] Thapar, R., Williams, J.G., and Campbell, S.L. **(2004)**. NMR characterization of full-length farnesylated and non-farnesylated H-Ras and its implications for Raf activation. *J. Mol. Biol. 343*, 1391–1408.

phase segregation into different (compared with the ambient pressure scenario) l_o or gel-like phases upon pressurisation. There is a clear idea of how the lipid membranes would behave or appear when acted upon by the above mentioned changes,[254] but how these pressure-induced changes would modulate the binding of lipidated proteins is little understood.

To this end, a high pressure mechanistic delineation based on activation volumes has long provided exciting vistas for scientists trying to comprehend the effect of pressure on membrane-associated processes,[255-256] and might provide valuable insights for assessing the transition state of the protein-membrane interaction process, which is attempted for the very first time here. In addition, if determined accurately, the activation volumes ($\Delta^{\ddagger}V$) for association and dissociation steps, respectively, may permit calculation of the overall reaction volume (ΔV_R), thus providing a glimpse of the physical properties of the final proteo-lipid system. Taken together, it would surely augment our perspectives about the very general yet crucial properties of the proteo-lipid system, tuning the pressure dependence of Ras–membrane interactions.

The pressure dependence of the effective association rate constant, $k^{+}_{\mathrm{eff},1}$, at a temperature T enables the calculation of the activation volume (Eq. 15), which is derived from transition state theory:

$$\Delta^{\ddagger}V_{\mathrm{ass}} = -RT\left(\frac{\partial \ln k^{+}_{\mathrm{eff},1}}{\partial p}\right)_T = \left(\frac{\partial \Delta^{\ddagger}G_{\mathrm{ass}}}{\partial p}\right)_T \qquad (15)$$

where, $\Delta^{\ddagger}V_{\mathrm{ass}}$ is the difference between the partial volumes of the transition state associated with the membrane association step, and that of the initial reactants (lipid, V_L and proteins, V_P). It embodies all volume changes occurring during the progression of the association

[254] Nicolini, C., Celli, A., Gratton, E., and Winter, R. **(2006b)**. Pressure tuning of the morphology of heterogeneous lipid vesicles: a two-photon-excitation fluorescence microscopy study. *Biophys. J. 91*, 2936–2942.
[255] Benz, R., and Conti, F. **(1986a)**. Effects of hydrostatic pressure on lipid bilayer membranes. I. Influence on membrane thickness and activation volumes of lipophilic ion transport. *Biophys. J.. 50*, 91–98.
[256] Benz, R., and Conti, F. **(1986b)**. Effects of hydrostatic pressure on lipid bilayer membranes. II. Activation and reaction volumes of carrier mediated ion transport. *Biophys. J. 50*, 99–107.

reaction from the initial to and within the transition state,[257] given by Eq. (16). $\Delta^{\ddagger} G_{ass}$ is the activation Gibbs energy for the association reaction.

$$\Delta^{\ddagger}V_{ass} = V^{\ddagger} - V_P - V_L, \quad (16)$$

From the presented data, the activation volume change, $\Delta^{\ddagger}V_{ass}$, for the association process of N-Ras to DOPC and raft-like membranes was found to be ~ -7.2 ± 0.21 and -16.99 ± 1.82 cm^3 mol^{-1}, respectively. Thus, the volume profile for the association process exhibits negative values for the transition state, revealing a compact transition state with reduced overall volume, probably dominated by the changes in the packing properties and hence free volume of the different lipid bilayer systems. This is due to higher acyl chain ordering and tighter packing of the lipid chains induced at high pressure, which is invariably accompanied by a reduction in volume.[258] For comparison, the pressure-induced increase of the packing density in a lipid bilayer (during a phase transition from the liquid-crystalline to the gel state, at 1 kbar) is accompanied by a reduction in volume by approximately ~ -30 cm^3 mol^{-1}. Use of Eq. (15), and assuming the same volume change to contribute to the decrease in activation volume, an increase in the rate constant at 2 kbar by a factor of 11 is obtained [i.e., $k^{+}_{eff,1}$ (2 kbar) = 11 x $k^{+}_{eff,1}$ (1 bar)]. Hence, increased van der Waals interactions between the lipid acyl chain and the protein's lipid anchors at high pressures, coupled with the decrease of conformational space in the lipid anchor region upon membrane insertion, would favour partitioning of the lipidated protein. Thereby, it leads to an overall volume reduction, and formation of a compact proteo-lipid transition state.

Minor changes in the activation volumes for the different membrane systems were observed, and are expected to arise from the respective volume fluctuations in the lipid bilayer systems. The phase boundary regions in the raft-like membranes are associated with higher area and volume fluctuations;[259] hence a larger reduction in the free volume is expected upon

[257] Jenner, G. In *High pressure Chemistry, Biochemistry and Material Sciences*, Winter, R., and Jonas, J. **(1993)** Kluwer: Dordrecht, 345–366.
[258] Böttner, M., Ceh, D., Jacobs, U., and Winter, R. **(1994)**. High Pressure Volumteric Measurements on Phospholipid Bilayers. *Zeit. Phys. Chem. 184*, 205–218.
[259] Kupiainen, M., Falck, E., Ollila, S., Niemelä, P., Gurtovenko, AA., Hyvönen, AT., Patra, M., Karttunen M., and Vattulainen, I. **(2005)**. Free Volume Properties of Sphingomyelin, DMPC, DPPC, and PLPC Bilayers. J. *Comput. Theor. Nanosci. 2*, 401–413.

pressurisation. However, within the accuracy of the data, these subtle differences have been omitted, and it has been assumed that the transition state is alike in both the membrane systems.

One question that remains at this point is the following: What does the final state looks like? Does it closely resemble the transition state (i.e. encompassing a compact protein-membrane packing), or does the Ras G-domain interact with the bilayer causing membrane perturbation (e.g. via thinning and lateral expansion), leading to a gain in the overall volume. In order to answer the above questions, information about the volume change for the partitioning reaction was required. Thus, experiments were performed by pressurising the membrane-bound Ras protein up to 2 kbar (Fig. 7.7). The pressure was increased upon equilibration of the association step (i.e. at~ 2 h). Upon increasing the pressure, a few events could be anticipated: A decrease in the FRET signal would imply that the protein is squeezed out of the membrane, or in other words, high pressure destabilises the membrane-bound Ras. The (partial) membrane desorption of the N-Ras protein is expected to be mediated by its bulky farnesyl lipid anchor. This would be in line with previous reports on farnesylated peptides that exhibit a reduced affinity for and higher desorption rates from the l_o phase in heterogeneous membranes.[251,260] Increased ordering of the membrane under pressure would nonetheless stabilise the saturated (HD) lipid chain of Ras, but this stability may not translate to the unsaturated farnesyl moiety. On the other hand, the HVR—which is deeply located within the interfacial region of the lipid interface at ambient pressure[165]—might undergo a conformational change, thus pulling out the farnesyl group from the membrane. This possibility has been already suggested in a more general context[261] and demonstrates an interesting potential: The affinity of lipidated proteins for a particular membrane (e.g. ordered) could be modulated by factors that modify the local conformation of the lipidated sequences. In either case, this would correspond to a positive reaction volume ($\Delta V_R > 0$) for the association reaction, where the protein insertion perturbs the membrane, and thereby increases the overall volume of the system.

---

[260] Wang, T.Y., Leventis, R., and Silvius, J.R. **(2001)**. Partitioning of lipidated peptide sequences into liquid-ordered lipid domains in model and biological membranes. *Biochemistry 40*, 13031–13040.

[261] Mesquita, R.M., Melo, E., Thompson, T.E., and Vaz, W.L. **(2000)**. Partitioning of amphiphiles between coexisting ordered and disordered phases in two-phase lipid bilayer membranes. *Biophys. J. 78*, 3019–3025.

On the other hand, an increase in the FRET signal (as measured experimentally) denotes that the partitioning of Ras is fostered under pressure resulting in a negative reaction volume, and implies that the final proteo-lipid system is still compact *en route* the transition state.

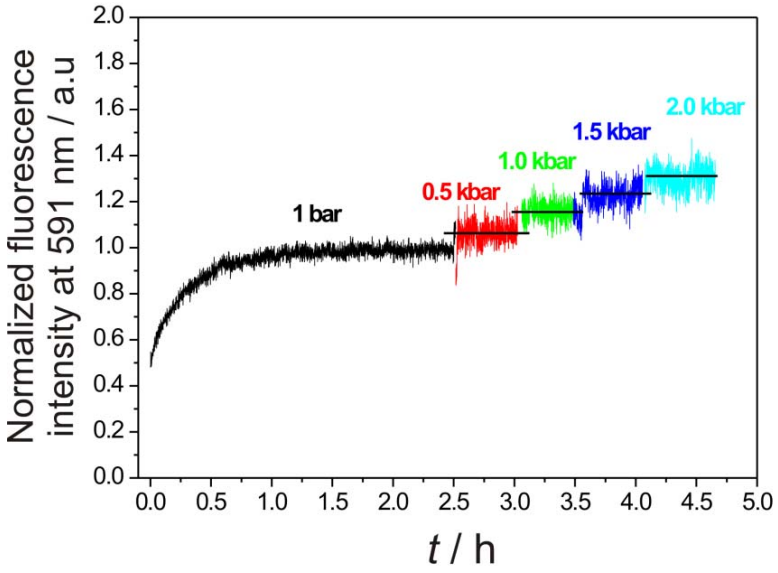

Figure 7.7: Pressure stability of membrane-bound N-Ras. Time-dependent changes in the normalised fluorescence intensity upon pressurisation of the membrane-bound protein. $c_{protein}$ = 0.35 µM, c_{BODIPY}= 0.125 µM; and $c_{vesicles}$ = 0.125 mM, $c_{N\text{-}Rh}$ = 0.25 µM The black curve represents the association step at 1 bar. After obtaining a stable baseline, pressure was increased and the measured data at each pressure were corrected for the background intensity from the pure BODIPY and *N*-Rh fluorophores, respectively. The pressure-induced increase in the signal intensity has been normalised to the maximum of the black curve (i.e. the plateau of the association curve).

An increase in the fluorescence intensity in Figure 7.7 can also, for instance, occur due to the decrease in the distance between the donor–acceptor pair, owing to the membrane's lateral compression. To ascertain this contribution, a simple calculation was attempted. From the cross sectional lipid chain area at 1 bar and 1 kbar, the ratio of the intermolecular distances between two lipids, given by R_p/R_1, was estimated to be 4.222 Å/4.478 Å = 0.94. Assuming the average distance between any labelled protein and lipid pair is roughly ~ 60 Å (giving an average E_{eff} of ~ 20 % at 1 bar), and that under high pressure this distance decreases by a factor of 0.94, an increase of E_{eff} at 1 kbar by roughly 23 % is obtained (being the maximum possible change). If the constant fluorescence signal at 1 bar is correlated to the $E_{eff,1bar}$ and

that at 2 kbar to $E_{\text{eff, 2 kbar}}$, an increase in $E_{\text{eff, 2 kbar}}$ by about ~ 27 % is obtained, as seen in Fig. 7.7. This demonstrates that the decreased distance contribution should not be neglected. Thus, the increase in the fluorescence intensity upon pressurisation of the membrane-bound Ras can have significant contributions from both, a decrease in the lateral distance (between the protein and the lipid), and an increased membrane partitioning. At the present stage, a clear cut distinction between the two contributions is difficult. However, as the partitioning coefficient of the lipidated protein in the vesicle is already rather large under ambient pressure conditions, the former contribution is more likely.

Nonetheless, the conclusions drawn from this section provide clues into the seemingly minor details in the volume fluctuations of lipid membranes, having a marked impact on the (pressure-modulated) Ras membrane association. The next section describes the pressure dependence of the dissociation step, which then also enabled the reaction volumes to be calculated, thus providing a clearer picture of the transition and a plausible final proteo-lipid state.

7.4.3 Intervesicle transfer of N-Ras under ambient and high pressure conditions: Time-resolved fluorescence spectroscopy results

Intervesicle transfer was performed by adding an eightfold excess of the unlabelled lipid vesicles (acceptor vesicles) of the same size and composition to the Ras-bound labelled vesicles (donor vesicles) once a stable baseline was reached in the association process. Such transfer experiments have already been shown as appropriate models to obtain kinetic details for the transfer of lipidated peptides.[251] A time-dependent decrease in the FRET signal resulted from the transfer of the BODIPY-labelled N-Ras from the donor to the acceptor vesicles. For the corresponding measurements under high pressure, there was a dead time of approximately five to eight minutes, due to the set-up and closure of the high pressure cell. To take into account the fluorescence intensity changes due to background scattering under pressure, control experiments were conducted with the same sample (but, without the protein) and the fluorescence change was found to be insignificant. The observed time-dependent fluorescence intensity at each pressure (F_{obs}) was corrected by subtracting the respective associated fluorescence signal from BODIPY-N-Ras (F_{b}), the cross excitation

intensity from *N*-Rh-PE labelled donor vesicles (F_a), and any from the unlabelled acceptor vesicles (F_u), using Eq. (17), to obtain F_{corr}:

$$F_{corr} = F_{obs} - F_b - F_a - F_u , \quad (17)$$

F_{corr} was analysed by curve-fitting to an equation of the form:

$$F_{corr} = A + B \exp(-k_{trans} \cdot t) \quad (18)$$

where k_{trans} is the apparent rate of the observed protein transfer from the donor to the acceptor vesicles. As the rate-limiting step for the intervesicle transfer process is the dissociation/desorption of the N-Ras protein from the donor vesicles, k_{trans} therefore represents the rate of dissociation (k_{diss}) of N-Ras from the lipid membrane.

7.4.3.1. Intervesicle transfer from the pure fluid (DOPC) membranes at ambient and under high pressures

Figure 7.8 shows the intervesicle transfer of the dually lipidated N-Ras protein from the fluid DOPC membranes as a function of pressure, and the associated k_{diss} (p) data are given in Table 7.3.

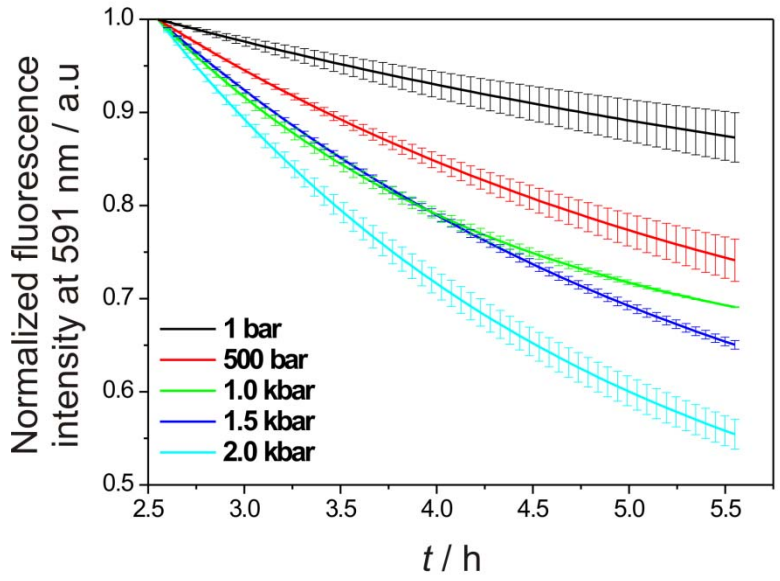

Figure 7.8: Intervesicle transfer of DOPC-bound dually lipidated N-Ras at various pressures. Time-dependent decrease in the normalised fluorescence intensity due to the loss of energy transfer from the BODIPY-N-Ras ($c_{protein}$ =0.35 µM, c_{BODIPY} = 0.125 µM) to the *N*-Rh labelled DOPC ($c_{vesicles}$ =0.125 mM, $c_{N\text{-}Rh}$ = 0.25 µM) upon addition of the unlabelled DOPC vesicles ($c_{vesicles}$ =1 mM). The measurements were carried out in a pressure range from 1 bar to 2.0 kbar and at 25 ˚C.

Table 7.3: Kinetic rate constants for the dissociation of the dually lipidated N-Ras from the pure fluid (DOPC) lipid membrane at different pressures. The effective association rate constants for the curves presented in Fig. 7.8 were obtained by use of Eq. (18). In the table, mean values ± standard deviation (n = 3-4) are given.

p / bar	k_{diss} / min^{-1}
1	$(3.20 \pm 0.36)\cdot 10^{-3}$
500	$(4.86 \pm 1.10)\cdot 10^{-3}$
1000	$(9.05 \pm 0.65)\cdot 10^{-3}$
1500	$(5.34 \pm 0.42)\cdot 10^{-3}$
2000	$(7.02 \pm 0.41)\cdot 10^{-3}$

The first-order dissociation rate constant at 1 bar corresponding to a half life ($t_{1/2}$) of approximately 3.6 h—as expected for a stably inserted dually lipidated protein—was obtained. Thus, the high binding stability imparted by a second lipid anchor slows down the

rate of spontaneous intermembrane transfer.[262] At 2 kbar, the protein showed a somewhat greater, but still very slow, dissociation rate with a $t_{1/2}$ of approx. 1.65 h. Previous studies probing the transfer rates of the N-Ras peptide sequence revealed a k_{diss} value of ~$3.7 \cdot 10^{-2}$ h^{-1}, with a corresponding half life of ~19 h.[262] The higher rate observed for the full length protein in this study may be, at least in part, attributed to a regain of configurational, translational, and rotational entropy upon transfer into the aqueous phase, which is lost when the lipidated protein is bound to the membrane. This effect has been predicted to increase the spontaneous intervesicle transfer rate of the full length lipidated proteins by typically five- to tenfold compared with the corresponding peptide alone. Surprisingly, the spontaneous intervesicle transfer for the peptide sequence corresponding to H-Ras C-terminal region *in vivo*, has a higher $t_{1/2}$ of ~ 2 h.[263]

These observations clearly suggest that the rate of intermembrane transfer of the full length Ras proteins occur over non-physiological time scales that raises important concerns. If the spontaneous desorption of lipidated protein is essential for its function, then some natural mechanisms must exist to counter the low transfer rates. As recently shown, one such determinant is the Ras acylation/deacylation cycle, which maintains the spatial localisation of the acylated Ras isoforms (such as, N- and H-Ras) on the different cellular membranes.[56] On the other hand, intracellular escort proteins (e.g. Calmodulin) that can extract specific membrane-bound Ras isoforms (e.g. K-Ras4B) have been elucidated. These escort proteins lower the activation energy of dissociation either by interacting with Ras itself or by modulating the Ras–membrane interactions, thus increasing the membrane desorption rates of Ras.[264] Such escort proteins—in contradiction to earlier perceptions—are also known for the dually lipidated G-proteins. For instance, Ytp1 is a doubly lipidated (GerGer) GTP-binding protein belonging to the small GTPases family of Rab proteins. It is known to be extracted from and subsequently delivered to the correct membrane compartment by its cognate GDI: yGDI E241A. Finally, rapid spontaneous membrane desorption rates for the

[262] Schroeder, H., Leventis, R., Rex, S., Schelhaas, M., Nagele, E., Waldmann, H., and Silvius, J.R. **(1997)**. S-acylation and plasma membrane targeting of the farnesylated carboxyl-terminal peptide of N-Ras in mammalian fibroblasts. *Biochemistry 36*, 13102–13109.
[263] Silvius, J.R., Bhagatji, P., Leventis, R., and Terrone, D. **(2006)**. K-ras4B and prenylated proteins lacking "second signals" associate dynamically with cellular membranes. *Mol. Biol. Cell 17*, 192–202.
[264] Sidhu, R.S., Clough, R.R., and Bhullar, R.P. **(2003)**. Ca2+/calmodulin binds and dissociates K-RasB from membrane. *Biochem. Biophys. Res. Commun. 304*, 655–660.

isoprenylated proteins[251] implicates that the protein–membrane interactions are relatively weak. Thus, these weak membrane interactions might embody substantial antagonization of the farnesyl lipid anchor's association with the membrane.

From Figure 7.8, it was concluded that the (spontaneous) intervesicle transfer rates of the full length N-Ras protein from the DOPC membranes increase upon pressurisation; this implies that the pressure-induced effects on the membrane and/or the protein serve as regulators for the protein–membrane interactions. The increased transfer rates were attributed to the nature of the membrane. The pure fluid DOPC membrane does not exhibit any phase transition to s_o or a gel-like phase in the pressure and temperature range covered. Thus, even at pressures of 2 kbar, the DOPC bilayer is still in a fluid phase, but with an overall higher order due to some pressure-induced acyl chain ordering. As a result of the chain ordering, probably no stable protein-membrane anchorage is achieved, and therefore the protein is still transferred. Notably, the pressure-induced lipid chain ordering was assumed to account for the higher membrane association rates of N-Ras, mainly mediated by the HD lipid anchor (outlined in Section 7.4.2.2), but the pressure dependence of the intervesicle transfer suggests that this effect is either mostly transient (but still rather slow) or that the protein dissociation is regulated by another mechanism. In this regard, a point to note is the relative orientation of the two N-Ras lipid anchors, which might be an important stability determinant for the membrane interaction. As such, no information is yet available to ascertain whether the membrane insertion of the Ras lipid anchors occurs in a concerted manner or not. However, from the studies presented in this section, it can be speculated that the saturated HD and the unsaturated Far lipid anchors serve as mutually exclusive sensors of the pressure-induced membrane ordering. Whereas the higher rates of association may be accounted for by the increased (though transient) stabilisation of the HD anchor within the ordered membrane, higher rates of dissociation may be controlled by the bulky Far anchor.

Using Eq. (15), the activation volume change for the dissociation step ($\Delta^{\ddagger}V_{diss}$) in the DOPC membrane was calculated to be -9.73 ± 0.67 cm^3 mol^{-1}. Combined with the $\Delta^{\ddagger}V_{ass}$ value for the association step, and simplistically assuming that the N-Ras–membrane interaction is a one-step process, a volume profile for this reaction could be obtained (Fig. 7.9). From this diagram, it can be stated—as initially predicted—that the final proteo-lipid system

rearranges, thereby increasing its volume *en route* from the transition state. One possible reason could be that the protein–membrane interaction modulates the interaction between the lipid acyl chains of the membrane and the Ras lipid anchors, i.e. the protein and its HVR interact and perturb the lipid bilayer, particularly in a clustered state, thereby inducing a lateral expansion and thinning (indentation) of the membrane.[261] A schematic view of such a hypothetical scenario is depicted in Fig. 7.9.

In conclusion, the increased rate of association and dissociation of the N-Ras proteins to and from the pure fluid DOPC membranes under higher pressure enables the protein to maintain the equilibrium even in the presence of an external mechanical stimulus, thus befittingly falling in the category of mechanosensor proteins.

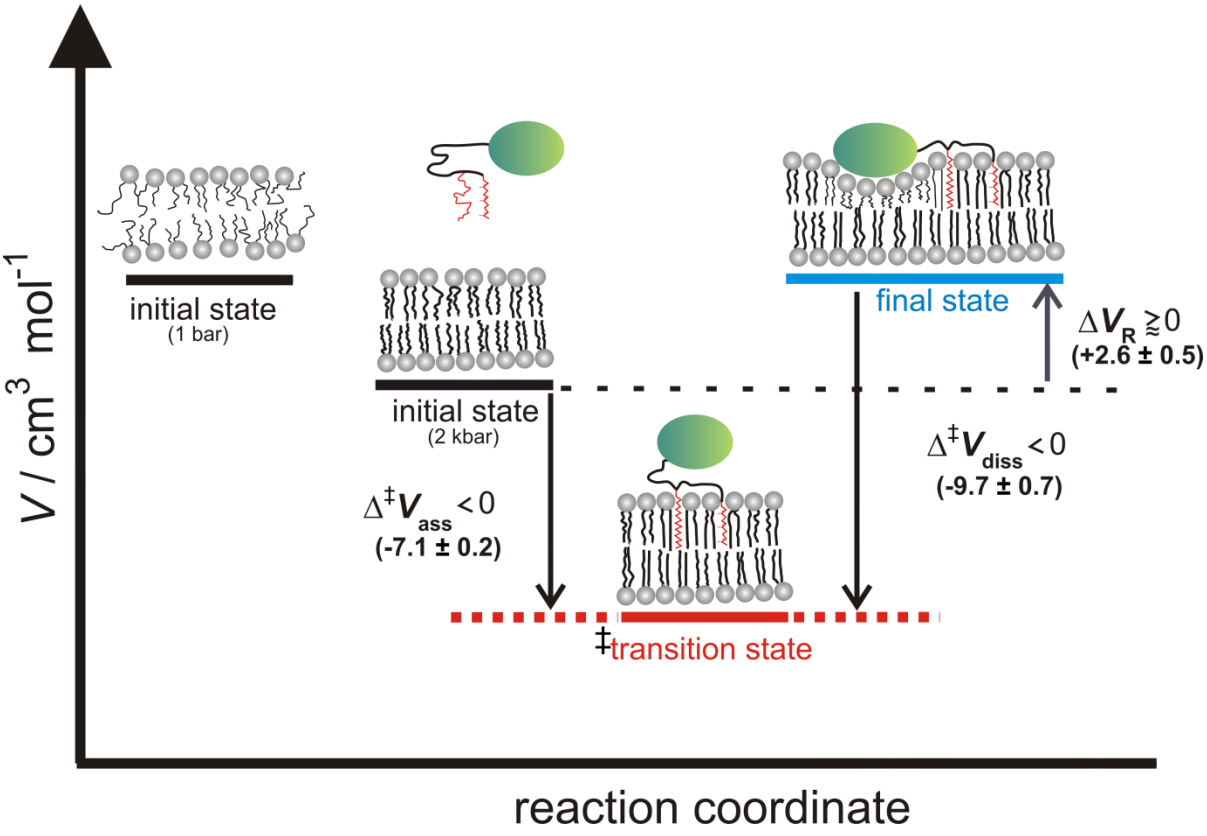

Figure 7.9: Volume profile for the interaction between dually lipidated N-Ras and a pure fluid (DOPC) membrane. The ordinate shows the relative changes in the volume of the proteo-lipid system and the abscissa delineates the reaction coordinate for the interaction/insertion process. Schematic representation of the structures of the initial states of the membrane at ambient and high pressures, the suggestive structure for the relatively compact transition state, and the relaxed final state of the Ras-DOPC interaction are depicted.

7.4.3.2. Inter-vesicle transfer from the neutral raft-like membranes at ambient and high pressures

Similar intervesicle studies were carried out with the neutral heterogeneous membrane system. These membranes can be envisioned as platforms of l_o domains dispersed in an l_d matrix of mostly the unsaturated lipids. The raft-like assemblies are more ordered and tightly packed, but they are still mobile, mainly due to lipid packing differences. This, in turn, is governed by the saturation level of the lipid chains in rafts, as compared with the unsaturated state of fatty acids in the l_d phase. Phase separation induced by rafts creates a unique compositional phase boundary or an interface, where the membrane properties change rather abruptly, and is bestowed with higher area and volume fluctuations. To Ras, such interface or domain boundaries represent the "hot spots", where the protein partitioning stabilises the interfaces. This translates to weaker repulsive interactions between the membrane domains. In addition, the still fluid character of these membranes enable them to rapidly respond to an incoming (mechanical) stimulus through the formation or dissipation of structurally and compositionally distinct lipid domains—which by virtue of the lipid's nearest neighbour contacts—allow the changes to be communicated and a cooperative response to follow. Can such a scenario reflect itself in modulating the membrane interaction of proteins, especially the peripheral proteins, under pressure? To this end, the present study aimed to examine how "tenaciously" the membrane composition or structural properties influence pressure effect on membrane dissociation of Ras.

In contrast to the pure fluid membranes, the spontaneous rate of N-Ras intervesicle transfer with neutral raft-like membranes decreased under pressure, by almost an order of magnitude (Fig. 7.10). The associated $k_{diss}(p)$ values are shown in Table 7.4.

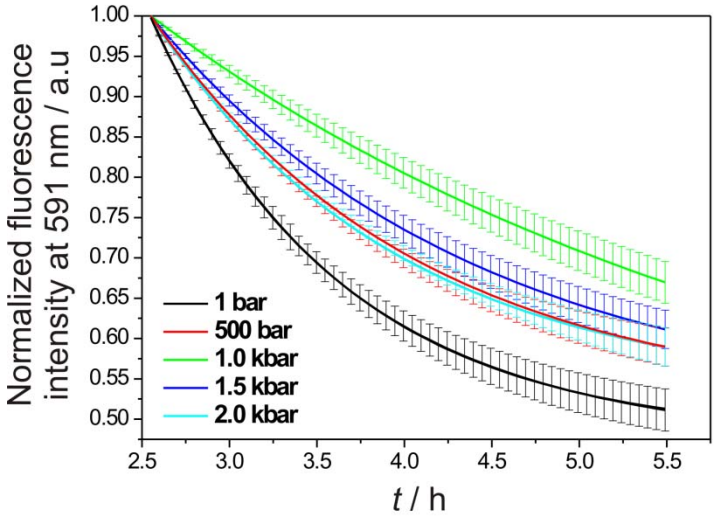

Figure 7.10: Intervesicle transfer of raft membrane-bound dually lipidated N-Ras at various pressures. Time-dependent decrease in the normalised fluorescence intensity due to the loss of energy transfer from the BODIPY-N-Ras ($c_{protein}$ =0.35 µM, c_{BODIPY} = 0.125 µM) to the *N*-Rh labelled neutral raft-like lipid vesicles ($c_{vesicles}$ =0.125 mM, $c_{N\text{-}Rh}$ = 0.25 µM) upon addition of the unlabelled raft-like vesicles ($c_{vesicles}$ =1 mM). The measurements were carried out in a pressure range from 1 bar to 2.0 kbar and at 25 ˚C.

Table 7.4: Kinetic rate constants for the dissociation of the dually lipidated N-Ras protein from the neutral raft-like lipid membrane at various pressures. The effective association rate constants for the curves presented in Fig. 7.11 were obtained by use of Eq. (18). In the table, mean values ± standard deviation (n = 3-4) are given.

***p* / bar**	**k_{diss} / min^{-1}**
1	$(1.54 \pm 0.11)\cdot10^{-2}$
500	$(1.18 \pm 0.14)\cdot10^{-2}$
1000	$(4.70 \pm 1.80)\cdot10^{-3}$
1500	$(8.97 \pm 0.36)\cdot10^{-3}$
2000	$(1.09 \pm 0.03)\cdot10^{-2}$

The first-order rate constant at 1 bar for the dissociation process from the raft-like membrane, corresponds to a half life ($t_{1/2}$) of approximately 1 h. The value is similar to that obtained at 2 kbar in the pure fluid DOPC membranes. This suggests that the pressure-induced ordering in the pure fluid DOPC membranes at approx. 2 kbar closely resembles the degree of ordering prevalent in the heterogeneous membranes under ambient pressure conditions. The

coexistence of l_o and l_d domains, with a certain percentage of saturated lipids and cholesterol also within the l_d phase, in heterogeneous membranes could account for a higher degree of order. The transfer rates upon pressurisation show the first signs of substantial change at about 1 kbar, which may be attributed to a phase-transition that occurs in this particular membrane composition. From the *p-T* phase diagram of this lipid membrane, a transformation from an l_d + l_o two-phase region to an l_d + l_o+ s_o three-phase region was observed. The s_o phase exhibits a gel-like or highly ordered (all-trans) acyl chain configuration, which is not likely to provide a suitable environment for the lipid anchors of Ras proteins. In fact, the phase sequence for preferential binding of the N-Ras protein in heterogeneous membranes was shown to be in the order of: $l_d > l_o >> s_o$. Thus, in the absence of any l_d phase, the protein shows a preference for partitioning into the l_o rather than the s_o phases.[265]

In the present case, a dominant pressure-induced effect is that of the steady reduction in the amount of l_d phase, in accordance with the Gibbs phase rule (outlined in Section. 7.1.2.1). As N-Ras would still prefer to partitions into these reduced l_d domains, which, by virtue of their small sizes (at high pressures), would drastically increase the local N-Ras concentration. As a result, a conformational or spatial constraint on the proteins might be imposed, which in turn, could ameliorate their clustering or reorganisation within the membrane plane. Hence, increased protein contacts might stabilise a particular N-Ras conformation that might confer a reduced dissociation rate under higher pressure, coupled with a higher activation volume required for membrane desorption in the clustered state.

This speculative suggestion for the reduced membrane desorption rates due to an increased stability of the Ras protein clusters, has indeed been experimentally observed for the K-Ras4B proteins *in vivo* (though qualitatively only and under ambient pressure conditions).[222,266] About 40 % of K-Ras proteins form nanoclusters (comprising ~ 9 protein molecules with a radius of about 9 nm), and the remaining 60 % diffuse as monomeric

[265] Nicolini, C., Baranski, J., Schlummer, S., Palomo, J., Lumbierres-Burgues, M., Kahms, M., Kuhlmann, J., Sanchez, S., Gratton, E., Waldmann, H., *et al.* **(2006a)**. Visualizing association of N-Ras in lipid microdomains: Influence of domain structure and interfacial adsorption. *J. Am. Chem. Soc. 128*, 192–201.
[266] Shalom-Feuerstein, R., Plowman, S.J., Rotblat, B., Ariotti, N., Tian, T., Hancock, J.F., and Kloog, Y. **(2008)**. K-ras nanoclustering is subverted by overexpression of the scaffold protein galectin-3. *Cancer Res. 68*, 6608–6616.

entities. Upon GTP loading, the protein exhibits decreased dissociation rates from the PM, which is further curtailed by interaction of the Ras nanoclusters with galectin-3 (β-galactoside binding protein) in a nucleotide-dependent manner. Galectin-3 constitutes a central and essential structural element in forming and stabilising the GTP-bound K-Ras nanoclusters at the PM. It decreases the K-Ras dissociation from the membranes. Furthermore, in the same study a mutated form of galectin-3 abrogated the clustering of K-Ras GTP, leading to the extraction (or dissociation) of K-Ras from the PM. Taken together, these data indicate that the activated K-Ras protein exhibits *decreased dissociation rates from the membrane*, when confined within (galectin-) stabilised *nanoclusters*. With the framework of such studies, it may be suggested that a similar scenario (i.e. a minor increase in the protein clustering) may occur for the dually lipidated N-Ras in the presence of the raft-like membranes (due to the presence of the phase boundaries). As such, high pressure would reduce the relative amount of l_d phase which may only further aggrandise Ras clustering, thereby (mostly likely) decreasing the dissociation rates.

Using Eq. (15), the activation volume for dissociation ($\Delta^{\ddagger}V_{diss}$) of the N-Ras protein from raft-like lipid membranes was calculated to be +4.3 ± 0.5 cm^3 mol^{-1}. Combining it with the activation volume of association ($\Delta^{\ddagger}V_{ass}$), a volume profile for its interaction with the heterogeneous membrane could be obtained, with a reaction volume of -20.9 ± 2.4 cm^3 mol^{-1} (Fig. 7.12). From this figure, it can be concluded that the final state of membrane-bound N-Ras exhibits an overall smaller volume compared to the initial state. This may arise due to the preferential insertion of the protein at the phase boundary of lipid domains, thus reducing the free volume of the system significantly. The volume is probably further reduced under higher pressures due to an increased clustering mediated by the decreasing amount of l_d phases. The schematic representation for such a scenario is depicted in Figure 7.11.

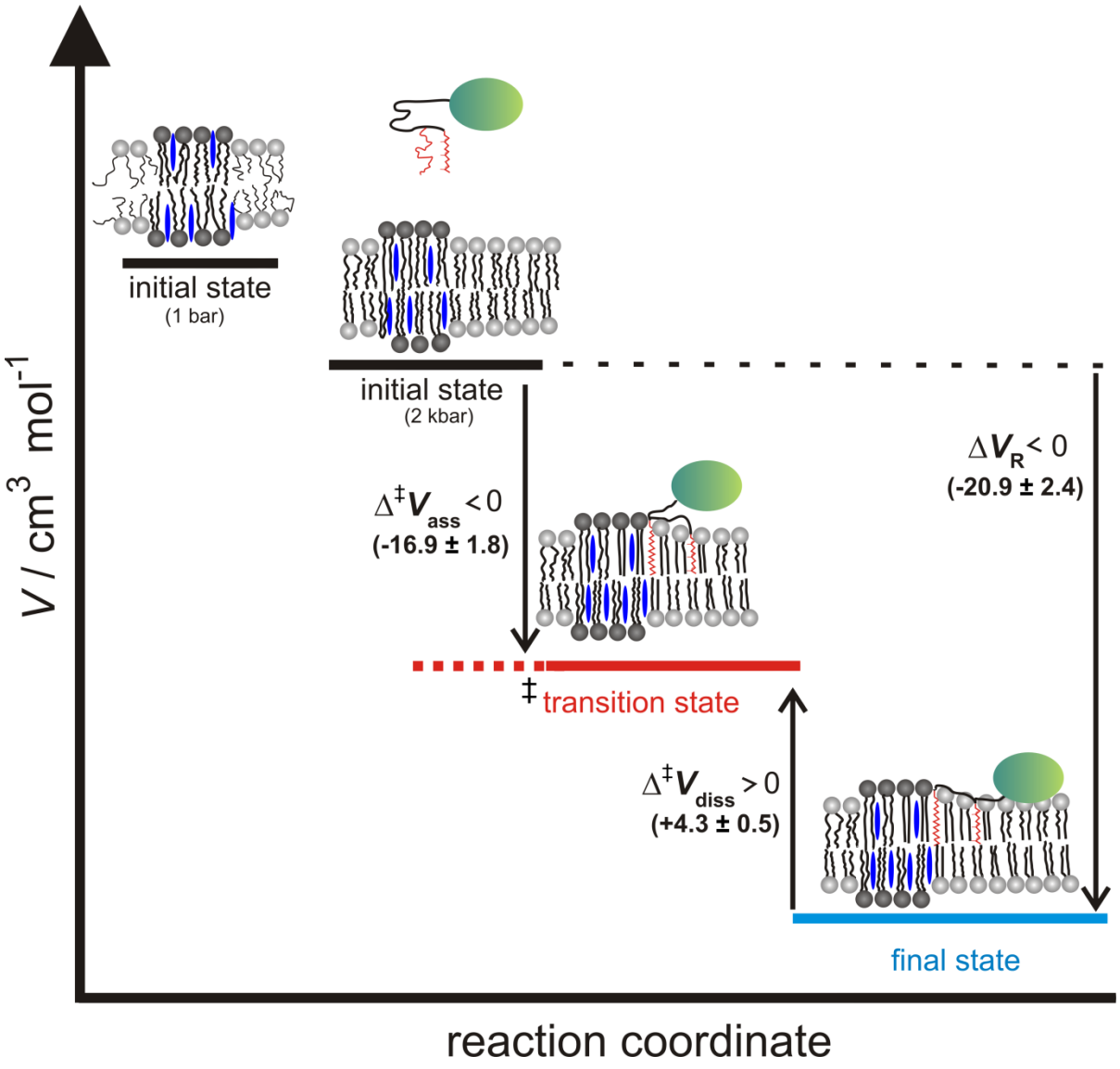

Figure 7.11: Volume profile for the interaction between dually lipidated N-Ras protein and a raft-like membrane. The ordinate shows the relative changes in the volume of the proteo-lipid system and the abscissa delineates the reaction coordinate for the interaction/insertion process. Schematic representations of the structures of the initial states of the raft-like membrane at ambient and high pressures, the suggestive structure for the relatively compact transition state, and the compact final state of the Ras-raft interaction are depicted.

Though the protein might still interact strongly with the phase-segregated membrane, it is an unlikely possibility that the interaction would produce a significant indentation of the outer-leaflet of the membrane (as depicted for pure DOPC N-Ras interaction, Fig. 7.9). This is due to a stable free energy minimum for membrane-bound N-Ras in heterogeneous membranes, in which partitioning at the domain boundary diminishes the repulsive forces between the

adjoining domains and stabilises them. Though this suggestion is quite innocuous, it nevertheless requires deeper investigation. At last, whatever the precise mechanism will be, the data presented in this section point towards pressure-induced changes in the membrane/protein as positive regulators of the N-Ras cluster formation. This could be further fined-tuned in the context of natural biological environments, by specific lipids or scaffolding proteins.

7.5 Summary and Outlook

Adaptation of proteins to external chemical and/or physical stimuli is of utmost importance in maintaining the cycle of life. Ras proteins attached to the PM frequently encounter mechanical stresses originating from extensive mesh-like structures of actin filaments (actin maintains the integrity and shape of biological membranes), hemodynamic flow and hydrostatic stresses. What criteria must the Ras protein fulfil to be able to respond to the different physical stimuli? Is is the sole fabric of the biological membrane that enables the Ras protein to achieve its selective functions under such conditions? Such questions have redefined the biophysics of Ras–membrane interactions, and are currently being investigated. The present study explored the effect of high hydrostatic pressure on the membrane association and dissociation of N-Ras proteins. Such studies inevitably help in understanding the effects of pressure perturbation on signalling events.

Using the FRET-based assay it was revealed that the Ras–membrane association is a two step process, where the first step includes an initial docking, reorientation and subsequent high affinity insertion of the protein into the membranes. The second step involves lateral-reorganisation of Ras proteins, eventually leading to cluster formation. In lipid membranes of different composition, only minor differences in the association rate constants were observed. High hydrostatic pressure fosters the association of membrane association of N-Ras proteins, independent of the lipid composition. Calculation of the activation volume for the association process revealed a highly compact transition state with reduced overall volume, dominated by the changes in free volume of the different lipid membranes. Higher ordering in the membrane's acyl chain region at high pressure dominates the association

process, possibly by an increased stabilisation of the saturated HD Ras anchor within the ordered membrane

Whereas the association step was only affected marginally by the lipid compositions, the dissociation process, both under ambient and high pressure conditions, showed a profound dependence. In the pure homogeneous fluid DOPC membranes, the dissociation rates of N-Ras protein increased upon pressurisation. The concomitant activation volume for this step revealed that the final proteo-lipid system rearranged, thus increasing its volume *en route* from the transition state to the final equilibrium structure. Thus, in pure homogenous membranes, the protein and its HVR interact and perturb the lipid bilayer, leading to lateral expansion and thinning of the lipid membrane eventually increasing the system's volume. Surprisingly, in heterogeneous lipid membranes, a retardation of the dissociation step was affirmed. The calculated activation volume for this step revealed the final proteo-lipid system to be even more compact than the transition state. This was accounted for by a stable free energy minimum for the heterogeneous membrane-bound N-Ras protein; partitioning at the domain boundary decreases the highline energy tension and diminishes the repulsive forces between the adjoining domains and stabilises them. In addition, high hydrostatic pressure was inferred as a positive regulator for N-Ras cluster formation, especially in heterogeneous membranes, contributing to the decreased dissociation rates. Future studies on pressure modulated Ras lateral organisation (e.g. via HHP fluorescence microscopy) could provide conclusive evidence for the pressure mediated Ras clustering in membranes. Furthermore, fast kinetic methods such as stopped-flow, under high pressure conditions, would furnish information on the intermolecular reaction rates (i.e. those governed by activation volumes), and in turn would enable studying the dynamic forces regulating clustering of lipidated proteins within membranes.

Finally, high pressure modulation studies of the association and dissociation process of N-Ras with different membrane systems avow that in addition to the hydrophobic mismatch, van der Waals attractive forces, lipid chain entropy, and packing of the lipid acyl chains against the protein's hydrophobic counterparts (i.e. lipid anchors), are critical and decisive factors in understanding Ras–membrane interactions. A further important conclusion that can be drawn from this study is the following: As the Ras proteins respond to external stimuli

they increase their membrane association rates, but the concomitant increases in dissociation rates was only observed for the pure fluid membranes. Thus, in pure fluid membranes, the equilibrium is mostly likely maintained. However, in case of the heterogeneous membrane, retardation in the dissociation rates, mediated by increased protein clustering, generates the need to restore the equilibrium. Extrapolating such a scenario towards physiological environments—especially deep sea conditions—implicates the need of, as yet, unidentified mechanisms. One plausible mechanism could be pressure-induced increased activity of trafficking-chaperons. In this regard, chaperones solubilising the doubly lipidated small GTPases are known to exist, but their role in N- and H-Ras biology remains unknown. In addition, interaction partners similar to galectins might exist, but with a reversed functional role, i.e. destabilising Ras clusters on the membranes, thereby increasing their dissociation rates. At last, the effect of high hydrostatic pressure on the activity of Acyl-Protein Thioesterase 1 (that catalyses the depalmitolyation of Ras proteins) should also be studied in the future, as a possible mechanism to restore equilibrium of Ras–membrane interactions under high pressure conditions. Intermembrane transfer experiments of the depalmitoylated N-Ras (i.e. farnesylated N-Ras) and the polycationic family of small GTPases such as K-Ras (containing eight lysines in its HVR) and RheB (containing two lysines in its peptide sequence) would allow the dominance of lipid anchor makeup and electrostatics in the protein–membrane interactions to be delineated, also under HHP conditions. Finally, pressure modulation of other Ras isoforms might reveal additional elements contributing to the isoform specificity in deep sea signalling.

VIII

SUMMARY AND FUTURE PERSPECTIVES

Ras GTPases sit near the top of the signalling pathways that regulate cell proliferation, differentiation, and apoptosis. These are *plasma membrane localised* molecular switches that function by shuttling between inactive GDP-bound and active GTP-bound forms. Two classes of regulatory proteins determine the life-time of these two binding states—guanine nucleotide exchange factors (GEFs) and GTPase activating proteins (GAPs). All cells harbour three Ras isoforms: H-Ras, K-Ras, and N-Ras; all three are encoded by distinct *ras genes*. Ras protein structures share a *common* catalytic G-domain fold, but each contains a *distinct* C-terminal region—the so-called hypervariable region (HVR). The HVR contains membrane targeting signals, such as a variable number of lipid anchors and/or a polybasic stretch of amino acids; these are both essential and sufficient for high membrane binding affinity. Detailed biophysical, biochemical, and biological investigations of Ras isoforms are urgent because of the high prevalence of Ras oncoproteins in many human cancer and tumour types. Therapeutic targeting of Ras oncoproteins has not yet been realised, largely due to their intricate complexities and those imparted by their interaction partners. In this respect, *lipid membranes* form the most abundant interaction partner for Ras proteins. The present study endeavours to gain a deeper understanding of Ras–membrane interactions using several different biophysical approaches.

Orientation flexibility of the G-domain at membranes contributes to the Ras isoform specificity

The Ras isoforms exhibit a high degree of sequence homology, but surprisingly are not functionally redundant. Even though they share a common spectrum of effectors and interaction partners, they still generate distinct signal outputs and diverse biological responses. One known contributor to the Ras isoform specificity is the HVR, targeting the different isoforms to distinct membrane microdomains that differ in their lipid and protein contents, eventually forming isoform-specific nanoclusters. Only recently has the following question gained substantial curiosity: If and how the conformational states of the G-domain affect Ras–membrane interactions. In this regard, the work presented has revealed that different sets of preferred G-domain orientations, bestowed with variable degrees of flexibility for the Ras isoforms, are modulated by the bound nucleotide state and the HVR upon membrane interaction. The results from infrared methods, namely, polarized ATR-FTIR and IRRAS together with IRRAS simulations, showed that the G-domain of N-Ras and

K-Ras orients itself with the majority of the α-helical secondary structure elements lying parallel to the interface of heterogeneous membranes. Specifically, for N-Ras it was revealed that the protein in the inactive GDP-bound form displays a weak interaction of its helical structures with the membrane, thus mediating the interaction mainly by its HVR. In the active GTP-bound form, the G-domain reorients itself and displays a relatively stronger interaction of its helical counterparts—helices α4 and α5—with the membrane. Contrariwise, K-Ras proteins show an opposite nucleotide-dependent behaviour. In the active state, a highly flexible conformation of the G-domain at the membrane was detected. In the inactive form, K-Ras shows a strong interaction with lipid membranes via its helical regions. Taken together, this study corroborates the already proposed idea that the Ras isoform specificity extends much beyond the hypervariable region to the highly conserved G-domain. Particular combinations of the nucleotide species and HVR are fine-tuned upon interaction with lipid membranes that lead to stabilising a defined orientation/conformation of the membrane-bound Ras proteins. Finally, combined with insights from the lateral membrane partitioning behaviour of Ras proteins, the data presented best fit to a molecular model as follows: Ras orientational dynamics is super-regulated via the constraints imposed by clustering of the Ras isoforms in the lipid bilayer plane and/or protein–protein interactions, further polishing the activity of proteins. The hypothesis derived from these simplistic model studies should be tested by exploring the orientational dynamics of Ras isoforms in macromolecular protein crowded membrane solutions, and finally progressing within the natural cell environments.

Lipid membranes modulate the conformational substates of Ras proteins

Proteins tend to harbour an intrinsic capability to coexist in a multitude of functional native and non-native higher energy conformations, preselecting suitable conformations for a particular biological event. This is now a well documented field of research, namely, protein conformational selection. A critical outlook points out that it is not always the most obvious *native* conformation of the protein, but rather a *non-native high energy* conformation that is primarily responsible for the biological function. Even in Ras, distinct chemical species in the nucleotide binding site—such as GTP, GDP, and GTP analogues—correlate with distinct global conformations. This enforces the idea that conformational selection is the predominant mechanism for regulation and functioning of Ras. The present work used pressure-

modulation in conjunction with FTIR and fluorescence spectroscopy to explore various conformational substates of the fully lipidated N-Ras protein. Pressure was chosen as the preferred perturbation tool because of its ability to populate low volume, high energy conformers in a reversible and mild fashion. Pressure perturbation shifts the conformational equilibrium from the native (probably crystallographic) state towards a more open and solvent-exposed high energy state in the bulk solution, for both the active and inactive N-Ras proteins. This non-native conformer most likely correlates to a functional state that interacts with GEFs by virtue of its enlarged solvated structure. Furthermore, the transition was facile in the inactive form due to the higher flexibility of its switch regions. The most important result of this study was the identification of the role of lipid membranes, which modulated the conformational selection by inducing a new substate. This is accompanied by significant structural reorientations of the G-domain at the lipid interface, particularly for the GTP-bound form of N-Ras. This new membrane-associated conformational substate is proposed to be a functional state that fosters interactions with other membrane-associated interaction partners. Future studies on the effect of pressure on membrane-bound Ras in the presence of its putative interaction partners will help in understanding the functional relevance of this new membrane-associated conformational substate.

Prenyl-binding protein and Ras-membrane interactions

Originally identified as a subunit of phosphodiesterase, PDEδ acts as a solubilisation factor for a large number of small GTPases including Ras. It shields the Ras hydrophobic lipid anchors from the cytosol, thereby facilitating their intracellular diffusion. In addition, PDEδ has been proposed to extract Ras proteins from the plasma membrane. The present work explored the interaction of farnesylated Ras isoforms (K-Ras and monofarnesylated N-Ras) with PDEδ in the presence of heterogeneous raft-like membranes of different compositions. The FRET and tryptophan-based findings revealed generic binding of PDEδ to Ras proteins, independent of nucleotide-loading and isoform specificity. No PDEδ mediated extraction of Ras (especially in case of K-Ras) was observed. Surprisingly, The FRET and IRRAS results showed that PDEδ itself interacts strongly with, but does not insert into membranes. A similar effect was also reported *in vivo* and suggests that this interaction should not exist without a defined biological function. Therefore, the PDEδ•Ras complex was preformed in

bulk solution and then exposed to heterogeneous membranes. This complex dissociates upon contact with the membrane, leading to stable membrane insertion of Ras proteins via their freed farnesyl anchor in both isoforms. Taken together, the results indicate an important role of lipids in modulating interactions of Ras with other interaction partners. A challenge now is to determine precisely how the lipid membrane regulates the biophysics of Ras-PDEδ binding. Future studies should include intervesicle transfer kinetic experiments using different Ras proteins and different membrane compositions in the presence and absence of PDEδ, in order to delineate the role of PDEδ as a diffusion facilitator. The crystal structures indicate that PDEδ spans at least two different conformations, each having a specific role in binding and releasing the bound prenylated protein. How this conformational dynamics is affected by lipid membranes is yet to be determined.

Biophysics of Ras membrane anchorage depends on the membrane composition and nature of the lipid anchors

High hydrostatic pressure (HHP) has been extensively used as a thermodynamic and kinetic tool to study structural and functional aspects of biological macromolecules. In the present work, this tool was employed to explore membrane-associated processes—specifically Ras–membrane association and dissociation—to underpin the associated kinetic and volumetric changes. The inherent low energy imparted by pressure may indicate crucial information regarding the type of forces involved or governing the protein–membrane interaction. FRET-based assays showed that Ras association with a lipid membrane proceeds in a two step process, where the first step is the initial docking, reorientation, and subsequent high affinity insertion of the protein into the membranes. The second step stems from a lateral reorganisation of Ras proteins, which eventually leads to cluster formation. The use of lipid membranes of different composition resulted in only minor differences in the association rate constants. High hydrostatic pressure conditions fostered the association of dually lipidated N-Ras protein to lipid membranes, independent of the lipid composition. Calculation of the activation volumes for the association process revealed a highly compact transition state with reduced overall volume, dominated by the changes in the free volume of the different lipid membranes. The dissociation process, both under ambient and high pressure conditions, displayed drastic differences depending on the lipid compositions. The dissociation rate of N-Ras is increased in pure homogeneous fluid membranes and the concomitant activation

volume for this step reveals a rearrangement of the final membrane-protein system that increases its volume *en route* to the transition state. Thus, in pure homogenous membranes, the protein and its HVR intuitively interact and perturb the lipid bilayer, leading to lateral expansion and thinning of the lipid membrane. In contrast, for heterogeneous raft-like lipid membranes, a retardation of the dissociation step was affirmed. The calculated activation volume for this step revealed that the final system is even more compact than the transition state. This could be explained by a stable free energy minimum for heterogeneous membrane-bound N-Ras, where partitioning at the domain boundary decrease the unfavourable line energy and diminishes the repulsive forces between the adjoining domains and stabilises them. In addition, high hydrostatic pressure was inferred as a positive regulator of N-Ras cluster formation, especially in the heterogeneous membranes. Future studies on pressure modulated Ras lateral organisation (e.g. by HHP fluorescence microscopy in combinations with FRET and FCS) could provide conclusive evidence for the pressure mediated Ras clustering in membranes. Furthermore, fast kinetic methods such as stopped-flow under high pressure conditions, would furnish information on the intermolecular reaction rates and would enable studying the dynamic forces regulating clustering of lipidated proteins within membranes. Taken together, this study provides evidence that the Ras lipid anchors serve as mutually exclusive sensors of the pressure-induced ordering in membranes. The stabilisation of the long saturated lipid anchor within the ordered membrane is reflected in higher association rates to the membranes, but higher rates of intervesicle transfer are controlled by the bulky unsaturated lipid anchor. In addition, the edifice of lipid membranes strongly regulates its interactions with Ras and probably other lipidated proteins by modulating the hydrophobic mismatch, van der Waals attractive forces, lipid chain entropy, and packing of the lipid chains against the protein's hydrophobic counterparts, i.e. the lipid anchors attached to the HVR. An important outlook that can be inferred from this study is the following: As the Ras proteins respond to an external mechanical stimulus, they increase their association rates, but the concomitant increase in dissociation rates is only observed for homogeneous membranes. Thus, the overall equilibrium is probably still maintained. However, in the case of heterogeneous membranes, retardation in the dissociation process, probably mediated by an increased protein clustering, generates the need to restore the equilibrium. Extrapolating these types of scenarios to physiological

environments requires identification of mechanisms and/or binding partners that would extract and solubilise Ras and release them from irreversible membrane binding, also under HHP conditions.

In conclusion, all of this work has demonstrated highly decisive and critical roles for lipid membranes in Ras protein biophysics, ranging from dictating Ras orientational flexibility, conformational dynamics, and mechanosensitivity, to modulating the interactions of Ras with other proteins.

VIII

ZUSAMMENFASSUNG UND AUSBLICK

Ras GTPasen sind ein zentrales Glied der Signaltransduktionswege, die sowohl die Zellproliferation als auch die Zelldifferenzierung und Apoptose regulieren. Diese in der Plasmamembran lokalisierten molekularen Schalter wechseln zwischen einer inaktiven GDP-gebundenen und aktiven GTP-gebundenen Form. Zwei Klassen von Regulatorproteinen bestimmen dabei die Lebenszeiten dieser beiden Zustände: die GTP-Austauschfaktoren (*engl.* guanine nucleotide exchange factors, GEFs) und die GTPase-aktivierenden Proteine (*engl.* GTPase-activating proteins, GAPs). Alle Zellen weisen drei Ras-Isoformen auf, die durch entsprechende Ras-Gene codiert werden: H-Ras, K-Ras und N-Ras. Die Struktur der Ras-Proteine umfasst ein universelles Faltungsmotiv für die katalytische G-Domäne und eine spezifische C-terminale Sequenz, die sogenannte hypervariable Region (*engl.* hypervariable region, HVR). Die HVR beinhaltet membrandirigierende Signalsequenzen, wie z. B. eine variable Anzahl von Lipidankern und/oder eine polybasische Aminosäuresequenz, die sowohl essentiell als auch ausreichend für eine hohe Membranbindungsaffinität sind. Die hohe Prävalenz onkogener Ras-Proteine in vielen humanen Krebs- und Tumorarten begründet die Dringlichkeit einer detaillierten biophysikalischen, biochemischen und biologischen Untersuchung der Ras-Isoformen. Ras-Onkoproteine sind bisher keine therapeutischen Angriffspunkte gewesen, was größtenteils auf ihre Komplexität und der ihrer Interaktionspartner zurückzuführen ist. In dieser Hinsicht bilden Lipidmembranen den am häufigsten vorkommenden Interaktionspartner für Ras-Proteine. Die vorliegende Studie strebt durch die Anwendung verschiedenster biophysikalischer Methoden ein tieferes Verständnis der Ras-Membranwechselwirkungen an.

Die Orientierungsflexibilität der G-Domäne an Membranen trägt zur Ras-Isoformspezifität bei

Die Ras-Isoformen weisen einen hohen Grad an Sequenzübereinstimmung auf, sind erstaunlicherweise aber nicht funktionell redundant. Obwohl sie ein gemeinsames Spektrum von Effektoren und Interaktionspartnern nutzen, generieren sie unterschiedliche Ausgangssignale und diverse biologische Reaktionen. Es ist bekannt, dass die HVR zur Ras-Isoformspezifität beiträgt indem sie die verschiedenen Isoformen zu unterschiedlichen Membranmikrodomänen dirigiert, die in der Lipid- und Proteinzusammensetzung variieren, wobei es schließlich zur Ausbildung isoformspezifischer Nanocluster kommt. Erst kürzlich

wurde folgende Frage mit einer erheblichen Aufmerksamkeit bedacht: Ob und wenn ja wie beeinflussen die Konformationszustände der G-Domäne die Ras-Membranwechselwirkung? Diesbezüglich konnte in der vorliegenden Arbeit gezeigt werden, dass unterschiedliche Verteilungen von bevorzugten G-Domänenorientierungen, die den Ras-Isoformen einen unterschiedlichen Grad an Flexibilität verleihen, durch den Zustand des gebundenen Nukleotids und die HVR bei der Membranwechselwirkung moduliert werden. Die Ergebnisse der infrarotspektroskopischen Methoden, d.h. der polarisierten ATR-FTIR- und IRRA-Spektroskopie in Kombination mit IRRAS-Simulierungen, zeigen, dass die G-Domäne von N-Ras und K-Ras sich an heterogenen Membranen mit dem Großteil der α-helikalen Sekundärstrukturelemente parallel zur Grenzfläche orientiert. Insbesondere für N-Ras konnte nachgewiesen werden, dass das Protein in der inaktiven GDP-gebundenen Form eine schwache Wechselwirkung seiner helikalen Strukturen mit der Membran besitzt, so dass die Interaktion im Wesentlichen durch die HVR vermittelt wird. Im aktiven GTP-gebundenen Zustand orientiert sich die G-Domäne um und weist eine vergleichsweise stärkere Interaktion ihrer helikalen Gegenstücke – Helices α4 und α5 – mit der Membran auf. Umgekehrt zeigten die K-Ras-Proteine ein gegensätzliches nukleotidabhängiges Verhalten. Im aktiven Zustand wurde eine hochflexible Konformation der G-Domäne an der Membran nachgewiesen. In der inaktiven Form wurde eine starke Interaktion des K-Ras mit Lipidmembranen über seine helikalen Bereiche gefunden. Zusammenfassend lässt sich feststellen, dass diese Arbeit die bereits vorgeschlagene Ansicht bestätigt, wonach sich die Ras-Isoformspezifität weit über die hypervariable Region hinaus bis zur hochkonservierten G-Domäne erstreckt. Bestimmte Kombinationen der Nukleotidart und HVR werden durch Wechselwirkungen mit Lipidmembranen feineingestellt, so dass eine definierte Orientierung/Konformation der Ras-Proteine stabilisiert wird. Abschließend zeigt die Verknüpfung der präsentierten Daten mit Erkenntnissen aus dem lateralen Verteilungsverhalten der Ras-Proteine in Membranen, dass die präsentierten Daten am besten wie folgt zu einem molekularen Modell passen: Die Ras-Orientierungsdynamik wird durch Einschränkungen reguliert, die durch Clusterbildung der Ras-Isoformen in der Lipiddoppelschichtebene und/oder Protein-Protein-Wechselwirkungen auferlegt werden, so dass ein weiteres Feintuning der Aktivität der Proteine erfolgt. Die sich von diesen vereinfachten Modellstudien ableitende Hypothese sollte durch die Erforschung der Orientierungsdynamik der Ras-Isoformen in einer makromolekularen,

proteinverdichteten Membranlösung getestet werden, sowie abschließend weiterführend in natürlichen zellulären Umgebungen.

Lipidmembranen modulieren die Konformationsunterzustände der Ras-Proteine

Proteine besitzen im Allgemeinen die intrinsische Fähigkeit zur Koexistenz in einer Vielzahl von funktionellen, nativen und nicht-nativen Konformationen höherer Energie, so dass eine Vorauswahl von geeigneten Konformationen für einen bestimmten biologischen Prozess erfolgen kann. Die Konformationsselektion von Proteinen ist mittlerweile ein gut dokumentiertes Forschungsgebiet. Eine kritische Betrachtung hebt hervor, dass nicht immer die naheliegende *native* Konformation des Proteins primär für die biologische Funktion verantwortlich ist, sondern eher auch *nicht-native Konformationen etwas höherer Energie*. Selbst bei Ras korrelieren bestimmte chemische Spezies in der Nukleotidbindungsstelle – wie z.B. GTP, GDP und GTP-Analoga – mit bestimmten globalen Konformationen. Dies stützt das Konzept, wonach konformationelle Selektion der vorherrschende Mechanismus für die Regulierung und Funktionsweise von Ras ist. In der vorliegenden Arbeit wurde Druckmodulation in Verbindung mit FT-IR- und Fluoreszenzspektroskopie verwendet, um verschiedene konformationelle Unterzustände des vollständig lipidierten N-Ras-Proteins zu untersuchen. Dabei wurde Druck als bevorzugter und milder Störfaktor gewählt, da er die Besetzung von Konformeren mit geringerem Volumen und höherer Energie in einer reversiblen Weise erlaubt. Sowohl für aktive als auch inaktive N-Ras-Proteine führt die Druckperturbation zu einer Verlagerung des konformationellen Gleichgewichts vom nativen (kristallographischen) Zustand zu einem offeneren und lösungsmittelexponierten, nicht-nativen Zustand etwas höherer Energie in der Volumenphase. Dieses nicht-native Konformer korreliert höchstwahrscheinlich mit einem funktionellen Zustand, der mit GEFs aufgrund seiner vergrößerten solvatisierten Struktur interagiert. Des Weiteren erfolgte der Übergang infolge der höheren Flexibilität der Switch-Regionen in der inaktiven Form schneller. Das wichtigste Ergebnis dieser Studie stellte die Identifikation der Rolle der Lipidmembranen dar, welche den Konformationsraum durch Population eines neuen Unterzustands (*engl.* substate) moduliert. Dies wird von einer signifikanten strukturellen Umorientierung der G-Domäne an der Lipidgrenzfläche begleitet, insbesondere im Fall der GTP-gebundenen Form von N-Ras. Es wird angenommen, dass dieser neue membranassoziierte

Konformationsunterzustand ein funktioneller Zustand ist, der die Interaktion mit anderen membranassoziierten Interaktionspartnern verstärkt. Zukünftige Studien zum Effekt des Drucks auf membrangebundenes Ras in Gegenwart seiner potentiellen Interaktionspartner werden die funktionelle Relevanz dieses neuen membranassoziierten Konformationsunterzustandes verstehen helfen.

Prenylbindende Proteine und Ras – Membranwechselwirkungen

Ursprünglich als eine Untereinheit der Phosphodiesterase identifiziert, fungiert PDEδ als Solubilisierungsfaktor für eine große Anzahl von kleinen GTPasen, einschließlich Ras. Es schirmt die hydrophoben Lipidanker des Ras vom Zytosol ab, wodurch die intrazelluläre Diffusion des Ras erleichtert wird. Des Weiteren wird angenommen, dass PDEδ Ras-Proteine aus der Plasmamembran extrahieren kann. Die vorliegende Arbeit untersuchte die Wechselwirkung farnesylierter Ras-Isoformen (K-Ras und monofarnesyliertes N-Ras) mit PDEδ in Anwesenheit heterogener Raft-ähnlicher Membranen unterschiedlicher Zusammensetzung. Die FRET- und Tryptophan-basierten Ergebnisse ließen eine allgemeine Bindung des PDEδ an Ras-Proteine unabhängig von der Nukleotidbeladung und Isoformspezifität erkennen. Dabei konnte keine PDEδ-vermittelte Extraktion von Ras beobachtet werden (insbesondere im Fall von K-Ras). Überraschenderweise zeigten die FRET- und IRRAS-Ergebnisse, dass PDEδ selbst stark mit Membranen interagiert, allerdings nicht in diese insertiert. Ein ähnlicher Effekt wurde auch *in vivo* berichtet und teleologische Überlegungen deuten darauf hin, dass diese Interaktion nicht ohne eine definierte biologische Funktion existieren sollte. Demzufolge wurde der PDEδ•Ras-Komplex in Bulklösung vorgebildet und dann heterogenen Membranen ausgesetzt. Dieser Komplex dissoziierte beim Kontakt mit der Membran, was bei beiden Isoformen zu einer stabilen Einlagerung der Ras-Proteine in die Membran über ihre freigesetzten Farnesylanker führte. Zusammenfassend lässt sich sagen, dass die Ergebnisse auf eine wichtige Rolle der Lipide hinsichtlich der Regulierung der Wechselwirkungen von Ras mit anderen Interaktionspartnern hindeuten. Eine Herausforderung besteht nun darin, genau zu bestimmen, wie die Lipidmembran die Bindung von Ras und PDEδ auf biophysikalischer Ebene reguliert. Zukünftige Studien sollten dabei kinetische, intervesikuläre Transferexperimente in An- und Abwesenheit von PDEδ unter Verwendung unterschiedlicher Ras-Proteine und Membranzusammensetzungen beinhalten,

um die Funktion von PDEδ als Diffusionsvermittler zu beschreiben. Die Kristallstrukturen deuten darauf hin, dass PDEδ mindestens zwei unterschiedliche Konformationen aufweist, wobei jeder eine spezifische Rolle bei der Bindung und Freisetzung des gebundenen prenylierten Proteins zukommt. Wie diese Konformationsdynamik durch Lipidmembranen beeinflusst wird, bleibt noch zu ermitteln.

Die Biophysik der Ras-Membranverankerung hängt von der Membranzusammensetzung und Art der Lipidanker ab

Hoher hydrostatischer Druck (*engl.* high hydrostatic pressure, HHP) wurde vielfach als thermodynamisches Werkzeug zum Studium struktureller und funktioneller Aspekte biologischer Makromoleküle eingesetzt. In der vorliegenden Arbeit wurde dieses Mittel zur Untersuchung membranassoziierter Prozesse eingesetzt – im Besonderen der Ras–Membranassoziation und -dissoziation, basierend auf einer Änderung kinetischer und volumetrischer Parameter. Die inhärente geringe Energie, die durch Druck zugeführt wird, kann auch wichtige Informationen bezüglich der Art der Kräfte, die für die Protein–Membranwechselwirkung verantwortlich sind, beeinflussen, . FRET-basierte Assays zeigten, dass die Assoziation von Ras mit einer Lipidmembran über einen zweistufigen Prozess erfolgt, wobei der erste Schritt die anfängliche Anbindung, Umorientierung und darauffolgende hochaffine Insertion des Proteins in die Membranen umfasst. Der zweite Schritt leitet sich von der lateralen Umorganisierung der Ras-Proteine ab, welche schließlich zur Clusterbildung führt. Die Verwendung von Lipidmembranen unterschiedlicher Zusammensetzung resultierte lediglich in geringfügigen Unterschieden in den Assoziationsgeschwindigkeitskonstanten. Hoher hydrostatischer Druck begünstigt die Assoziation des doppelt lipidierten N-Ras-Proteins mit Lipidmembranen, unabhängig von der Lipidzusammensetzung. Die Berechnung der Aktivierungsvolumina für den Prozess der Assoziation ergab einen hochkompakten Übergangszustand mit einem reduzierten Gesamtvolumen, der durch Änderungen im freien Volumen der unterschiedlichen Lipidmembranen hervorgerufen wurde. Der Dissoziationsprozess wies sowohl unter Umgebungs- als auch Hochdruckbedingungen drastische Unterschiede in Abhängigkeit der Lipidzusammensetzung auf. Die Dissoziationsgeschwindigkeit von N-Ras wurde in reinen homogenen, fluiden Membranen erhöht und das damit einhergehende Aktivierungsvolumen

dieses Schrittes ließ eine Änderung des endgültigen Membran-Protein-Systems erkennen, welche das Volumen *en route* zum Übergangszustand vergrößerte. Folglich interagieren das Protein und seine HVR effektiv mit der Lipiddoppelschicht und stören diese in reinen homogenen Membranen, was zu einer lateralen Expansion und Verkleinerung der Lipidschichtdicke führt. Im Gegensatz dazu wurde für heterogene Raft-ähnliche Lipidmembranen eine Verlangsamung des Dissoziationsschrittes bestätigt. Das für diesen Schritt berechnete Aktivierungsvolumen ergab, dass das gebildete Proteo-Lipid-System sogar kompakter als der Übergangszustand ist. Dies könnte mit einem stabilen Minimum der freien Energie für an heterogene Membranen gebundenes N-Ras erklärt werden, wobei die Verteilung an der Domänengrenze die abstoßenden Kräfte zwischen den benachbarten Domänen verringert und diese stabilisiert. Zudem erwies sich hoher hydrostatischer Druck insbesondere in den heterogenen Membranen als ein positiver Regulator der N-Ras-Clusterbildung. Zusammengefasst belegt diese Studie, dass der Lipidanker der Ras-Proteine als Sensor für druckinduzierte Ordnung in Lipidmembranen dient. Die Stabilisierung des gesättigten Lipidankers in der geordneten Membran spiegelt sich in höheren Assoziationsgeschwindigkeiten für Ras an Membranen wider; andererseits werden höhere Geschwindigkeiten des intervesikulären Transfers durch den sterisch anspruchsvollen, ungesättigten Lipidanker kontrolliert. Außerdem reguliert die Beschaffenheit der Lipid-membranen stark deren Interaktionen mit Ras und wahrscheinlich anderen lipidierten Proteinen aufgrund von Unterschieden in der hydrophoben Kettenlänge, der anziehenden van-der-Waals-Kräfte, der Entropie der Lipidketten sowie der Packung der Lipidketten gegen die hydrophoben Bereiche des Proteins, d.h. die an die HVR angegliederten Lipidanker. Eine wichtige aus dieser Arbeit hervorgehende Perspektive ist die Folgende: Indem die Ras-Proteine auf einen externen mechanischen Reiz ansprechen, erhöhen sie ihre Assoziationsgeschwindigkeiten; allerdings wird der damit einhergehende Anstieg der Dissoziationsgeschwindigkeiten nur für fluide Membranen beobachtet. Folglich ist das Gleichgewicht in reinen fluiden Membranen vermutlich noch aufrechterhalten. Im Fall der heterogenen Membranen dagegen ruft die durch die gesteigerte Proteinclusterbildung vermittelte Verlangsamung des Dissoziationsprozesses die Notwendigkeit zur Wiederherstellung des Gleichgewichts hervor. Die Extrapolation dieser Szenarien auf physiologische Membranen erfordert daher die Identifizierung der Mechanismen und/oder

Bindungspartner, die die Proteine extrahieren und solubilisieren, wodurch sie von einer irreversiblen Bindung an die Membran befreit werden.

Abschließend lässt sich sagen, dass die vorliegende Arbeit entscheidende Funktionen von Lipidmembranen in der Biophysik der Ras-Proteine aufzeigen konnte. Eine wichtige Rolle spielt die Induktion bevorzugter Orientierungen, die Konformationsdynamik und Mechanosensitivität sowie die Lipid-vermittelte Modulation der Wechselwirkungen von Ras mit anderen Proteinen.

IX

APPENDICES

9.1 Determination of the Secondary Structure Content of Proteins

The vibrational spectrum of a protein can be obtained from Raman scattering and/or infrared spectroscopy (used in this work). Absorption of the infrared light is plotted against the wavenumber, $\tilde{\nu} = 1/\lambda$ (in units of cm^{-1}). The horizontal coordinate of the spectrum runs from higher to lower wavenumber, in accordance with the IUPAC recommendation.[267] The infrared light is absorbed by a molecular vibration when the frequencies of light and the respective vibration coincide. Since the frequency of a vibration and the probability of absorption depend on the strength and polarity of the vibrating bond, they are strongly influenced by inter- and intramolecular environmental effects. As a direct consequence, the effect of environment (e.g. membranes) on the protein's vibrational frequencies is a telltale of how proteins interact with them. Proteins exhibit a vast number of vibrational bands (reviewed in ref. 268), among which the most prominent is the amide-I vibration. It spans a frequency range from 1700 to 1600 cm^{-1} and is dominated by the backbone C=O vibrations, which encodes for the secondary structure of a given protein. Given the diverse secondary structure components of a protein, absorbing at different positions in the amide-I region, the resultant observed amide-I band is broad and featureless (due to overlapping components bands). This precludes a direct evaluation of the secondary structures. To this end, two approaches are known to determine the secondary structure components and their respective contributions to the protein structure. The first is the band narrowing and curve-fitting method.[63] The second is based on using a calibration set of spectra from proteins with known structures, to perform a pattern-based recognition calculation, similar to that used in circular dichroism spectroscopy.[269-270] In this work the curve-fitting approach was employed to elucidate the secondary structural changes in the proteins Ras and PDEδ.

---

[267] Mills, I., Cvitas, T., Homann, K., Kallay, N., and Kuchitsu, K. **(1988)**. Quantities, Units and Symbols in Physical Chemistry, Blackwell Scientific publications, Oxford; Lamola, A.A. and Wrighton, M.S. **(1984)** Recommended standards for reporting photochemical data. *Pure Appl. Chem. 56*, 939–944.

[268] Barth, A. **(2007)**. Infrared spectroscopy of proteins. *Biochim. Biophys. Acta 1767*, 1073–1101.

[269] Baumruk, V., Pancoska, P., and Keiderling, T.A. **(1996)**. Predictions of secondary structure using statistical analyses of electronic and vibrational circular dichroism and Fourier transform infrared spectra of proteins in H_2O. *J. Mol. Biol. 259*, 774–791.

[270] Rahmelow, K., and Hubner, W. **(1996)**. Secondary structure determination of proteins in aqueous solution by infrared spectroscopy: a comparison of multivariate data analysis methods. *Anal. Biochem. 241*, 5–13.

9.1.1. Mathematical Procedures of Band Narrowing

Two independent mathematical procedures of band-narrowing were used to obtain the number of component bands and their positions: Second derivative[271] and Fourier self deconvolution (FSD)[272].

Fourier Derivatisation

In Fourier derivatisation, the Fourier transform $\mathscr{F}\{\}$, of the spectrum $A(v)$ given by $F(x)$ [$F(x)= \mathscr{F}\{ A(v)\}$], is multiplied by a function x^p and a smoothing function $S(x)$. An inverse Fourier transform then yields the derivative spectrum $D(v)$.

$$D(v) = \mathscr{F}\{ F(x) \bullet x^p \bullet S(x)\} \quad (1)$$

where, x is an independent variable with units of cm, and p is the order of the derivative (in this case 2). When p is an even integer, the output is congruent with the corresponding derivative of the input spectrum smoothed by $S(x)$. In practice, Fourier derivatisation is performed over the smoothed spectra to reduce noise amplification. The recommended smoothing filter is the Boxcar function,[273] however when the smoothing is done in combination with derivation, then the $Sinc^2$ filter is recommended[274]. The calculation of the second derivative of a spectrum, in the present work is based on the convolution technique described by Savistzky and Golay[275]. Briefly, a least squared linear regression fit of a polynomial of degree k (=6, in this case) over at least k+1 data points (15-17, in this case) around each point in the spectrum is applied to smoothen the data (analogous to $S(x)$). The derivative given by Eq. (1) is then the derivative of the fitted polynomial at each point. This calculation was performed using the GRAMS software, which in turn uses a matrix

[271] Cameron, D.G., and Moffatt, D.J. **(1987)**. A Generalized-Approach to Derivative Spectroscopy. *Appl. Spectrosc. 41*, 539–544.
[272] Kauppinen, J.K., Moffatt, D.J., Mantsch, H.H., and Cameron, D.G. **(1981)**. Fourier Self-Deconvolution - a Method for Resolving Intrinsically Overlapped Bands. *Appl. Spectrosc. 35*, 271–276.
[273] Kauppinen, J.K., Moffatt, D.J., Mantsch, H.H., and Cameron, D.G. **(1982)**. Smoothing of Spectral Data in the Fourier Domain. *Applied Optics 21*, 1866–1872.
[274] Moffatt, D.J., and Mantsch, H.H. **(1992)**. Fourier Resolution Enhancement of Infrared Spectral Data. *Methods Enzymol. 210*, 192–200.
[275] Savitzky, A., and Golay, M.J.E. **(1964)**. Smoothing + Differentiation of Data by Simplified Least Squares Procedures. *Anal. Chem.36*, 1627–1639.

formalism described by Steiner and Madden[276] to generate the Savitzky–Golay convolution coefficients. Since the line width of the second derivative of a band is smaller than that of the original band[271], it permits resolving the overlapping bands, where the minima in the second derivative spectrum denote the positions of the overlapping components (Fig 9.1).

Fourier Deconvolution

The positions of the overlapping bands obtained by the above method were further crosschecked by the Fourier Deconvolution approach. Though the concept of FSD was introduced much earlier, Kauppinen and co-workers were the first to apply this concept in context of infrared spectroscopy. It works on the principle of using a high pass FFT filter which synthetically narrows the effective trace bandwidth features without seriously distorting the spectrum, as described below.

Assuming the profile of each band in the infrared spectrum of a protein in the condensed phase as Lorentzian, the absorbance of the i^{th} band at a wavenumber ($\tilde{\nu}$) is given by Eq. (2):

$$A_i(\tilde{\nu}) = A_i^o \frac{\gamma_i^2}{\gamma_i^2 + (\tilde{\nu} - \tilde{\nu}_i^o)^2} \tag{2}$$

where, A_i^o is the maximum absorbance of the band, $\tilde{\nu}_i^o$ is the wavenumber for A_i^o and γ_i is the half-width at half-height (HWHH).

Similarly, a spectrum with *N* bands may be approximated by Eq. (3):

$$A(\tilde{\nu}) = \sum_{i=1}^{N} A_i^o \frac{\gamma_i^2}{\gamma_i^2 + (\tilde{\nu} - \tilde{\nu}_i^o)^2} \tag{3}$$

If in the spectral region between any two wavenumbers ($\tilde{\nu}_1$ and $\tilde{\nu}_2$), the number of bands (*N*) exceeds the spectral range divided by the average full width at half-height (FWHH) of each of the overlapping bands, then not all of these bands can be resolved (which is invariably met in most of the cases dealing with proteins).

[276] Steinier, J., Termonia, Y., and Deltour, J. **(1972)**. Smoothing and differentiation of data by simplified least square procedure. *Anal. Chem. 44*, 1906–1909.

$$N > \frac{\left|\tilde{\nu}_1 - \tilde{\nu}_2\right|}{2\sum_{i=1}^{n}\gamma_i} \tag{4}$$

According to Eq. (4), if the width of each component band is reduced, then the number of resolvable peaks would increase, and thereby informational content will be drastically improved. To this end, FSD provides by far the most superior means of resolution enhancement, whereby the values of γ_i for each component band may be reduced (as shown below). The underlying principle is the multiplication of the Fourier transform of the original spectrum (given by Eq. 5), by a line-shape-dependent function of the form —$\exp(2\pi\gamma' x)$— that increases with increasing distance from the centre peak.

The cosine Fourier transform of the original band (described by Eq. 2) is given by:[67]

$$F(x) = \int_0^\infty A_i(\tilde{\nu})\cos(2\pi\tilde{\nu}x)\partial\tilde{\nu} = 0.5A_i^o\gamma_i\cos(2\pi x\tilde{\nu}_i^o)\exp(-2\pi x\gamma_i) \tag{5}$$

where x is the spatial frequency or wavenumber (cm^{-1}).

The multiplication of $F(x)$ by the exponentially increasing term—$\exp(2\pi\gamma' x)$, yields a new function, $F'(x)$, described by Eq. (6):

$$F'(x) = F(x)\exp(2\pi\gamma' x) = 0.5A_i^o\gamma_i\cos(2\pi x\tilde{\nu}_i^o)\exp[-2\pi(\gamma_i - \gamma')x] \tag{6}$$

After back-transformation of $F'(x)$, the HWHH of each band is reduced to ($\gamma_i - \gamma'$) cm^{-1}.

As a direct consequence of these manipulations, those regions of the Fourier transform that encode for the fine structures in the original spectrum are weighed more strongly. After back-transformation into a spectrum, those components that change more strongly with wavenumber are amplified (i.e. the overlapping component bands appear to be sharper). Similar to the minima in the second derivative spectrum, the maxima of the Fourier self-deconvoluted spectrum give the positions of the overlapping components (Fig. 9.1). However, as this procedure increases the apparent noise in the data, counteraction by applying a low pass smoothing filter (i.e. apodisation function, either involving Bessel or

Boxcar) is required. These spectral processing procedures were performed using the GRAMS software, based on the method described by P.R. Grifiths and G. Pariente.[67]

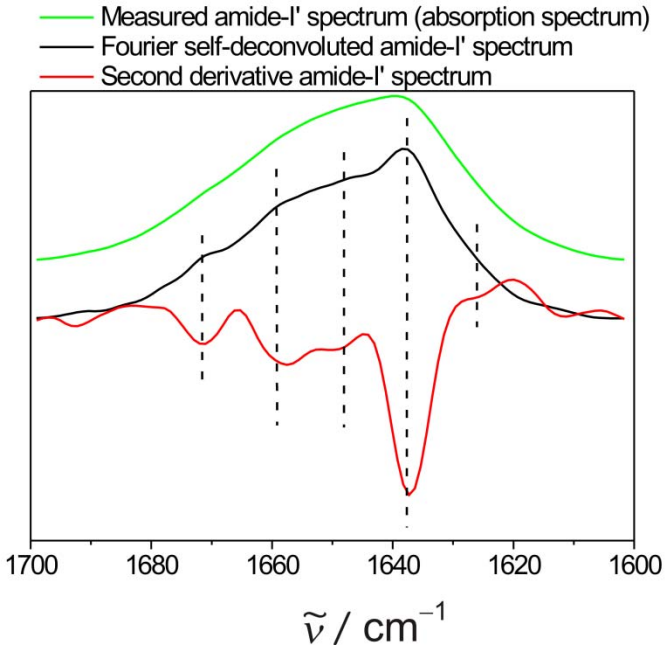

Figure 9.1: Narrowing of the amide-I' band of the Ras protein: The original absorption spectrum (green), spectrum after self-deconvolution (black), and the second derivate spectrum (red). The dashed lines show the most plausible number of components bands overlapping the original spectrum, which were assigned to different secondary structure according to Table 9.1.

Table 9.1: Assignment of the amide-I/I' band positions to the different secondary structure elements in proteins. The values in the table are based on experimental data and assignments of various authors, collected and evaluated by Goormagtigh et al. [277]

	Band position in H_2O/ cm^{-1}		Band position in D_2O/ cm^{-1}	
Secondary structure	Average	Extremes	Average	Extremes
α-helix	1654	1648-1657	1652	1642-1660
β-sheet	1633	1623-1641	1630	1615-1638
β-sheet	1684	1674-1695	1679	1672-1694
turns and loops	1672	1662-1686	1671	1653-1691
unordered/random coils	1654	1642-1657	1645	1639-1654

[277] Goormaghtigh, E., Cabiaux, V., and Ruysschaert, J.M. **(1994)**. Determination of soluble and membrane protein structure by Fourier transform infrared spectroscopy. I. Assignments and model compounds. *Subcell. Biochem. 23*, 329–362.

9.1.2. Curve-Fitting

Curve-fitting is a non-linear regression method for modelling experimental data to get the best agreement between the experimental data and the appropriate model. The least square solution is obtained by minimising the function:

$$\sum_{i=1}^{N}\left(y(\tilde{\nu}_i)-f(\tilde{\nu}_i;a)\right)^2 \tag{7}$$

where $y(\tilde{\nu}_i)$ is the experimental data, N is the number of experimental data, and $f(\tilde{\nu}_i;a)$ is the fitted data.

Different methods are available to minimise Eq. (7) with respect to a, for instance, Newton-Raphson, Gauss-Newton, the Steepest Descent, and Levenberg-Marquard method. The most commonly used method is the Levenberg-Marquard.[68] Briefly, it is an interactive method that starts with a set of some initial values for the peak parameters (such as peak numbers, heights, widths, and band shapes) and modifies them until the variation in the goodness of fit, χ^2 (also known as reduced chi-square), reaches a specified minimum. This implies that prior to performing a curve fit on a given Fourier spectrum, knowledge of some parameters (mentioned below) are required.

These are:

1. Number of peaks: These are obtained by performing band narrowing via derivatisation and deconvolution of the Fourier spectrum as discussed above.
2. Parametric band-shape: In vibrational spectroscopy of molecules in solution, the band shape is dominated by the T_2 relaxation (dephasing), giving approximately Voigtian band-shapes (given by Eq. (8).[278] Thus, the use of Voigtian bands is appropriate and recommended for curve-fitting, which in some cases may be substituted by Lorentzian or Gaussian bands.

[278] Oxtoby, D.W. **(1981)**. Vibrational-Relaxation in Liquids. *Annu. Rev. Phys. Chem. 32*, 77–101.

$$f(\tilde{\nu}) = \frac{2A\gamma_L}{\pi\left(\gamma_L^2 + (\tilde{\nu} - \tilde{\nu}_o)^2\right)} \otimes \frac{2\sqrt{\ln 2}}{\gamma_G^2\sqrt{\pi}} \times \exp\left(-\left(\frac{2\nu\sqrt{\ln 2}}{\gamma_G^2}\right)^2\right) \quad (8)$$

where, $\tilde{\nu}$ stands for the wavenumber; $\tilde{\nu}_o$ for the position of the band; γ_G, γ_L for the Gaussian and Lorentzian full-width at half-height respectively, and A for the area of the band; $\otimes$ stands for convolution. As many bands compose the original amide-I spectrum, Eq. (8) is expressed as a summation.

3. Initial guess about band parameters (i.e. the positions and widths of the overlapping bands in the original spectrum): The peak positions can be estimated by the band-narrowing method, while the widths or FWHH (both Gaussian and Lorentzian) of the bands can be obtained from the estimation of the average bandwidth of the band in the original spectrum as described elsewhere.[279] The range of FWHH used in this study was between 7-15 cm^{-1}. It is important to note here that these guesses do not affect the final results, as long as the curve-fit converges to the global minimum of Eq. (7).

These initial parameters were used to obtain the "best" fit of the sum of the calculated peaks/bands to that of the measured peak/band or the global minimum of Eq. (7). The curve-fitting was performed using the GRAMS software. In addition, the fitting was also performed by fixing some of the initial parameters (e.g. the peak position and/or widths). The final results presented in this work are an average of all the fits of a given spectrum, measured at least in triplicate.

Finally, to ascertain the goodness of the fit, a few statistical measures were considered. These are:

1. Reduced Chi Square

$$\chi^2 = \frac{\sum_{i=1}^{n}\left(y(\tilde{\nu}_i) - f(\tilde{\nu}_i; a)\right)^2}{\sigma_i^2} \Big/ \left(n - p\right) \quad (9)$$

[279] Saarinen, P.E., Kauppinen, J.K., and Partanen, J.O. **(1995)**. New Method for Spectral-Line Shape Fitting and Critique on the Voigt Line-Shape Model. *Appl. Spectrosc. 49*, 1438–1453.

where, n is the number of data points in the fitted region, p is total number of variable from all the peak functions, and σ_i^2 is the variance related to the measurement error. The variance was estimated by the Root Mean Squared noise (***RMSNoise***) in the measured data over the fitted region by the GRAMS software. This was done by performing a Savitzky–Golay smoothing on the measured spectrum trace using third-degree polynomial by the following equation:

$$RMSNoise = \frac{\sqrt{\sum_{i=1}^{n} (raw)^2 - (smoothed)^2}}{n} \tag{10}$$

2. The correlation (R^2) given by Eq. (11) is the ratio of the estimated variance of the fitted data over the estimated variance of the raw (measured) data. If the fitting function accurately predicts the means of the raw data distribution, then R^2 should be close to 1. In this study, the values of R^2 ranged between 0.992-0.998.

$$R^2 = \frac{\sum_{i=1}^{n} (fitted)^2 - (average)^2}{\sum_{i=1}^{n} (raw)^2 - (average)^2} \tag{11}$$

9. 2. Curve-Fitting Results for Ras and PDEδ

Figure 9.2 **A** and **B** show the curve-fit results for Ras and PDEδ, obtained by performing the steps outlined in section 9.1.

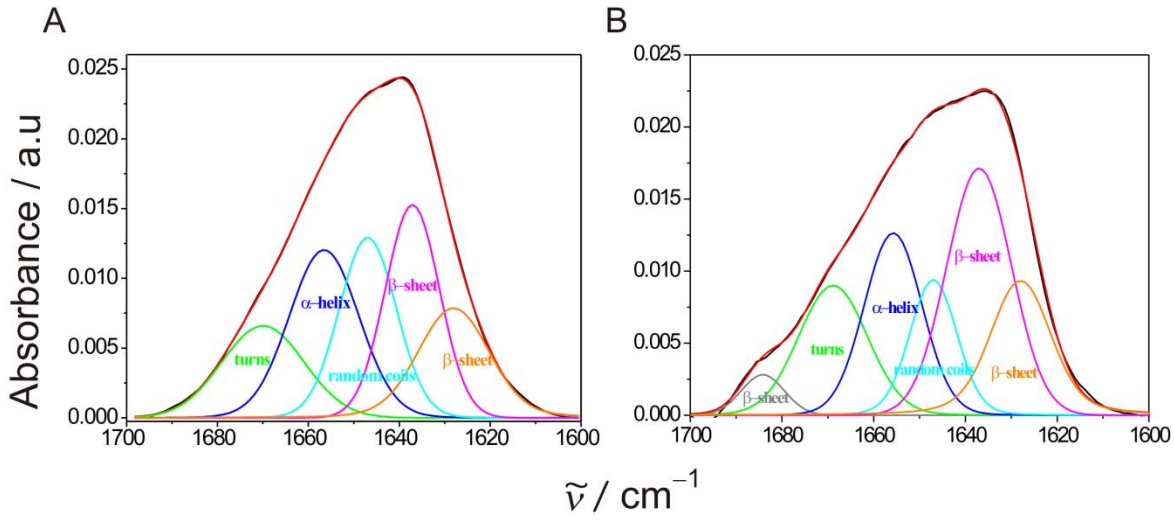

Figure 9.2: Infrared-based secondary structure analysis of proteins. Curve fitting results for (**A**) Ras and (**B**) PDEδ with the raw spectrum (measured data) in black, fitted spectrum in red, and the components bands assigned to the designated secondary structures, from Table 9.1.

The band integrals determined the fraction of the position-dependently assigned structure, regarding the overall amide integral (assuming similar transition dipole moments for the different conformers). The band positions were assigned to the secondary structures according to Table 9.1.

9. 3. IRRAS Spectral Simulations

The amide-I′ region of the IRRA spectra for p-polarized light was simulated according to ref. 92, with the modification that instead of using rough estimates for the orientations of the secondary structure elements relative to the air-water interface, the values were determined by the method described below.

The tilt angles of the α-helices (as defined in ref. 91) were derived by superimposing a reference helix (program "superpose", CCP4 suite),[93] and calculating the angle between the vector parallel to the long axis of the reference helix and the normal to the air-water interface (*z*-axis). For β-sheets, the orientation of the carbonyl bonds relative to the direction of the individual strands (as defined by a vector from the carbonyl C-atom to the carbonyl C-atom of the neighbouring residue) was used to indicate the orientation of the inter-chain hydrogen bonds and the transition dipole moment of the amide-I mode. The angle between the strand vector and the *z*-axis defines the tilt angle, Θ. The angle between the direction vector of a C=O bond and the cross product of the *z*-axis with the strand vector defines the twist angle, ψ. The values were calculated using a C program. All contributions of the secondary structure element sections to the respective amide-I bands were weighted by the number of contributing residues in the respective sections. These were then summed up for the spectral calculations using the Matlab implementation of the methods published by Mendelsohn et al.[86] and Flach et al.[87] and outlined in the section 2.2.3, of chapter 2. The simulations were performed using the protein crystal structure PDB entry 3CON, for the orientations described by the two models in ref. 155. Fig. 9.3 shows the simulated spectra for the N-Ras protein in its two nucleotide-bound states. Table 9.2 and 9.3 list the orientational coordinates (i.e. the tilt and twist angles, depicted in Fig. 2.6) for the α-helix and β-sheet structures in the proteins.

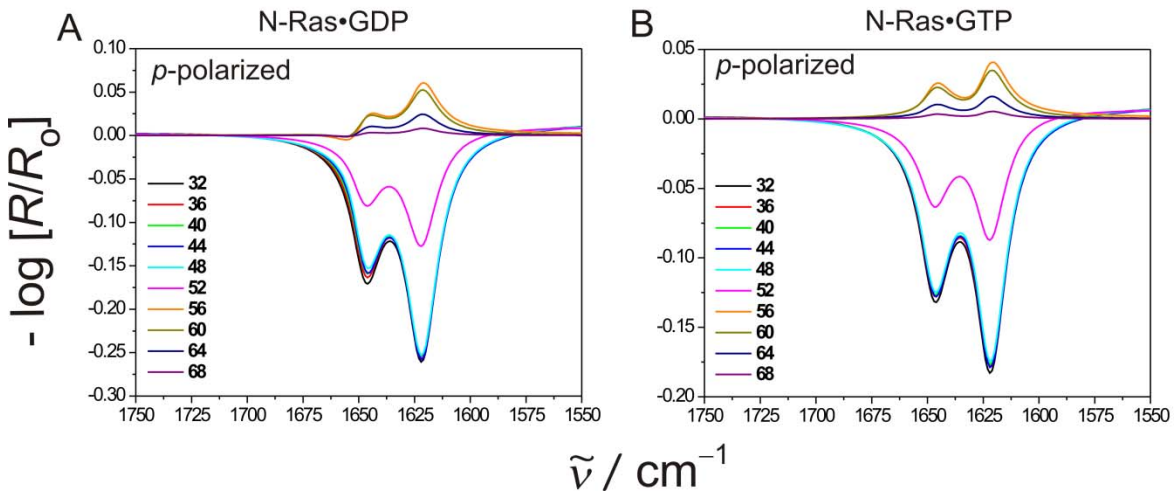

Figure 9.3: Simulated IRRA spectra for N-Ras in the two different nucleotide-bound states. Simulated IRRA spectra of the α-helical and β-sheet elements of the (**A**) GDP-bound N-Ras occupying the orientation denoted as model 1 and (**B**) GTP-bound N-Ras occupying the orientation denoted as model 2, relative to the normal of the air-D_2O interface. The calculations were performed for p-polarized light for different angles of incidence ranging from 32˚ - 68˚.

Table 9.2: Tilt angle Θ for the α-helices in the two different orientations

Secondary structure	Θ (model 1)	Θ (model 2)
α–1	12 x 38.9°	12 x 65.0°
α̃–3	20 x 55.3°	20 x 85.2°
α̃–4	13 x 59.0°	13 x 86.6°
α̃–5	17 x 59.2°	17 x 84.4°

Tilt-angle Θ for α-helices: α-1 (residues 15-26), α-3 (residues 86-105), α-4 (residues 126-138), α-5 (residues 151-167) of N-Ras (PDB entry 3CON) for model 1 and model 2, relative to the normal of the air-water interface. α-2 corresponds to the switch-II region and is disordered in this N-Ras structure. The twist-angle Ψ was set 45° for all the α-helical elements, due to an uniaxial distribution of the vibrational dipole moments in an α-helix around the helix-axis.

Table 9.2: Tilt angle Θ and twist angle Ψ for strands of β-sheets in the two different orientations

Secondary structure	Θ (model 1)	Ψ (model 1)	Θ (model 2)	Ψ (model 2)
β–1	3 x 18.1°	3 x 58.9°	3 x 57.2°	3 x 52.8°
	3 x 27.8°	3 x 45.4°	3 x 73.8°	3 x 41.5°
	2 x 47.8°	2 x 26.4°	2 x 88.4°	2 x 6.7°
β–2	2 x 25.3°	2 x 58.1°	2 x 53.4°	2 x 35.8°
	3 x 22.8°	3 x 57.7°	3 x 34.2°	3 x 55.8°
	3 x 64.9°	3 x 25.4°	3 x 24.4°	3 x 11.6°
β–3	3 x 25.4°	3 x 50.0°	3 x 28.2°	3 x 15.2°
	3 x 13.7°	3 x 35.5°	3 x 49.6°	3 x 53.8°
	2 x 12.2°	2 x 38.8°	2 x 50.1°	2 x 28.1°
β–4	3 x 40.2°	3 x 21.7°	3 x 83.9°	3 x 24.0°
	2 x 35.5°	2 x 54.1°	2 x 68.5°	2 x 17.8°
	2 x 59.1°	2 x 45.7°	2 x 77.9°	2 x 41.2°
β–5	3 x 51.0°	3 x 16.9°	3 x 89.2°	3 x 8.9°
	3 x 58.6°	3 x 29.9°	3 x 77.9°	3 x 15.4°
β–6	3 x 68.1°	3 x 33.9°	3 x 74.9°	3 x 12.6°

Tilt-angle Θ and twist-angle Ψ for six strands of β-sheets: β1 (residues 2-9), β2 (residues 38-45), β3 (residues 50-57), β4 (residues 77-83), β5 (residues 11-116), β6 (residues 141-143) of N-Ras (PDB entry 3CON) for model 1 and model 2, relative to the normal of the air-water interface.

9. 4. Pressure Dependence of BODIPY-FL and *N*-Rh-PE

High hydrostatic pressure marginally decreased and increased the fluorescence intensity of pure BODIPY-FL (Fig. 9.4 **A**) and *N*-Rh-PE labelled lipid vesicles (Fig. 9.4 **B**) in solution, respectively. The pressure was increased in steps of 250-500 bars and at each step the sample was allowed to equilibrate for 10 min, prior to recording the spectra.

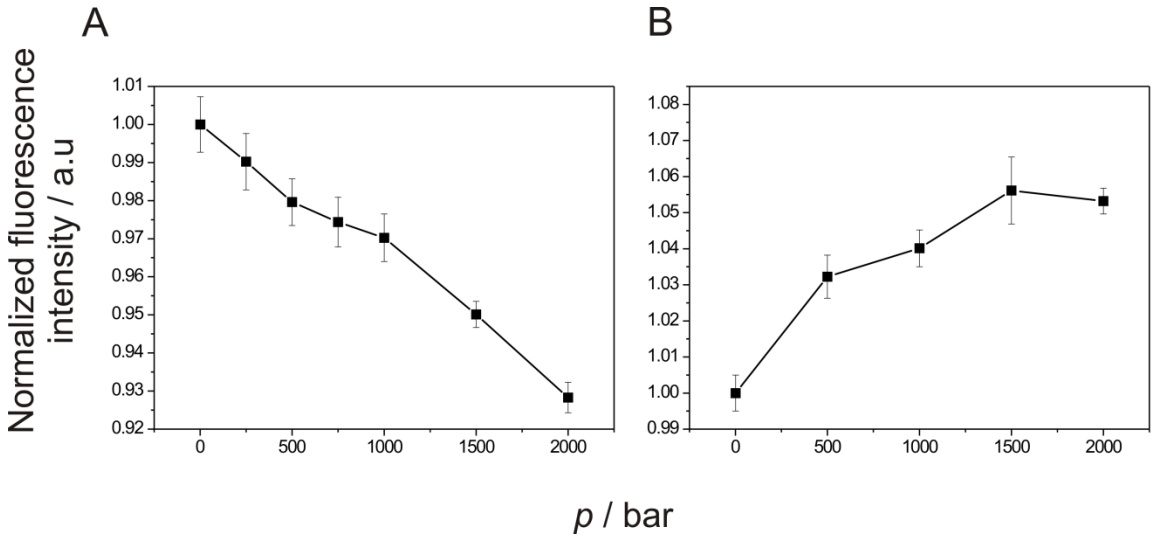

Figure 9.4*: *Pressure dependence of the fluorescence intensity of BODIPY-FL and N-Rh-PE fluorophores. Pressure induced changes on the fluorescence of (**A**) pure BODIPY-FL in solution (c_{BODIPY} = 0.125 µM, ex: 488 nm, em: 505 nm) and (**B**) on pure *N*-Rh labelled lipid vesicles (c_{lipids} = 0.125 mM, $c_{N\text{-}Rh}$ = 0.25 µM, ex: 568 nm, em: 591) at 25 ˚C.

The decrease in fluorescence intensity of BODIPY-FL was not accompanied by a significant change in the emission maximum (i.e. neither a blue nor a red shift upon increasing pressure). The decrease in this case can most appropriately be attributed to the increased non-specific interactions between water molecules and BODIPY. The water density increases with increasing pressure [for instance: at 5 kbar the water density is 15 % higher than at 1 bar][280], which could increase the frequency of collisions between water molecules and the fluorophores, resulting in a decreased fluorescence intensity (i.e. collision quenching). As the increase in the density of water at about 2 kbar is not very large [approximately 6 %], it substantiates the marginal decrease observed. Moreover, increasing pressure is also expected

[280] Burnham, C.W., Holloway, J.R., and Davis, N.F. **(1969)**. Specific Volume of Water in Range 1000 to 8900 Bars 20 Degrees to 900 Degrees C. *Am. J. Sci. 267*, 70–95.

to increase the solubility of O_2 in the medium, which itself is a well known fluorescence quencher. On the other hand, reasons for the increase in the fluorescence intensity of *N*-Rh-PE coupled with a minor red shift in the emission maxima with pressure are many fold. The foremost reason could be the movement of the fluorophore to more hydrophobic regions within the membrane, as also reported previously for other lipid-labelled fluorophores. However, this should result in a blue shift which was not observed experimentally, so was safely ruled out. The other reason could be related to changes in the Stokes shift of *N*-Rh-PE, caused by pressure-induced changes in the static dielectric constant and/or refractive index of the water medium, related to each other by Eq. (12).[281] It is well known that increasing pressures increases the dielectric constant (ε) of water [complied from data in literature which report a linear increase in ε by approximately 14 % in the pressure range of 1-3 kbar],[282-283] which in accordance with Eq. (12), should at least partially account for the increased Stokes shift (i.e. a red-shift of the emission relative to the absorption).

$$\tilde{\nu}_a - \tilde{\nu}_f = \frac{2\left(\mu^* - \mu\right)^2}{hca^3} \cdot \left[\frac{\varepsilon - 1}{2\varepsilon + 1} - \frac{n^2 - 1}{2n^2 + 1} \right] \qquad (12)$$

where, $\tilde{\nu}_a$ and $\tilde{\nu}_f$ are the absorption and emission wavenumbers in cm^{-1}, respectively; μ^* and μ are the dipole moments of the fluorophore in the excited and ground states, respectively; *h* is the Planck's constant, *c* is the speed of light, and *a* is the Onsager radius of the cavity within which the fluorophore resides. The red shift in the emission spectra of the fluorophores is usually accompanied by a decrease in the fluorescence intensity, but the opposite has also been reported.[284] When pressure promotes ionisation in the fluorophore, these charged species usually exhibit a higher quantum yield, thus producing an increase in the fluorescence intensity under pressure.[284] So far such effect has not been reported for *N*-Rhodamine, but seems like a plausible explanation. In either case, the changes in the

[281] Lippert, E. **(1957)**. Habilitationsschrift Zur Erlangung Der Lehrberichtigung (Venia Legendi) Fur Das Fach Physikalische Chemie Ander Techischen-Hochschule-Stuttgart - Spektroskopische Bestimmung Des Dipolmomentes Aromatischer Verbindungen Im Ersten Angeregten Singulettzustand. *Zeitschrift Fur Elektrochemie 61*, 962–975.
[282] Bridgman, P.W. **(1931)**. *The Physics of High Pressure*, G. Bell and Sons, London.
[283] Owen, B.B., Milner, C.E., Miller, R.C., and Cogan, H.L. **(1961)**. Dielectric Constant of Water as a Function of Temperature and Pressure. *J. Phys. Chem. 65*, 2065–2070.
[284] Ruan, K.C., Tian, S.M., Lange, R., and Balny, C. **(2000)**. Pressure effects on tryptophan and its derivatives. *Biochem. Biophys. Res. Comm. 269*, 681–686.

fluorescence intensity of pure fluorophores were minor compared with the change expected due to FRET, and were taken into account in the final data analysis.

9.5. Stability of the Lipid Monolayer Film at the Air-Water Interface

The heterogeneous or raft-like lipid monolayer comprising of neutral and anionic lipid mixtures, when spread at the air-water interface at approximately 30 mN m^{-1}, exhibited a stable surface-pressure over 20-22 h (Fig. 9.5 **A**). This indicates a high stability of the lipid film, suitable for studies with proteins, which (might) show spectral changes (related to the changes in conformation and/or orientations) spread out in time. Such control experiments enabled to unambiguously assign the changes in the surface pressure either due to protein insertion into the membrane, or an only slight perturbation due to protein adsorption at the membrane interface. Similarly, the IRRA spectra monitoring the lipid acyl chain vibration (Fig. 9.5 **B**) also displayed a constant intensity and wavenumber position, ruling out any disturbance to the integrity of the lipid film.

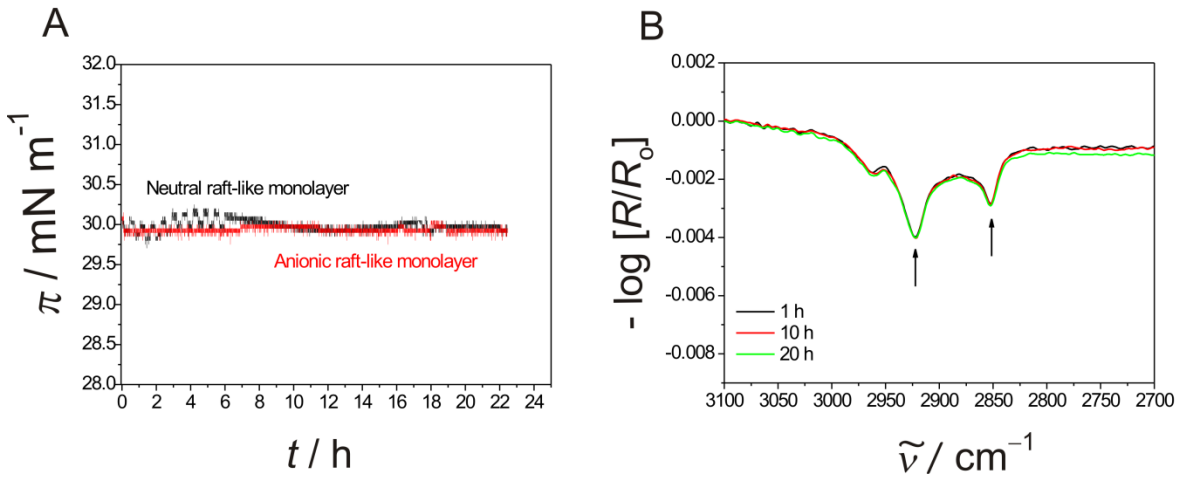

Figure 9.5: Long-term stability of the pure lipid monolayer film at the air-water interface. (**A**) Surface pressure profile of the anionic (DOPC:DOPCDPPC:DPPG:Chol 20:5:45:5:25 (molar ratio)) and the neutral (DOPC:DPPC:Chol 25:50:25 (molar ratio)) raft-like lipid monolayers, respectively. Films were spread at 30 mN m^{-1} at 20 ˚C and 1 bar. (**B**) IRRA spectra depicting the CH_2 asymmetric (at 2923 cm^{-1}) and symmetric (at 2853 cm^{-1}) vibrations of the lipid acyl chain region in the anionic lipid monolayer. IRRA spectra were acquired at 20 ˚C, 1 bar and with p-polarized light at an angle of incidence of 35˚.

9. 6. Measurement of the Surface Pressure in Langmuir Films

The surface pressure of monolayer films in a typical IRRAS set up was measured by a Wilhelmy plate, attached to an electro-balance. Surface pressure refers to a change in the surface tension, given by Eq. (13):[285]

$$\pi = \gamma^{o} - \gamma \tag{13}$$

where, γ^{o} is the surface tension of the pure air-water interface; surface tension (pressure) is expressed in SI units of mN m^{-1}.

The surface tension was measured using a Wilhelmy plate (a thin filter paper in the present case). The vertically oriented plate makes contact with the water surface, such that water wets the plate surface upwards, thereby creating a meniscus. The surface area of water is expanded and surface tension tends to contract the surface area as a counteraction, and pushes the plate downwards (Fig. 9.6). The force that brings the plate downwards (in the presence of lipids and proteins) is used to calculate the surface tension using the Wilhelmy equation, given by Eq. (14):

$$\gamma = \frac{F}{(2w + 2d).\cos\theta} \tag{14}$$

where, w, d and θ stand for the plate's width, thickness and contact angle to the water surface, respectively (Fig. 9.6). Prior to each measurement, the plate was submerged in the subphase to ensure complete wetting, thus approximating the contact angle to zero.

[285] Barrow, R.E. and Hills, B.A. **(1979)**. A critical assessment of the Wilhelmy method in studying lung surfactants. *J. Physiol. 295*, 217–227.

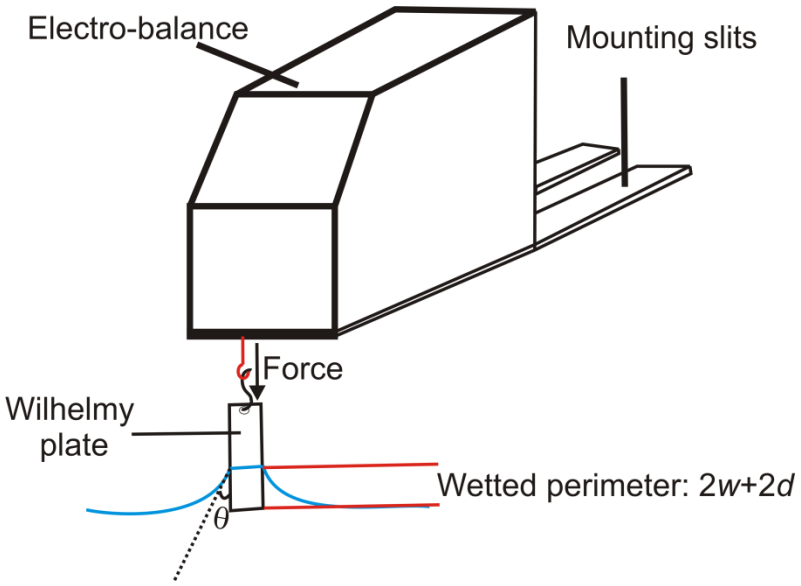

Figure 9.6: Schematic representation of the pressure sensing unit in the IRRAS setup. The Wilhelmy plate is connected to the electro-balance that transforms the force on the plate into a voltage, proportional to the surface tension of the interface. Symbols are explained in the text.

The electro-balance connected to the Wilhelmy plate via a thin wire, transforms the force acted upon the plate into a voltage that is proportional to the surface pressure. This voltage is used for the data recording and subsequently for automatic pressure controls, where needed. The working principle of the electro-balance is based on measuring the force necessary to maintain the Wilhelmy plate at a constant height. The force measured on the plate depends on its weight (constant), buoyancy (due to immersion of the plate into the subphase) and width (that is proportional to the surface tension component by Eq. (14)). As the buoyancy differs for every experimental condition, the electro-balance had to be adjusted prior to each measurement by the inbuilt potentiometers.

9.7. Ongoing project: Stopped-Flow Analysis of Ras–Membrane Interactions

Introduction

A comprehensive description of protein–membrane interactions is an essential step in the understanding of signalling from small GTPases in general, and Ras in specific. Modifications of Ras protein with covalently attached lipid moieties and polybasic regions are fundamental in their proper subcellular (membraneous) localisation, thereby regulating inter-/intra-protein interactions and hence their functions. Heterogeneity of the plasma membrane has attracted immense interest due to their principal role in mediating protein sorting and signalling specificity. Thus, proteins have evolved to recognise the diverse membrane morphologies to develop their specific functions, which often involve the interplay between lipids and proteins. There is abundant evidence for spatial reorganisation and dynamic clustering of lipid anchored proteins (e.g. Ras) in cellular (highly complex) membranes.[286-287] Thus, membrane-mediated reorganisation of lipidated proteins (e.g. Ras), at least in part, is expected to ameliorate protein clustering which in turn allows for highly precise coding of time-dependent inputs termed as high fidelity signalling.[288] Moreover, Ras signalling platforms have been demonstrated to be isoform-specific which supports the notion of differential lateral organisation/clustering properties of all the three Ras isoforms in their respective signalling platforms.[170,289] In this regard, explicit roles of the Ras lipid anchor makeup (which define the isoforms, *per se*) and the host membrane composition remain little understood.

In the present work, a FRET-based, time-resolved analysis of Ras–membrane interactions has been been attempted to provide detailed kinetic insights into the membrane association

[286] Murakoshi, H., Fujiwara, T., Akihiko, K., Takahiro, O., Chika I, et al. **(2004)**. Single molecule imaging analysis of Ras activation in living cells. *Proc. Natl. Acad. Sci. USA. 101*, 7317–7322.
[287] Hancock, J.F., and Parton, R.G. **(2005)**. Ras plasma membrane signalling platforms. *Biochem. J. 389*, 1–11.
[288] Harding, A.S., and Hancock, J.F. **(2008)**. Using plasma membrane nanoclusters to build better signaling circuits. *Trends Cell. Biol. 18*, 364–371.
[289] Plowman, S.J., Muncke, C., Parton, R.G., and Hancock, J.F. **(2005)**. H-ras, K-ras, and inner plasma membrane raft proteins operate in nanoclusters with differential dependence on the actin cytoskeleton. *Proc. Natl. Acad. Sci. USA. 102*, 15500–15505.

and dissociation processes. For this study, N-Ras proteins with different kinds of lipid anchor motifs, i.e. farnesyl and hexadecyl (a stable palmitoyl analogue) were used. In addition, different membrane compositions enabled to address the role of lipid domains (e.g. rafts-like structures) in mediating protein–membrane interactions.

RESULTS AND DISCUSSIONS

Biphasic membrane association of lipidated N-Ras proteins

The association of dually- or monolipidated N-Ras proteins was studied using a fluorescence-based stopped-flow assay. The proteins were labelled with the BODIPY fluorophore at their N-terminus, and the unilamellar model membranes, composed of either DOPC or DOPC/DPPC/Chol, were incorporated symmetrically with 0.2 mole % *N*-Rh-PE. The spatial information of N-Ras to membranes was obtained by FRET from BODIPY to *N*-Rh-PE, allowing the emission to be observed at 591 nm (i.e. the em_{max} of *N*-Rh-PE). The change in the fluorescence intensity upon Ras–membrane binding was in the range of 3-16 %. The membrane association was found to be a biphasic process, both for the monolipidated (N-Ras Far) and the dually lipidated (N-Ras HD/Far) protein, independent of the membrane composition. The time-course of the process (Fig. 9.7) could be described by a bi-exponential function (given by Eq. (13) of Ch.7)

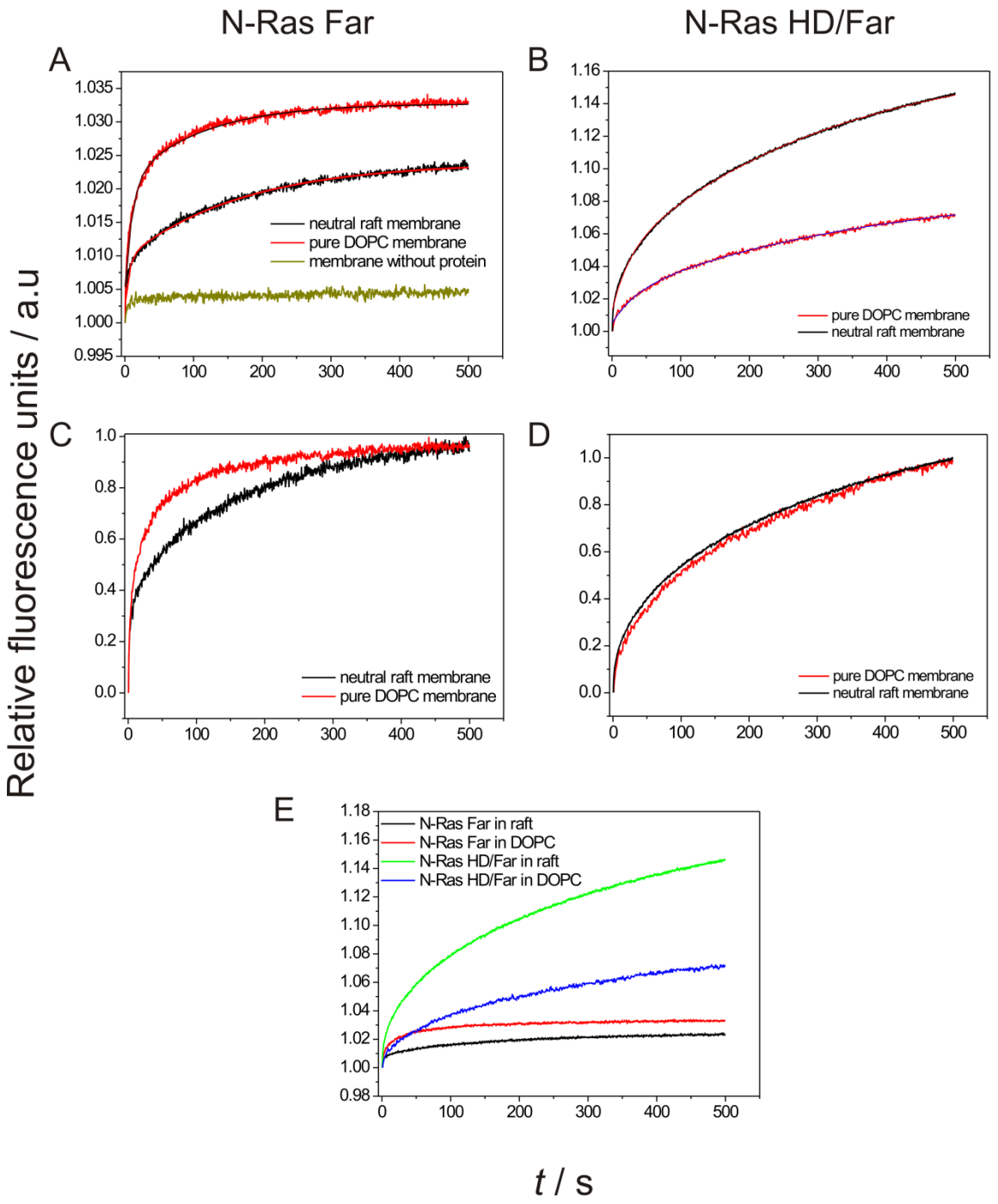

Figure 9.7: Ras association to membranes is a biphasic process. Representative association curves of (**A**) monofarnesylated and (**B**) dually lipidated N-Ras to the membranes of different composition, at 1 bar and 25 ˚C. (**C**) and (**D**) represent curves after normalisation of the ordinate in Figs. 9.7 **A** and **B**, respectively. (E) depicts the affect of the second lipid anchor on the membrane binding process. $c_{protein}$ = 0.35 µM, c_{BODIPY} = 0.125 µM, $c_{vesicles}$= 0.125 mM, and $c_{N\text{-}Rh\text{-}PE}$ = 0.25 µM. The curves in (A, B) have been fitted to a bi-exponential function, given by Eq. (13) of Ch.7.

For the monolipdated Ras protein, i.e. N-Ras Far, the fast association process showed an observed rate (k_1) almost ten times higher than that of the slower process (k_2) in the pure fluid DOPC membrane, whereas in heterogeneous membranes, it was almost thirty times higher (Table 9.4). The second process contributed approximately ~ 40 % and 60% of the observed FRET signal in DOPC and in raft-like membranes, respectively. For the dually lipidated Ras protein, i.e. N-Ras HD Far, in both membrane systems, the fast association process displayed an observed rate constant (k_1) almost ten times higher than that of the slow process (k_2). The second process contributed approximately 80 % of the observed FRET signal in both cases and dominated the association process (Table 9.4). No major changes were observed in the association kinetics for the first step in different membrane systems, implying that the insertion in heterogeneous membranes occurs preferentially into the fluid (l_d) domains, in accord with previous reports.[290]

Table 9.4: Kinetic rate constants for the membrane association of N-Ras at 1 bar. The observed apparent rate constants for the curves presented in Fig. 9.7 by use of Eq. (13) of Ch. 7. In the table, mean values ± standard deviations are given.

Membrane composition	*Obs.* k_1 (s^{-1})	*Obs.* k_2 (s^{-1})	A_1	A_2
		N-Ras Far		
DOPC	0.10 ± 0.003	$9.2 \times 10^{-3} \pm 2 \times 10^{-4}$	$0.016 \pm 2 \times 10^{-4}$	$0.012 \pm 1 \times 10^{-4}$
raft	0.17 ± 0.001	$5.9 \times 10^{-3} \pm 9 \times 10^{-5}$	$0.007 \pm 1 \times 10^{-4}$	$0.014 \pm 6 \times 10^{-5}$
		N-Ras HD/Far		
DOPC	0.03 ± .0002	$2.7 \times 10^{-3} \pm 1 \times 10^{-4}$	$0.017 \pm 6 \times 10^{-4}$	$0.067 \pm 6 \times 10^{-4}$
raft	0.04 ± 0.001	$3.2 \times 10^{-3} \pm 1 \times 10^{-4}$	$0.032 \pm 3 \times 10^{-4}$	$0.126 \pm 2 \times 10^{-4}$

[290] Gohlke, A., Triola, G., Waldmann, H., and Winter, R. **(2010)**. Influence of the lipid anchor motif of N-Ras on the interaction with lipid membranes: A surface plasmon resonance study. *Biophys. J. 98*, 2226–2235.

The kinetics of binding can be described by a simple two-step model, with a second-order association process followed by a first-order process:

$$Ras_{monomer} + Membrane \Leftrightarrow Ras_{monomer} - membrane \Leftrightarrow Ras_{clustered} - membrane^{*}$$

The first observable phase is attributed to the initial association, governed by hydrophobic effects (i.e. the non-polar lipid anchors of Ras insert into the membrane, after Ras docks at the membrane surface) or electrostatic interactions, in accordance with previously reported studies.[291] This is followed by (membrane-mediated) protein/lipid–protein interactions and a reorganisation (clustering) of the proteins within the membrane plane. This assumption is in line with insights gained from the lateral partitioning of Ras proteins into various membranes.[125,149] This step may be governed by factors such as hydrophobic mismatch between the lipid chain of Ras and that of phospholipids in the membrane, electrostatic contributions arising from the interaction of amino acid residues of the protein and the phospholipids' headgroups, and eventually from the lateral heterogeneity in membranes (especially, in phase segregated membranes).

Upon comparison between monolipidated N-Ras Far and dually lipidated N-Ras HD/Far, a few conclusions about the association kinetics can be drawn:

$$obs.k_1(Far)_{DOPC/Raft} \approx 3-4 \bullet obs.k_1(HD/Far)_{DOPC/Raft}$$

$$obs.k_2(Far)_{DOPC/Raft} \approx 2-3 \bullet obs.k_2(HD/Far)_{DOPC/Raft}$$

The initial docking and subsequent insertion into membranes (first step), as observed, is expected to be more facile for a protein bearing only one lipid anchor. Moreover, the dually lipidated N-Ras proteins have been demonstrated to exist as dimers in solution (A. Werkmüller, unpublished results), further antagonising the docking and the subsequent membrane insertion. The slower process, which (most likely) involves diffusion-controlled lateral reorganization of the protein-lipid assembly within the membrane plane, was observed for both the N-Ras proteins, but with different rates. It is found to be faster—though was still

[291] Gerlach, H., Laumann, V., Martens, S., Becker, C.F.W., Goody, R.S., and Geyer, M. **(2009)**. HIV-1 Nef membrane association depends on charge, curvature, composition and sequence. *Nat. Chem. Biol. 6*, 46–53.

a rather slow reorganisation process—in the monolipidated Ras, mainly due to a faster diffusion of N-Ras Far within membranes (A. Werkmüller, unpublished results). Thus, double lipidation in Ras leads to an overall decrease of the association process. Furthermore, no major lipid composition-dependent changes could be elucidated for the membrane binding kinetics, suggesting that N-Ras proteins preferentially partition into the fluid phase of membranes of different composition.

However, the amplitudes of the two distinct association steps for the individual N-Ras proteins were different in the two membrane systems. They suggest a stronger (in magnitude) formation of association clusters in the raft-like membranes (Table 9.4). This could be explained based on the evidence that Ras with at least one farnesyl lipid anchor laterally diffuses and concentrates at the phase-boundaries or interfaces of heterogeneous membranes.[125] This is expected to accentuate inter-protein collisions, thus increasing intermolecular (attractive) interactions and finally clustering. The attractive forces may originate via hydrophobic, van der Waals or electrostatic interactions,[287] and may also be mediated by scaffolding proteins and specific lipids (in natural biological systems).[238]

In addition to the membrane composition, the presence of a second membrane targeting signal (in this case, a hexadecyl lipid chain) in N-Ras proteins substantially contributes to the observable slower association process. Whereas in N-Ras Far, the slower association process had a share of ~40 to 60 % in the total FRET signal increase, for N-Ras HD/Far it was about ~80%. Since, double or triple lipidation in N-Ras is responsible for essentially irreversible membrane binding,[290] selective collisions between the N-Ras HD/Far molecules (due to a longer residence time in membranes facilitating inter-protein interactions) might account for a higher magnitude of membrane-associated protein clusters.

Nature of the Ras lipid anchor and clustering dominate the dissociation (off) rates from the membrane

The dissociation process was accomplished by adding an eightfold excess of unlabelled vesicles of the same size and composition, and the decrease in the fluorescence intensity (as the protein transferred from labelled to unlabelled vesicles) was fitted either to a mono-exponential or bi-exponential decay.

The dissociation of N-Ras Far from DOPC membranes exhibited a fast dissociation phase with an observed rate constant ($k_{diss,1}$) of 11.55 ± 1 s^{-1} and a slower phase ($k_{diss,2}$) with 0.13 ± 0.015 s^{-1} (Fig. 9.8). The amplitude of the fast phase (A_1 = 0.016±0.0008) accounted for approximately 60 % of FRET signal decay. The amplitude of the slow phase (A_2) was 0.011 ± 0.0004. Surprisingly, no fast dissociation step of the same protein, when bound to the raft-like membrane, was detected. As such, the measurement time was reduced to 2 s, to resolve the fast phase in the dissociation process for N-Ras Far in the raft-like membranes, if any. From Figure 9.8 it can be seen that the fast dissociation step was observed only in pure DOPC membranes.

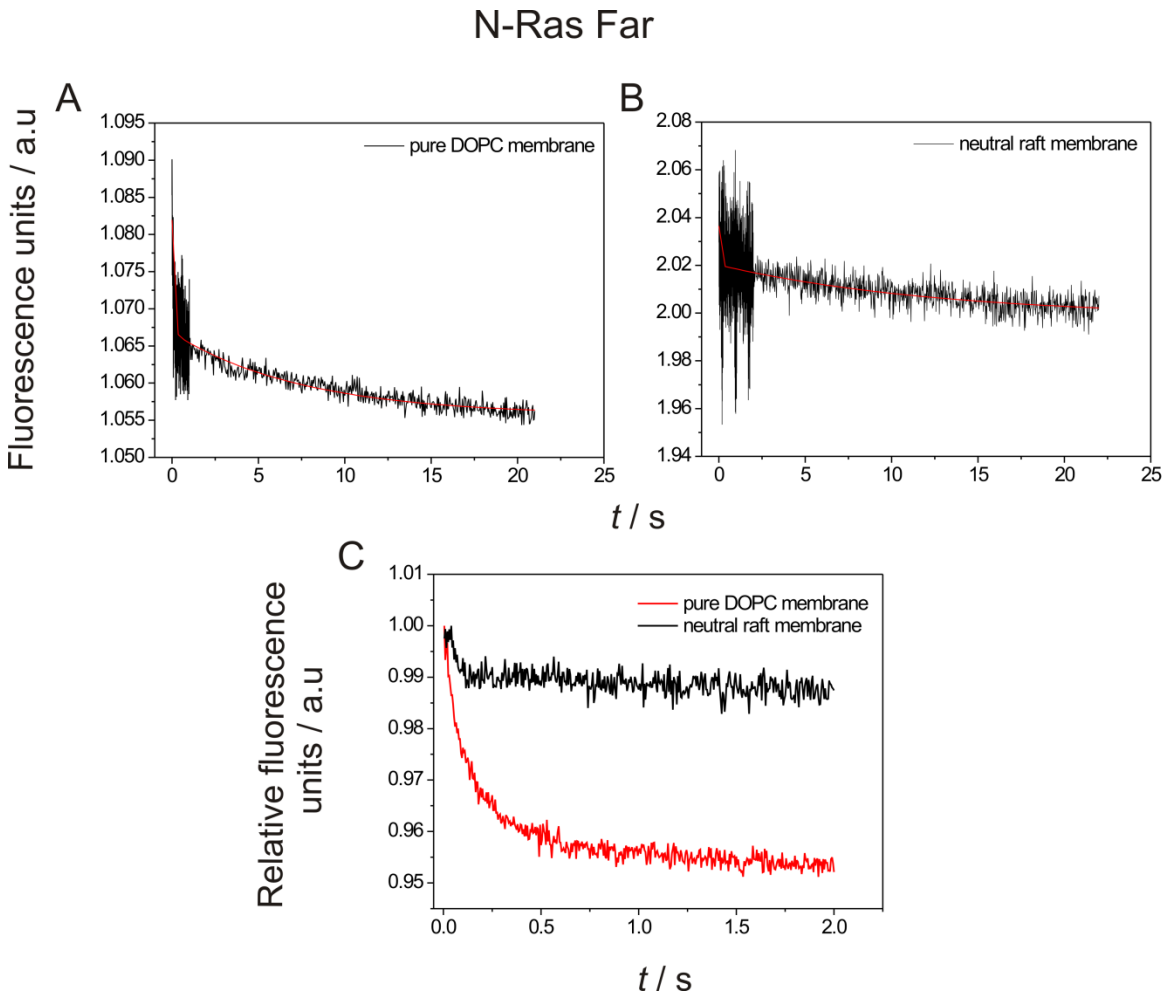

Figure 9.8: Membrane dissociation of Ras depends on the nature of the lipid anchor and protein clustering. Representative dissociation curves of monofarnesylated N-Ras from (**A**) pure DOPC and (**B**) neutral raft-like (DOPC:DPPC:Chol 1:2:1 (molar ratio)) membrane up to 22 s, at 1 bar and 25 ˚C. $c_{protein}$ = 0.35 µM, c_{BODIPY} = 0.125 µM, $c_{vesicles}$= 0.125 mM, and $c_{N\text{-}Rh\text{-}PE}$ = 0.25 µM. The dissociation reaction was accomplished by adding

eightfold excess of the unlabelled lipid vesicles. In (**C**) the corresponding dissociation curves were collected up to 2 s.

For the kinetics of dissociation process, the observable phases could be best ascribed by the following model:

$$Ras_{monomer} - membrane \Leftrightarrow Ras_{clustered} - membrane$$

where the rate constant for the dissociation from membrane-bound monomeric Ras is k_{diss}^{m} and that from the clustered fraction is denoted as k_{diss}^{c}. Within the same membrane system, dissociation from monomeric (loosely bound) protein is expected to be higher than from the clustered fraction due to clustering constraints and intermolecular interactions. Thus, it may stated that at a given membrane composition, invariably $k_{diss}^{m} >> k_{diss}^{c}$.

For N-Ras Far, the amplitude of the slower association phase (designated for clustering within the membrane plane) was higher in raft-like (60 %) compared with DOPC (40%) membranes. This suggests that the equilibrium was towards the clustered fraction in heterogeneous membranes. This may, in part, explain why in the raft-like membranes, no fast dissociation process was observed (or was slow), as a higher fraction of proteins was constrained by the clustering contact. For N-Ras HD/Far, no fast phase in the dissociation process could be observed in the stopped-flow set-up reflecting more stable binding to lipid bilayers. In addition, the dually lipidated N-Ras is suggested (from the previous section) to exist mainly in the clustered fractions on the membrane, further contributing to the low dissociation rates. However, the slower phase in the dissociation process observed at long times (fluorescence results **cf. Ch.7, Fig. 7.10**) showed a relatively faster (4 times) dissociation of the protein from the raft-like membranes, implying formation of kinetically rather unstable Ras clusters in heterogeneous membranes. In conclusion, the fastest dissociation of the initial binding step—in pure fluid bilayers—could only be observed for N-Ras Far, mainly attributed to the lower binding energy of the farnesyl moiety to lipid bilayers. This is consistent with the weak membrane interaction proposed for monofarnesylated N-Ras.

CONCLUSIONS

In the present kinetic study, binding of N-Ras bearing a variable number of lipid anchors with membranes of different composition was explored using a stopped-flow based fluorescence method. The non-simple-exponential association curves reflect complex interaction behaviour for all the proteins in different membrane systems. The membrane binding was shown to be a two step process, in accordance with previously published reports. The first observable phase is most likely the initial docking and reorientation of proteins leading to a stable membrane insertion. The second phase includes lateral reorganisation and subsequent clustering of Ras in the membrane plane. In general, both N-Ras proteins preferentially insert into the fluid phase of different membranes. Minor observed differences in the association rates in different membrane systems are attributed to a more ordered fluid phase in heterogeneous membranes, mainly due to the presence of saturated lipid and cholesterol in the vicinity of the l_d phase. Monofarnesylated N-Ras exhibits a higher association rate independent of the lipid composition, and fastest dissociation process from fluid lipid membranes. No fast phase in the dissociation process could be elucidated for N-Ras Far in raft-like membranes, suggesting a higher tendency of proteins to self-associate in heterogeneous membranes. On the other hand, double lipidation in N-Ras leads to an overall decrease of the association kinetics in both membrane systems. No fast phase in the dissociation process of the doubly lipidated N-Ras was observed, indicative of a stable membrane binding and presence of kinetically rather stable association clusters. In addition, we posit that the membrane composition plays a very crucial role in maintaining the Ras monomer-cluster equilibrium, as deduced from the relative changes in the amplitude of the two distinct steps in the association process. This is ascribed to the presence of domain boundaries in heterogeneous membranes that have been previously revealed to act as 'hot spots' for Ras (bearing at least one farnesyl anchor) to get selectively enriched at these interfaces, facilitating favourable intermolecular interactions and subsequently stronger clustering. The stability of these clusters are altogether a different issue and further studies are required to unravel the different forces maintaining and regulating the clustered domains of proteins. Furthermore, the additional lipid anchor (HD) in N-Ras seems to substantially shift the equilibrium towards the clustered fraction, leading to overall decreased dissociation rates from the membrane, as observed experimentally.

X

BIBLIOGRAPHY

1. Cox, A.D., and Der, C.J. **(2010)**. Ras history: The saga continues. *Small GTPases 1*, 2–27.
2. Hurley, J.B., Simon, M.I., Teplow, D.B., Robishaw, J.D., and Gilman, A.G. **(1984)**. Homologies between signal transducing G proteins and ras gene products. *Science 226*, 860–862.
3. Parada, L.F., Tabin, C.J., Shih, C., and Weinberg, R.A. **(1982)**. Human EJ bladder carcinoma oncogene is homologue of Harvey sarcoma virus ras gene. *Nature 297*, 474–478.
4. Harvey, J.J. **(1964)**. Unidentified Virus Which Causes Rapid Production of Tumours in Mice. *Nature*. *204*, 1104–1105.
5. Kirsten, W.H., and Mayer, L.A. **(1967)**. Morphologic responses to a murine erythroblastosis virus. *J. Natl. Cancer Inst. 39*, 311–335.
6. Shimizu, K., Goldfarb, M., Perucho, M., and Wigler, M. **(1983)**. Isolation and preliminary characterization of the transforming gene of a human neuroblastoma cell line. *Proc. Natl. Acad. Sci. U.S.A. 80*, 383–387.
7. Hall, A., Marshall, C.J., Spurr, N.K., and Weiss, R.A. **(1983)**. Identification of transforming gene in two human sarcoma cell lines as a new member of the ras gene family located on chromosome 1. *Nature 303*, 396–400.
8. Shih, T.Y., Weeks, M.O., Young, H.A., and Scolnick, E.M. **(1979)**. Identification of a Sarcoma Virus–Coded Phosphoprotein in Nonproducer Cells Transformed by Kirsten or Harvey Murine Sarcoma–Virus. *Virology 96*, 64–79.
9. Langbeheim, H., Shih, T.Y., and Scolnick, E.M. **(1980)**. Identification of a normal vertebrate cell protein related to the p21 src of Harvey murine sarcoma virus. *Virology*. *106*, 292–300.
10. Scolnick, E.M., Papageorge, A.G., and Shih, T.Y. **(1979)**. Guanine nucleotide-binding activity as an assay for src protein of rat-derived murine sarcoma viruses. *Proc. Natl. Acad. Sci. U.S.A. 76*, 5355–5359.
11. Willingham, M.C., Pastan, I., Shih, T.Y., and Scolnick, E.M. **(1980)**. Localization of the src gene product of the Harvey strain of MSV to plasma membrane of transformed cells by electron microscopic immunocytochemistry. *Cell 19*, 1005–1014.
12. Papageorge, A., Lowy, D., and Scolnick, E.M. **(1982)**. Comparative biochemical properties of p21 ras molecules coded for by viral and cellular ras genes. *J. Virol. 44*, 509–519.
13. Bos, J.L. **(1989a)**. Ras Oncogenes in Human Cancer – a Review. *Cancer Research 49*, 4682–4689.
14. Karnoub, A.E., and Weinberg, R.A. **(2008)**. Ras oncogenes: split personalities. *Nat. Rev. Mol. Cell Biol. 9*, 517–531.
15. Vetter, I.R., and Wittinghofer, A. **(2001)**. The guanine nucleotide-binding switch in three dimensions. *Science 294*, 1299–1304.
16. Van Dyke, K., Robinson, R., Urquilla, P., Smith, D., Taylor, M., Trush, M., and Wilson, M. **(1977)**. An analysis of nucleotides and catecholamines in bovine medullary granules by anion exchange high pressure liquid chromatography and fluorescence. Evidence that most of the catecholamines in chromaffin granules are stored without associated ATP. *Pharmacology 15*, 377–391.
17. Chardin, P., Camonis, J.H., Gale, N.W., van Aelst, L., Schlessinger, J., Wigler, M.H., and Bar-Sagi, D. **(1993)**. Human Sos1: a guanine nucleotide exchange factor for Ras that binds to GRB2. *Science 260*, 1338–1343.
18. Wittinghofer, A., Scheffzek, K., and Ahmadian, M.R. **(1997)**. The interaction of Ras with GTPase-activating proteins. *FEBS Lett 410*, 63–67.
19. Neal, S.E., Eccleston, J.F., Hall, A., and Webb, M.R. **(1988)**. Kinetic analysis of the hydrolysis of GTP by p21N-ras. The basal GTPase mechanism. *J. Biol. Chem. 263*, 19718–19722.
20. Trahey, M., and McCormick, F. **(1987)**. A cytoplasmic protein stimulates normal N-ras p21 GTPase, but does not affect oncogenic mutants. *Science 238*, 542–545.
21. de Vos, A.M., Tong, L., Milburn, M.V., Matias, P.M., Jancarik, J., Noguchi, S., Nishimura, S., Miura, K., Ohtsuka, E., and Kim, S.H. **(1988)**. Three-dimensional structure of an oncogene protein: catalytic domain of human c–H-ras p21. *Science*. *239*, 888–893.
22. Pai, E.F., Kabsch, W., Krengel, U., Holmes, K.C., John, J., and Wittinghofer, A. **(1989)**. Structure of the guanine-nucleotide-binding domain of the Ha-ras oncogene product p21 in the triphosphate conformation. *Nature 341*, 209–214.
23. Bourne, H.R., Sanders, D.A., and McCormick, F. **(1991)**. The GTPase superfamily: conserved structure and molecular mechanism. *Nature 349*, 117–127.

24. Milburn, M.V., Tong, L., deVos, A.M., Brunger, A., Yamaizumi, Z., Nishimura, S., and Kim, S.H. **(1990)**. Molecular switch for signal transduction: structural differences between active and inactive forms of protooncogenic ras proteins. *Science 247*, 939–945.
25. Vetter, I.R., Nowak, C., Nishimoto, T., Kuhlmann, J., and Wittinghofer, A. **(1999)**. Structure of a Ran-binding domain complexed with Ran bound to a GTP analogue: implications for nuclear transport. *Nature 398*, 39–46.
26. Goldberg, J. **(1998)**. Structural basis for activation of ARF GTPase: mechanisms of guanine nucleotide exchange and GTP-myristoyl switching. *Cell 95*, 237–248.
27. Kamata, T., and Feramisco, J.R. **(1984)**. Epidermal Growth-Factor Stimulates Guanine-Nucleotide Binding-Activity and Phosphorylation of Ras Oncogene Proteins. *Nature 310*, 147–150.
28. Van Aelst, L., Barr, M., Marcus, S., Polverino, A., and Wigler, M. **(1993)**. Complex formation between RAS and RAF and other protein kinases. *Proc. Natl. Acad. Sci. U.S.A. 90*, 6213–6217.
29. Moodie, S.A., Willumsen, B.M., Weber, M.J., and Wolfman, A. **(1993)**. Complexes of Ras.GTP with Raf-1 and mitogen-activated protein kinase kinase. *Science 260*, 1658–1661.
30. Kyriakis, J.M., App, H., Zhang, X.F., Banerjee, P., Brautigan, D.L., Rapp, U.R., and Avruch, J. **(1992)**. Raf-1 activates MAP kinase-kinase. *Nature 358*, 417–421.
31. Howe, L.R., Leevers, S.J., Gomez, N., Nakielny, S., Cohen, P., and Marshall, C.J. **(1992)**. Activation of the MAP kinase pathway by the protein kinase raf. *Cell 71*, 335–342.
32. Mitin, N., Rossman, K.L., and Der, C.J. **(2005)**. Signaling interplay in Ras superfamily function. *Curr. Biol*. *15*, R563–574.
33. Tidyman, W.E., and Rauen, K.A. **(2009)**. The RASopathies: developmental syndromes of Ras/MAPK pathway dysregulation. *Curr. Opin. Genet. Dev. 19*, 230–236.
34. Ulsh, L.S., and Shih, T.Y. **(1984)**. Metabolic turnover of human c-rasH p21 protein of EJ bladder carcinoma and its normal cellular and viral homologs. *Mol. Cell. Biol. 4*, 1647–1652.
35. Willumsen, B.M., Christensen, A., Hubbert, N.L., Papageorge, A.G., and Lowy, D.R. **(1984a)**. The p21 ras C-terminus is required for transformation and membrane association. *Nature 310*, 583–586.
36. Willumsen, B.M., Norris, K., Papageorge, A.G., Hubbert, N.L., and Lowy, D.R. **(1984b)**. Harvey murine sarcoma virus p21 ras protein: biological and biochemical significance of the cysteine nearest the carboxy terminus. *EMBO J. 3*, 2581–2585.
37. Buss, J.E., and Sefton, B.M. **(1986)**. Direct identification of palmitic acid as the lipid attached to p21ras. *Mol*. *Cell Biol. 6*, 116–122.
38. Fujiyama, A., and Tamanoi, F. **(1990)**. RAS2 protein of Saccharomyces cerevisiae undergoes removal of methionine at N terminus and removal of three amino acids at C terminus. *J. Biol. Chem. 265*, 3362–3368.
39. Gutierrez, L., Magee, A.I., Marshall, C.J., and Hancock, J.F. **(1989)**. Post-translational processing of p21ras is two-step and involves carboxyl-methylation and carboxy-terminal proteolysis. *EMBO J. 8*, 1093–1098.
40. Hancock, J.F., Magee, A.I., Childs, J.E., and Marshall, C.J. **(1989)**. All Ras Proteins Are Polyisoprenylated but Only Some Are Palmitoylated. *Cell 57*, 1167–1177.
41. Hancock, J.F., Paterson, H., and Marshall, C.J. **(1990)**. A Polybasic Domain or Palmitoylation Is Required in Addition to the Caax Motif to Localize P21ras to the Plasma Membrane. *Cell 63*, 133–139.
42. Magee, A.I., Gutierrez, L., McKay, I.A., Marshall, C.J., and Hall, A. **(1987)**. Dynamic fatty acylation of p21N-ras. *EMBO J. 6*, 3353–3357.
43. Casey, P.J., Solski, P.A., Der, C.J., and Buss, J.E. **(1989)**. p21ras is modified by a farnesyl isoprenoid. *Proc. Natl. Acad. Sci. U.S.A. 86*, 8323–8327.
44. Magee, A.I., Newman, C.M.H., Giannakouros, T., Hancock, J.F., Fawell, E., and Armstrong, J. **(1992)**. Lipid Modifications and Function of the Ras Superfamily of Proteins. *Biochem. Soc.Trans. 20*, 497–499.
45. Casey, P.J., and Seabra, M.C. **(1996).** Protein prenyltransferases. *J. Biol. Chem. 271*, 5289–5292.
46. Maurer-Stroh, S., and Eisenhaber, F. **(2005)**. Refinement and prediction of protein prenylation motifs. *Genome Biol. 6*, R55.

47. Pepinsky, R.B., Zeng, C., Wen, D., Rayhorn, P., Baker, D.P., Williams, K.P., Bixler, S.A., Ambrose, C.M., Garber, E.A., Miatkowski, K*., et al.* **(1998)**. Identification of a palmitic acid-modified form of human Sonic hedgehog. *J. Biol. Chem. 273*, 14037–14045.
48. Resh, M.D. **(2006)**. Palmitoylation of ligands, receptors, and intracellular signaling molecules. *Sci. STKE*. *2006*, re14.
49. Resh, M.D. **(1999)**. Fatty acylation of proteins: new insights into membrane targeting of myristoylated and palmitoylated proteins. *Biochim. Biophys. Acta. 1451*, 1–16.
50. McGrath, J.P., Capon, D.J., Smith, D.H., Chen, E.Y., Seeburg, P.H., Goeddel, D.V., and Levinson, A.D. **(1983)**. Structure and organization of the human Ki-ras proto-oncogene and a related processed pseudogene. *Nature 304*, 501–506.
51. Lowy, D.R., and Willumsen, B.M. **(1993)**. Function and regulation of ras. *Annu. Rev. Biochem*. *62*, 851–891.
52. van Meer, G., Voelker, D.R., and Feigenson, G.W. **(2008)**. Membrane lipids: where they are and how they behave. *Nat. Rev. Mol. Cell. Biol. 9*, 112–124.
53. Crouthamel, M., Thiyagarajan, M.M., Evanko, D.S., and Wedegaertner, P.B. **(2008)**. N-terminal polybasic motifs are required for plasma membrane localization of Galpha(s) and Galpha(q). *Cell Signal. 20*, 1900–1910.
54. Rocks, O., Peyker, A., and Bastiaens, P.I. **(2006)**. Spatio-temporal segregation of Ras signals: one ship, three anchors, many harbors. *Curr. Opin. Cell. Biol. 18*, 351–357.
55. Hancock, J.F., Cadwallader, K., Paterson, H., and Marshall, C.J. **(1991)**. A Caax or a Caal Motif and a 2nd Signal Are Sufficient for Plasma-Membrane Targeting of Ras Proteins. *EMBO J. 10*, 4033–4039.
56. Rocks, O., Peyker, A., Kahms, M., Verveer, P.J., Koerner, C., Lumbierres, M., Kuhlmann, J., Waldmann, H., Wittinghofer, A., and Bastiaens, P.I. **(2005)**. An acylation cycle regulates localization and activity of palmitoylated Ras isoforms. *Science 307*, 1746–1752.
57. Bivona, T.G., Quatela, S.E., Bodemann, B.O., Ahearn, I.M., Soskis, M.J., Mor, A., Miura, J., Wiener, H.H., Wright, L., Saba, S.G*., et al.* **(2006)**. PKC regulates a farnesyl-electrostatic switch on K-Ras that promotes its association with Bcl-XL on mitochondria and induces apoptosis. *Mol. Cell. 21*, 481–493.
58. Brunsveld, L., Kuhlmann, J., Alexandrov, K., Wittinghofer, A., Goody, R.S., and Waldmann, H. **(2006a)**. Lipidated ras and rab peptides and proteins--synthesis, structure, and function. *Angew. Chem. Int. Ed. 45*, 6622–6646, Brunsveld, L., Kuhlmann, J., and Waldmann, H. **(2006b)**. Synthesis of palmitoylated Ras-peptides and -proteins. *Methods 40*, 151–165, Kuhn, K., Owen, D.J., Bader, B., Wittinghofer, A., Kuhlmann, J., and Waldmann, H. **(2001)**. Synthesis of functional Ras lipoproteins and fluorescent derivatives. *J. Am. Chem. Soc. 123*, 1023–1035, Nagele, E., Schelhaas, M., Kuder, N., and Waldmann, H. **(1998)**. Chemoenzymatic synthesis of N-Ras lipopeptides. *J. Am. Chem. Soc. 120*, 6889–6902, Reents, R., Wagner, M., Kuhlmann, J., and Waldmann, H. **(2004).** Synthesis and application of fluorescence-labeled Ras-proteins for live-cell imaging. *Angew. Chem. Int. Ed. 43*, 2711–2714.
59. Chen, Y.X., Koch, S., Uhlenbrock, K., Weise, K., Das, D., Gremer, L., Brunsveld, L., Wittinghofer, A., Winter, R., Triola, G*., et al.* **(2010).** Synthesis of the Rheb and K-Ras4B GTPases. *Angew. Chem. Int. Ed. 49*, 6090–6095.
60. Lenzen, C., Cool, R.H., Prinz, H., Kuhlmann, J., and Wittinghofer, A. **(1998)**. Kinetic analysis by fluorescence of the interaction between Ras and the catalytic domain of the guanine nucleotide exchange factor Cdc25Mm. *Biochemistry 37*, 7420–7430, Lenzen, C., Cool, R.H., and Wittinghofer, A. **(1995)**. Analysis of intrinsic and CDC25-stimulated guanine nucleotide exchange of p21ras-nucleotide complexes by fluorescence measurements. *Methods Enzymol. 255*, 95–109.
61. Papahadjopoulos, D., Vail, W.J., Pangborn, W.A., and Poste, G. **(1976)**. Studies on membrane fusion. II. Induction of fusion in pure phospholipid membranes by calcium ions and other divalent metals. *Biochim. Biophys. Acta. 448*, 265–283.
62. Timasheff, S.N., Susi, H., and Stevens, L. **(1967)**. Infrared spectra and protein conformations in aqueous solutions. II. Survey of globular proteins. *J. Biol. Chem. 242*, 5467–5473.
63. Byler, D.M., and Susi, H. **(1986)**. Examination of the Secondary Structure of Proteins by Deconvolved FTIR Spectra. *Biopolymers 25*, 469–487.

64. Wong, P.T.T. and Moffat, D.J. **(1989)**. A new internal pressure calibrant fro high-pressure infrared spectroscopy in aqueous systems. *App. Spectrosc. 43*, 1279–1281.
65. Dunstan, D.J., and Spain, I.L. **(1989)**. The Technology of Diamond Anvil High-Pressure Cells .1. Principles, Design and Construction*. J. Phys. E-Sci. Inst. 22*, 913–923.
66. Spain, I.L., and Dunstan, D.J. **(1989)**.The Technology of Diamond Anvil High-Pressure Cells .2. Operation and Use*. . J. Phys. E-Sci. Inst. 22*, 923–933.
67. Griffiths, P.R., and Pariente, G.L. **(1986)**. Introduction to Spectral Deconvolution. *Trends in Anal. Chem*. *5*, 209–215.
68. Marquardt, D.W. **(1963)**. An Algorithm for Least-Squares Estimation of Nonlinear Parameters. *J. Soc. Indust. and Appl. Math. 11*, 431–441.
69. Born, M., and Wolf, E. **(1965)**. Principles of optics; electromagnetic theory of propagation, interference and diffraction of light, 3d Rev. Ed. (Oxford, New York, Pergamon Press).
70. Harrick, N.J. **(1967)**. *Internal Reflection Spectroscopy*. Interscience, New York.
71. Fahrenfort, J. **(1961)**. Attenuated Total Reflection - a New Principle for the Production of Useful Infra-Red Reflection Spectra of Organic Compounds. *Spect. Acta. 17*, 698–712.
72. Goos, F., and Hanchen, H. **(1947)**. Ein Neuer Und Fundamentaler Versuch Zur Totalreflexion. *Annal. Der Phys. 1*, 333–346.
73. Carniglia,C.K, and Mandel, L. **(1971)**. Quantization of Evanescent Electromagnetic Waves. *Phys. Rev. D. 3*, 280–290.
74. Harrick, N.J. **(1971)**. Principles of Internal Reflection Spectroscopy. *Appl. Spect. 25*, 142–170.
75. Tatulian, S.A., Jones, L.R., Reddy, L.G., Stokes, D.L., and Tamm, L.K. **(1995)**. Secondary structure and orientation of phospholamban reconstituted in supported bilayers from polarized attenuated total reflection FTIR spectroscopy. *Biochemistry 34*, 4448–4456.
76. Marsh, D. **(1997)**. Dichroic ratios in polarized Fourier transform infrared for nonaxial symmetry of beta-sheet structures. *Biophys. J. 72*, 2710–2718.
77. Tamm, L.K., and Tatulian, S.A. **(1997)**. Infrared spectroscopy of proteins and peptides in lipid bilayers. *Q. Rev. Biophys. 30*, 365–429.
78. Bechinger, B., Ruysschaert, J.M., and Goormaghtigh, E. **(1999)**. Membrane helix orientation from linear dichroism of infrared attenuated total reflection spectra. *Biophys J. 76*, 552–563.
79. Axelsen, P.H., and Citra, M.J. **(1996)**. Orientational order determination by internal reflection infrared spectroscopy. *Prog. Biophys. Mol. Bio. 66*, 227–253.
80. Goormaghtigh, E., Raussens, V., and Ruysschaert, J.M. **(1999)**. Attenuated total reflection infrared spectroscopy of proteins and lipids in biological membranes. *Biochim. Biophys. Acta, Biomembr. 1422*, 105–185.
81. Ausili, A., Corbalan-Garcia, S., Gomez-Fernandez, J.C., and Marsh, D. **(2011)**. Membrane docking of the C2 domain from protein kinase C alpha as seen by polarized ATR-IR. The role of PIP2. *Biochim. Biophys. Acta, Biomembr. 1808*, 684–695.
82. Wittebort, R.J., Schmidt, C.F., and Griffin, R.G. **(1981)**. Solid-State C-13 Nuclear Magnetic-Resonance of the Lecithin Gel to Liquid-Crystalline Phase-Transition. *Biochemistry 20*, 4223–4228.
83. Lewis, R.N., and McElhaney, R.N. **(1992)**. Structures of the subgel phases of n-saturated diacyl phosphatidylcholine bilayers: FTIR spectroscopic studies of 13C = O and 2H labeled lipids. *Biophys. J. 61*, 63–77.
84. Dluhy, R.A., and Cornell, D.G. **(1985)**. Insitu Measurement of the Infrared-Spectra of Insoluble Monolayers at the Air-Water-Interface. *J. Phys. Chem. 89*, 3195–3197.
85. Mendelsohn, R., Mao, G.R., and Flach, C.R. **(2010)**. Infrared reflection-absorption spectroscopy: Principles and applications to lipid-protein interaction in Langmuir films. *Biochim. Biophys. Acta, Biomembr. 1798*, 788–800.
86. Mendelsohn, R., Brauner, J.W., and Gericke, A. **(1995)**. External Infrared Reflection-Absorption Spectrometry Monolayer Films at the Air-Water-Interface. *Annu. Rev. Phys. Chem. 46*, 305–334.
87. Flach, C.R., Gericke, A., and Mendelsohn, R. **(1997)**. Quantitative determination of molecular chain tilt angles in monolayer films at the air/water interface: Infrared reflection/absorption spectroscopy of behenic acid methyl ester*. J. Phys. Chem. B. 101*, 58–65.
88. Abelès, F. **(1950)**. "Recherches sur la propagation des ondes électromagnétique sinussoïdales dans les milieux stratifiés. Application aux couches minces." *Ann. Phys. 5*, 596–640.

89. Schopper, H. **(1952)**. Zur Optik Dunner Doppelbrechender Und Dichroitischer Schichten. *Z. Phys. 132*, 146–170.
90. Kuzmin, V.L., Romanov, V.P., and Mikhailov, A.V. **(1992)**. Light-Reflection on the Boundary of Liquid-Systems and Surface-Layer Structure. *Opt. Spekt. 73*, 3–47.
91. Korte, E.H. **(1983)**. Influence of the Order Parameter-D on the Linear Dichroism of Nematic Liquid-Crystals. *Mol. Crys. Liq. Crys. 100*, 127–135.
92. Meister, A., Nicolini, C., Waldmann, H., Kuhlmann, J., Kerth, A., Winter, R., and Blume, A. **(2006)**. Insertion of lipidated Ras proteins into lipid monolayers studied by infrared reflection absorption spectroscopy (IRRAS). *Biophys. J. 91*, 1388–1401.
93. Bailey, S. **(1994)**. The Ccp4 Suite - Programs for Protein Crystallography. *Acta. Crystall. D. 50*, 760–763.
94. Bertie, J.E., Ahmed, M.K., and Eysel, H.H. **(1989)**. Infrared Intensities of Liquids .5. Optical and Dielectric-Constants, Integrated-Intensities, and Dipole-Moment Derivatives of H_2O and D_2O at 22 ˚C. *J. Phys Chem. 93,* 2210–2218.
95. Gericke, A., Michailov, A.V., and Huhnerfuss, H. **(1993)**. Polarized External Infrared Reflection Absorption Spectrometry at the Air-Water-Interface - Comparison of Experimental and Theoretical Results for Different Angles of Incidence. *Vib. Spect. 4*, 335–348.
96. Thomas, L. **(1971)**. Notes of a Biology-Watcher - Lives of a Cell. *N. Engl. J. Med. 284*, 1082–1083.
97. Roux, M., Auzely-Velty, R., Djedaini-Pilard, F., and Perly, B. **(2002)**. Cyclodextrin-induced lipid lateral separation in DMPC membranes: H-2 nuclear magnetic resonance study. *Biophys. J. 82*, 813–822.
98. Hartmann, W., and Galla, H.J. **(1978)**. Binding of Polylysine to Charged Bilayer Membranes - Molecular-Organization of a Lipid - Peptide Complex. *Biochim. Biophys. Acta. 509*, 474–490.
99. Wilkinson, D.A., and Nagle, J.F. **(1979)**. Dilatometric Study of Binary-Mixtures of Phosphatidylcholines. *Biochemistry 18*, 4244–4249.
100. Knoll, W., Schmidt, G., Rotzer, H., Henkel, T., Pfeiffer, W., Sackmann, E., Mittlerneher, S., and Spinke, J. **(1991)**. Lateral Order in Binary Lipid Alloys and Its Coupling to Membrane Functions. *Chem. Phys. Lipids 57*, 363–374.
101. Feigenson, G.W. **(2006)**. Phase behavior of lipid mixtures. *Nat. Chem.Biol. 2*, 560–563.
102. Feigenson, G.W. **(2007)**. Phase boundaries and biological membranes. *Ann. Rev. Biophy. Biomol. Str. 36*, 63–77.
103. Silvius, J.R., delGiudice, D., and Lafleur, M. **(1996)**. Cholesterol at different bilayer concentrations can promote or antagonize lateral segregation of phospholipids of differing acyl chain length. *Biochemistry 35*, 15198–15208.
104. Ahmed, S.N., Brown, D.A., and London, E. **(1997)**. On the origin of sphingolipid/cholesterol-rich detergent-insoluble cell membranes: Physiological concentrations of cholesterol and sphingolipid induce formation of a detergent-insoluble, liquid-ordered lipid phase in model membranes. *Biochemistry*. *36*, 10944–10953.
105. Veatch, S.L., and Keller, S.L. **(2002)**. Organization in lipid membranes containing cholesterol. *Phys. Rev. Lett. 89*.
106. Sankaram, M.B., and Thompson, T.E. **(1990)**. Modulation of Phospholipid Acyl Chain Order by Cholesterol - a Solid-State H-2 Nuclear-Magnetic-Resonance Study. *Biochemistry 29*, 10676–10684.
107. Nielsen, M., Miao, L., Ipsen, J.H., Zuckermann, M.J., and Mouritsen, O.G. **(1999)**. Off-lattice model for the phase behavior of lipid-cholesterol bilayers. *Phys. Rev. E. 59*, 5790–5803.
108. Czeslik, C., Reis, O., Winter, R., and Rapp, G. **(1998)**. Effect of high pressure on the structure of dipalmitoylphosphatidylcholine bilayer membranes: a synchrotron x-ray diffraction and FTIR spectroscopy study using the diamond anvil technique. *Chem. Phys. Lipids. 91*, 135–144.
109. Winter, R., and Jeworrek, C. **(2009)**. Effect of pressure on membranes. *Soft Matter 5*, 3157–3173.
110. Jeworrek, C., Puhse, M., and Winter, R. **(2008).** X-ray Kinematography of Phase Transformations of Three-Component Lipid Mixtures: A Time-Resolved Synchrotron X-ray Scattering Study Using the Pressure-jump Relaxation Technique. *Langmuir 24*, 11851–11859.
111. Brown, D.A., and London, E. **(1998)**. Functions of lipid rafts in biological membranes. *Ann. Rev. Cell Dev. Biol. 14*, 111–136.
112. Simons, K., and Ikonen, E. **(1997)**. Functional rafts in cell membranes. *Nature 387*, 569–572.

113. Simons, K., and Ehehalt, R. **(2002)**. Cholesterol, lipid rafts, and disease. *J. Clin. Invest. 110*, 597–603.
114. Nicolini, C., Kraineva, J., Khurana, M., Periasamy, N., Funari, S.S., and Winter, R. **(2006c)**. Temperature and pressure effects on structural and conformational properties of POPC/SM/cholesterol model raft mixtures - a FTIR, SAXS, DSC, PPC and Laurdan fluorescence spectroscopy study. *Biochim. Biophys. Acta, Biomembr. 1758*, 248–258.
115. Varma, R., and Mayor, S. **(1998)**. GPI-anchored proteins are organized in submicron domains at the cell surface. *Nature 394*, 798–801.
116. Pralle, A., Keller, P., Florin, E.L., Simons, K., and Horber, J.K.H. **(2000)**. Sphingolipid-cholesterol rafts diffuse as small entities in the plasma membrane of mammalian cells*. J. Cell Biol. 148*, 997–1007.
117. Wilson, B.S., Pfeiffer, J.R., and Oliver, J.M. **(2000)**.Observing Fc epsilon RI signaling from the inside of the mast cell membrane. *J. Cell Biol 149*, 1131–1142.
118. Levental, I., Grzybek, M., and Simons, K. **(2011)**. Raft domains of variable properties and compositions in plasma membrane vesicles. *Proc. Natl. Acad. Sci. U.S.A. 108*, 11411–11416.
119. Irwin, M.E., Bohin, N., and Boerner, J.L. **(2011)**. Src family kinases mediate epidermal growth factor receptor signaling from lipid rafts in breast cancer cells. *Cancer Biology & Therapy 12*, 718–726.
120. Parton, R.G., and Hancock, J.F. **(2004)**. Lipid rafts and plasma membrane microorganization: insights from Ras. *Trends Cell Biol. 14*, 141–147.
121. Lucero, H.A., and Robbins, P.W. **(2004)**. Lipid rafts-protein association and the regulation of protein activity. *Arch. Biochem. Biophys. 426*, 208–224.
122. Roy, S., Luetterforst, R., Harding, A., Apolloni, A., Etheridge, M., Stang, E., Rolls, B., Hancock, J.F., and Parton, R.G. **(1999)**. Dominant-negative caveolin inhibits H-Ras function by disrupting cholesterol-rich plasma membrane domains. *Nat. Cell. Biol. 1*, 98–105.
123. Sheets, E.D., Petersen, N.O., Holowka, D., and Baird, B. **(1999)**. Interactions between the high affinity IgE receptor and detergent-resistant membranes measured by image cross-correlation spectroscopy. *Biophys. J. 76*, A391–A391.
124. Rietveld, A., Neutz, S., Simons, K., and Eaton, S. **(1999)**. Association of sterol- and glycosylphosphatidylinositol-linked proteins with Drosophila raft lipid microdomains. *J. Biol. Chem. 274*, 12049–12054.
125. Weise, K., Triola, G., Brunsveld, L., Waldmann, H., and Winter, R. **(2009)**. Influence of the Lipidation Motif on the Partitioning and Association of N-Ras in Model Membrane Subdomains. *J. Am. Chem. Soc. 131*, 1557–1564.
126. Williamson, P., and Schlegel, R.A. **(1994)**. Back and Forth - the Regulation and Function of Transbilayer Phospholipid Movement in Eukaryotic Cells. *Mol. Mem. Biol. 11*, 199–216.
127. Glaser, M., Wanaski, S., Buser, C.A., Boguslavsky, V., Rashidzada, W., Morris, A., Rebecchi, M., Scarlata, S.F., *et al.* **(1996)**. Myristoylated alanine-rich C kinase substrate (MARCKS) produces reversible inhibition of phospholipase C by sequestering phosphatidylinositol 4,5-bisphosphate in lateral domains. *J. Biol. Chem. 271*, 26187–26193.
128. Pike, L.J., and Casey, L. **(1996)**. Localization and turnover of phosphatidylinositol 4,5-bisphosphate in caveolin-enriched membrane domains. *J. Biol. Chem. 271*, 26453–26456.
129. Wong, P.T.T., Siminovitch, D.J., and Mantsch, H.H. **(1988)**. Structure and Properties of Model Membranes - New Knowledge from High-Pressure Vibrational Spectroscopy. *Biochim. Biophys. Acta*. *947*, 139–171.
130. Mendelsohn, R., Davies, M.A., Brauner, J.W., Schuster, H.F., and Dluhy, R.A. **(1989)**. Quantitative-Determination of Conformational Disorder in the Acyl Chains of Phospholipid-Bilayers by Infrared-Spectroscopy. *Biochemistry 28*, 8934–8939.
131. Davies, M.A., Schuster, H.F., Brauner, J.W., and Mendelsohn, R. **(1990)**. Effects of Cholesterol on Conformational Disorder in Dipalmitoylphosphatidylcholine Bilayers - a Quantitative IR Study of the Depth Dependence. *Biochemistry*. *29*, 4368–4373.
132. Reis, O., and Winter, R. **(1998)**. Pressure and temperature effects on conformational and hydrational properties of lamellar and bicontinuous cubic phases of the fully hydrated monoacylglyceride monoelaidin - A Fourier transform infrared spectroscopy study using the diamond anvil technique. *Langmuir 14*, 2903–2909.

133. Senak, L., Davies, M.A., and Mendelsohn, R. **(1991)**. A Quantitative Ir Study of Hydrocarbon Chain Conformation in Alkanes and Phospholipids - CH_2 Wagging Modes in Disordered Bilayer and HII Phases. *J. Phys. Chem. 95*, 2565–2571.
134. Puehse, M., Jeworrek, C., and Winter, R. **(2008)**. The temperature-pressure phase diagram of a DPPC-ergosterol fungal model membrane - a SAXS and FTIR spectroscopy study. *Chem. Phys. Lipids 152*, 57–63.
135. Kapoor, S., Werkmuller, A., Denter, C., Zhai, Y., Markgraf, J., Weise, K., Opitz, N., and Winter, R. **(2011)**. Temperature-pressure phase diagram of a heterogeneous anionic model biomembrane system: Results from a combined calorimetry, spectroscopy and microscopy study. *Biochim. Biophys.Acta, Biomembr. 1808*, 1187–1195.
136. Colicelli, J. **(2004)**. Human RAS superfamily proteins and related GTPases. *Sci. STKE 2004*, RE13.
137. Wennerberg, K., Rossman, K.L., and Der, C.J. **(2005)**. The Ras superfamily at a glance. *J. Cell. Sci. 118*, 843–846.
138. Rodriguez-Viciana, P., Sabatier, C., and McCormick, F. **(2004)**. Signaling specificity by Ras family GTPases is determined by the full spectrum of effectors they regulate. *Mol. Cell. Biol. 24*, 4943–4954.
139. Umanoff, H., Edelmann, W., Pellicer, A., and Kucherlapati, R. **(1995)**. The murine N-ras gene is not essential for growth and development. *Proc. Natl. Acad. Sci. U.S.A. 92*, 1709–1713.
140. Kataoka, T., Powers, S., Mcgill, C., Fasano, O., Strathern, J., Broach, J., and Wigler, M. **(1984)**. Genetic-Analysis of Yeast Ras1 and Ras2 Genes. *Cell 37*, 437–445.
141. Leon, J., Guerrero, I., and Pellicer, A. **(1987)**. Differential Expression of the Ras Gene Family in Mice. *Mol. Cell. Biol. 7*, 1535–1540.
142. Koera, K., Nakamura, K., Nakao, K., Miyoshi, J., Toyoshima, K., Hatta, T., Otani, H., Aiba, A., and Katsuki, M. **(1997)**. K-ras is essential for the development of the mouse embryo. *Oncogene 15*, 1151–1159.
143. Johnson, L., Greenbaum, D., Cichowski, K., Mercer, K., Murphy, E., Schmitt, E., Bronson, R.T., Umanoff, H., Edelmann, W., Kucherlapati, R*., et al.* **(1997)**. K-ras is an essential gene in the mouse with partial functional overlap with N-ras. *Genes Dev. 11*, 2468–2481.
144. Casar, B., Arozarena, I., Sanz-Moreno, V., Pinto, A., Agudo-Ibanez, L., Marais, R., Lewis, R.E., Berciano, M.T., and Crespo, P. **(2009)**. Ras Subcellular Localization Defines Extracellular Signal-Regulated Kinase 1 and 2 Substrate Specificity through Distinct Utilization of Scaffold Proteins. *Mol. Cell. Biol. 29*, 1338–1353.
145. Choy, E., Chiu, V.K., Silletti, J., Feoktistov, M., Morimoto, T., Michaelson, D., Ivanov, I.E. and Philips, M.R. **(1999)**. Endomembrane trafficking of Ras: The CAAX motif targets proteins to the ER and Golgi. *Cell 98*, 69–80.
146. Apolloni, A., Prior, I.A., Lindsay, M., Parton, R.G., and Hancock, J.F. **(2000)**. H-ras but not K-ras traffics to the plasma membrane through the exocytic pathway. *Mol. Cell. Biol. 20*, 2475–2487.
147. Chandra, A., Grecco, H.E., Pisupati, V., Perera, D., Cassidy, L., Skoulidis, F., Ismail, S.A., Hedberg, C., Hanzal-Bayer, M., Venkitaraman, A.R*., et al.* **(2012)**. The GDI-like solubilizing factor PDE delta sustains the spatial organization and signalling of Ras family proteins. *Nat. Cell Biol. 14*, 148–158.
148. Prior, I.A., Harding, A., Yan, J., Sluimer, J., Parton, R.G., and Hancock, J.F. **(2001)**. GTP-dependent segregation of H-ras from lipid rafts is required for biological activity. *Nat. Cell Biol. 3*, 368–375.
149. Weise, K., Kapoor, S., Denter, C., Nikolaus, J., Opitz, N., Koch, S., Triola, G., Herrmann, A., Waldmann, H., and Winter, R. **(2011)**. Membrane-Mediated Induction and Sorting of K-Ras Microdomain Signaling Platforms. *J. Am. Chem. Soc. 133*, 880–887.
150. Yan, J., Roy, S., Apolloni, A., Lane, A., and Hancock, J.F. **(1998)**. Ras isoforms vary in their ability to activate Raf-1 and phosphoinositide 3-kinase. *J. Biol. Chem. 273*, 24052–24056.
151. Voice, J.K., Klemke, R.L., Le, A., and Jackson, J.H. **(1999)**. Four human Ras homologs differ in their abilities to activate Raf-1, induce transformation, and stimulate cell motility. *J. Biol. Chem.. 274*, 17164–17170.
152. Morrison, D.K., and Cutler, R.E. **(1997)**. The complexity of Raf-1 regulation. *Curr. Opin. Cell Biol. 9*, 174–179.
153. Clark, G.J., Drugan, J.K., Rossmann, K.L., Carpenter, J.W., RogersGraham, K., Fu, H., Der, C.J., and Campbell, S.L. **(1997)**. 14-3-3 zeta negatively regulates Raf-1 activity by interactions with the Raf-1 cysteine-rich domain. *J. Biol. Chem. 272*, 20990–20993.

154. Abankwa, D., Gorfe, A.A., Inder, K., and Hancock, J.F. **(2010)**. Ras membrane orientation and nanodomain localization generate isoform diversity. *Proc. Natl. Acad. Sci. U.S.A. 107*, 1130–1135.
155. Gorfe, A.A., Hanzal-Bayer, M., Abankwa, D., Hancock, J.F., and McCammon, J.A. **(2007)**. Structure and dynamics of the full-length lipid-modified H-ras protein in a 1,2-dimyristoylglycero-3-phosphocholine bilayer. *J. Med. Chem. 50*, 674–684.
156. Abankwa, D., Hanzal-Bayer, M., Ariotti, N., Plowman, S.J., Gorfe, A.A., Parton, R.G., McCammon, J.A., and Hancock, J.F. **(2008b)**. A novel switch region regulates H-ras membrane orientation and signal output. *EMBO J. 27*, 727–735.
157. Abankwa, D., Gorfe, A.A., and Hancock, J.F. **(2008a)**. Mechanisms of Ras membrane organization and signaling: Ras on a rocker. *Cell Cycle 7*, 2667–2673.
158. Brunger, A.T., Milburn, M.V., Tong, L., deVos, A.M., Jancarik, J., Yamaizumi, Z., Nishimura, S., Ohtsuka, E., and Kim, S.H. **(1990)**. Crystal structure of an active form of RAS protein, a complex of a GTP analog and the HRAS p21 catalytic domain. *Proc. Natl. Acad. Sci. U.S.A. 87*, 4849–4853.
159. Guldenhaupt, J., Adiguzel, Y., Kuhlmann, J., Waldmann, H., Kotting, C., and Gerwert, K. **(2008)**. Secondary structure of lipidated Ras bound to a lipid bilayer. *FEBS J. 275*, 5910–5918.
160. Rojas, A.M., Fuentes, G., Rausell, A., and Valencia, A. **(2012)**. The Ras protein superfamily: evolutionary tree and role of conserved amino acids*. J. Cell Biol. 196*, 189–201.
161. Abraham, S.J., Nolet, R.P., Calvert, R.J., Anderson, L.M., and Gaponenko, V. **(2009)**. The hypervariable region of K-Ras4B is responsible for its specific interactions with calmodulin. *Biochemistry 48*, 7575–7583.
162. Lukman, S., Grant, B.J., Gorfe, A.A., Grant, G.H., and McCammon, J.A. **(2010)**. The Distinct Conformational Dynamics of K-Ras and H-Ras A59G. *PLoS Comput. Biol. 6*.
163. Marsh, D. **(1999)**. Quantitation of secondary structure in ATR infrared spectroscopy. *Biophys. J. 77*, 2630–2637.
164. Marsh, D., Muller, M., and Schmitt, F.J. **(2000)**. Orientation of the infrared transition moments for an alpha-helix. *Biophys. J.. 78*, 2499–2510.
165. Huster, D., Vogel, A., Katzka, C., Scheidt, H.A., Binder, H., Dante, S., Gutberlet, T., Zschornig, O., Waldmann, H., and Arnold, K. **(2003)**. Membrane insertion of a lipidated ras peptide studied by FTIR, solid-state NMR, and neutron diffraction spectroscopy. *J. Am. Chem. Soc. 125*, 4070–4079.
166. Evers, F., Jeworrek, C., Weise, K., Tolan, M., and Winter, R. **(2012)**. Detection of lipid raft domains in neutral and anionic Langmuir monolayers and bilayers of complex lipid composition. *Soft Matter 8*, 2170–2175.
167. Janmey, P.A., and Kinnunen, P.K. **(2006)**. Biophysical properties of lipids and dynamic membranes. *Trends Cell Biol. 16*, 538–546.
168. Bringezu, F., Majerowicz, M., Wen, S.Y., Reuther, G., Tan, K.T., Kuhlmann, J., Waldmann, H., and Huster, D. **(2007)**. Membrane binding of a lipidated N-Ras protein studied in lipid monolayers. *Eur. Biophys. J. Biophys. Lett. 36*, 491–498.
169. Hancock, J.F. **(2003)**. Ras proteins: Different signals from different locations. *Nat. Rev. Mol. Cell Biol. 4*, 373–384.
170. Prior, I.A., Muncke, C., Parton, R.G., and Hancock, J.F. **(2003)**. Direct visualization of Ras proteins in spatially distinct cell surface microdomains. *J. Cell Biol. 160*, 165–170.
171. Kapoor, S., Weise, K., Erlkamp, M., Triola, G., Waldmann, H., and Winter, R. **(2012)**. The role of G-domain orientation and nucleotide state on the Ras isoform-specific membrane interaction. *Eur. Biophys. J. 41*, 801–813.
172. Linderstrøm-Lang, K. U. & Schellman, J. A. **(1959)** Protein Structure and Enzyme Activity in *"The Enzymes" Vol 1*, Second Ed. 443–510 Boyer, Lardy, Myrbäk Eds. Academic Press, New York.
173. Ansari, A., Berendzen, J., Bowne, S.F., Frauenfelder, H., Iben, I.E. Sauke, T.B., Shyamsunder, E., and Young, R.D. **(1985)**. Protein states and proteinquakes. *Proc. Natl. Acad. Sci. U.S.A. 82*, 5000–5004.
174. Frauenfelder, H., Parak, F., and Young, R.D. **(1988)**. Conformational substates in proteins. *Annu. Rev. Biophys. Biophys. Chem. 17*, 451–479.
175. Frauenfelder, H., Sligar, S.G., and Wolynes, P.G. **(1991)**. The energy landscapes and motions of proteins. *Science 254*, 1598–1603.
176. Frauenfelder, H., Alberding, N.A., Ansari, A., Braunstein, D., Cowen, B.R., Hong, M.K., Iben, I.E.T., *et al.* **(1990)**. Proteins and Pressure. *J. Phys. Chem. 94*, 1024–1037.

177. Dill, K.A., and Chan, H.S. **(1997)**. From Levinthal to pathways to funnels. *Nat. Struct. Biol. 4*, 10–19.
178. Monod, J., Wyman, J., and Changeux, J.P. **(1965)**. On the Nature of Allosteric Transitions: A Plausible Model. *J. Mol. Biol. 12*, 88–118.
179. Boehr, D.D., Nussinov, R., and Wright, P.E. **(2009)**. The role of dynamic conformational ensembles in biomolecular recognition. *Nat. Chem. Biol. 5*, 789–796.
180. Akasaka, K. **(2003)**. Exploring the entire conformational space of proteins by high-pressure NMR. *Pure Appl. Chem. 75*, 927–936.
181. Li, P., Martins, I.R., Amarasinghe, G.K., and Rosen, M.K. **(2008)**. Internal dynamics control activation and activity of the autoinhibited Vav DH domain. *Nat. Struct. Mol. Biol. 15*, 613–618.
182. Kuwata, K., Li, H., Yamada, H., Legname, G., Prusiner, S.B., Akasaka, K., and James, T.L. **(2002)**. Locally disordered conformer of the hamster prion protein: a crucial intermediate to PrPSc? *Biochemistry 41*, 12277–12283.
183. Privalov, P.L., and Gill, S.J. **(1988)**. Stability of protein structure and hydrophobic interaction. *Adv. Prot. Chem. 39*, 191–234.
184. Ravindra, R., and Winter, R. **(2003)**. On the temperature--pressure free-energy landscape of proteins. *Chemphyschem 4*, 359–365.
185. Winter, R., and Dzwolak, W. **(2005)**. Temperature-pressure configurational landscape of lipid bilayers and proteins. *Phil. Trans. R. Soc. A 363,* 537–563.
186. Akasaka, K. **(2006)**. Probing conformational fluctuation of proteins by pressure perturbation. *Chem. Rev, 106*, 1814–1835.
187. McCoy, J., and Hubbell, W.L. **(2011)**. High-pressure EPR reveals conformational equilibria and volumetric properties of spin-labeled proteins. *Proc. Natl. Acad. Sci. U.S.A. 108*, 1331–1336.
188. Collins, M.D., Kim, C.U., and Gruner, S.M. **(2011)** High-pressure protein crystallography and NMR to explore protein conformations. *Annu. Rev. Biophys. 40*, 81–98.
189. Silva, J.L., Foguel, D., and Royer, C.A. **(2001)**. Pressure provides new insights into protein folding, dynamics and structure. *Trends Biochem. Sci. 26*, 612–618.
190. Roche, J., Caro, J.A., Norberto, D.R., Barthe, P., Roumestand, C., Schlessman, J.L., Garcia, A.E., Garcia-Moreno, B.E., and Royer, C.A. **(2012)**Cavities determine the pressure unfolding of proteins. *Proc. Natl. Acad. Sci. U.S.A. 109*, 6945–6950.
191. Grant, B.J., McCammon, J.A., and Gorfe, A.A. **(2010)**. Conformational Selection in G-Proteins Lessons from Ras and Rho. *Biophys. J. 99*, L87–L89.
192. Meierhofer, T., Rosnizeck, I.C., Graf, T., Reiss, K., Konig, B., Kalbitzer, H.R., and Spoerner, M. **(2011)**. Cu2+-cyclen as probe to identify conformational states in guanine nucleotide binding proteins. *J. Am. Chem. Soc. 133*, 2048–2051.
193. Geyer, M., Schweins, T., Herrmann, C., Prisner, T., Wittinghofer, A., and Kalbitzer, H.R. **(1996)**. Conformational transitions in p21ras and in its complexes with the effector protein Raf-RBD and the GTPase activating protein GAP. *Biochemistry 35*, 10308–10320.
194. Spoerner, M., Hozsa, C., Poetzl, J.A., Reiss, K., Ganser, P., Geyer, M., and Kalbitzer, H.R. **(2010)**. Conformational states of human rat sarcoma (Ras) protein complexed with its natural ligand GTP and their role for effector interaction and GTP hydrolysis. *J. Biol. Chem. 285*, 39768–39778.
195. Spoerner, M., Nuehs, A., Ganser, P., Herrmann, C., Wittinghofer, A., and Kalbitzer, H.R. **(2005)**. Conformational states of Ras complexed with the GTP analogue GppNHp or GppCH2p: implications for the interaction with effector proteins. *Biochemistry 44*, 2225–2236.
196. Spoerner, M., Wittinghofer, A., and Kalbitzer, H.R. **(2004)**. Perturbation of the conformational equilibria in Ras by selective mutations as studied by ^{31}P-NMR spectroscopy. *FEBS Lett. 578*, 305–310.
197. Spoerner, M., Herrmann, C., Vetter, I.R., Kalbitzer, H.R., and Wittinghofer, A. **(2001)**. Dynamic properties of the Ras switch I region and its importance for binding to effectors. *Proc. Natl. Acad. Sci. U.S.A. 98*, 4944–4949.
198. Kalbitzer, H.R., Spoerner, M., Ganser, P., Hozsa, C., and Kremer, W. **(2009)**. Fundamental link between folding states and functional states of proteins. *J. Am. Chem. Soc. 131*, 16714–16719.
199. Heremans, K., and Smeller, L. **(1998)**. Protein structure and dynamics at high pressure. *Biochim. Biophys. Acta 1386*, 353–370.

200. Dzwolak, W., Kato, M., and Taniguchi, Y. **(2002)**. Fourier transform infrared spectroscopy in high-pressure studies on proteins. *Biochim. Biophys. Acta*. *1595*, 131–144.
201. Sonavane, S., and Chakrabarti, P. **(2008)**. Cavities and atomic packing in protein structures and interfaces. *PLoS Comput. Biol. 4*, e1000188.
202. Panick, G., Malessa, R., Winter, R., Rapp, G., Frye, K.J., and Royer, C.A. **(1998)**. Structural characterization of the pressure-denatured state and unfolding/refolding kinetics of staphylococcal nuclease by synchrotron small-angle X-ray scattering and Fourier-transform infrared spectroscopy. *J. Mol. Biol. 275*, 389–402.
203. Sanner, M.F., Olson, A.J., and Spehner, J.C. **(1996)**. Reduced surface: an efficient way to compute molecular surfaces. *Biopolymers 38*, 305–320.
204. Gekko, K., Kamiyama, T., Ohmae, E., and Katayanagi, K. **(2000)**. Single amino acid substitutions in flexible loops can induce large compressibility changes in dihydrofolate reductase. *J. Biochem. 128*, 21–27.
205. Matos, P.M., Franquelim, H.G., Castanho, M.A., and Santos, N.C. **(2010)**. Quantitative assessment of peptide–lipid interactions. Ubiquitous fluorescence methodologies. *Biochim. Biophys. Acta 1798*, 1999–2012.
206. Bekard, I.B., and Dunstan, D.E. **(2009)**. Tyrosine autofluorescence as a measure of bovine insulin fibrillation. *Biophys. J. 97*, 2521–2531.
207. Amaro, M., Birch, D.J., and Rolinski, O.J. **(2011)**. Beta-amyloid oligomerisation monitored by intrinsic tyrosine fluorescence. *Phys. Chem. Chem. Phys. 13*, 6434–6441.
208. Kapoor, S., Triola, G., Vetter, I.R., Erlkamp, M., Waldmann, H., and Winter, R. **(2012)**. Revealing conformational substates of lipidated N-Ras protein by pressure modulation. *Proc. Natl. Acad. Sci. U.S.A. 109*, 460–465.
209. Beavo, J.A. **(1995)**. Cyclic nucleotide phosphodiesterases: functional implications of multiple isoforms. *Physiol. Rev. 75*, 725–748.
210. Baehr, W., Devlin, M.J., and Applebury, M.L. **(1979)**. Isolation and characterization of cGMP phosphodiesterase from bovine rod outer segments. *J. Biol. Chem. 254*, 11669–11677.
211. Deterre, P., Bigay, J., Forquet, F., Robert, M., and Chabre, M. **(1988)**. cGMP phosphodiesterase of retinal rods is regulated by two inhibitory subunits. *Proc. Natl. Acad. Sci. U.S.A. 85*, 2424–2428.
212. Qin, N., Pittler, S.J., and Baehr, W. **(1992)**. In vitro isoprenylation and membrane association of mouse rod photoreceptor cGMP phosphodiesterase alpha and beta subunits expressed in bacteria. *J. Biol. Chem. 267*, 8458–8463.
213. Gillespie, P.G., Prusti, R.K., Apel, E.D., and Beavo, J.A. **(1989)**. A soluble form of bovine rod photoreceptor phosphodiesterase has a novel 15-kDa subunit. *J. Biol. Chem.. 264*, 12187–12193.
214. Cook, T.A., Ghomashchi, F., Gelb, M.H., Florio, S.K., and Beavo, J.A. **(2000)**. Binding of the delta subunit to rod phosphodiesterase catalytic subunits requires methylated, prenylated C-termini of the catalytic subunits. *Biochemistry 39*, 13516–13523.
215. Florio, S.K., Prusti, R.K., and Beavo, J.A. **(1996)**. Solubilization of membrane–bound rod phosphodiesterase by the rod phosphodiesterase recombinant delta subunit. *J. Biol. Chem. 271*, 24036–24047.
216. Cook, T.A., Ghomashchi, F., Gelb, M.H., Florio, S.K., and Beavo, J.A. **(2001)**. The delta subunit of type 6 phosphodiesterase reduces light-induced cGMP hydrolysis in rod outer segments. *J. Biol. Chem*. *276*, 5248–5255.
217. Marzesco, A.M., Galli, T., Louvard, D., and Zahraoui, A. **(1998)**. The rod cGMP phosphodiesterase delta subunit dissociates the small GTPase Rab13 from membranes. *J. Biol. Chem.. 273*, 22340–22345.
218. Linari, M., Hanzal-Bayer, M., and Becker, J. **(1999)**. The delta subunit of rod specific cyclic GMP phosphodiesterase, PDE delta, interacts with the Arf-like protein Arl3 in a GTP specific manner. *FEBS Lett. 458*, 55–59.
219. Hanzal-Bayer, M., Renault, L., Roversi, P., Wittinghofer, A., and Hillig, R.C. **(2002)**. The complex of Arl2-GTP and PDE delta: from structure to function. *EMBO J. 21*, 2095–2106.
220. Zhang, H., Liu, X.H., Zhang, K., Chen, C.K., Frederick, J.M., Prestwich, G.D., and Baehr, W. **(2004)**. Photoreceptor cGMP phosphodiesterase delta subunit (PDEdelta) functions as a prenyl-binding protein. *J. Biol. Chem. 279*, 407–413.

221. Nancy, V., Callebaut, I., El Marjou, A., and de Gunzburg, J. **(2002)**. The delta subunit of retinal rod cGMP phosphodiesterase regulates the membrane association of Ras and Rap GTPases. *J. Biol. Chem. 277*, 15076–15084.
222. Bhagatji, P., Leventis, R., Rich, R., Lin, C.J., and Silvius, J.R. **(2010)**. Multiple Cellular Proteins Modulate the Dynamics of K-ras Association with the Plasma Membrane. *Biophys. J. 99*, 3327–3335.
223. Ismail, S.A., Chen, Y.X., Rusinova, A., Chandra, A., Bierbaum, M., Gremer, L., Triola, G., Waldmann, H., Bastiaens, P.I.H., and Wittinghofer, A. **(2011)**. Arl2-GTP and Arl3-GTP regulate a GDI-like transport system for farnesylated cargo. *Nat. Chem. Biol. 7*, 942–949.
224. Weise, K., Kapoor, S., Wekmüller, A., Möbitz, S., Zimmermann, G., Triola, G., Waldmann, H., and Winter, R. **(2012)**. Dissociation of the K-Ras4B/PDEδ complex upon contact with lipid membranes: Membrane delivery instead of extraction. *134*, 11503–11510.
225. Myszka, D.G. **(1997)**. Kinetic analysis of macromolecular interactions using surface plasmon resonance biosensors. *Curr. Opin. Biotechnol. 8*, 50–57.
226. Myszka, D.G. **(2000)**. Kinetic, equilibrium, and thermodynamic analysis of macromolecular interactions with BIACORE. *Methods Enzymol. 323*, 325–340.
227. Heo, W.D., Inoue, T., Park, W.S., Kim, M.L., Park, B.O., Wandless, T.J., and Meyer, T. **(2006)**. PI(3,4,5)P3 and PI(4,5)P2 lipids target proteins with polybasic clusters to the plasma membrane. *Science 314*, 1458–1461.
228. McLaughlin, S., and Aderem, A. **(1995)**. The myristoyl-electrostatic switch: a modulator of reversible protein-membrane interactions. *Trends Biochem. Sci. 20*, 272–276.
229. Alexander, M., Gerauer, M., Pechlivanis, M., Popkirova, B., Dvorsky, R., Brunsveld, L., Waldmann, H., and Kuhlmann, J. **(2009)**. Mapping the Isoprenoid Binding Pocket of PDE delta by a Semisynthetic, Photoactivatable N-Ras Lipoprotein. *Chembiochem 10*, 98–108.
230. Wu, H.J., Zhang, Z.Q., Yu, B., Liu, S., Qin, K.R., and Zhu, L. **(2010)**. Pressure activates Src-dependent FAK-Akt and ERK1/2 signaling pathways in rat hepatic stellate cells. *Cell Physiol. Biochem. 26*, 273–280.
231. Salvador-Silva, M., Aoi, S., Parker, A., Yang, P., Pecen, P., and Hernandez, M.R. **(2004)**. Responses and signaling pathways in human optic nerve head astrocytes exposed to hydrostatic pressure in vitro. *Glia 45*, 364–377.
232. Sukharev, S.I., Blount, P., Martinac, B., Blattner, F.R., and Kung, C. **(1994)**. A large-conductance mechanosensitive channel in E. coli encoded by mscL alone. *Nature 368*, 265–268.
233. Paoletti, P., and Ascher, P. **(1994)**. Mechanosensitivity of NMDA receptors in cultured mouse central neurons. *Neuron 13*, 645–655.
234. Gudi, S., Nolan, J.P., and Frangos, J.A. **(1998)**. Modulation of GTPase activity of G proteins by fluid shear stress and phospholipid composition. *Proc. Natl. Acad. Sci. U.S.A. 95*, 2515–2519.
235. Ferraro, J.T., Daneshmand, M., Bizios, R., and Rizzo, V. **(2004)**. Depletion of plasma membrane cholesterol dampens hydrostatic pressure and shear stress-induced mechanotransduction pathways in osteoblast cultures. *Am. J. Physiol. Cell. Physiol. 286*, C831–839.
236. Li, Y.S., Shyy, J.Y., Li, S., Lee, J., Su, B., Karin, M., and Chien, S. **(1996)**. The Ras–JNK pathway is involved in shear-induced gene expression. *Mol. Cell Biol. 16*, 5947–5954.
237. Tzima, E. **(2006)**. Role of small GTPases in endothelial cytoskeletal dynamics and the shear stress response. *Circ. Res. 98*, 176–185.
238. McLaughlin, S. **(1989)**. The electrostatic properties of membranes. *Annu. Rev. Biophys. Biophys. Chem. 18*, 113–136.
239. Weise, K., Huster, D., Kapoor, S., Triola, G., Waldmann, H., and Winter, R. **(2012)**. Gibbs energy determinants of lipoprotein insertion into lipid membranes: The case study of Ras proteins. *Faraday Discussions*. DOI: 10.1039/C2FD20100C
240. Scarlata, S.F., and Rosenberg, M. **(1990)**. Effect of increased lipid packing on the surface charge of micelles and membranes. *Biochemistry 29*, 10233–10240.
241. Montich, G., Scarlata, S., McLaughlin, S., Lehrmann, R., and Seelig, J. **(1993)**. Thermodynamic characterization of the association of small basic peptides with membranes containing acidic lipids. *Biochim. Biophys. Acta 1146*, 17–24.
242. Teng, Q., and Scarlata, S. **(1993)**. Effect of high pressure on the association of melittin to membranes. *J. Biol. Chem. 268*, 12434–12442.

243. Plager, D.A., and Nelsestuen, G.L. **(1992)**. Dissociation of peripheral protein–membrane complexes by high pressure. *Protein Sci. 1*, 530–539.
244. Pagano, R.E., Martin, O.C., Schroit, A.J., and Struck, D.K. *(1981)*. Formation of asymmetric phospholipid membranes via spontaneous transfer of fluorescent lipid analogues between vesicle populations. *Biochemistry 20*, 4920–4927.
245. Nichols, J.W., and Pagano, R.E. **(1982)**. Use of resonance energy transfer to study the kinetics of amphiphile transfer between vesicles. *Biochemistry*. *21*, 1720–1726.
246. Wimley, W.C., and Thompson, T.E. **(1991)**. Transbilayer and interbilayer phospholipid exchange in dimyristoylphosphatidylcholine/dimyristoylphosphatidylethanolamine large unilamellar vesicles. *Biochemistry*. *30*, 1702–1709.
247. Nichols, J.W. **(1988)**. Kinetics of Fluorescent-Labeled Phosphatidylcholine Transfer between Nonspecific Lipid Transfer Protein and Phospholipid-Vesicles. *Biochemistry*. *27*, 1889–1896.
248. Lapinski, M.M., and Blanchard, G.J. **(2007)**. The role of phospholipid headgroups in mediating bilayer organization. Perturbations induced by the presence of a tethered chromophore. *Chem. Phys. Lipids 150*, 12–21.
249. Yang, J., Chen, H., Vlahov, I.R., Cheng, J.X., and Low, P.S. **(2006)**. Evaluation of disulfide reduction during receptor-mediated endocytosis by using FRET imaging. *Proc. Natl. Acad. Sci. U.S.A. 103*, 13872–13877.
250. Haas, E., Wilchek, M., Katchalski-Katzir, E., and Steinberg, I.Z. **(1975)**. Distribution of end-to-end distances of oligopeptides in solution as estimated by energy transfer. *Proc. Natl. Acad. Sci. U.S.A.*. *72*, 1807–1811.
251. Silvius, J.R., and l'Heureux, F. **(1994)**. Fluorimetric evaluation of the affinities of isoprenylated peptides for lipid bilayers. *Biochemistry 33*, 3014–3022.
252. Nordlund, J.R., Schmidt, C.F., Dicken, S.N., and Thompson, T.E. **(1981)**. Transbilayer distribution of phosphatidylethanolamine in large and small unilamellar vesicles. *Biochemistry*. *20*, 3237–3241.
253. Thapar, R., Williams, J.G., and Campbell, S.L. **(2004)**. NMR characterization of full-length farnesylated and non-farnesylated H-Ras and its implications for Raf activation. *J. Mol. Biol. 343*, 1391–1408.
254. Nicolini, C., Celli, A., Gratton, E., and Winter, R. **(2006b)**. Pressure tuning of the morphology of heterogeneous lipid vesicles: a two-photon-excitation fluorescence microscopy study. *Biophys. J. 91*, 2936–2942.
255. Benz, R., and Conti, F. **(1986a)**. Effects of hydrostatic pressure on lipid bilayer membranes. I. Influence on membrane thickness and activation volumes of lipophilic ion transport. *Biophys. J.*. *50*, 91–98.
256. Benz, R., and Conti, F. **(1986b)**. Effects of hydrostatic pressure on lipid bilayer membranes. II. Activation and reaction volumes of carrier mediated ion transport. *Biophys. J. 50*, 99–107.
257. Jenner, G. In *High pressure Chemistry, Biochemistry and Material Sciences*, Winter, R., and Jonas, J. **(1993)** Kluwer: Dordrecht, 345–366.
258. Böttner, M., Ceh, D., Jacobs, U., and Winter, R. **(1994)**. High Pressure Volumteric Measurements on Phospholipid Bilayers. *Zeit. Phys. Chem. 184*, 205–218.
259. Kupiainen, M., Falck, E., Ollila, S., Niemelä, P., Gurtovenko, AA., Hyvönen, AT., Patra, M., Karttunen M., and Vattulainen, I. **(2005)**. Free Volume Properties of Sphingomyelin, DMPC, DPPC, and PLPC Bilayers. J. Comput. Theor. Nanosci. 2, 401–413.
260. Wang, T.Y., Leventis, R., and Silvius, J.R. **(2001)**. Partitioning of lipidated peptide sequences into liquid-ordered lipid domains in model and biological membranes. *Biochemistry 40*, 13031–13040.
261. Mesquita, R.M., Melo, E., Thompson, T.E., and Vaz, W.L. **(2000)**. Partitioning of amphiphiles between coexisting ordered and disordered phases in two-phase lipid bilayer membranes. *Biophys. J. 78*, 3019–3025.
262. Schroeder, H., Leventis, R., Rex, S., Schelhaas, M., Nagele, E., Waldmann, H., and Silvius, J.R. **(1997)**. S-acylation and plasma membrane targeting of the farnesylated carboxyl-terminal peptide of N-Ras in mammalian fibroblasts. *Biochemistry 36*, 13102–13109.

263. Silvius, J.R., Bhagatji, P., Leventis, R., and Terrone, D. **(2006)**. K-ras4B and prenylated proteins lacking "second signals" associate dynamically with cellular membranes. *Mol. Biol. Cell 17*, 192–202.
264. Sidhu, R.S., Clough, R.R., and Bhullar, R.P. **(2003)**. Ca2+/calmodulin binds and dissociates K-RasB from membrane. *Biochem. Biophys. Res. Commun. 304*, 655–660.
265. Nicolini, C., Baranski, J., Schlummer, S., Palomo, J., Lumbierres-Burgues, M., Kahms, M., Kuhlmann, J., Sanchez, S., Gratton, E., Waldmann, H., *et al.* **(2006a)**. Visualizing association of N-Ras in lipid microdomains: Influence of domain structure and interfacial adsorption. *J. Am. Chem. Soc. 128*, 192–201.
266. Shalom-Feuerstein, R., Plowman, S.J., Rotblat, B., Ariotti, N., Tian, T., Hancock, J.F., and Kloog, Y. **(2008)**. K-ras nanoclustering is subverted by overexpression of the scaffold protein galectin-3. *Cancer Res. 68*, 6608–6616.
267. Mills, I., Cvitas, T., Homann, K., Kallay, N., and Kuchitsu, K. **(1988)**. Quantities, Units and Symbols in Physical Chemistry, Blackwell Scientific publications, Oxford; Lamola, A.A. and Wrighton, M.S. **(1984)** Recommended standards for reporting photochemical data. *Pure Appl. Chem. 56*, 939–944.
268. Barth, A. **(2007)**. Infrared spectroscopy of proteins. *Biochim. Biophys. Acta 1767*, 1073–1101.
269. Baumruk, V., Pancoska, P., and Keiderling, T.A. **(1996)**. Predictions of secondary structure using statistical analyses of electronic and vibrational circular dichroism and Fourier transform infrared spectra of proteins in H_2O. *J. Mol. Biol. 259*, 774–791.
270. Rahmelow, K., and Hubner, W. **(1996)**. Secondary structure determination of proteins in aqueous solution by infrared spectroscopy: a comparison of multivariate data analysis methods. *Anal. Biochem. 241*, 5–13.
271. Cameron, D.G., and Moffatt, D.J. **(1987)**. A Generalized-Approach to Derivative Spectroscopy. *Appl. Spectrosc. 41*, 539–544.
272. Kauppinen, J.K., Moffatt, D.J., Mantsch, H.H., and Cameron, D.G. **(1981)**. Fourier Self-Deconvolution - a Method for Resolving Intrinsically Overlapped Bands. *Appl. Spectrosc*. *35*, 271–276.
273. Kauppinen, J.K., Moffatt, D.J., Mantsch, H.H., and Cameron, D.G. **(1982)**. Smoothing of Spectral Data in the Fourier Domain. *Applied Optics 21*, 1866–1872.
274. Moffatt, D.J., and Mantsch, H.H. **(1992)**. Fourier Resolution Enhancement of Infrared Spectral Data. *Methods Enzymol. 210*, 192–200.
275. Savitzky, A., and Golay, M.J.E. **(1964)**. Smoothing + Differentiation of Data by Simplified Least Squares Procedures. *Anal. Chem.36*, 1627–1639.
276. Steinier, J., Termonia, Y., and Deltour, J. **(1972)**. Smoothing and differentiation of data by simplified least square procedure. *Anal. Chem. 44*, 1906–1909.
277. Goormaghtigh, E., Cabiaux, V., and Ruysschaert, J.M. **(1994)**. Determination of soluble and membrane protein structure by Fourier transform infrared spectroscopy. I. Assignments and model compounds. *Subcell. Biochem. 23*, 329–362.
278. Oxtoby, D.W. **(1981)**. Vibrational-Relaxation in Liquids. *Annu. Rev. Phys. Chem. 32*, 77–101.
279. Saarinen, P.E., Kauppinen, J.K., and Partanen, J.O. **(1995)**. New Method for Spectral-Line Shape Fitting and Critique on the Voigt Line-Shape Model. *Appl. Spectrosc. 49*, 1438–1453.
280. Burnham, C.W., Holloway, J.R., and Davis, N.F. **(1969)**. Specific Volume of Water in Range 1000 to 8900 Bars 20 Degrees to 900 Degrees C. *Am. J. Sci. 267*, 70–95.
281. Lippert, E. **(1957)**. Habilitationsschrift Zur Erlangung Der Lehrberichtigung (Venia Legendi) Fur Das Fach Physikalische Chemie Ander Techischen–Hochschule-Stuttgart - Spektroskopische Bestimmung Des Dipolmomentes Aromatischer Verbindungen Im Ersten Angeregten Singulettzustand. *Zeitschrift Fur Elektrochemie 61*, 962–975.
282. Bridgman, P.W. **(1931)**. *The Physics of High Pressure*, G. Bell and Sons, London.
283. Owen, B.B., Milner, C.E., Miller, R.C., and Cogan, H.L. **(1961)**. Dielectric Constant of Water as a Function of Temperature and Pressure. *J. Phys. Chem. 65*, 2065–2070.
284. Ruan, K.C., Tian, S.M., Lange, R., and Balny, C. **(2000)**. Pressure effects on tryptophan and its derivatives. *Biochem. Biophys. Res. Comm. 269*, 681–686.
285. Barrow, R.E. and Hills, B.A. **(1979)**. A critical assessment of the Wilhelmy method in studying lung surfactants. *J. Physiol. 295*, 217–227.

286. Harding, A.S., and Hancock, J.F. **(2008)**. Using plasma membrane nanoclusters to build better signaling circuits. *Trends Cell. Biol. 18*, 364–371.
287. Murakoshi, H., Fujiwara, T., Akihiko, K., Takahiro, O., Chika I, et al. **(2004)**. Single molecule imaging analysis of Ras activation in living cells*. Proc. Natl. Acad. Sci. USA. 101*, 7317–7322.
288. Hancock, J.F., and Parton, R.G. **(2005)**. Ras plasma membrane signalling platforms. *Biochem. J. 389*, 1–11.
289. Plowman, S.J., Muncke, C., Parton, R.G., and Hancock, J.F. **(2005)**. H-ras, K-ras, and inner plasma membrane raft proteins operate in nanoclusters with differential dependence on the actin cytoskeleton. *Proc. Natl. Acad. Sci. USA. 102*, 15500–15505.
290. Gohlke, A., Triola, G., Waldmann, H., and Winter, R. **(2010)**. Influence of the lipid anchor motif of N-Ras on the interaction with lipid membranes: A surface plasmon resonance study. *Biophys. J. 98*, 2226–2235.
291. Gerlach, H., Laumann, V., Martens, S., Becker, C.F.W., Goody, R.S., and Geyer, M. **(2009)**. HIV-1 Nef membrane association depends on charge, curvature, composition and sequence. *Nat. Chem. Biol. 6*, 46–53.

XI

PUBLICATIONS AND PRESENTATIONS

Results presented in this thesis have contributed to the following peer-reviewed publications

1. Kapoor, S., Weise, K., Erlkamp, M., Triola, G., Waldmann, H., and Winter, R. **(2012)**. The role of G-domain orientation and nucleotide state on the Ras isoform-specific membrane interaction. *Eur. Biophys. J.41,*801–813.
2. Kapoor, S., Triola, G., Vetter, I.R., Erlkamp, M., Waldmann, H., and Winter, R. **(2012)**. Revealing conformational substates of lipidated N-Ras protein by pressure modulation. *Proc. Natl. Acad. Sci. U.S.A. 109*, 460–465.
3. Weise, K., Kapoor, S., Wekmüller, A., Möbitz, S., Zimmermann, G., Triola, G., Waldmann, H., and Winter, R. **(2012)**. Dissociation of the K-Ras4B/PDEδ complex upon contact with lipid membranes: Membrane delivery instead of extraction. *J. Am. Chem. Soc. 134*, 11503–11510.
4. Weise, K., Huster, D., Kapoor, S., Triola, G., Waldmann, H., and Winter, R. **(2012)**. Gibbs energy determinants of lipoprotein insertion into lipid membranes: The case study of Ras proteins. *Faraday Discussions*. (Accepted, In press) DOI: 10.1039/C2FD20100C.
5. Weise, K., Kapoor, S., Denter, C., Nikolaus, J., Opitz, N., Koch, S., Triola, G., Herrmann, A., Waldmann, H., and Winter, R. **(2011)**. Membrane-Mediated Induction and Sorting of K-Ras Microdomain Signaling Platforms. *J. Am. Chem. Soc. 133*, 880–887.
6. Kapoor, S., Werkmüller, A., Denter, C., Zhai, Y., Markgraf, J., Weise, K., Opitz, N., and Winter, R. **(2011)**. Temperature-pressure phase diagram of a heterogeneous anionic model biomembrane system: Results from a combined calorimetry, spectroscopy and microscopy study. *Biochim. Biophys. Acta, Biomembr. 1808*, 1187–1195.

Work undertaken in collaborations has contributed to the following peer-reviewed publications

7. Seeliger, J., Evers, F., Jeworrek, C., Kapoor, S., Weise, K., Andreetto, E., Tolan, M., Kapurniotu, A., and Winter, R. **(2012).** Cross-amyloid interaction of Aβ and IAPP at lipid membranes. *Angew. Chem. Int. Ed. 51*, 679–683.
8. Barackov, I., Mause, A., Kapoor, S., Winter, R., Schembecker, G., and Burghoff, B. (2012). Investigation of structural changes of β-casein and lysozyme at the gas-liquid interface during foam fractionation. *J. Biotech. 161*, 138–146.
9. Henke, S., Schneemann, A., Kapoor, S., Winter, R., and Fischer, RA. **(2012).** Zinc-1, 4-benzenedicarboxylate-bipyridine frameworks - Linker functionalization impacts network topology during solvothermal synthesis. *J. Mat. Chem. 22*, 909–918

Conferences Proceeding and Talks

1. 7th International Conference on High Pressure Biosciences and Biotechnology, Otsu, Japan. October-November 2012. **Poster**
2. Cold Spring Harbor Asia Conference, Suzhou, China. September 2012. **Poster**
3. Bunsentagung Annual German Conference on Physical Chemistry, Leipzig, Germany. May 2012. **Poster**
4. MPI-RIKEN Kick *Off* Symposium, Dortmund, Germany. March 2012. **Talk**
5. Annual Biophysical Society Conference, California, USA. February 2012. Poster
6. Tag Der Chemie, Technische Universität Dortmund, Germany. February 2012. **Talk**
7. Bunsentagung Annual German Conference on Physical Chemistry, Berlin, Germany. June 2011. **Poster (Poster Prize)**
8. University of Utrecht and International Max Planck Research School Joint Symposium on Chemical Biology, Utrecht, Netherlands. May 2011. **Talk**
9. Tag Der Chemie, Technische Universität Dortmund, Germany. February 2011. **Poster**
10. IMPRS Symposium: Chemical Biology-Exploring the interface, Max Planck Institute of Molecular Physiology, Dortmund, Germany. September 2011. **Poster**
11. Annual Meeting of German Biophysical Society, Rühr-Universität, Bochum, Germany**.** October 2010. **Poster**
12. Collaborative Research Center (SFB) 642 "GTP- and ATP-Dependent Membrane Processes-Summer School, Wenden, Germany. September 2011. **Talk**

XII

CURRICULUM VITAE

Personal Details

Name: Shobhna Kapoor
Address: Kleyer Weg 86, 44149 Dortmund, Germany
Telephone: +49-176-64958443
Email: kapoor_shobhna@yahoo.co.in; shobhna.kapoor@tu-dortmund.de
Date of Birth: 24th April 1985
Nationality: Indian
University Matriculation Number: 136875 (TU Dortmund)

Education and Scientific Research Experiences

- *Doctoral Thesis*
  Institution: Technische Universität Dortmund, Germany & International Max Planck Research School in Chemical Biology
  Duration: August 2009 - Present
  Title: Biophysical Inisghts into the Ras–Membrane Ballet: Orientational Flexibilty, Conformational Substates and Mechanosensitivity of Ras proteins.
  Supervisor: Prof. Dr. Roland Winter

- *Master of Science in Chemical Sciences*
  Institution: Indian Institute of Science, Bangalore, India
  Duration: 2006-2009
  Grade: CGPA (Cumulative Grade Point Average) 7.1/8.0
  Thesis: Nano-structured inorganic materials for biotechnological applications.
  Supervisor: Prof. Aninda J. Bhattacharyya

- *Bachelor of Science in Chemistry (Honors Degree)*
  Institution: St. Stephen's College, Delhi University, India
  Duration: 2003-2006
  Grade: First class with distinction (77.7 %)

- *Research Internship*
  Institution: School of Studies in Neuroscience & Bio-Informatics Center, Jiwaji University, Gwalior, India
  Duration: Dec 2007 – Jan 2008

Title: Molecular Histopathology of HIV-Tuberculosis meningitis.
Supervisor: Prof. Ishan Patro

- *Research Internship*
  Institution: LIONEX, Diagonstics and Therapeutics GmbH, Braunschweig, Germany
  Duration: May 2007 – July 2007
  Title: A biochemical route to rational drug design
  Supervisors: Prof. Ralf Spalleck, Prof. Mahavir Singh and Dr. Wulf Oehlmann

- *Research Internship*
  Institution: Dr. B. R. Ambedkar Center for Biomedical Research, Delhi University, India
  Duration: June 2005 – Aug 2005
  Title: Purification of mouse α-2 macroglobulin and preparation of mouse albumin-malondialdehyde acetaldehyde.
  Supervisor: Dr. Anju Katyal

- *Research Internship*
  Institution: Department of Chemistry, Delhi University, India
  Duration: Oct 2003 – Jan 2004
  Title: Study of Heme oxygenase activity and its role in progression of oxidative stress in carbon tetrachloride induced mice model.
  Supervisor: Prof. Ritu Anjea

Educational Awards

- ***PCCP* Hot Topic Prize** at the 110th Bunsentagung Annual German Conference on Physical Chemistry, Berlin, Germany, 2011.
- **NRW Young Scientist Award** in Chemistry, 2009, Düsseldorf, Germany. (http://www.young-scientist-award.de/)
- **Dr. A. Nagaraja Rao Gold Medal** for the "*Best Master's Student"* in Chemical Sciences Division presented by the Council of Indian Institute of Science, India, 2009.
- **Virendra Kumar Memorial Prize** for showing "*greatest proficiency in laboratory work"* during the Academic year 2005-2006 by the Chemistry Department, St. Stephen's College, Delhi, India.
- **Meritorious Student Award**- Book Grant for the year 2004 by the Faculty of Science, University of Delhi, India.